



Faculty of Engineering



Port Said University

Modeling Barrette Foundations under Lateral Loads

By

Mahmoud Mohamed Mossad El Gendy

M. Sc. in Civil Engineering

Faculty of Engineering, Port Said University, 2016

A Thesis

Submitted for the Partial Fulfillment of the Requirements for the
Doctor of Philosophy Degree in Civil Engineering

Under the Supervision of

Prof. Hassan Mohamed Hassan

Prof. of Concrete Structures

Faculty of Engineering

Port Said University

Dr. Ibrahim Ahmed El Arabi

Assoc. Prof. of Structural Engineering

Faculty of Engineering

Port Said University

2021

Modeling Barrette Foundations under Lateral Loads

A THESIS

Submitted in Partial Fulfillment of the
Requirements for the Doctor of Philosophy
Degree in Civil Engineering

By

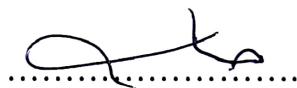
Mahmoud Mohamed Mossad El Gendy

M. Sc. Faculty of Engineering

Port Said University, 2016

APPROVED BY

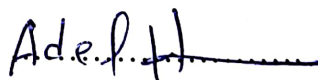
Prof. Dr. Tarek Nageeb Abd Allah Salem
Prof. of Soil Mechanics and Foundations
Faculty of Engineering, Zagazig University



Prof. Dr. Hassan Mohamed Hassan Ibrahim
Prof. of Concrete Structures, Faculty of Engineering
Port Said University



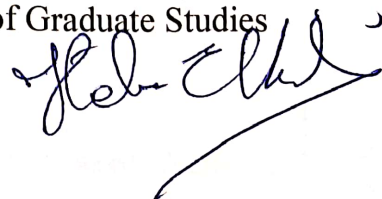
Prof. Dr. Adel Hashem Hammam Mohamed
Prof. of Soil Mechanics and Geotechnical
Engineering, Housing and Building National
Research Center



Prof. Hassan Mohamed Hassan
Dean



Prof. Heba Al Kilany
Vice – Dean of Graduate Studies



2021



Author	Mahmoud Mohamed Mossad El Gendy
Title	Modeling Barrette Foundations under Lateral Loads
Faculty	Faculty of Engineering
Department	Civil Engineering
Location	Port Said
Degree	Doctor of Philosophy Degree
Date	7-7-2021
Language	English
Supervision Committee	Prof. Dr. Hassan Mohamed Hassan Ibrahim Dr. Ibrahim Ahmed Ahmed El Arabi
Approval Committee	Prof. Dr. Tarek Nageeb Abd Allah Salem Prof. Dr. Hassan Mohamed Hassan Ibrahim Prof. Dr. Adel Hashem Hammam Mohamed

English Abstract

Barrette is a vital solution to minimize soil displacement problems of massive structures due to its high axial and lateral load capacities. The traditional methods for analyzing barrettes are mainly modeling the barrette and surrounding soil using three-dimensional finite elements. These methods require a huge-computational effort. In this thesis, a numerical hybrid technique is developed for analyzing laterally loaded barrettes and barrette groups. In this technique, the flexibility coefficient is used to determine the soil deformation based on *Mindlin's* solution considering the full interaction between barrettes and surrounding soil. Also, it takes into consideration the group interaction of every single barrette on the group of barrettes. On the other hand, the barrette in the vertical direction is discretized to one-dimensional finite elements. The soil stiffness along the barrette surface is reduced by the Composed Coefficient Technique (*CCT*) to be one-dimensional along the barrette vertical axis having variable displacements along the barrette height. This technique enables adding the soil stiffness to the barrette stiffness matrix generating the full stiffness matrix of the single barrettes/barrette groups to be solved. As a result, the number of equations is reduced. Besides the soil nonlinearity using the hyperbolic function is considered. A series of validations are carried out to verify the hybrid technique. In addition, a comparative study of laterally loaded single barrettes in a real-subsoil is carried out, in which east Port-Said soil properties are considered. Also, parametric studies are carried out to investigate the behavior of laterally loaded barrette/barrette groups. The study presents guidelines for analyzing laterally loaded single barrettes and barrette groups.

Keywords	Soil structure interaction, Deep foundations, Rectangular piles, Barrettes, Single barrettes, barrette groups, lateral load, Composed Coefficient Technique.
-----------------	--

ACKNOWLEDGMENT

I would first like to thank my father **Pro. Mohamed El Gendy**, and my uncle **Dr. Amin El Gendy** the authors of the program *ELPLA*. This accomplishment would not have been possible without them.

I must express my very profound to my **mother** and to my **wife** for providing me with unfailing support and continuous encouragement throughout my years of researching and writing this thesis. Thank you.

I would also like to thank my thesis advisors **Pro. Hassan Mohamed Hassan** and **Dr. Ibrahim El Arabi** for their kind supervision, valuable suggestions, advice, and continuous encouragement.

I would also like to thank **Prof. Tarek Naguib**, **Prof. Adel Hashem**, and **Dr. Darwin Fox** for their kind revision, and advice.

Mahmoud El Gendy

ABSTRACT

Barrette is a vital solution to minimize soil displacement problems of massive structures due to its high axial and lateral load capacities. The traditional methods for analyzing barrettes are mainly modeling the barrette and surrounding soil using three-dimensional finite elements. These methods require a huge-computational effort. In this thesis, a numerical hybrid technique is developed for analyzing laterally loaded barrettes and barrette groups. In this technique, the flexibility coefficient is used to determine the soil deformation based on *Mindlin's* solution considering the full interaction between barrettes and surrounding soil. Also, it takes into consideration the group interaction of every single barrette on the group of barrettes. On the other hand, the barrette in the vertical direction is discretized to one-dimensional finite elements. The soil stiffness along the barrette surface is reduced by the Composed Coefficient Technique (*CCT*) to be one-dimensional along the barrette vertical axis having variable displacements along the barrette height. This technique enables adding the soil stiffness to the barrette stiffness matrix generating the full stiffness matrix of the single barrettes/barrette groups to be solved. As a result, the number of equations is reduced. Besides the soil nonlinearity using the hyperbolic function is considered. A series of validations are carried out to verify the hybrid technique. In addition, a comparative study of laterally loaded single barrettes in a real-subsoil is carried out, in which east Port-Said soil properties are considered. Also, parametric studies are carried out to investigate the behavior of laterally loaded barrette/barrette groups. The study presents guidelines for analyzing laterally loaded single barrettes and barrette groups.

Table of Contents

ACKNOWLEDGMENT	VIII
ABSTRACT	IX
TABLE OF CONTENTS.....	X
LIST OF TABLES	XIII
LIST OF FIGURES	XIV
NOTATIONS.....	XIX
CHAPTER 1	1
1 INTRODUCTION.....	1
1.1 General	1
1.2 Aims of the Study	2
1.3 Objectives of the Study	3
1.4 Significance of the Study	3
1.5 Organization of Thesis	3
CHAPTER 2	5
2 LITERATURE REVIEW	5
2.1 Introduction	5
2.2 Axially Loaded Barrettes	7
2.3 Laterally Loaded Barrettes	9
2.4 Composed Coefficient Technique (<i>CCT</i>)	9
CHAPTER 3	11
3 MATHEMATICAL MODEL	11
3.1 Introduction	11
3.2 Modeling Laterally Loaded Single Barrette.....	11
3.2.1 Soil flexibility matrix	13
3.2.2 Soil stiffness matrix	15
3.2.3 Barrette stiffness matrix	18
3.2.4 Multi-layered soil	22
3.2.5 Nonlinear analysis of barrette	23
3.3 Modeling Laterally Loaded Barrette Groups	24

3.3.1	Soil flexibility matrix	25
3.3.2	Soil stiffness matrix.....	27
3.3.3	Barrette stiffness matrix	32
CHAPTER 4	34
4	VALIDATION OF THE PROGRAM.....	34
4.1	Introduction	34
4.2	The Validity of Linear Analysis.....	34
4.2.1	Description of the test problem	34
4.2.2	Numerical analysis	38
4.2.3	Results and discussion.....	40
4.3	The Validity of Dimensionless Barrette Displacements	46
4.3.1	Description of the test problem	46
4.3.2	Numerical analysis	46
4.3.3	Results and discussion.....	50
4.4	The Validity of Nonlinear Analysis	50
4.4.1	Description of the test problem	50
4.4.2	Numerical analysis	52
4.4.3	Results and discussion.....	53
4.5	Case Study of Lateral Load Tests.....	55
4.5.1	Description of the test problem	55
4.5.2	Numerical analysis	58
4.5.3	Results and discussion.....	59
4.6	Comparative Study of the Present Hybrid Technique.....	61
4.6.1	Description of the examination problem	61
4.6.2	Numerical analysis	64
4.6.3	Results and discussion.....	68
CHAPTER 5	72
5	ANALYSIS OF BARRETTES.....	72
5.1	Introduction	72
5.2	Comparative Study of a Single Barrette in a Real Subsoil.....	72
5.2.1	Introduction	72
5.2.2	Barrette properties	73
5.2.3	Soil properties.....	74

5.2.4	Effective barrette height.....	75
5.2.5	The maximum bending moment and barrette head displacement..	88
5.2.6	Limit barrette load.....	95
5.2.7	Guideline for analyzing single barrettes	96
5.3	Parametric Study of Single Barrettes	98
5.3.1	Introduction.....	98
5.3.2	Material properties and parameters of interest.....	98
5.3.3	Results and discussion	98
5.4	Parametric Study of Barrette Groups	104
5.4.1	Introduction.....	104
5.4.2	Material properties and parameters of interest.....	104
5.4.3	Results and discussion	105
CHAPTER 6	114
6	CONCLUSIONS AND RECOMMENDATIONS.....	114
6.1	Summary	114
6.2	Conclusions.....	115
6.3	Recommendations for Future Works	116
6.4	Research extracted from this thesis.....	117
7	REFERENCES.....	118
8	APPENDIX.....	125
8.1	APPENDIX (A)	125
8.2	APPENDIX (B).....	129
8.3	APPENDIX (C).....	149

LIST OF TABLES

Table No.	Title	Page
Table 4.1	Barrette geometries, <i>Basu et al.</i> (2007, 2008) [6], [7] and <i>Choi et al.</i> (2014, 2015) [14], [15].	36
Table 4.2	Soil properties, <i>Basu et al.</i> (2007, 2008) [6], [7] and <i>Choi et al.</i> (2014, 2015) [14], [15].	36
Table 4.3	Comparison between Max. Bending moment obtained from <i>Basu et al.</i> (2007, 2008) [6], [7] and <i>Choi et al.</i> (2014, 2015) [14], [15] with those obtained from the present analysis using flexibility coefficient.	40
Table 4.4	Barrette geometries, <i>Poulos et al.</i> (2019) [48].	51
Table 4.5	Subsoil properties, <i>Poulos et al.</i> (2019) [48].	51
Table 4.6	Barrette geometries, <i>Zhang</i> (2003) [63].	57
Table 4.7	The subsoil properties of case (1), <i>Zhang</i> (2003) [63].	57
Table 4.8	Subsoil properties of case (2), <i>Zhang</i> (2003) [63].	58
Table 4.9	Soil properties.	62
Table 4.10	Barrette geometries.	62
Table 5.1	Barrette material properties.	73
Table 5.2	Studied cases of a single barrette.	73
Table 5.3	Subsoil properties, <i>Hamza et al.</i> (2000) [25].	74
Table 5.4	The equivalent horizontal modulus of soil reaction, n_{eq} .	78
Table 5.5	Effective barrette height using method (1), first iteration.	79
Table 5.6	Effective barrette height, Method (1).	79
Table 5.7	The equivalent modulus of elasticity, E_{seq} kN/m ² .	81
Table 5.8	Effective barrette height using method (2), first iteration.	82
Table 5.9	Effective barrette height, Method (2).	82
Table 5.10	Effective barrette height, the present analysis.	84
Table 5.11	The ultimate lateral load of the barrettes H_{ult} , [kN].	96
Table 5.12	The horizontal limit load of the barrettes H_{lim} , [kN].	96
Table 5.13	Summary results of analyzing single barrettes using nonlinear analysis.	97
Table 5.14	Dimensionless groups of parameters used in the analysis.	98
Table 5.15	Dimensionless groups of parameters used in the analysis.	105

LIST OF FIGURES

Figure No.	Title	Page
Figure 1.1	Barrette construction sequence, [67].	2
Figure 2.1	Dubai Creek Tower's barrettes, [65].	6
Figure 2.2	Dubai Creek Tower's pile cap, [66].	7
Figure 3.1	Barrette geometry and elements.	12
Figure 3.2	The geometry of a point load beneath the ground surface.	13
Figure 3.3	The surface mesh of a single barrette.	15
Figure 3.4	The beam element with the applied load.	18
Figure 3.5	The finite element mesh of the barrette and the element geometry..	20
Figure 3.6	The geometry of the shaft element lies between two layers.	23
Figure 3.7	The barrette load-displacement curve (hyperbolic relation).	24
Figure 3.8	The surface mesh of the barrette group.	25
Figure 3.9	The barrette group displacement in one-dimension.	28
Figure 3.10	Finite element mesh of the barrette group and element geometry.	32
Figure 4.1	The subsoil of single barrettes.	35
Figure 4.2	Boring logs.	37
Figure 4.3	The surface element of the barrette for all cases except case (3).	38
Figure 4.4	The surface element of the barrette for case (3).	39
Figure 4.5	Barrette in 1D finite elements.	39
Figure 4.6	Comparison between Max. Displacements.	41
Figure 4.7	Comparison between Min. Displacements.	41
Figure 4.8	Displacement u with the barrette height (case 1).	42
Figure 4.9	Displacement u with the barrette height (case 2).	42
Figure 4.10	Displacement u with the barrette height (case 3).	43
Figure 4.11	Bending moment with the barrette height (case 3).	43
Figure 4.12	Displacement u with the barrette height (case 4).	44
Figure 4.13	Bending moment with the barrette height (case 4).	44
Figure 4.14	Displacement u with the barrette height (case 5).	45
Figure 4.15	Bending moment with the barrette height (case 5).	45
Figure 4.16	Displacement u with the barrette height (case 6).	46
Figure 4.17	The ratio $u_{2\text{-layer}}/u_{\text{homog.}}$ in two-layer soil and versus h_s/H .	47
Figure 4.18	The normalized u_n in two-layer soil and versus ratio E_p/G_s^* avg..	48
Figure 4.19	The normalized u_n in three-layer soil and versus ratio E_p/G_s^* avg..	49
Figure 4.20	The normalized u_n against the ratio H/B^* .	49

Figure 4.21 Single barrette with subsoil.....	51
Figure 4.22 The surface element of the barrette.....	53
Figure 4.23 Load-displacement curve (x -direction).....	54
Figure 4.24 Load-displacement curve (y -direction).....	54
Figure 4.25 Single barrette with subsoil.....	55
Figure 4.26 Boring logs.....	56
Figure 4.27 The surface element of the barrette.....	59
Figure 4.28 Linear load-displacement curve, case (1).....	60
Figure 4.29 Nonlinear load-displacement curve, case (1).....	60
Figure 4.30 Load-displacement curve, case (2).....	61
Figure 4.31 Boring logs.....	63
Figure 4.32 The surface element of the barrette for model (1).....	64
Figure 4.33 Element mesh of the single barrette - model (2) - Soil A&B.	65
Figure 4.34 Element mesh of the single barrette - model (2) - Soil C&D.	65
Figure 4.35 Barrette with interface elements - model (3).....	66
Figure 4.36 Plan of element mesh of the single barrette - model (3).....	66
Figure 4.37 Element mesh of the single barrette - model (3) - Soil A&B.	67
Figure 4.38 Element mesh of the single barrette - model (3) - Soil C&D.	67
Figure 4.39 Comparison between Max. Displacements.....	69
Figure 4.40 Comparison between Min. Displacements.	69
Figure 4.41 Comparison between Max. Bending moments.	70
Figure 4.42 Displacement u for case (1) with subsoil (A&C).....	70
Figure 4.43 Bending moment for case (1) with subsoil (A&C).....	71
Figure 4.44 Shear force for case (1) with subsoil (A&C).....	71
Figure 5.1 East Port-Said location.....	73
Figure 5.2 East Port-Said boring log.....	75
Figure 5.3 The geometry of the barrette lies between different soil layers.....	77
Figure 5.4 The geometry of the barrette lies between different soil layers.....	80
Figure 5.5 The surface element of the single barrette.....	83
Figure 5.6 Displacement u with the barrette height (case 1).....	84
Figure 5.7 Reaction forces R_x with the barrette height (case 1).....	85
Figure 5.8 Shear forces Q_x with the barrette height (case 1).....	85
Figure 5.9 Bending moments M_y with the barrette height (case 1).....	86
Figure 5.10 Barrette rotations Θ_y with the barrette height (case 1).....	86
Figure 5.11 Comparison of effective barrettes height L_e	87

Figure 5.12 Comparison of modified effective barrettes height L_e88

Figure 5.13 Comparison of barrette head displacement u_o ($M_{y_o}=0$).89

Figure 5.14 Comparison of maximum bending moment of the barrette M_{max} ($M_{y_o}=0$).90

Figure 5.15 Comparison of modified barrette head displacement u_o ($M_{y_o}=0$)..91

Figure 5.16 Comparison of modified maximum bending moment of the barrette M_{max} ($M_{y_o}=0$).91

Figure 5.17 Comparison of barrette head displacement u_o ($P_{x_o}=0$).92

Figure 5.18 Comparison of modified barrette head displacement u_o ($P_{x_o}=0$)...93

Figure 5.19 Comparison of barrette head displacement u_o94

Figure 5.20 Comparison of maximum bending moment of the barrette M_{max} ...94

Figure 5.21 Comparison of modified maximum bending moment of the barrette M_{max}95

Figure 5.22 The load-displacement curve for Case (1).....97

Figure 5.23 The displacement ratio R_s for $L/W = 1.5$ [-].99

Figure 5.24 The displacement ratio R_s for $L/W = 2.0$ [-].100

Figure 5.25 The displacement ratio R_s for $L/W = 2.5$ [-].100

Figure 5.26 The displacement ratio R_s for $L/W = 3.0$ [-].101

Figure 5.27 The displacement ratio R_s for various barrette L/W101

Figure 5.28 The displacement ratio R_s for the effect of v_s102

Figure 5.29 The displacement ratio R_s for the effect of H/W103

Figure 5.30 The geometry of two barrettes as a barrette group.104

Figure 5.31 The displacement ratio R_g for $L/W = 1.0$ [-].105

Figure 5.32 The displacement ratio R_g for $L/W = 1.5$ [-].106

Figure 5.33 The displacement ratio R_g for $L/W = 2.0$ [-].106

Figure 5.34 The displacement ratio R_g for $L/W = 2.5$ [-].107

Figure 5.35 The displacement ratio R_g for $L/W = 3.0$ [-].107

Figure 5.36 The displacement ratio R_g with various L/W108

Figure 5.37 The displacement ratio R_g for the effect of v_s109

Figure 5.38 The displacement ratio R_g for the effect of H/W110

Figure 5.39 The groups of three barrettes.110

Figure 5.40 The groups of four barrettes.110

Figure 5.41 The displacement ratio R_g for the effect of barrettes number.111

Figure 5.42 The displacement ratio R_g for the effect of α , Group of 2 barrettes.112

Figure 5.43 The displacement ratio R_g for the effect of α , Group of 3 barrettes, B1.	112
Figure 5.44 The displacement ratio R_g for the effect of α , Group of 3 barrettes, B2&B3.....	113
Figure 5.45 The displacement ratio R_g for the effect of α , Group of 4 barrettes.	113
Figure A.1 Displacement for case (1) with subsoil (B&D).....	125
Figure A.2 Bending moment for case (1) with subsoil (B&D).....	125
Figure A.3 Shear force for case (1) with subsoil (B&D).	126
Figure A.4 Displacement u for case (2) with subsoil (A&C).....	126
Figure A.5 Bending moment for case (2) with subsoil (A&C).....	127
Figure A.6 Shear force for case (2) with subsoil (A&C).	127
Figure A.7 Displacement u for case (2) with subsoil (B&D).....	128
Figure A.8 Bending moment for case (2) with subsoil (B&D).....	128
Figure A.9 Shear force for case (2) with subsoil (B&D).	129
Figure A.10 Displacement u with the barrette height (case 2).	129
Figure A.11 Reaction forces R_x with the barrette height (case 2).....	130
Figure A.12 Shear forces Q_x with the barrette height (case 2).	130
Figure A.13 Bending moments M_y with the barrette height (case 2).....	131
Figure A.14 Barrette rotations Theta-y with the barrette height (case 2).....	131
Figure A.15 Displacement u with the barrette height (case 3).	132
Figure A.16 Reaction forces R_x with the barrette height (case 3).....	132
Figure A.17 Shear forces Q_x with the barrette height (case 3).	133
Figure A.18 Bending moments M_y with the barrette height (case 3).....	133
Figure A.19 Barrette rotations Theta-y with the barrette height (case 3).....	134
Figure A.20 Displacement u with the barrette height (case 4).	134
Figure A.21 Reaction forces R_x with the barrette height (case 4).....	135
Figure A.22 Shear forces Q_x with the barrette height (case 4).	135
Figure A.23 Bending moments M_y with the barrette height (case 4).....	136
Figure A.24 Barrette rotations Theta-y with the barrette height (case 4).....	136
Figure A.25 Displacement u with the barrette height (case 5).	137
Figure A.26 Reaction forces R_x with the barrette height (case 5).....	137
Figure A.27 Shear forces Q_x with the barrette height (case 5).	138
Figure A.28 Bending moments M_y with the barrette height (case 5).....	138
Figure A.29 Barrette rotations Theta-y with the barrette height (case 5).....	139
Figure A.30 Displacement u with the barrette height (case 6).	139

Figure A.31 Reaction forces R_x with the barrette height (case 6).	140
Figure A.32 Shear forces Q_x with the barrette height (case 6).	140
Figure A.33 Bending moments M_y with the barrette height (case 6).	141
Figure A.34 Barrette rotations $\Theta_{\theta-y}$ with the barrette height (case 6).	141
Figure A.35 Displacement u with the barrette height (case 7).	142
Figure A.36 Reaction forces R_x with the barrette height (case 7).	142
Figure A.37 Shear forces Q_x with the barrette height (case 7).	143
Figure A.38 Bending moments M_y with the barrette height (case 7).	143
Figure A.39 Barrette rotations $\Theta_{\theta-y}$ with the barrette height (case 7).	144
Figure A.40 Displacement u with the barrette height (case 8).	144
Figure A.41 Reaction forces R_x with the barrette height (case 8).	145
Figure A.42 Shear forces Q_x with the barrette height (case 8).	145
Figure A.43 Bending moments M_y with the barrette height (case 8).	146
Figure A.44 Barrette rotations $\Theta_{\theta-y}$ with the barrette height (case 8).	146
Figure A.45 Displacement u with the barrette height (case 9).	147
Figure A.46 Reaction forces R_x with the barrette height (case 9).	147
Figure A.47 Shear forces Q_x with the barrette height (case 9).	148
Figure A.48 Bending moments M_y with the barrette height (case 9).	148
Figure A.49 Barrette rotations $\Theta_{\theta-y}$ with the barrette height (case 9).	149
Figure A.50 The load-displacement curve for Case (2).	149
Figure A.51 The load-displacement curve for Case (3).	150
Figure A.52 The load-displacement curve for Case (4).	150
Figure A.53 The load-displacement curve for Case (5).	151
Figure A.54 The load-displacement curve for Case (6).	151
Figure A.55 The load-displacement curve for Case (7).	152
Figure A.56 The load-displacement curve for Case (8).	152
Figure A.57 The load-displacement curve for Case (9).	153

NOTATIONS

L	Length of the barrette in X -direction, [m].
W	Width of the barrette in Y -direction, [m].
H	Height of the barrette in Z -direction, [m].
l	Length of the element in X -direction, [m].
w	Width of the element in Y -direction, [m].
h	Height of the element in Z -direction, [m].
c	Depth of the point load j from the ground surface, [m].
z	Depth of the studied point i from the ground surface, [m].
r	Radial distance between points i and j , [m].
x	Horizontal distance in plan between points i and j , [m].
E_s	Modulus of elasticity of the soil, [kN/m ²].
ν_s	<i>Poisson's</i> ratio of the soil, [-].
G_s	Soil shear modulus, [kN/m ²].
u_{si}	Soil displacement in the x -direction of any shaft or base node i , [m].
Qx_j	Contact force in the x -direction on any shaft or base node j , [kN].
n	Total number of nodes.
$Ix_{i,j}$	Flexibility coefficient of node i due to a concentrated force in the x -direction on node j , [m/kN].
$\{u_s\}$	n Soil displacement vector of the single barrette in the x -direction.
$\{Qx\}$	n Contact force vector of the single barrette in the x -direction.
$[Ix]$	$n \times n$ Soil flexibility matrix of the single barrette.
$[Sx]$	$n \times n$ Soil stiffness matrix of the single barrette.
$Sx_{i,j}$	Soil stiffness coefficient of the single barrette, [kN/m].
n_b	Number of barrette levels.
$Sx_{bi,j}$	Composed coefficient of level i in 1D single barrette due to a concentrated force in the x -direction at level j , [kN/m].
u_{bi}	Soil displacement of level i in 1D single barrette in the x -direction, [m].
Qx_{bi}	Contact force of level i in 1D single barrette in the x -direction, [kN].
$\{u_b\}$	n_b Soil displacement vector of the single barrette levels in the x -direction.

- $\{Qx\}$ n_b Contact force vector of the single barrette levels in the x -direction.
- $[Sx_b]$ $n_b \times n_b$ Composed soil stiffness matrix of the single barrette.
- E_p Modulus of elasticity of the barrette material, [kN/m²].
- I_{pe} Moment of inertia of the barrette element e , [m⁴].
- h_e Height of the barrette element e , [m].
- Px_i External force in the x -direction on node i , [kN].
- My_i External moment about the y -axis on node i , [kN.m].
- u_i Displacement in the x -direction of node i , [m].
- θ_{y_i} Rotation about the y -axis at node i , [°].
- $\{Px\}$ $2 \times n_b$ Vector of applied load on the single barrette levels.
- $\{\delta x\}$ $2 \times n_b$ Deformation vector of the single barrette levels.
- $[Bx]$ $(2 \times n_b) \times (2 \times n_b)$ Beam stiffness matrix of the single barrette levels.
- $u_{i,j}$ Lateral soil displacement on any shaft or base node i due to a lateral point load at point j , [m].
- E_{si} Soil modulus of elasticity of layer i , [kN/m²].
- ν_{si} *Poisson's* ratio of the soil of layer i , [-].
- u_n Nonlinear displacement in the x -direction of the barrette, [m].
- H_{lim} Horizontal limit load, [kN].
- n_g Total number of nodes in barrette group.
- u_{sg_i} Soil displacement of the barrette group in the x -direction on any shaft or base node i , [m].
- Qx_{g_j} Contact force of the barrette group in the x -direction on any shaft or base node j , [kN].
- $Ix_{g_i,j}$ Flexibility coefficient of the barrette group of node i due to a concentrated force in the x -direction on node j , [m/kN].
- $\{u_{sg}\}$ n_g Soil displacement vector of the barrette group in the x -direction.
- $\{Qx_g\}$ n_g Contact force vector of the barrette group in the x -direction.
- $[Ix_g]$ $n_g \times n_g$ Soil flexibility matrix of the barrette group.
- $[Sx_g]$ $n_g \times n_g$ Soil stiffness matrix of the barrette group.
- $Sx_{g_i,j}$ Soil stiffness coefficient of the barrette group, [kN/m].

u_{bgi}	Soil displacement of the barrette group levels in the x -direction in node i of 1D barrette group, [m].
Qx_{bgi}	Contact force of the barrette group levels in the x -direction on node i of 1D barrette group, [kN].
$Sx_{bg\ i, j}$	Composed coefficient of the barrette group of level i due to a concentrated force in the x -direction at level j , [kN/m].
n_{bg}	Total number of barrette levels in barrette group.
$\{u_{bg}\}$	n_{bg} Soil displacement vector of the barrette group levels in the x -direction.
$\{Qx_{bg}\}$	n_{bg} Contact force vector of the barrette group levels in the x -direction.
$[Sx_{bg}]$	$n_{bg} \times n_{bg}$ Composed soil stiffness matrix of the barrette group.
Px_{gi}	Barrette group external force in the x -direction at level i , [kN].
My_{gi}	Barrette group external moment about the y -axis at level i , [kN.m].
u_{gi}	Barrette group displacement in the x -direction of level i , [m].
θy_{gi}	Barrette group rotation about the y -axis at level i , [°].
$\{Px_g\}$	$2 \times n_b$ Vector of applied load on barrettes in the barrette group levels.
$\{\delta x_g\}$	$2 \times n_b$ Deformation vector of the barrette group levels.
$[Bx_g]$	$(2 \times n_b) \times (2 \times n_b)$ Beam stiffness matrix of the barrette group levels.
n_{eq}	Equivalent horizontal modulus of soil reaction, [kN/m ³].
n_i	Horizontal modulus of soil reaction for layer i , [kN/m ³].
H_i	The barrette height that crosses layer i , [m].
t	Elastic barrette height, [m].
H_e	Effective barrette height, [m].
E_{seq}	Equivalent modulus of elasticity of the soil, [kN/m ²].
P_{xo}	The lateral load at the barrette head, [kN].
M_{yo}	The bending moment at the barrette head, [kN.m].
u_o	The barrette head displacement, [cm].
M_{max}	The maximum bending moment along the barrette height, [kN.m].
K_p	Passive earth pressure coefficient, [-].
γ'	Submerged unit weight of soil, [kN/m ³].
D	The diameter of the pile with the same moment of inertia, [m].
c_u	Undrained cohesion of clay, [kN/m ²].

H_{ult}	Ultimate lateral load, [kN].
S	Spacing between the centerline of barrettes, [m].
R_s	Single barrette displacement ratio R_s , [-].
u_s	Studied single barrette displacement with different load directions α , [m].
u_o	Single barrette displacement with load direction $\alpha = 0^\circ$, [m].
R_g	Barrette group displacement ratio R_g , [-].
u_g	Studied barrette group displacement, [m].

CHAPTER 1

1 INTRODUCTION

1.1 General

The civilization development, especially that has taken place in Egypt in recent times, such as the tallest tower in Africa with a height of 345 m, Towers of the financial and business district, New El Alamein Towers, and others. These mega structures cause extreme heavy axial and lateral loads, which need a special system of foundations to transmit these loads into the surrounding soils. Many structural problems for these structures arise mainly from large soil displacements. Barrette foundation is a major solution for avoiding large soil displacement problems. It reduces soil displacements, especially if the underlying layers contain weak soil, because of it is large dimensions compared to piles.

Several barrettes research appeared at the end of the last century. It became more frequently used at the beginning of the 21st century, especially in the past ten years. Early researches were based on field results of loading tests and using the three-dimensional finite element (3D-FE) to analyze it. Few researches are available for these loading tests due to the difficulty of conducting barrettes loading tests because of their high vertical and lateral load capacities. These capacities reached a world record test load of 363 MN. Different methods of analyzing barrettes appeared based on traditional methods of analyzing piles. These methods are mainly modeling the barrette and surrounding soil using 3D-FE, which requires large-computational effort. So, large-systems of equations need to be solved. Similar methods for analyzing piles are used as a less complicated problem than that of the barrettes. Usually, Piles are circular with a relatively smaller cross-sectional area, while barrettes are rectangular with a large cross-sectional area. Therefore, piles are treated as a beam element subjected to point loads on its nodes, while barrettes are treated as block members. Although these methods are used for analyzing barrettes by treating barrettes as piles with equivalent cross-section area, Its disadvantage is that it ignores the three-dimensional natural geometry of the barrette and soil.

The Composed Coefficient Technique (*CCT*) was presented by *El Gendy* (2007) [17] and *Russo* (1998) [51] to reduce the size of the soil stiffness matrix for piled rafts. This technique was developed by the author (2016) [18] for analyzing vertically-loaded single barrettes. In this thesis, the *CCT* is extended to analyze laterally loaded single barrettes and barrette groups. *Mindlin's* solution (1936) [40] is used to determine the soil deformation, considering the full three-dimensional interactions between the barrette/barrette groups and surrounding soil. The soil stiffness matrix is determined considering the group interaction

between barrettes in the barrette groups. Subsequently, The *CCT* is used to reduce the soil stiffness to be one-dimensional. On the other hand, the barrette is divided into vertical elements to determine the barrette stiffness by one-dimensional finite elements. The soil stiffness is added to the barrette stiffness generating the full stiffness matrix of barrette/barrette groups to be solved. As a result, this hybrid technique reduces the number of equations to be solved. Also, it enables applying the nonlinear response in of the barrettes by a hyperbolic function. [Figure 1.1](#) shows the barrette construction sequence.

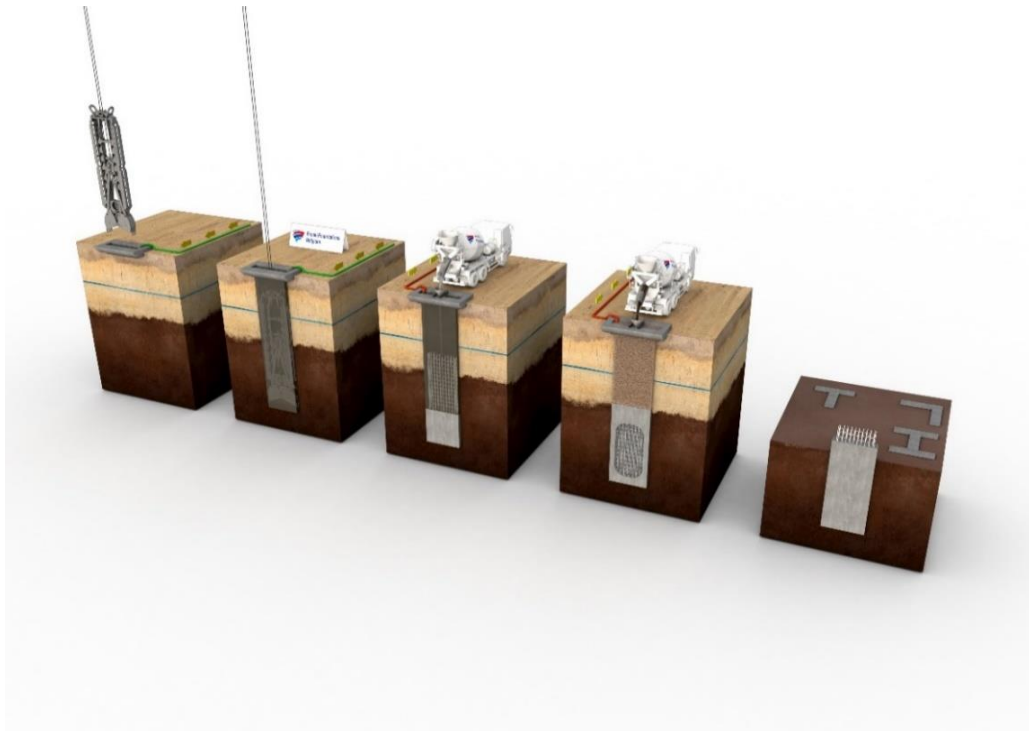


[Figure 1.1](#) Barrette construction sequence, [67].

1.2 Aims of the Study

Analyzing laterally loaded barrettes is a complex problem. It is related to the difficulty of modeling the problem with the real conditions of loading and surrounding subsoil. Pile foundations are used as traditional deep foundation systems to overcome displacement problems. On the other hand, barrette foundations are not a preferred option based on cost considerations. In the present study, barrette foundations are studied as an alternative to overcome lateral displacement problems. The main aims of the study are:

- 1- To develop a practical method for analyzing laterally loaded barrettes.

- 2- To examine the developed method for analyzing laterally loaded barrettes considering various soil conditions and parameters.
- 3- To assess the appropriateness of laterally loaded barrettes choice as a foundation system for heavy-loaded structures.
- 4- To provide the geotechnical engineer with guidelines and recommendations for the analysis of laterally loaded single barrettes constructed at the east Port-Said area.

1.3 Objectives of the Study

To achieve the above aims. The following objectives have been set:

- 1- Adopting a suitable numerical model for analyzing laterally loaded single barrettes and barrette groups considering barrette-soil interaction.
- 2- Collecting the available subsoil information to get the soil parameters, which can be used in the proposed numerical model.
- 3- Performing a sensitivity study to assess the importance of the main parameters: barrette width, barrette length, barrette height, the effective barrette height, and spacing between barrettes.

1.4 Significance of the Study

Present a developed program for analyzing laterally loaded single barrettes/barrette groups with both linear and nonlinear subsoil models. Present guidelines to be a basis for designing laterally loaded barrette foundations in the east Port-Said area. These are similar to the soil formation of London, Frankfurt, Rome, Hong kong, and Dammam.

1.5 Organization of Thesis

The thesis consists of six chapters, as follows:

Chapter (1): Introduction.

This chapter introduces the research topic and illustrates the organization of this thesis. Also, presented aims, objectives, and significance of the study.

Chapter (2): Literature Review.

Reviews of the available literature related to the scope of the thesis are presented in this chapter.

Chapter (3): Numerical Model.

This chapter presents the developed mathematical models using flexibility coefficient and finite element methods based on *CCT* for analyzing laterally loaded single barrettes and barrette groups.

Chapter (4): Validation of the program.

This chapter presents verification examples to test the accuracy of the program used in the analysis. Besides the linearly and nonlinearly results from analyzing laterally loaded barrettes embedded in multi-layered soil are compared with those in the available literature, the verification by comparing results from the present technique with two different 3D-FE models available in well-known software.

Chapter (5): Analysis of Barrettes.

This chapter presents a comparative study of laterally loaded single barrettes in a real-subsoil to study different methods for determining the effective barrette height, the linear and nonlinear soil models. Also, parametric studies are presented to investigate the behavior of laterally loaded barrette/barrette groups.

Chapter (6): Conclusions and Recommendations.

This chapter presents the summary and conclusions derived from the thesis, followed by recommendations for future work. Also, a list of research extracted from this thesis is presented.

CHAPTER 2

2 LITERATURE REVIEW

2.1 Introduction

Modeling barrettes considering their geometry and surrounding soil is a complicated problem. Methods for analyzing piles are used to simplify this problem. In those methods, Barrettes are treated as piles with an equivalent cross-sectional area. Most of these methods are verified with the results of the in-site pile-load test. For example, behaviors of laterally loaded piles were studied by comparing numerical results with those obtained from the full-scale in-site pile-load test, *Russo et al.* (2008) [52]. A simplified numerical analysis of barrettes was carried out by *Poulos et al.* (2019) [48], considering the barrette as a pile with an equivalent cross-sectional area. The simplified solutions of an equivalent pile are compared to finite element results for the barrette/barrette group in their analysis. *Kumari et al.* (2020) [32] used the three-dimensional finite element (3D-FE) for comparing the barrette load capacities with those of circular piles with the same cross-section area.

Many researchers modeled barrettes using the 3D-FE and verified their analyses with the results of load tests. *Zhang* (2003) [63] and *Mansour et al.* (2021) [38] presented some of those analyses of laterally loaded barrettes tested in Hong Kong. *Rafa et al.* (2018) [50] followed their studies with vertically loaded single barrettes in Bangkok. Besides, *Leszczynski* (2009) [35] analyzed the barrette raft for a high-rise building in Warsaw. *Znamenskii et al.* (2019) [64] presented the analysis of the barrette raft of a 56-story residential building in Moscow. In their studies, using 3D-FE for modeling barrettes take into account the full interaction between barrettes, surrounding soil, and considering the geometry of barrettes. However, it leads to a large stiffness matrix. Consequently, the analysis takes a long computational time, even with today's fast computers.

Limited methods for analyzing laterally and vertically loaded barrettes rather than 3D-FE methods are used. Some of these methods were developed by *Basu* (2006) [4], *Basu et al.* (2008) [7] and *Choi et al.* (2014) [14] for analyzing laterally and vertically loaded piles and barrettes embedded in multi-layered soil. These methods are based on the differential equations governing displacements of the pile-soil system derived from energy principles. On the other hand, *Kacprzak* (2015) [29] proposed a method to determine the load settlement characteristic of a single barrette in the group of barrettes.

Barrette foundations are already used in many foundation systems, as in Dubai Creek Tower. It will be rising to a height of 1.3 kilometers into the sky. Upon completion in 2021, it will become the tallest tower in the world. The foundation of this tower consists of 145 barrettes. These barrettes are 58 m in-depth with a cross-sectional of $2.8 \text{ m} \times 1.5 \text{ m}$, those are arranged into a dense grid of $5 \text{ m} \times 5 \text{ m}$, as shown in [Figure 2.1](#). Dubai Creek Tower's pile cap is an approximately 20 m thick multi-layered, tiered reinforced concrete top that covers and transfers the load to the foundation barrettes, as shown in [Figure 2.2](#). Barrettes used for the foundation have been tested to a world record test load of 363 MN (36,300 tons), [\[44\]](#). Other heavy-loaded structures constructed on barrette foundation such as the Grand Paris Express in France, The One tower in Brussels, the Eastern quay wall for east Port-Said port, and The Petronas Towers, Kuala Lumpur.



[Figure 2.1](#) Dubai Creek Tower's barrettes, [\[65\]](#).



Figure 2.2 Dubai Creek Tower's pile cap, [66].

2.2 Axially Loaded Barrettes

Thasnanipan et al. (1998) [60] reported the construction practice and the performance of a barrette constructed in a Bangkok metropolis, using trial trenching near a canal for trench assessment stability and soil deformation. Also discussed the choice of the barrette and common defects found in a barrette.

Thasnanipan et al. (1999) [58] and *Thasnanipan et al.* (2001) [59] compared the result of load test on the barrette, and its performance embedded in identical ground conditions with those from load test on bored pile having the same length.

Lei (2001) [33] presented a new analytical elastic solution and developed calculation charts and tables for calculating the horizontal stress changes and displacements caused by the installation of a barrette.

Charles and Lei (2003) [13] investigated long barrette behaviors under vertical loading to improve the design and analysis.

Lei et al. (2007) [34] presented an approximate 3D semi-analytical method for analyzing single barrettes, barrette group, and barrette-cap system.

Basu et al. (2008) [5] and *Seo et al.* (2009) [54] presented a user-friendly spreadsheet program (ALPAXL) for analyzing axially loaded barrettes embedded in layered soil.

Nossan et al. (2009) [43] used the 3D FE Method for analyzing barrette as deep foundations of two viaducts to sustain lateral earth pressures from a large sliding soil mass.

Shulyatiev et al. (2013) [55] studied the soil parameters for analyzing barrette foundation based on the barrette static load-test results.

Lin et al. (2014) [36] studied the axial performance of two heavily instrumented barrettes in Taipei, with and without grouting. The analysis was evaluated based on the results of barrette load tests. Also simulated the t-z curves interpreted from the measured data with depth by the hyperbolic model.

Musarra et al. (2015) [41] evaluated results obtained from the barrette test for the new Petrobras headquarters building in Salvador, Bahia, northwest of Brazil, without discussing the designer assumption.

Nguyen et al. (2016) [42] analyzed the result of bidirectional static loading tests on two shaft-grouted barrettes in Vietnam. The soil profile consisted of organic-soft clay on silty sand with some gravel and silty clay.

Hsu et al. (2017) [26] carried out a comprehensive analysis for barrettes based on five load tests on barrettes in the Taipei Basin and Kaohsiung City. Based on the strains measured at several depths along the pile shaft, complete side resistance t-z curves for various soil strata are retrieved.

Poulos et al. (2017) [46] presented the foundation system of Entisar Tower in Dubai. It will be one of the tallest buildings in the world, the foundation system consisting of barrettes with high-performance concrete, up to 80 m in depth, embedded in soft rock.

Rabaiotti et al. (2018) [49] showed how barrette was adopted and tested for anchoring a high retaining wall in the rock on a slope located in the center of Zurich.

Teparaksa et al. (2018) [57] carried out a load test on the fully instrumented barrettes. These tests are compared with the calculated ultimate capacity by the estimated adhesion factor of clay, friction/end bearing of sand.

Manoj et al. (2020) [37] presented a case study of the design for the 100-storey La Maison tower in Dubai. Barrette raft was selected as an efficient foundation system to transfer 55 MN load per barrette. Redesign by back-analysis of reinforced concrete barrette raft, resulting in a reduction of barrette length by about 11%.

Mert et al. (2020) [39] presented a new hyperbolic method based on the load transfer method for settlement analysis of axially loaded single friction piles. This method is obtained by examining 14 pile load tests. Two of them were barrettes.

Tested barrettes were loaded until they failed. These barrettes were chosen from friction piles having variable dimensions and located in different regions.

Cao et al. (2020) [12] presented an analysis method of dynamic response for a rectangular barrette subjected to a time-harmonic vertical force with the aid of a modified *Vlasov* foundation model in multilayered viscoelastic soil.

2.3 Laterally Loaded Barrettes

Abbas et al. (2008) [2] presented the results of the 3D-FE analysis of a lateral loaded single pile. Also investigated the effect of pile shape for both circular and square cross-sections on the pile response. Besides, studied the effectiveness of slenderness ratio L/B . Mohr-Coulomb model is used to simulate surrounding soil and linear elastic model for modeling piles.

El Wakil et al. (2013) [23] presented the results of small-scale laterally loaded barrettes in the laboratory. It has been reported that the lateral response of the barrette is influenced by loading direction, and the lateral load capacity is the greatest when the loading is toward the largest side of the barrette.

Conte et al. (2013) [16] proposed a 3D-FE approach for analyzing laterally loaded barrettes. This approach was used to analyze the results from some well-documented loading tests concerning large-diameter piles and large-section rectangular piles (barrettes) embedded in sandy soils.

Behloul et al. (2016) [8] studied the effect of different soil constitutive models on the laterally loaded barrette.

Keawsawasvong et al. (2016) [30] presented a numerical solution for determining the ultimate lateral capacity of barrettes in clay. The 2D plane strain FE is employed to determine the limit load for this problem.

Ukritchon et al. (2017) [61] investigated new upper and lower bound solutions for the undrained lateral capacity of barrettes under a general loading direction and full flow mechanism by using FE limit analysis with plane strain conditions.

Nasser (2020) [28] used Plaxis 3D [45] to investigate the lateral performance of single and group of barrettes in cohesionless soils.

2.4 Composed Coefficient Technique (CCT)

El Gendy (2007) [17] used the CCT to reduce the size of the soil stiffness matrix of single piles, pile groups, and piled rafts. It was a modification of the technique proposed by *Russo* (1998) [51]. This technique is dependent on treating piles as a rigid member having a uniform settlement for all nodes along its shaft and base. The CCT enables the assembly of pile coefficients into composed coefficients. Also, applying the nonlinear response of piles by a hyperbolic relation between

loads and settlements. There is no approximation when generating the flexibility coefficients of the soil by the *CCT*. This technique is examined and used efficiently in many studies. *Russo et al.* (2012) [53] and *El Gendy et al.* (2018) [19] applied this technique efficiently to re-assessment foundation settlements for the Burj Khalifa, the tallest building all over the world.

The *CCT* is developed by the author (2016) [18], [27], [20], [21], [22] for analyzing single barrettes, barrette groups and barrette raft under vertical load as a rigid and elastic body. In the developed technique, the barrette elasticity is considered by the finite element method, while that of the soil by the flexibility coefficient method. This technique is applied efficiently for vertically loaded barrettes.

In this thesis, the numerical hybrid technique is extended for analyzing laterally loaded single barrettes/barrette groups. In which the full three-dimensional interactions between barrettes and the surrounding soil are taken into consideration. In addition, the *CCT* reduces the number of equations to be solved considerably. Also, it enables applying the nonlinear response in the lateral direction of the barrettes by a hyperbolic relation between the load and displacement of the barrette.

CHAPTER 3

3 MATHEMATICAL MODEL

3.1 Introduction

A numerical technique for analyzing vertically loaded barrettes previously presented by the author (2016) [18] is extended to analyze laterally loaded single barrettes and barrette groups. The soil deformation is determined by the flexibility coefficient method based on *Mindlin's* solution (1936) [40], considering the full interaction between barrettes and surrounding soil. The barrette surface is divided into elements considering the compatibility between soil and barrette displacements at the barrette-soil interface. Then, the soil stiffness matrix is determined considering the group interaction between barrettes in the barrette groups. Subsequently, the *CCT* is used for condensing the soil stiffness along the barrette surface to be one-dimension along the barrette vertical axis having variable displacements along the barrette height. On the other hand, the barrette in the vertical direction is discretized to one-dimensional finite elements. The barrette-applied load is transformed to the soil interface as contact forces. The soil stiffness is added to the barrette stiffness generating the full stiffness matrix of barrette groups to be solved. As a result, the hybrid technique reduces the number of equations to be solved. Consequently, the analysis requires less computing time. In addition, it enables the soil nonlinearity response to be applied by a hyperbolic relation between loads and displacements of the barrette.

3.2 Modeling Laterally Loaded Single Barrette

Following the *CCT* for modeling single barrette, barrette group, and barrette raft by the author (2016) [18], a composed coefficient Sx_b [kN/m] representing the soil stiffness of the barrette is developed.

The barrette is divided into many shaft and base elements with n nodes, as shown in [Figure 3.1](#). Each one is acted upon by a distributed stress. The stresses acting on the shaft and base elements are replaced by a series of concentrated forces acting on the nodes to carry out the analysis. The soil displacement is determined by *Mindlin's* flexibility coefficient [40], considering the compatibility between soil and barrette displacements at the barrette-soil interface.

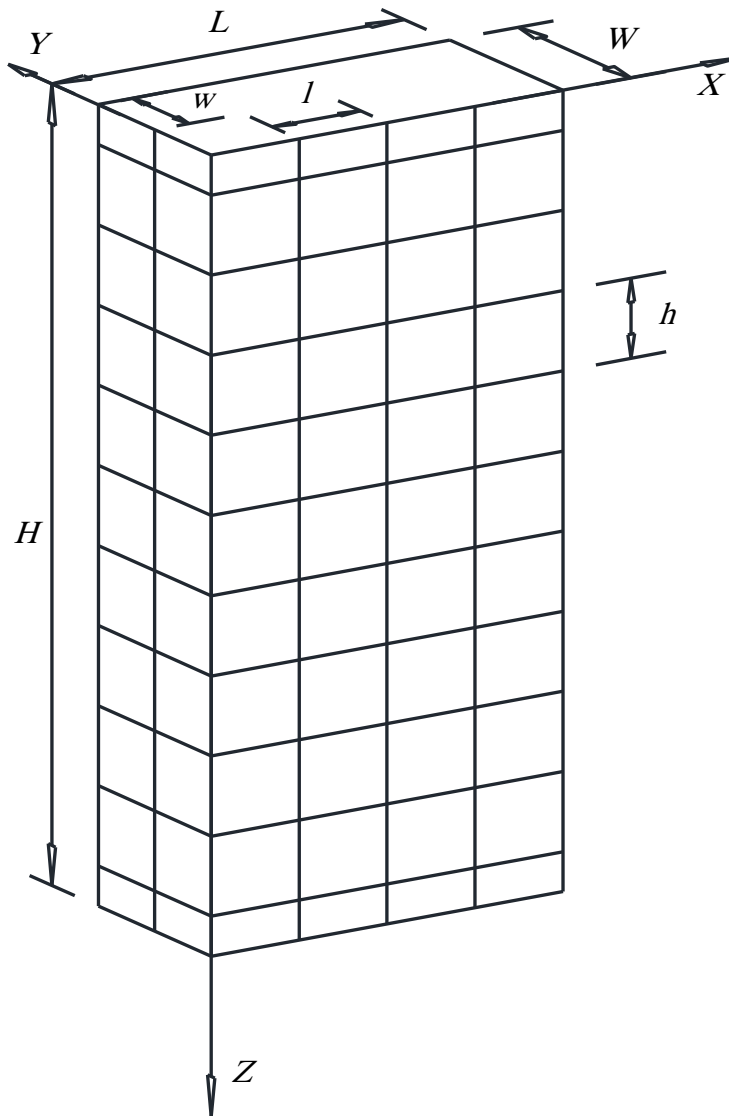


Figure 3.1 Barrette geometry and elements.

Where:

- L Length of the barrette in X-direction, [m];
- W Width of the barrette in Y-direction, [m];
- H Height of the barrette in Z-direction, [m];
- l Length of the element in X-direction, [m];
- w Width of the element in Y-direction, [m];
- h Height of the element in Z-direction, [m].

3.2.1 Soil flexibility matrix

Mindlin (1936) [40] presented a mathematical solution for determining stresses and displacements in soil resulting from a point load acting beneath the ground surface. This solution often employed in the numerical analysis of piled foundations, *Poulos* and *Davis* (1968) [47]. *Russo* (2016) [52] used this solution to predict the pile-soil interaction based on a hybrid boundary element model (BEM) approach. The displacement factor Ix_{ij} of the point i due to a point load Qx_j , kN, acting at point j beneath the surface (Figure 3.2) is expressed according to *Mindlin's* solution as:

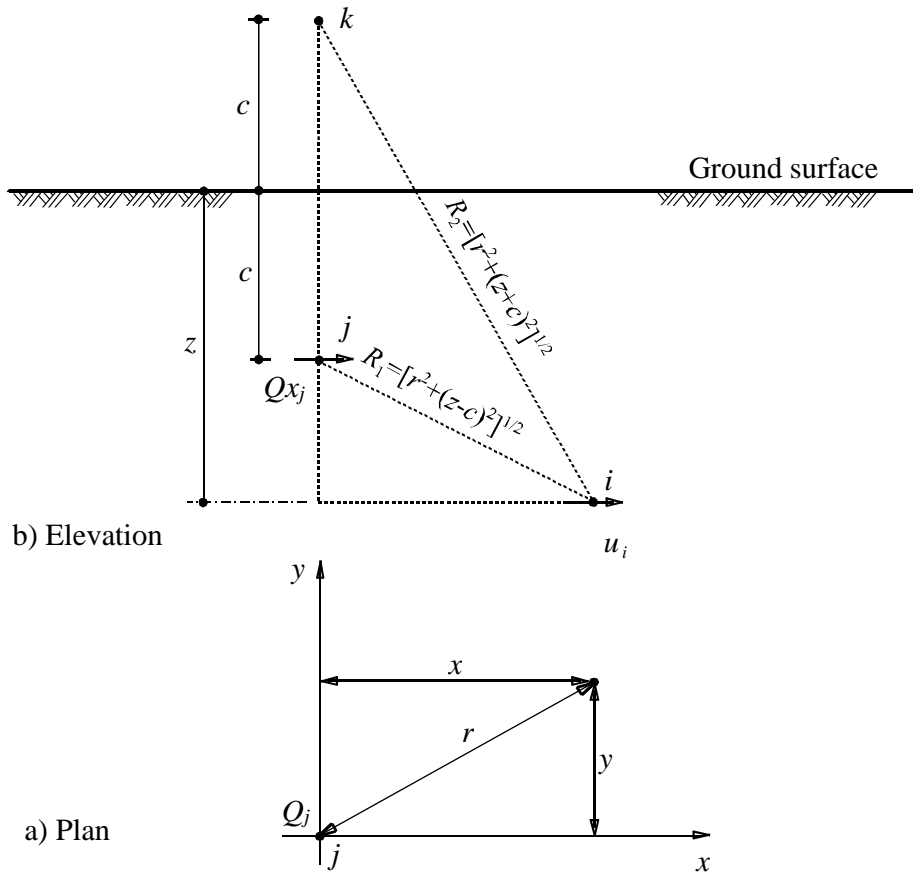


Figure 3.2 The geometry of a point load beneath the ground surface.

$$Ix_{ij} = \frac{1}{16\pi G_s(1-v_s)} \left(\frac{3-4v_s}{R_1} + \frac{1}{R_2} + \frac{x^2}{R_1^3} + \frac{(3-4v_s)x^2 + 2cz}{R_2^3} - \frac{6czx^2}{R_2^5} + \frac{4(1-v_s)(1-2v_s)}{R_2+z+c} - \frac{4(1-v_s)(1-2v_s)x^2}{R_2(R_2+z+c)^2} \right) \quad (1)$$

Where:

$$R_1 = \sqrt{r^2 + (z - c)^2}, \quad R_2 = \sqrt{r^2 + (z + c)^2}$$

- c Depth of the point load j from the ground surface, [m];
 z Depth of the studied point i from the ground surface, [m];
 r Radial distance between points i and j , [m];
 x Horizontal distance in plan between points i and j , [m];
 ν_s *Poisson's* ratio of the soil, [-]; and
 G_s Soil shear modulus, [kN/m²].

$$G_s = \frac{E_s}{2(1 + \nu_s)} \quad (2)$$

Where, E_s Modulus of elasticity of the soil, [kN/m²].

Now, the displacement in x -direction u_{sij} [m] at the point i due to a point load Qx_j [kN] acting at point j beneath the surface (Figure 3.2) can be expressed as:

$$u_{sij} = Ix_{i,j} Qx_j \quad (3)$$

Where:

- u_{si} Soil displacement in the x -direction of any shaft or base node i , [m];
 Qx_j Contact force in the x -direction on any shaft or base node j , [kN];
 n Total number of nodes; and
 $Ix_{i,j}$ Flexibility coefficient of node i due to a concentrated force in the x -direction on node j , [m/kN].

Or in matrix form:

$$\{u_s\} = [Ix]\{Qx\} \quad (4)$$

Where:

- $\{u_s\}$ n Soil displacement vector of the single barrette in the x -direction;
 $\{Qx\}$ n Contact force vector of the single barrette in the x -direction; and
 $[Ix]$ $n \times n$ Soil flexibility matrix of the single barrette.

Inverting the soil flexibility matrix in Eq. (4) leads to:

$$\{Qx\} = [Sx]\{u_s\} \quad (5)$$

Where $[Sx]$ are $n \times n$ soil stiffness matrix of the single barrette, $[Sx] = [Ix]^{-1}$.

3.2.2 Soil stiffness matrix

To describe the formulation of composed coefficients for generating the soil stiffness matrix. Consider, as an example, the simple barrette shown in [Figure 3.3a](#), which has a total of $n = 60$ surface nodes in this case.

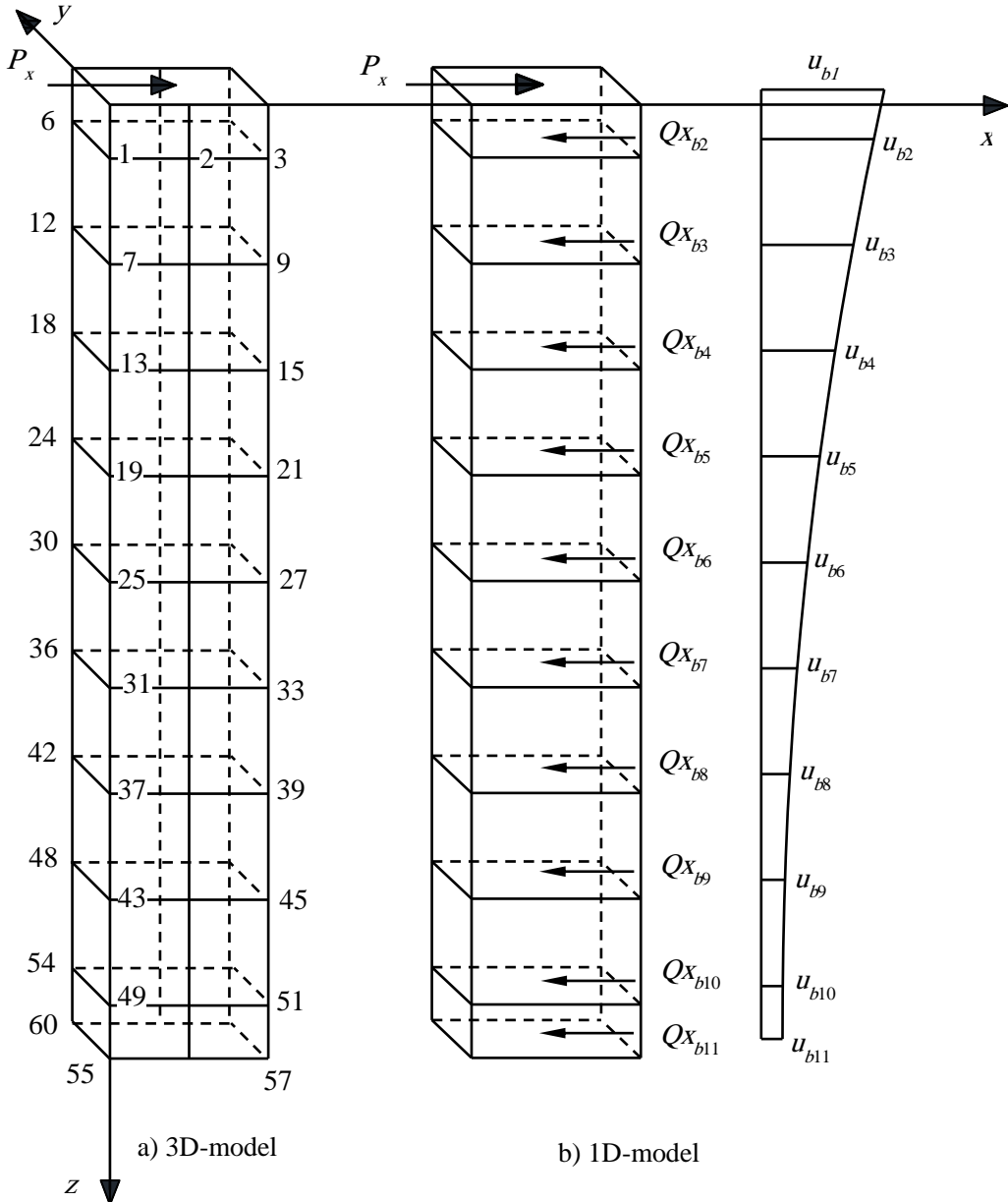


[Figure 3.3](#) The surface mesh of a single barrette.

The barrette of 3D is converted into a 1D model as presented in [Figure 3.3b](#), which has $n_b = 11$ nodes in 11 levels only. Each node has a force and a displacement in the horizontal direction. This problem unknowns are reduced to

be 11 contact forces Qx_{bi} and 11 horizontal displacements u_{bi} on the soil-barrette interface.

Displacements of the soil adjacent to all nodes of the single barrette shown in Figure 3.3a is rewritten in an expanded matrix as:

$$\begin{Bmatrix} u_{s1} \\ \dots \\ u_{s25} \\ \dots \\ u_{s60} \end{Bmatrix} = \begin{bmatrix} Ix_{1,1} & \dots & Ix_{1,25} & \dots & Ix_{1,60} \\ \dots & \dots & \dots & \dots & \dots \\ Ix_{25,1} & \dots & Ix_{25,25} & \dots & Ix_{25,60} \\ \dots & \dots & \dots & \dots & \dots \\ Ix_{60,1} & \dots & Ix_{60,25} & \dots & Ix_{60,60} \end{bmatrix} \begin{Bmatrix} Qx_1 \\ \dots \\ Qx_{25} \\ \dots \\ Qx_{60} \end{Bmatrix} \quad (6)$$

The total soil flexibility matrix in Eq. (6) can be written in a matrix form as Eq. (4). Inverting the soil flexibility matrix in Eq. (6) leads to the total soil stiffness matrix in Eq. (7), which can be written in a matrix form as Eq. (5).

$$\begin{Bmatrix} Qx_1 \\ \dots \\ Qx_{25} \\ \dots \\ Qx_{60} \end{Bmatrix} = \begin{bmatrix} Sx_{1,1} & \dots & Sx_{1,25} & \dots & Sx_{1,60} \\ \dots & \dots & \dots & \dots & \dots \\ Sx_{25,1} & \dots & Sx_{25,25} & \dots & Sx_{25,60} \\ \dots & \dots & \dots & \dots & \dots \\ Sx_{60,1} & \dots & Sx_{60,25} & \dots & Sx_{60,60} \end{bmatrix} \begin{Bmatrix} u_{s1} \\ \dots \\ u_{s25} \\ \dots \\ u_{s60} \end{Bmatrix} \quad (7)$$

Where $Sx_{i,j}$ is the soil stiffness coefficient of the single barrette, [kN/m].

The barrette is represented by a vertical member having a variable horizontal displacement along its height to reduce the number of unknown values in this problem. All nodes in the 3D model, which have the same level, are assumed to have the same displacement. For example, nodes 1 to 6 in Figure 3.3a will have the same displacement u_{b1} . Another point of view in choosing this approach is that the designer is interested in the soil displacement and contact forces at different levels on the barrette height, not at each barrette node. This assumption can establish the relationship between displacement and the contact force on each node in 1D. In Eq. (7), the summation of rows and columns corresponds to the barrette node i in 1D, leads to:

$$\begin{Bmatrix} \left\{ \sum_{i=1}^6 Qx_i \right\}_1 \\ \dots \\ \left\{ \sum_{i=25}^{30} Qx_i \right\}_5 \\ \dots \\ \left\{ \sum_{i=55}^{60} Qx_i \right\}_{11} \end{Bmatrix} = \begin{bmatrix} \sum_{i=1}^6 \sum_{j=1}^6 Sx_{i,j} & \dots & \sum_{i=1}^6 \sum_{j=25}^{30} Sx_{i,j} & \dots & \sum_{i=1}^6 \sum_{j=55}^{60} Sx_{i,j} \\ \dots & \dots & \dots & \dots & \dots \\ \sum_{i=25}^{30} \sum_{j=1}^6 Sx_{i,j} & \dots & \sum_{i=25}^{30} \sum_{j=25}^{30} Sx_{i,j} & \dots & \sum_{i=25}^{30} \sum_{j=55}^{60} Sx_{i,j} \\ \dots & \dots & \dots & \dots & \dots \\ \sum_{i=55}^{60} \sum_{j=1}^6 Sx_{i,j} & \dots & \sum_{i=55}^{60} \sum_{j=25}^{30} Sx_{i,j} & \dots & \sum_{i=55}^{60} \sum_{j=55}^{60} Sx_{i,j} \end{bmatrix} \begin{Bmatrix} \left\{ \sum_{i=1}^6 u_{si} \right\}_1 \\ \dots \\ \left\{ \sum_{i=25}^{30} u_{si} \right\}_5 \\ \dots \\ \left\{ \sum_{i=55}^{60} u_{si} \right\}_{11} \end{Bmatrix} \quad (8)$$

Accordingly, Eq. (7) of the soil stiffness matrix can be rewritten for the barrette of 1D in composed coefficients as:

$$\begin{Bmatrix} Qx_{b2} \\ \dots \\ Qx_{b5} \\ \dots \\ Qx_{b11} \end{Bmatrix} = \begin{bmatrix} Sx_{b2,2} & \dots & Sx_{b2,5} & \dots & Sx_{b2,11} \\ \dots & \dots & \dots & \dots & \dots \\ Sx_{b5,2} & \dots & Sx_{b5,5} & \dots & Sx_{b5,11} \\ \dots & \dots & \dots & \dots & \dots \\ Sx_{b11,2} & \dots & Sx_{b11,5} & \dots & Sx_{b11,11} \end{bmatrix} \begin{Bmatrix} u_{b2} \\ \dots \\ u_{b5} \\ \dots \\ u_{b11} \end{Bmatrix} \quad (9)$$

Where:

$Sx_{bi,j}$ Composed coefficient of level i in 1D single barrette due to a concentrated force in the x -direction at level j , [kN/m];

u_{bi} Soil displacement of level i in 1D single barrette in the x -direction, [m],
 $u_{b2} = u_{s1} = u_{s2} = \dots = u_{s6}, \dots, u_{b11} = u_{s55} = \dots = u_{s60}$; and

Qx_{bi} Contact force of level i in 1D single barrette in the x -direction, [kN],
 $Qx_{b2} = Qx_1 + Qx_2 + \dots + Qx_6, \dots, Qx_{b11} = Qx_{55} + \dots + Qx_{60}$.

The first level of each barrette has no contact with the surrounding soil. So $Qx_{b1} = 0$, $Sx_{b1,i} = 0$, and u_{b1} is the barrette-head displacement in the x -direction, where i is barrette level. Consequently, the composed soil stiffness matrix of the single barrette in Eq. (9) can be expressed in a matrix as:

$$\begin{Bmatrix} 0 \\ Qx_{b2} \\ \dots \\ Qx_{b5} \\ \dots \\ Qx_{b11} \end{Bmatrix} = \begin{bmatrix} 0 & 0 & 0 & 0 & 0 & 0 \\ 0 & Sx_{b2,2} & \dots & Sx_{b2,5} & \dots & Sx_{b2,11} \\ 0 & \dots & \dots & \dots & \dots & \dots \\ 0 & Sx_{b5,2} & \dots & Sx_{b5,5} & \dots & Sx_{b5,11} \\ 0 & \dots & \dots & \dots & \dots & \dots \\ 0 & Sx_{b11,2} & \dots & Sx_{b11,5} & \dots & Sx_{b11,11} \end{bmatrix} \begin{Bmatrix} u_{b1} \\ u_{b2} \\ \dots \\ u_{b5} \\ \dots \\ u_{b11} \end{Bmatrix} \quad (10)$$

Eq. (10) shows that the soil stiffness matrix in Eq. (7) of size 60×60 is reduced considerably to an equivalent soil stiffness matrix of 11×11 . The composed soil stiffness matrix in Eq. (10) is written in a matrix form as:

$$\{Qx_b\} = [Sx_b]\{u_b\} \quad (11)$$

Where:

$\{u_b\}$ n_b Soil displacement vector of the single barrette levels in the x -direction;

$\{Qx\}$ n_b Contact force vector of the single barrette levels in the x -direction; and

$[Sx_b]$ $n_b \times n_b$ Composed soil stiffness matrix of the single barrette.

3.2.3 Barrette stiffness matrix

In this analysis, the elasticity of the barrette is considered. The one-dimensional finite element method is used for analyzing the barrette body, which is exposed to external forces on the soil-barrette interface as soil reactions in addition to the applied load on its head as an action. The compatibility between horizontal displacements of the barrette and the soil displacements at the soil-barrette interface is taken in the horizontal direction.

From the finite element, the beam stiffness matrix of the barrette element e is expressed as (Figure 3.4):

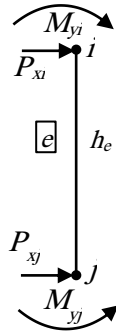


Figure 3.4 The beam element with the applied load.

$$\begin{Bmatrix} P_{x_i} \\ M_{y_i} \\ P_{x_j} \\ M_{y_j} \end{Bmatrix}_e = \frac{E_p I_{pe}}{h_e^3} \begin{bmatrix} 12 & 6h_e & -12 & 6h_e \\ 6h_e & 4h_e^2 & -6h_e & 2h_e^2 \\ -12 & -6h_e & 12 & -6h_e \\ 6h_e & 2h_e^2 & -6h_e & 4h_e^2 \end{bmatrix} \begin{Bmatrix} u_i \\ \theta y_i \\ u_j \\ \theta y_j \end{Bmatrix}_e \quad (12)$$

Where:

E_p Modulus of elasticity of the barrette element e , [kN/m²];

I_{pe} Moment of inertia of the barrette element e , [m⁴];

h_e Height of the barrette element e , [m];

P_{x_i} External force in the x -direction on node i , [kN];

M_{y_i} External moment about the y -axis on node i , [kN.m];

u_i Displacement in the x -direction of node i , [m]; and

θy_i Rotation about the y -axis at node i , [°].

Eq. (12) could be written as:

$$\begin{Bmatrix} Px_i \\ My_i \\ Px_j \\ My_j \end{Bmatrix}_e = \begin{bmatrix} Bu_{i,i} & Bu\theta_{i,i} & Bu_{i,j} & Bu\theta_{i,j} \\ B\theta u_{i,i} & B\theta_{i,i} & B\theta u_{i,j} & B\theta_{i,j} \\ Bu_{j,i} & Bu\theta_{j,i} & Bu_{j,j} & Bu\theta_{j,j} \\ B\theta u_{j,i} & B\theta_{j,i} & B\theta u_{j,j} & B\theta_{j,j} \end{bmatrix} \begin{Bmatrix} u_i \\ \theta y_i \\ u_j \\ \theta y_j \end{Bmatrix}_e \quad (13)$$

Where:

$$Bu_{i,i} = Bu_{j,j} = \frac{12E_p I_{pe}}{h_e^3},$$

$$Bu_{i,j} = Bu_{j,i} = -\frac{12E_p I_{pe}}{h_e^3},$$

$$B\theta u_{i,i} = Bu\theta_{i,i} = B\theta u_{i,i} = B\theta u_{j,i} = \frac{6E_p I_{pe}}{h_e^2},$$

$$B\theta u_{i,j} = Bu\theta_{j,i} = Bu\theta_{j,j} = B\theta u_{j,j} = -\frac{6E_p I_{pe}}{h_e^2},$$

$$B\theta u_{i,i} = Bu\theta_{j,j} = \frac{4E_p I_{pe}}{h_e},$$

$$B\theta_{i,j} = B\theta_{j,i} = \frac{2E_p I_{pe}}{h_e}.$$

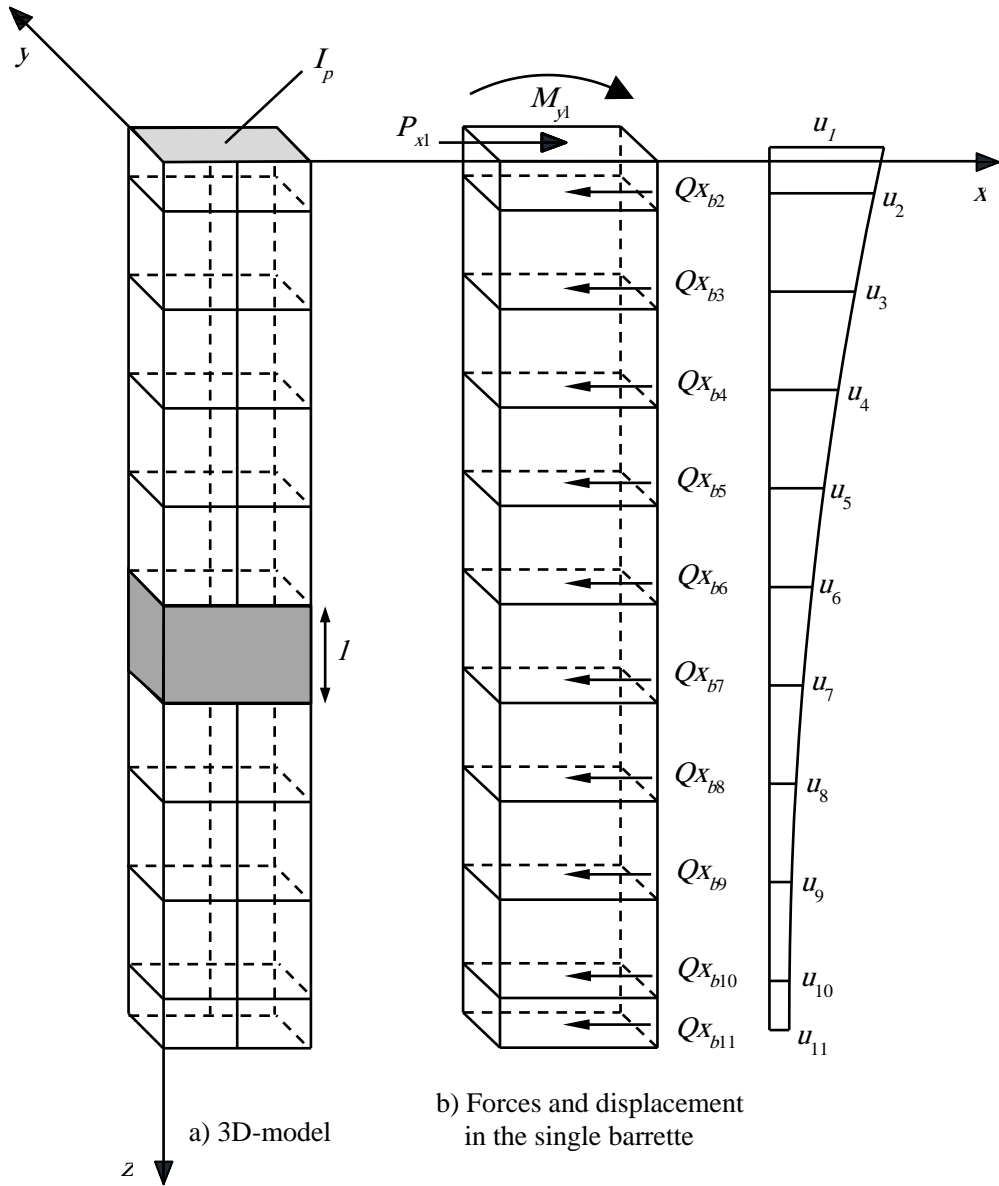


Figure 3.5 The finite element mesh of the barrette and the element geometry.

From Eq. (13), the assembled beam stiffness matrix for the single barrette shown in Figure 3.5 is:

$$\{Px\} = [Bx]\{\delta x\} \tag{14}$$

Where:

$\{Px\}$ $2 \times n_b$ Vector of applied load on the single barrette levels, $\{P_{x1}, M_{x1}, 0, 0, \dots\}$;

$\{\delta x\}$ $2 \times n_b$ Deformation vector of the single barrette levels; $\{u_1, \theta_1, u_2, \theta_2, \dots\}$;
and

$[Bx]$ $(2 \times n_b) \times (2 \times n_b)$ Beam stiffness matrix of the single barrette levels.

Eq. (14) can be expressed in an expanded matrix as:

$$\begin{Bmatrix} Px_i \\ My_i \\ 0 \\ 0 \\ 0 \\ 0 \\ \dots \\ \dots \end{Bmatrix} = \begin{bmatrix} Bu_{1,1} & Bu\theta_{1,1} & Bu_{1,2} & Bu\theta_{1,2} & 0 & 0 & \dots & \dots \\ B\theta u_{1,1} & B\theta_{1,1} & B\theta u_{1,2} & B\theta_{1,2} & 0 & 0 & \dots & \dots \\ Bu_{2,1} & Bu\theta_{2,1} & 2Bu_{2,2} & 2Bu\theta_{2,2} & Bu_{2,3} & Bu\theta_{2,3} & \dots & \dots \\ B\theta u_{2,1} & B\theta_{2,1} & 2B\theta u_{2,2} & 2B\theta_{2,2} & B\theta u_{2,3} & B\theta_{2,3} & \dots & \dots \\ 0 & 0 & Bu_{2,3} & Bu\theta_{2,3} & Bu_{3,3} & Bu\theta_{3,3} & \dots & \dots \\ 0 & 0 & B\theta u_{2,3} & B\theta_{2,3} & B\theta u_{3,3} & B\theta_{3,3} & \dots & \dots \\ \dots & \dots \\ \dots & \dots \end{bmatrix} \begin{Bmatrix} u_1 \\ \theta y_1 \\ u_2 \\ \theta y_2 \\ u_3 \\ \theta y_3 \\ \dots \\ \dots \end{Bmatrix} \quad (15)$$

To consider the compatibility between barrette and soil displacements at the soil-barrette interface, Eq. (14) is expressed as:

$$[Bx]\{\delta x\} = \{Px\} - \{Qx_b\} \quad (16)$$

Substituting Eq. (11) into Eq. (16) leads to:

$$[Bx]\{\delta x\} = \{Px\} - [Sx_b]\{u_b\} \quad (17)$$

The *CCT* is used to formulate the soil stiffness matrix for the barrette as a vertical member. This soil stiffness matrix takes into account the interaction effect among all the soil-barrette interface nodes. By assuming full compatibility between barrette and soil displacements u_{bi} and u_i , the following equation is obtained:

$$[[Bx] + [Sx_b]]\{\delta x\} = \{Px\} \quad (18)$$

The full soil stiffness matrix of the single barrette in Eq. (18) can be expressed in an expanded matrix, Eq. (19).

$$\begin{Bmatrix} Px_i \\ My_i \\ 0 \\ 0 \\ 0 \\ \dots \\ \dots \end{Bmatrix} = \begin{bmatrix} Bu_{1,1} & Bu\theta_{1,1} & Bu_{1,2} & Bu\theta_{1,2} & 0 & 0 & \dots & \dots \\ B\theta u_{1,1} & B\theta_{1,1} & B\theta u_{1,2} & B\theta_{1,2} & 0 & 0 & \dots & \dots \\ Bu_{2,1} & Bu\theta_{2,1} & 2Bu_{2,2} + Sx_{b2,2} & 2Bu\theta_{2,2} & Bu_{2,3} + Sx_{b2,3} & Bu\theta_{2,3} & \dots & \dots \\ B\theta u_{2,1} & B\theta_{2,1} & 2B\theta u_{2,2} & 2B\theta_{2,2} & B\theta u_{2,3} & B\theta_{2,3} & \dots & \dots \\ 0 & 0 & Bu_{2,3} + Sx_{b3,2} & Bu\theta_{2,3} & Bu_{3,3} + Sx_{b3,3} & Bu\theta_{3,3} & \dots & \dots \\ 0 & 0 & B\theta u_{2,3} & B\theta_{2,3} & B\theta u_{3,3} & B\theta_{3,3} & \dots & \dots \\ \dots & \dots \\ \dots & \dots \end{bmatrix} \begin{Bmatrix} u_{b1} \\ \theta y_{b1} \\ u_{b2} \\ \theta y_{b2} \\ u_{b3} \\ \theta y_{b3} \\ \dots \\ \dots \end{Bmatrix} \quad (19)$$

Solving the system of linear equations of Eq. (19) gives displacements and rotations at each node. These are equal to the soil deformations at that node. Substituting soil displacement from Eq. (19) into Eq. (11) gives contact forces $Q_{x_{bi}}$ on the barrette.

3.2.4 Multi-layered soil

Computing soil displacement u_{sij} using *Mindlin* solution is applied by characterizing soil layers around the barrette by the soil modulus of elasticity and *Poisson's* ratio of points j . Where u_{sij} is lateral soil displacement on any shaft or base node i due to a lateral point load at point j .

In case the shaft element crosses two soil layers, the soil properties will take as a ratio of the element height that crosses these layers, as shown in Figure 3.6.

$$E_s = \frac{E_{s1}h_1 + E_{s2}h_2}{h_1 + h_2} \quad (20)$$

$$v_s = \frac{v_{s1}h_1 + v_{s2}h_2}{h_1 + h_2} \quad (21)$$

Where:

E_s Modulus of elasticity of the soil that used in *Mindlin* solution, [kN/m²];

v_s *Poisson's* ratio of the soil that used in *Mindlin* solution, [-];

E_{si} Soil modulus of elasticity of layer i , [kN/m²]; and

v_{si} *Poisson's* ratio of the soil of layer i , [-].

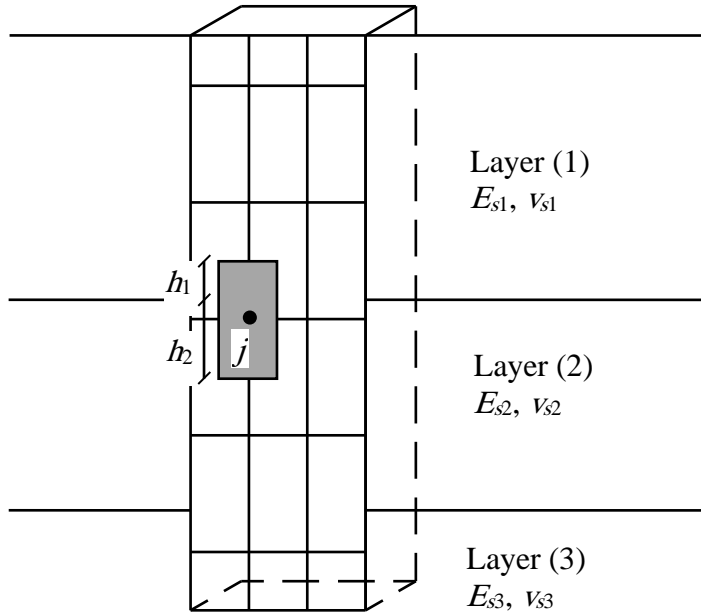


Figure 3.6 The geometry of the shaft element lies between two layers.

3.2.5 Nonlinear analysis of barrette

Russo (1998) [51] presented a numerical method for analyzing piled raft. In this method, piles were modeled as interactive linear or nonlinear springs. This nonlinear method is extended by the author (2016) [18] for analyzing vertically loaded barrette. The nonlinear relation between loads and displacements of the barrette is determined by following this method. A hyperbolic function between the load on the barrette head and the settlement is considered.

The nonlinear behavior of the barrette load-displacement in the horizontal direction is:

$$P_x = \frac{u_n}{\frac{1}{S_x} + \frac{u_n}{H_{lim}}} \quad (22)$$

Where:

u_n Nonlinear displacement in the x -direction of the barrette, [m]; and

H_{lim} Horizontal limit load, [kN].

In Figure 3.7, the initial tangent modulus of the barrette is obtained from the linear analysis. This modulus is equal to the modulus of soil stiffness S_x . The horizontal limit load H_{lim} is a geometrical parameter of the hyperbolic relation.

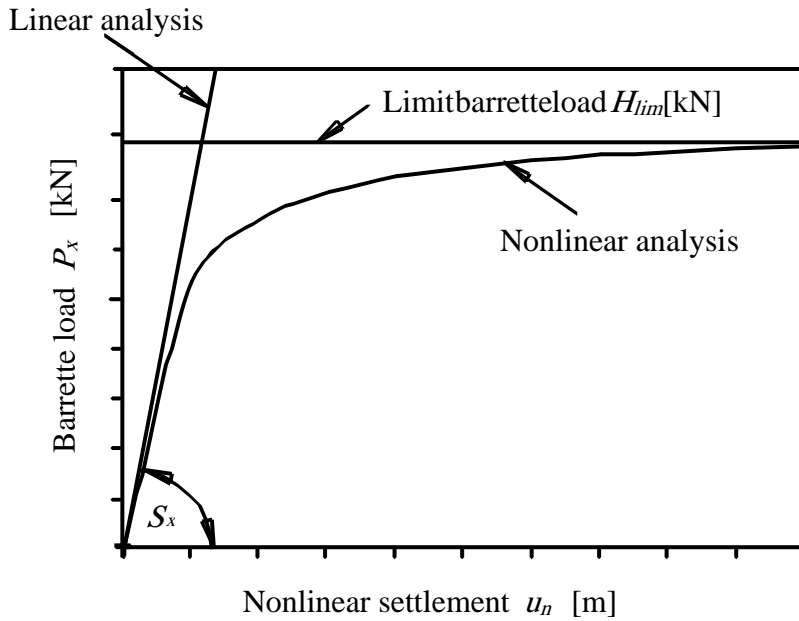


Figure 3.7 The barrette load-displacement curve (hyperbolic relation).

3.3 Modeling Laterally Loaded Barrette Groups

The developed hybrid technique is extended to analyze laterally loaded barrette groups. This technique takes into account the interactions of soil elements with the barrette elements. The soil stiffness matrix is determined considering the group interaction between barrettes in the barrette groups. As for the single barrette, the barrette itself is analyzed using FE. The nonlinear response is considered by a hyperbolic relation between the lateral load and displacement of the barrette.

3.3.1 Soil flexibility matrix

To explain the proposed technique, consider the barrette group in [Figure 3.8](#), which consists of $n_b = 3$ barrettes. Barrettes are divided into shaft and base elements with a total number of nodes $n_g = 166$. Each barrette i in the group system is subjected to a head force in x -directions P_{xgi} .

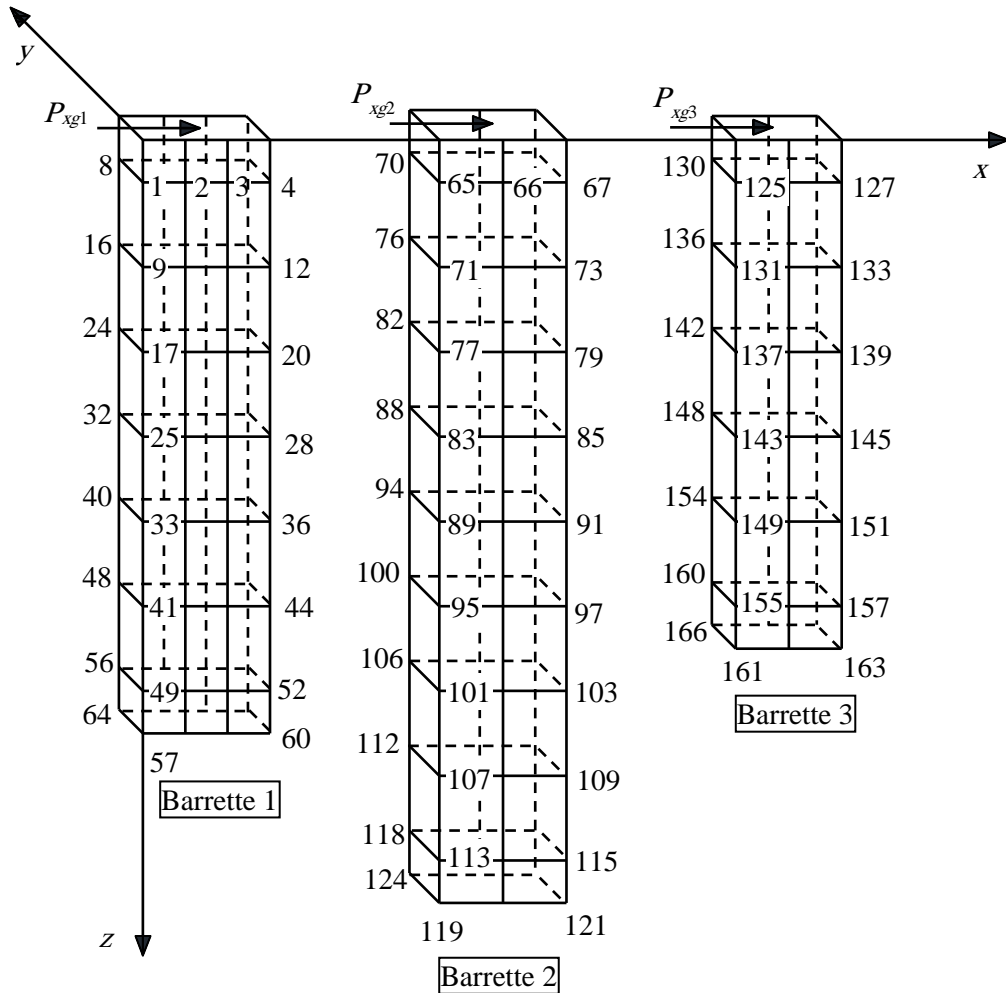


[Figure 3.8](#) The surface mesh of the barrette group.

The total soil flexibility matrix of the barrette group can be expressed in an expanded matrix as:

$$\begin{matrix}
 \left. \begin{matrix} \left\{ \begin{matrix} u_{sg1} \\ \dots \\ u_{sg64} \end{matrix} \right\}_1 \\ \left\{ \begin{matrix} u_{sg65} \\ \dots \\ u_{sg124} \end{matrix} \right\}_2 \\ \left\{ \begin{matrix} u_{sg125} \\ \dots \\ u_{sg166} \end{matrix} \right\}_3
 \end{matrix} \right\} = \\
 \left[\begin{matrix} Ix_{g1,1} & \dots & Ix_{g1,64} & Ix_{g1,65} & \dots & Ix_{g1,124} & Ix_{g1,125} & \dots & Ix_{g1,166} \\ \dots & \dots \\ Ix_{g64,1} & \dots & Ix_{g64,64} & Ix_{g64,65} & \dots & Ix_{g64,124} & Ix_{g64,125} & \dots & Ix_{g64,166} \\ Ix_{g65,1} & \dots & Ix_{g65,64} & Ix_{g65,65} & \dots & Ix_{g65,124} & Ix_{g65,125} & \dots & Ix_{g65,166} \\ \dots & \dots \\ Ix_{g124,1} & \dots & Ix_{g124,64} & Ix_{g124,65} & \dots & Ix_{g124,124} & Ix_{g124,125} & \dots & Ix_{g124,166} \\ Ix_{g125,1} & \dots & Ix_{g125,64} & Ix_{g125,65} & \dots & Ix_{g125,124} & Ix_{g125,125} & \dots & Ix_{g125,166} \\ \dots & \dots \\ Ix_{g166,1} & \dots & Ix_{g166,64} & Ix_{g166,65} & \dots & Ix_{g166,124} & Ix_{g166,125} & \dots & Ix_{g166,166}
 \end{matrix} \right] \left\{ \begin{matrix} \left\{ Qx_{g1} \right\} \\ \dots \\ \left\{ Qx_{g64} \right\}_1 \\ \left\{ Qx_{g65} \right\} \\ \dots \\ \left\{ Qx_{g124} \right\}_2 \\ \left\{ Qx_{g125} \right\} \\ \dots \\ \left\{ Qx_{g166} \right\}_3
 \end{matrix} \right\}
 \end{matrix} \quad (23)$$

Where:

n_g Total number of nodes in barrette group;

u_{sgi} Soil displacement of the barrette group in the x -direction on any shaft or base node i , [m] ;

Qx_{gj} Contact force of the barrette group in the x -direction on any shaft or base node j , [kN]; and

$Ix_{gi,j}$ Flexibility coefficient of the barrette group of node i due to a concentrated force in the x -direction on node j , [m/kN].

The total soil flexibility matrix of the barrette group in Eq. (23) can be written in a matrix form as:

$$\{u_{sg}\} = [Ix_g]\{Qx_g\} \quad (24)$$

Where:

$\{u_{sg}\}$ n_g Soil displacement vector of the barrette group in the x -direction;

$\{Qx_g\}$ n_g Contact force vector of the barrette group in the x -direction; and

$[Ix_g]$ $n_g \times n_g$ Soil flexibility matrix of the barrette group.

Inverting the barrette group flexibility matrix in Eq. (24) leads to:

$$\{Qx_g\} = [Sx_g]\{u_{sg}\} \quad (25)$$

Where $[Sx_g]$ are $n_g \times n_g$ Soil stiffness matrix of the barrette group, $[Sx_g]=[Ix_g]^{-1}$.

3.3.2 Soil stiffness matrix

Consider the simple barrette groups shown in [Figure 3.8](#). All nodes in the 3D model, which have the same level for each barrette, are assumed to have the same displacement. For example, nodes 1 to 8 in barrette number 1 will have approximately the same displacement u_{bg2} . This assumption reduces the size of the soil stiffness matrix. Also, it can establish the relationship between displacements and forces on each barrette level in 1D. It can be done by equating all displacements in each barrette levels in 3D by only an equivalent displacement, as shown in [Figure 3.9](#).

The barrette group of 3D is converted into a 1D model as presented in [Figure 3.9](#), which has a total number of barrette levels $n_{bg} = 28$ with nodes numbers 28 only. Each node has a force and a displacement in the horizontal direction. The unknowns of the problem will be reduced to n_{bg} contact forces Qx_{bgi} and displacements u_{bgi} on the soil-barrette interface for all barrette nodes.

The total soil stiffness matrix of the barrette group in Eq. (25) can be expressed in an expanded matrix as:

$$\left\{ \begin{array}{l} \left(\begin{array}{c} Qx_{g1} \\ \dots \\ Qx_{g64} \end{array} \right)_1 \\ \left(\begin{array}{c} Qx_{g65} \\ \dots \\ Qx_{g124} \end{array} \right)_2 \\ \left(\begin{array}{c} Qx_{g125} \\ \dots \\ Qx_{g166} \end{array} \right)_3 \end{array} \right\} = \left[\begin{array}{cccccccc} Sx_{g1,1} & \dots & Sx_{g1,64} & Sx_{g1,65} & \dots & Sx_{g1,124} & Sx_{g1,125} & \dots & Sx_{g1,166} \\ \dots & \dots \\ Sx_{g64,1} & \dots & Sx_{g64,64} & Sx_{g64,65} & \dots & Sx_{g64,124} & Sx_{g64,125} & \dots & Sx_{g64,166} \\ Sx_{g65,1} & \dots & Sx_{g65,64} & Sx_{g65,65} & \dots & Sx_{g65,124} & Sx_{g65,125} & \dots & Sx_{g65,166} \\ \dots & \dots \\ Sx_{g124,1} & \dots & Sx_{g124,64} & Sx_{g124,65} & \dots & Sx_{g124,124} & Sx_{g124,125} & \dots & Sx_{g124,166} \\ Sx_{g125,1} & \dots & Sx_{g125,64} & Sx_{g125,65} & \dots & Sx_{g125,124} & Sx_{g125,125} & \dots & Sx_{g125,166} \\ \dots & \dots \\ Sx_{g166,1} & \dots & Sx_{g166,64} & Sx_{g166,65} & \dots & Sx_{g166,124} & Sx_{g166,125} & \dots & Sx_{g166,166} \end{array} \right] \left\{ \begin{array}{l} \left(\begin{array}{c} u_{sg1} \\ \dots \\ u_{sg64} \end{array} \right)_1 \\ \left(\begin{array}{c} u_{sg65} \\ \dots \\ u_{sg124} \end{array} \right)_2 \\ \left(\begin{array}{c} u_{sg125} \\ \dots \\ u_{sg166} \end{array} \right)_3 \end{array} \right\} \quad (26)$$

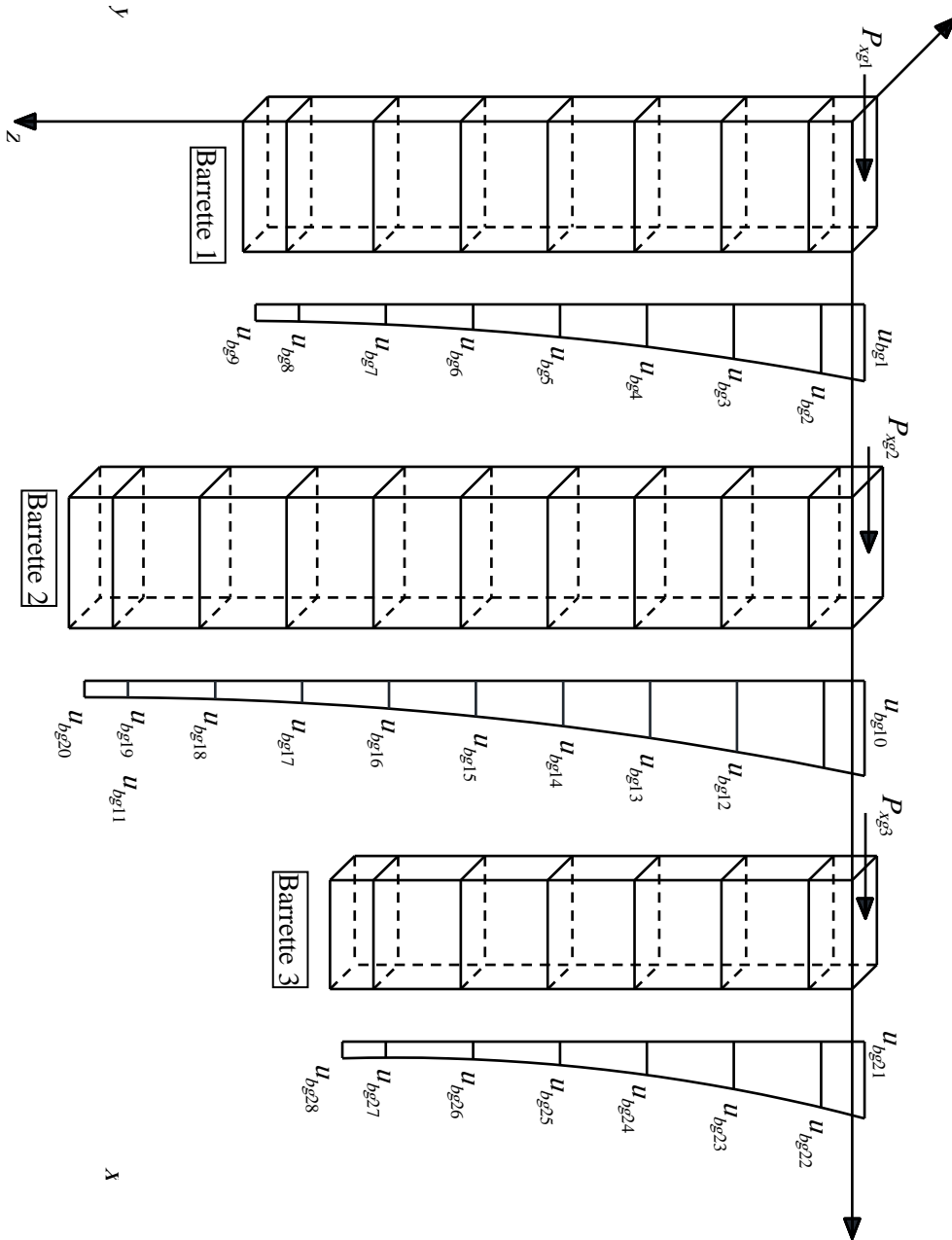


Figure 3.9 The barrette group displacement in one-dimension.

The summation of rows and columns corresponds to the barrette node i in 1D of the barrette group in Eq. (26), leads to:

$$\left. \begin{array}{l} \left\{ \begin{array}{l} \sum_{i=1}^8 Qx_{gi} \\ \dots \\ \sum_{i=57}^{64} Qx_{gi} \end{array} \right\}_1 \\ \left\{ \begin{array}{l} \sum_{i=65}^{70} Qx_{gi} \\ \dots \\ \sum_{i=119}^{124} Qx_{gi} \end{array} \right\}_2 \\ \left\{ \begin{array}{l} \sum_{i=125}^{130} Qx_{gi} \\ \dots \\ \sum_{i=161}^{166} Qx_{gi} \end{array} \right\}_3 \end{array} \right\} = \left[\begin{array}{cccccc} \sum_{i=1}^8 \sum_{j=1}^{64} Sx_{gi,j} & \dots & \sum_{i=1}^8 \sum_{j=57}^{64} Sx_{gi,j} & \dots & \sum_{i=1}^8 \sum_{j=65}^{70} Sx_{gi,j} & \dots \\ \sum_{i=57}^{64} \sum_{j=1}^8 Sx_{gi,j} & \dots & \sum_{i=57}^{64} \sum_{j=57}^{64} Sx_{gi,j} & \dots & \sum_{i=57}^{64} \sum_{j=65}^{70} Sx_{gi,j} & \dots \\ \sum_{i=65}^{70} \sum_{j=1}^8 Sx_{gi,j} & \dots & \sum_{i=65}^{70} \sum_{j=57}^{64} Sx_{gi,j} & \dots & \sum_{i=65}^{70} \sum_{j=65}^{70} Sx_{gi,j} & \dots \\ \sum_{i=119}^{124} \sum_{j=1}^8 Sx_{gi,j} & \dots & \sum_{i=119}^{124} \sum_{j=57}^{64} Sx_{gi,j} & \dots & \sum_{i=119}^{124} \sum_{j=65}^{70} Sx_{gi,j} & \dots \\ \sum_{i=125}^{130} \sum_{j=1}^8 Sx_{gi,j} & \dots & \sum_{i=125}^{130} \sum_{j=57}^{64} Sx_{gi,j} & \dots & \sum_{i=125}^{130} \sum_{j=65}^{70} Sx_{gi,j} & \dots \\ \sum_{i=161}^{166} \sum_{j=1}^8 Sx_{gi,j} & \dots & \sum_{i=161}^{166} \sum_{j=57}^{64} Sx_{gi,j} & \dots & \sum_{i=161}^{166} \sum_{j=65}^{70} Sx_{gi,j} & \dots \end{array} \right] \left\{ \begin{array}{l} \left\{ \begin{array}{l} u_{bg1} \\ \dots \\ u_{bg9} \end{array} \right\}_1 \\ \left\{ \begin{array}{l} u_{bg11} \\ \dots \\ u_{bg20} \end{array} \right\}_2 \\ \left\{ \begin{array}{l} u_{bg22} \\ \dots \\ u_{bg28} \end{array} \right\}_3 \end{array} \right\}$$

(27)

Accordingly, Eq. (26) of the soil stiffness matrix for the barrette of 1D can be rewritten in composed coefficients as:

$$\begin{aligned}
 & \left. \begin{array}{l} \left\{ \begin{array}{l} Qx_{bg2} \\ \dots \\ Qx_{bg9} \end{array} \right\}_1 \\ \left\{ \begin{array}{l} Qx_{bg11} \\ \dots \\ Qx_{bg20} \end{array} \right\}_2 \\ \left\{ \begin{array}{l} Qx_{bg22} \\ \dots \\ Qx_{bg28} \end{array} \right\}_3 \end{array} \right\} = \\
 & \left[\begin{array}{cccccccc} Sx_{bg2,2} & \dots & Sx_{bg2,9} & Sx_{bg2,11} & \dots & Sx_{bg2,20} & Sx_{bg2,22} & \dots & Sx_{bg2,28} \\ \dots & \dots \\ Sx_{bg9,2} & \dots & Sx_{bg9,9} & Sx_{bg9,11} & \dots & Sx_{bg9,20} & Sx_{bg9,22} & \dots & Sx_{bg9,28} \\ Sx_{bg11,2} & \dots & Sx_{bg11,9} & Sx_{bg11,11} & \dots & Sx_{bg11,20} & Sx_{bg11,22} & \dots & Sx_{bg11,28} \\ \dots & \dots \\ Sx_{bg20,2} & \dots & Sx_{bg20,9} & Sx_{bg20,11} & \dots & Sx_{bg20,20} & Sx_{bg20,22} & \dots & Sx_{bg20,28} \\ Sx_{bg22,2} & \dots & Sx_{bg22,9} & Sx_{bg22,11} & \dots & Sx_{bg22,20} & Sx_{bg22,22} & \dots & Sx_{bg22,28} \\ \dots & \dots \\ Sx_{bg28,2} & \dots & Sx_{bg28,9} & Sx_{bg28,11} & \dots & Sx_{bg28,20} & Sx_{bg28,22} & \dots & Sx_{bg28,28} \end{array} \right] \left. \begin{array}{l} \left\{ \begin{array}{l} u_{bg2} \\ \dots \\ u_{bg9} \end{array} \right\}_1 \\ \left\{ \begin{array}{l} u_{bg11} \\ \dots \\ u_{bg20} \end{array} \right\}_2 \\ \left\{ \begin{array}{l} u_{bg22} \\ \dots \\ u_{bg28} \end{array} \right\}_3 \end{array} \right\} \quad (28)
 \end{aligned}$$

Where:

u_{bgi} Soil displacement of the barrette group levels in the x -direction in node i of 1D barrette group, [m]; $u_{bg2} = u_{sg1} = u_{sg2} = \dots = u_{sg8}, \dots, u_{bg20} = u_{sg119} = \dots = u_{sg124}, \dots, u_{bg28} = u_{sg161} = \dots = u_{sg166}$;

Qx_{bgi} Contact force of the barrette group levels in the x -direction on node i of 1D barrette group, [kN]; $Qx_{bg2} = Qx_{g1} + Qx_{g2} + \dots + Qx_{g8}, \dots, Qx_{bg9} = Qx_{g57} + \dots + Qx_{g64}, \dots, Qx_{gb28} = Qx_{g161} + \dots + Qx_{g166}$; and

$Sx_{bg\ i,j}$ Composed coefficient of the barrette group of level i due to a concentrated force in the x -direction at level j , [kN/m].

The first level of each barrette has no contact with the surrounding soil. So $Qx_{bg1} = Qx_{bg10} = Qx_{bg21} = 0$, $Sx_{bg\ 1,i} = Sx_{bg\ 10,i} = Sx_{bg\ 21,i} = 0$, and $u_{bg1}, u_{bg10}, u_{bg21}$ are barrette head displacements in the x -direction, where i is barrette level. Eq. (28) can be written as:

$$\begin{aligned}
& \left\{ \begin{array}{l} 0 \\ Qx_{bg2} \\ \dots \\ Qx_{bg9} \end{array} \right\}_1 \\
& \left\{ \begin{array}{l} 0 \\ Qx_{bg11} \\ \dots \\ Qx_{bg20} \end{array} \right\}_2 \\
& \left\{ \begin{array}{l} 0 \\ Qx_{bg22} \\ \dots \\ Qx_{bg28} \end{array} \right\}_3
\end{aligned} \Bigg\} =
\begin{bmatrix}
0 & 0 & 0 & 0 & 0 & 0 & 0 & 0 & 0 & 0 & 0 \\
0 & Sx_{bg2,2} & \dots & Sx_{bg2,9} & Sx_{bg2,11} & \dots & Sx_{bg2,20} & Sx_{bg2,22} & \dots & Sx_{bg2,28} & \\
0 & \dots & \\
0 & Sx_{bg9,2} & \dots & Sx_{bg9,9} & Sx_{bg9,11} & \dots & Sx_{bg9,20} & Sx_{bg9,22} & \dots & Sx_{bg9,28} & \\
0 & Sx_{bg11,2} & \dots & Sx_{bg11,9} & Sx_{bg11,11} & \dots & Sx_{bg11,20} & Sx_{bg11,22} & \dots & Sx_{bg11,28} & \\
0 & \dots & \\
0 & Sx_{bg20,2} & \dots & Sx_{bg20,9} & Sx_{bg20,11} & \dots & Sx_{bg20,20} & Sx_{bg20,22} & \dots & Sx_{bg20,28} & \\
0 & Sx_{bg22,2} & \dots & Sx_{bg22,9} & Sx_{bg22,11} & \dots & Sx_{bg22,20} & Sx_{bg22,22} & \dots & Sx_{bg22,28} & \\
0 & \dots & \\
0 & Sx_{bg28,2} & \dots & Sx_{bg28,9} & Sx_{bg28,11} & \dots & Sx_{bg28,20} & Sx_{bg28,22} & \dots & Sx_{bg28,28} &
\end{bmatrix}
\begin{bmatrix}
\left\{ \begin{array}{l} u_{bg1} \\ u_{bg2} \\ \dots \\ u_{bg9} \end{array} \right\}_1 \\
\left\{ \begin{array}{l} u_{bg10} \\ u_{bg11} \\ \dots \\ u_{bg20} \end{array} \right\}_2 \\
\left\{ \begin{array}{l} u_{bg21} \\ u_{bg22} \\ \dots \\ u_{bg28} \end{array} \right\}_3
\end{bmatrix}
\tag{29}$$

The composed soil stiffness matrix in Eq. (29) is written in a matrix form as:

$$\{Qx_{bg}\} = [Sx_{bg}]\{u_{bg}\} \tag{30}$$

Where:

$\{u_{bg}\}$ n_{bg} Soil displacement vector of the barrette group levels in the x -direction;

$\{Qx_{bg}\}$ n_{bg} Contact force vector of the barrette group levels in the x -direction;

and

$[Sx_{bg}]$ $n_{bg} \times n_{bg}$ Composed soil stiffness matrix of the barrette group.

Eq. (29) shows that the soil stiffness matrix in Eq. (26) of size 166×166 is reduced considerably to an equivalent soil stiffness matrix of 28×28 .

3.3.3 Barrette stiffness matrix

The one-dimensional finite element method is used for analyzing barrettes, as shown in Figure 3.10. The composed coefficient technique is used to formulate the soil stiffness matrix of barrettes as vertical members, Eq. (30).

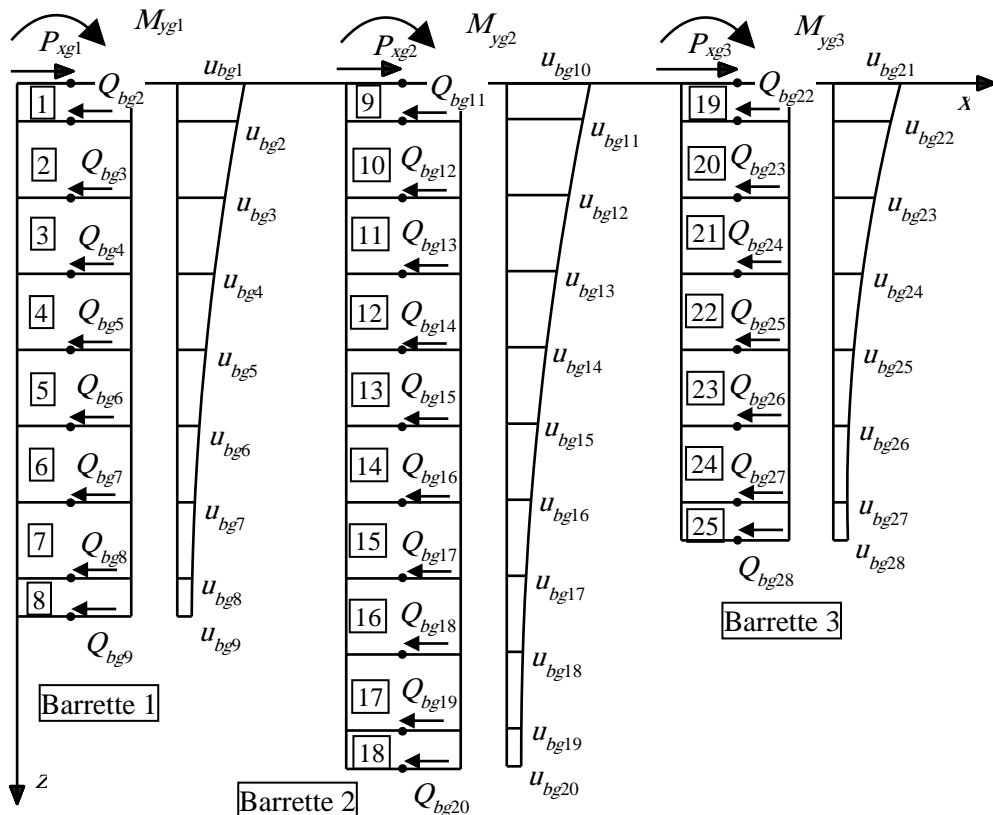


Figure 3.10 Finite element mesh of the barrette group and element geometry.

The barrette stiffness matrix of the barrette group is formulated according to Eq. (12) to be:

$$\begin{Bmatrix} Px_{gi} \\ My_{gi} \\ Px_{gj} \\ My_{gj} \end{Bmatrix}_e = \begin{bmatrix} Bu_{i,i} & Bu\theta_{i,i} & Bu_{i,j} & Bu\theta_{i,j} \\ B\theta u_{i,i} & B\theta_{i,i} & B\theta u_{i,j} & B\theta_{i,j} \\ Bu_{j,i} & Bu\theta_{j,i} & Bu_{j,j} & Bu\theta_{j,j} \\ B\theta u_{j,i} & B\theta_{j,i} & B\theta u_{j,j} & B\theta_{j,j} \end{bmatrix} \begin{Bmatrix} u_{gi} \\ \theta y_{gi} \\ u_{gj} \\ \theta y_{gj} \end{Bmatrix}_e \quad (31)$$

Where:

Px_{gi} Barrette group external force in the x -direction at level i , [kN];

My_{gi} Barrette group external moment about the y -axis at level i , [kN.m];

u_{gi} Barrette group displacement in the x -direction of level i , [m]; and

θy_{gi} Barrette group rotation about the y -axis at level i , [°].

$$\{Px_g\} = [Bx_g]\{\delta x_g\} \quad (32)$$

Where:

$\{Px_g\}$ $2 \times n_b$ Vector of applied load on the barree group levels, $\{Px_{g1}, Mx_{g1}, 0, 0, \dots\}$;

$\{\delta x_g\}$ $2 \times n_b$ Deformation vector of the barrette group levels; $\{u_{g1}, \theta_{g1}, u_{g2}, \theta_{g2}, \dots\}$; and

$[Bx_g]$ $(2 \times n_b) \times (2 \times n_b)$ Beam stiffness matrix of the barrette group levels.

From the finite element method, assuming full compatibility between barrette and soil displacements at the soil-barrette interface, Eq. (32) can be expressed as:

$$[Bx_g]\{\delta x_g\} = \{Px_g\} - \{Qx_b\} \quad (33)$$

Substituting Eq. (30) into Eq. (33) leads to:

$$[Bx_g]\{\delta x_g\} = \{Px_g\} - [Sx_{bg}]\{u_{bg}\} \quad (34)$$

This soil stiffness matrix takes into account the interaction effect among all the soil-barrette interface nodes. Also, it considered the group effect of the single barrette in the group of barrettes. By assuming full compatibility between barrettes and soil displacements u_{bgi} and u_{gi} , the following equation is obtained:

$$\left[[Bx_g] + [Sx_{bg}] \right] \{\delta x_g\} = \{Px_g\} \quad (35)$$

Solving the system of the linear equation (35) gives displacements and rotations of each node. These deformations are equal to those of the soil at that node. Substituting soil displacement from Eq. (35) into Eq. (30) gives contact forces Qx_{bgi} on barrettes.

CHAPTER 4

4 Validation of the program

4.1 Introduction

The developed program is used for analyzing laterally loaded single barrettes/barrette groups embedded in multi-layered soil, linear and nonlinear models. Firstly, barrette displacements and bending moments with barrette heights obtained by the present hybrid-technique are compared with those from an analytical analysis in the available literature to verify the program. Another comparison between dimensionless barrette-head displacements obtained by this hybrid analysis and the analytical solution is also presented. The nonlinear analysis of a laterally loaded single barrette is verified by comparing results from this model with those using an equivalent circular shafted pile to represent the barrette. Also, case studies are performed using the developed technique to compare the results with those from load tests of the laterally loaded single barrette and 3D-FE model. In addition, two different models using 3D-FE are used to compare the results from these models with those from using the presented program. These models are available in the well-known program Plaxis [45]. In this comparison, the results of barrette displacements, shear forces, and bending moments along the barrette height obtained from the different models are compared.

4.2 The Validity of Linear Analysis

4.2.1 Description of the test problem

The barrette displacements with barrette heights obtained by the present analysis using flexibility coefficient and CCT are compared with those obtained by *Basu et al.* (2007, 2008) [6], [7] and *Choi et al.* (2014, 2015) [14], [15], to verify the present analysis of a laterally loaded single barrette in multi-layered soil.

An analytical analysis of a laterally loaded single barrette embedded in a multi-layered soil medium is available in the references *Basu et al.* (2007, 2008) [6], [7] and *Choi et al.* (2014, 2015) [14], [15] and compared with those by equivalent 3D-FE using ABAQUS [1]. In this analysis, the differential equations governing the barrette-soil system displacements were obtained using the principle of minimum potential energy and calculus of variations. Closed-form solutions were produced for barrette displacements and forces along the barrette shaft by using the initial parameters method for a circular pile analysis with an equivalent diameter with the same second moment of inertia as that of the barrette.

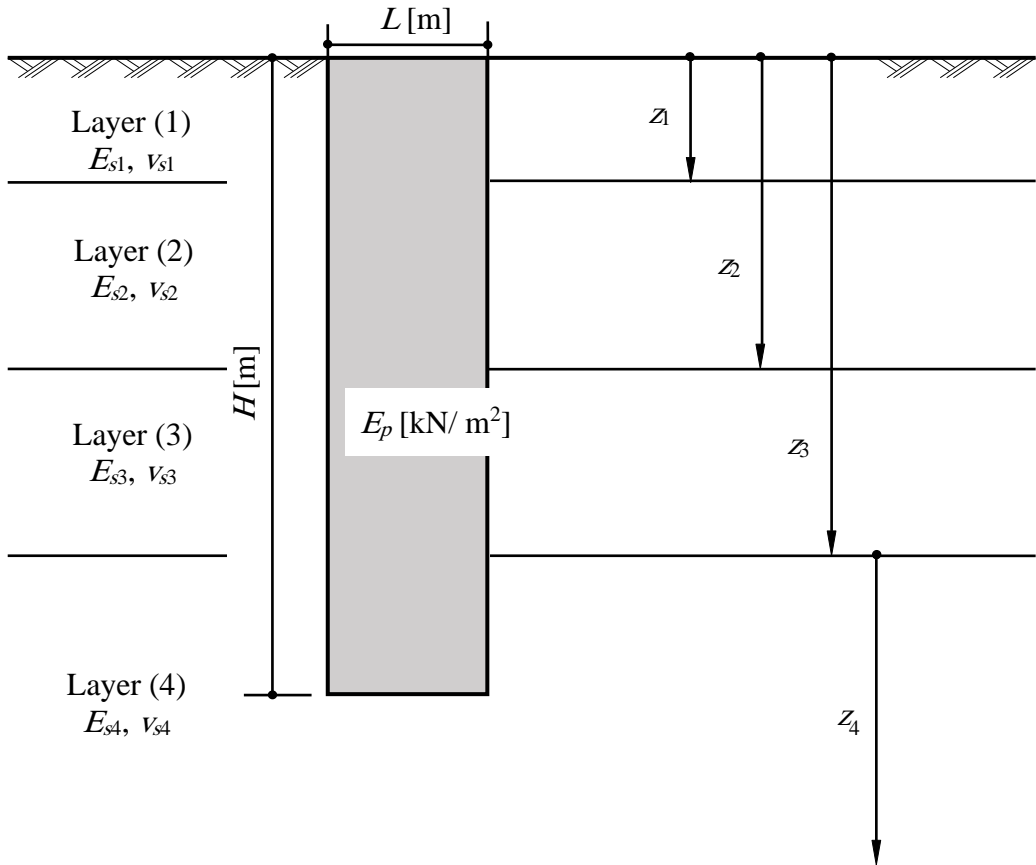


Figure 4.1 The subsoil of single barrettes.

The single barrette shown in Figure 4.1 is analyzed for seven different cases with different geometries, lateral loads, and subsoil conditions. Barrettes geometry, lateral loads on the barrettes head, and modulus of elasticity of barrettes E_p for the chosen cases are listed in Table 4.1. The subsoil of each case consists of different layers. Each layer has a different modulus of elasticity E_s , and *Poisson's* ratio ν_s are listed in Table 4.2 and shown in Figure 4.2.

Table 4.1 Barrette geometries, *Basu et al.* (2007, 2008) [6], [7] and *Choi et al.* (2014, 2015) [14], [15].

Case	Cross-section [m ²]	Height [m]	Modulus of elasticity of the barrette [kN/m ²]	Load [kN]
1	0.5 × 0.5	10	24×10 ⁶	300
2	0.7 × 0.4	15	24×10 ⁶	300
3	2.8 × 0.8	40	25×10 ⁶	3000
4	0.7 × 0.4	10	25×10 ⁶	300
5	0.53 × 0.53	10	25×10 ⁶	300
6	0.7 × 0.4	15	24×10 ⁶	300
7	0.5 × 0.5	15	25×10 ⁶	500

Table 4.2 Soil properties, *Basu et al.* (2007, 2008) [6], [7] and *Choi et al.* (2014, 2015) [14], [15].

Case	Layer No. I	Soil type	Layer depth from the ground surface z [m]	Modulus of elasticity E_s [MN/m ²]	<i>Poisson's</i> ratio ν_s [-]
1, 2, 4, 5	1	Very stiff clay	2	20	0.35
	2	Medium dense sand	5	35	0.25
	3	Dense sand	8	50	0.20
	4	Dense sand	∞	80	0.15
3	1	Very stiff clay	1.5	20	0.35
	2	Loose sand	3.5	25	0.30
	3	Medium dense sand	8.5	40	0.25
	4	Dense sand	∞	80	0.20
6	1	Dense sand	∞	50	0.20
7	1	Medium dense sand	∞	40	0.25

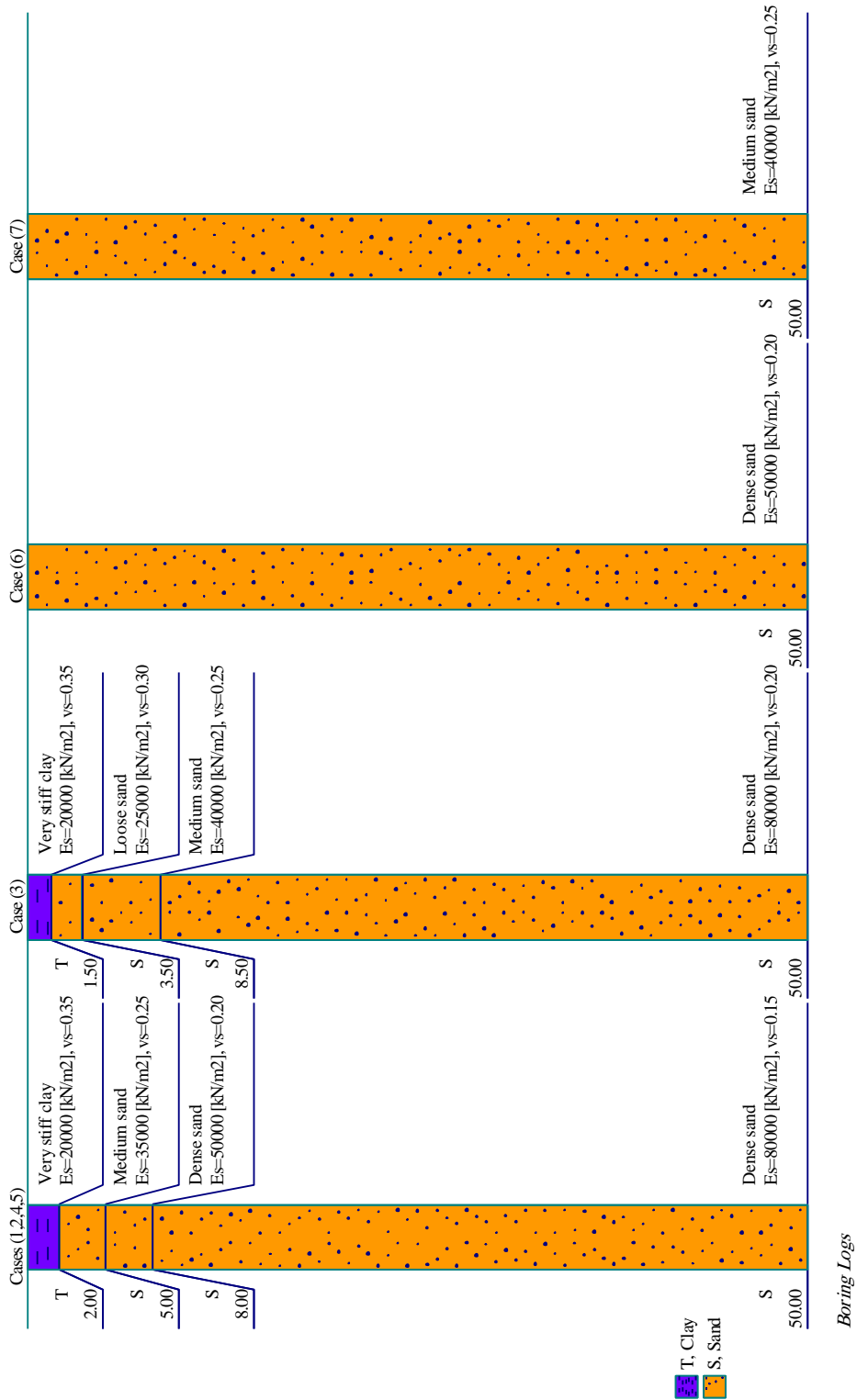


Figure 4.2 Boring logs.

4.2.2 Numerical analysis

A comparison of results of the laterally loaded single barrette in a multi-layered soil medium of the present analysis with those by *Basu et al.* (2007, 2008) [6], [7] and *Choi et al.* (2014, 2015) [14], [15] is presented here. Both the barrette lengths and widths are taken as two elements. Barrettes heights are divided into vertical elements with $h = 0.5$ [m], in all cases, as shown in Figure 4.3. Except for case (3), the barrette length and width are taken as four elements. The Barrette height is divided into vertical elements with $h = 2$ [m], as shown in Figure 4.4. In the analysis, the barrette material is considered to be elastic. The barrette is analyzed as a 1D finite element, as shown in Figure 4.5.

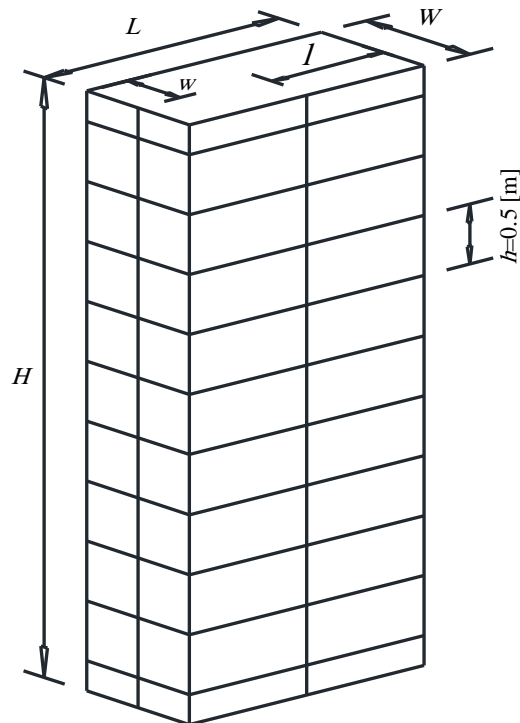


Figure 4.3 The surface element of the barrette for all cases except case (3).

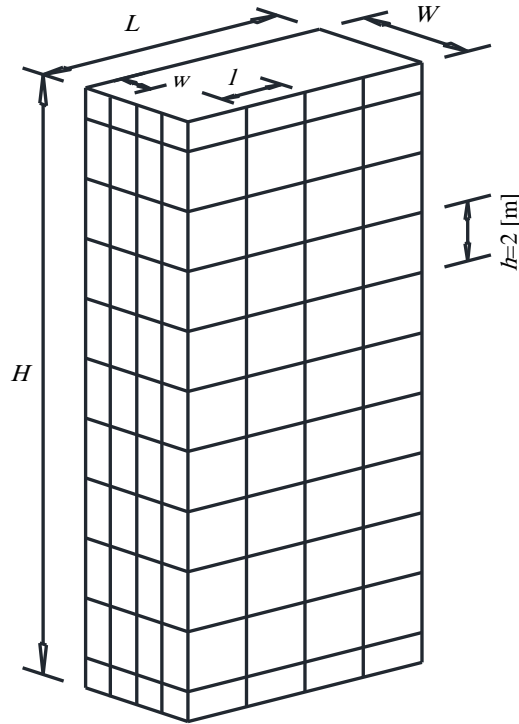


Figure 4.4 The surface element of the barrette for case (3).

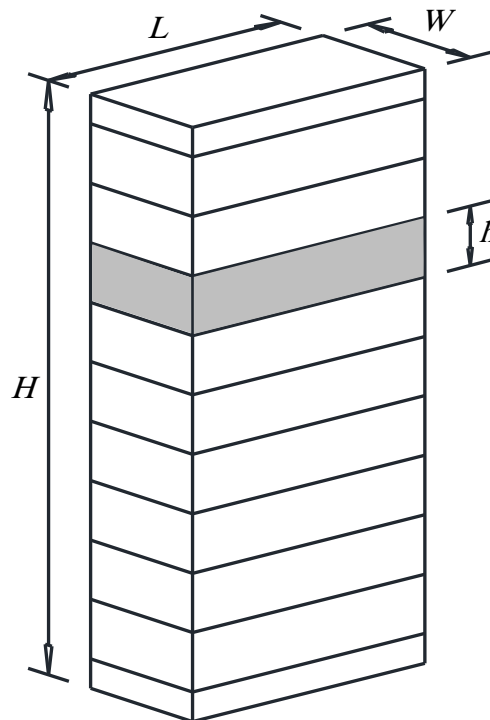


Figure 4.5 Barrette in 1D finite elements.

4.2.3 Results and discussion

The barrette displacement u and bending moment along the barrette height obtained from the present analysis using flexibility coefficient and CCT for the seven cases are compared with those by *Basu et al.* (2007, 2008) [6], [7] and *Choi et al.* (2014, 2015) [14], [15], as shown in Figure 4.6 to Figure 4.16 and listed in Table 4.3.

Results show that the absolute difference between the barrette head displacements in the present analysis and that by *Basu et al.* (2007, 2008) [6], [7] and *Choi et al.* (2014, 2015) [14], [15] is less than 0.05 [cm] for all cases except case (3) which is 0.11 [cm]. This difference when using FEA is less than 0.08 [cm] for cases (1, 2, 6) and 0.2 cm for the third one, as shown in Figure 4.6.

Also, the absolute difference between the computed barrette base displacements in the present analysis and those by *Basu et al.* (2007, 2008) [6], [7] and *Choi et al.* (2014, 2015) [14], [15] is less than 0.04 [cm] for all cases except case (3) which is 0.06 [cm]. This difference when using FEA is less than 0.03 [cm] for cases (1, 2, 6) and 0.07 [cm] for the third one, as shown in Figure 4.7.

Comparing the maximum bending moment using the present analysis and those from *Basu et al.* (2007, 2008) [6], [7] and *Choi et al.* (2014, 2015) [14], [15], the differences is less than 11 %, as listed in Table 4.3.

In general, it can be concluded that the results of the present analyses using flexibility coefficient and CCT are in good agreement with both analytical results and numerical results using full 3D FEA.

Table 4.3 Comparison between Max. Bending moment obtained from *Basu et al.* (2007, 2008) [6], [7] and *Choi et al.* (2014, 2015) [14], [15] with those obtained from the present analysis using flexibility coefficient.

Case	Max. Bending moment [kN.m]		Difference [%]
	<i>Basu et al.</i> (2007, 2008) and <i>Choi et al.</i> (2014, 2015)	Present analysis	
Case (3)	7681.2	7258.1	-5.51%
Case (4)	224.4	201	-10.43%
Case (5)	184.2	164.3	-10.80%
Case (7)	202.6	204.5	0.94%

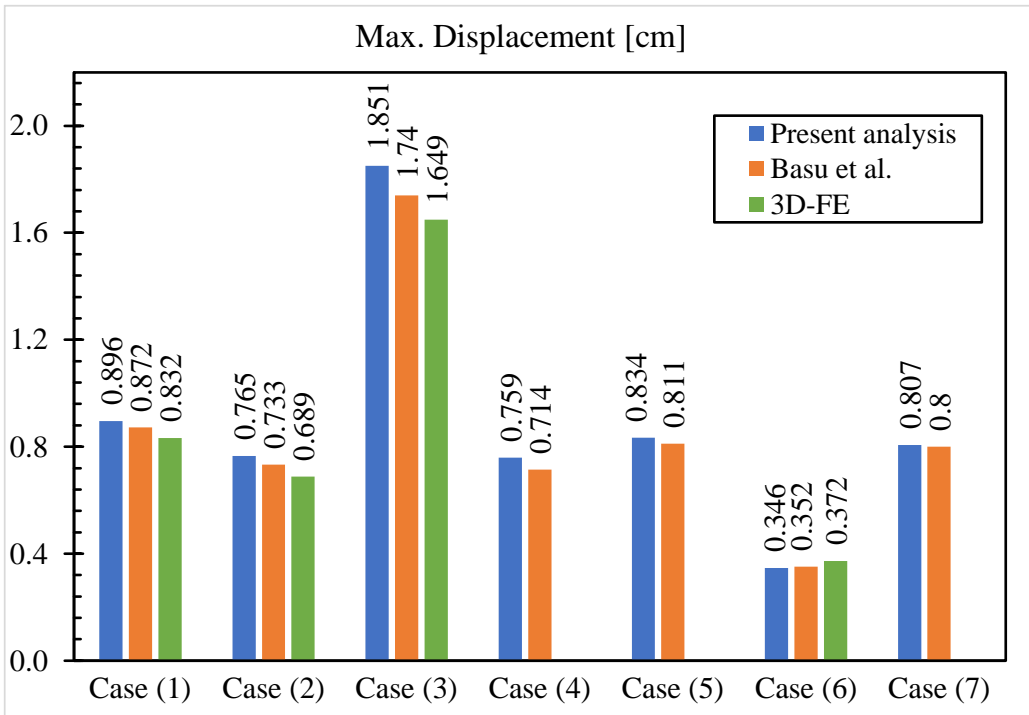


Figure 4.6 Comparison between Max. Displacements.

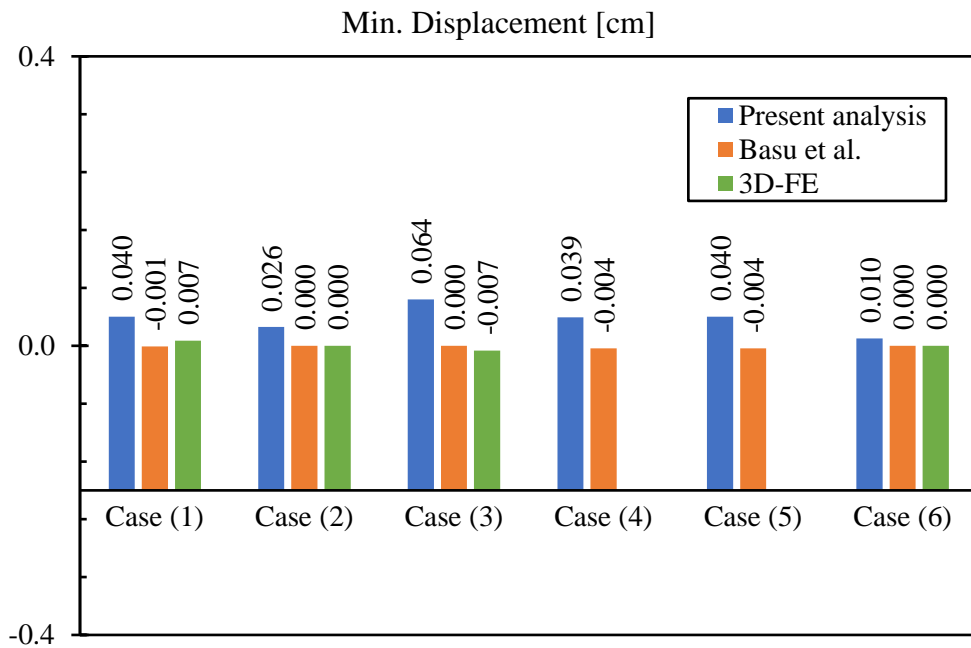


Figure 4.7 Comparison between Min. Displacements.

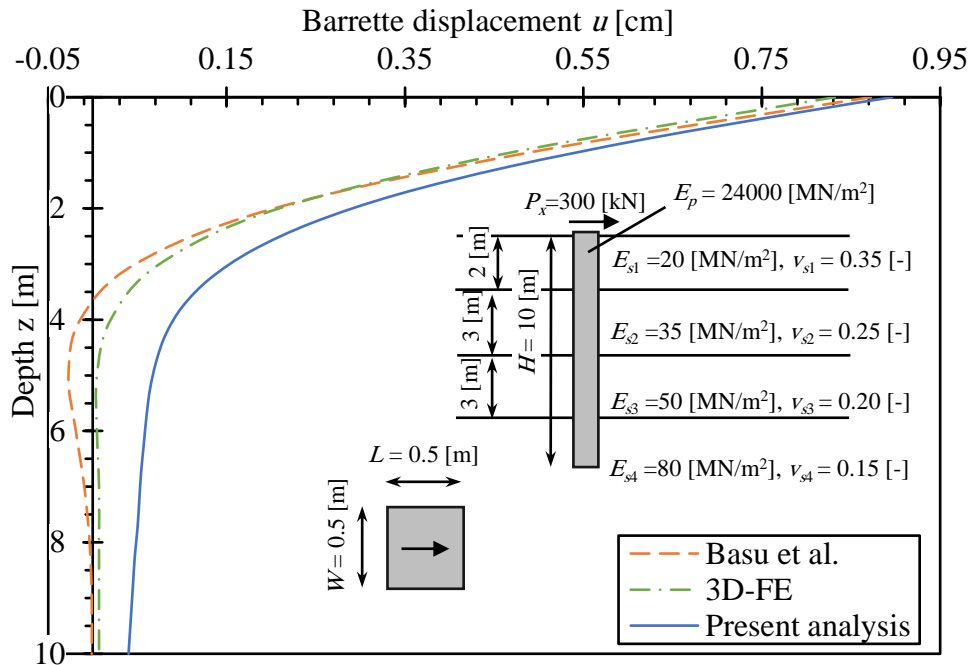


Figure 4.8 Displacement u with the barrette height (case 1).

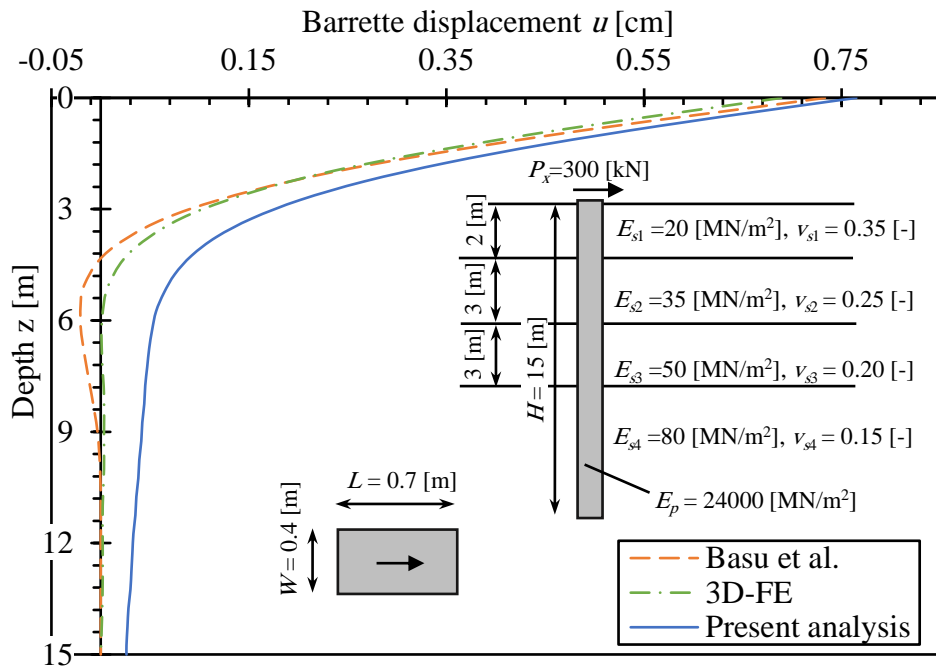


Figure 4.9 Displacement u with the barrette height (case 2).

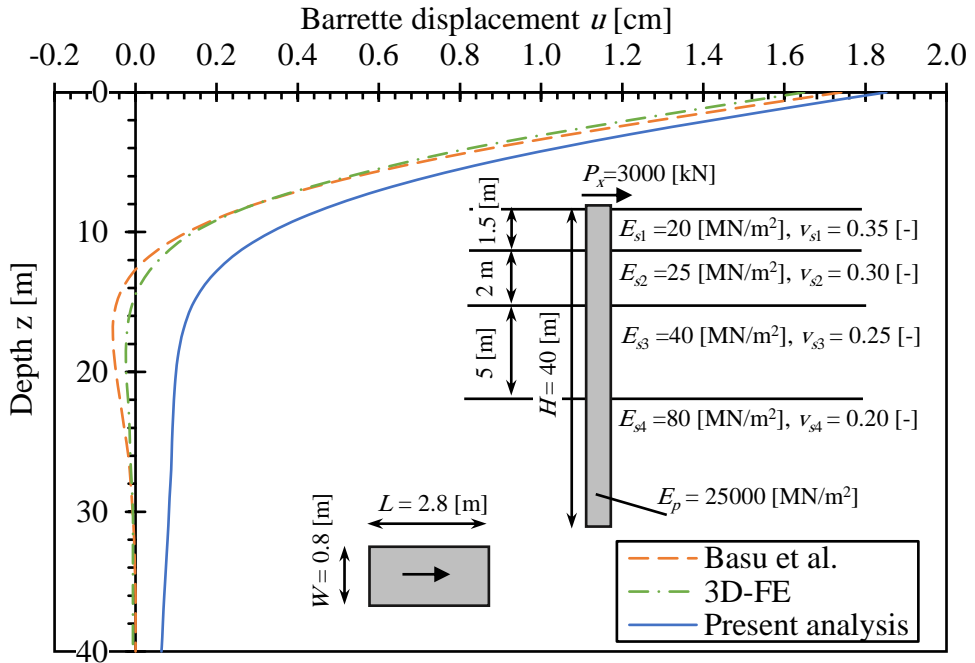


Figure 4.10 Displacement u with the barrette height (case 3).

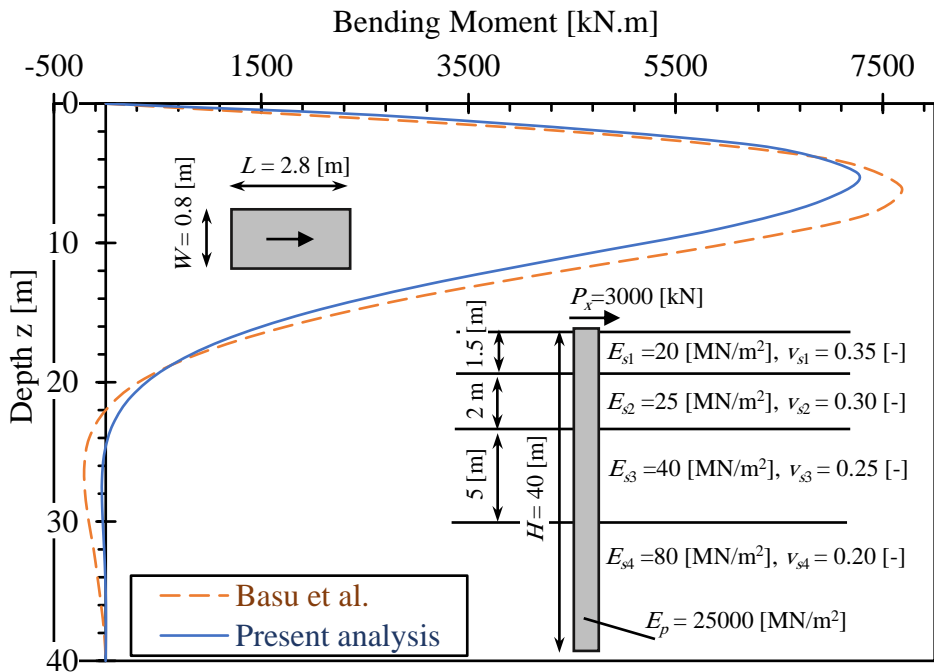


Figure 4.11 Bending moment with the barrette height (case 3).

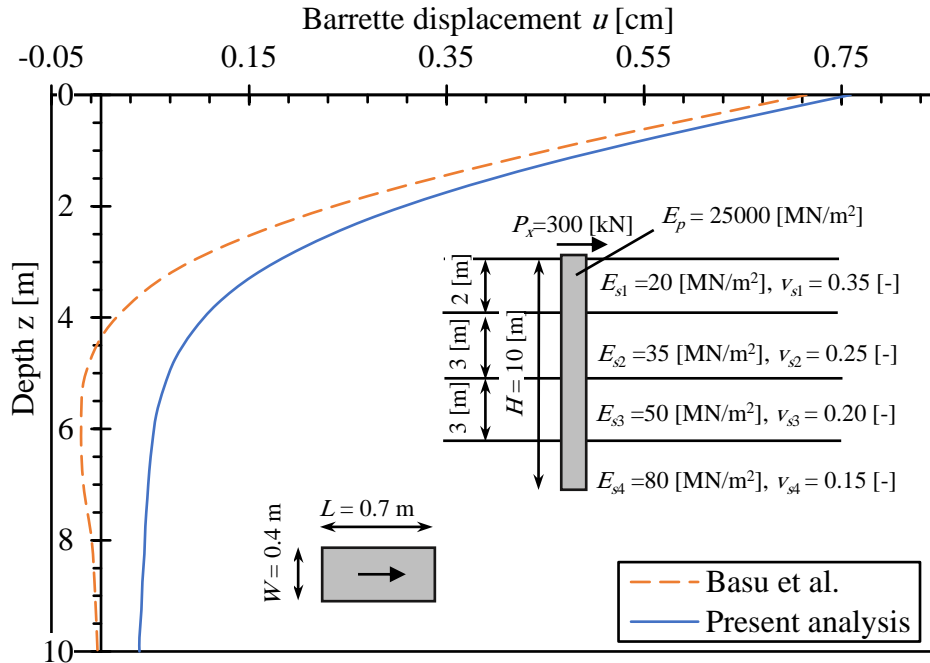


Figure 4.12 Displacement u with the barrette height (case 4).

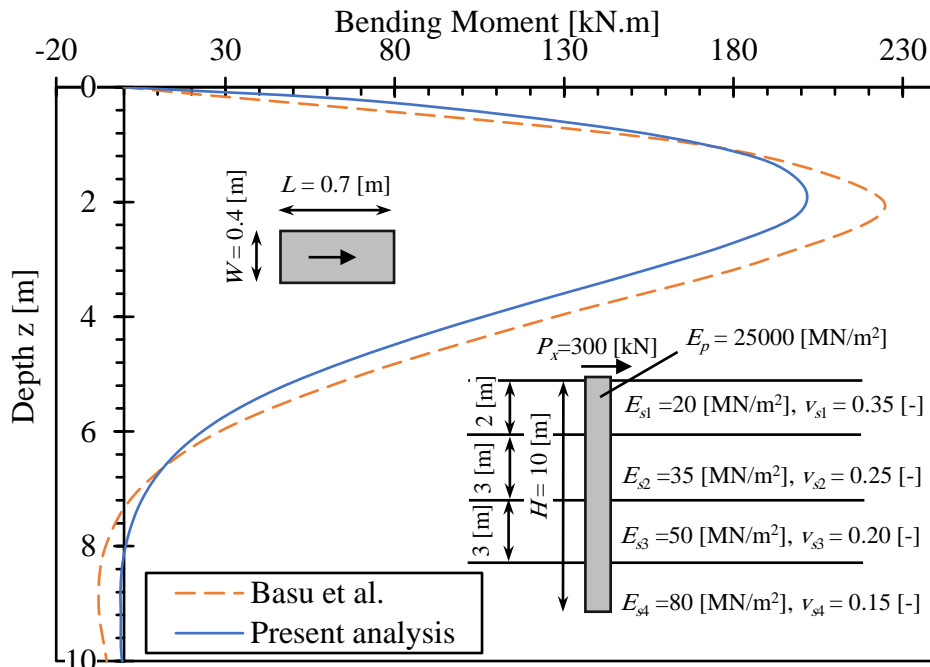


Figure 4.13 Bending moment with the barrette height (case 4).

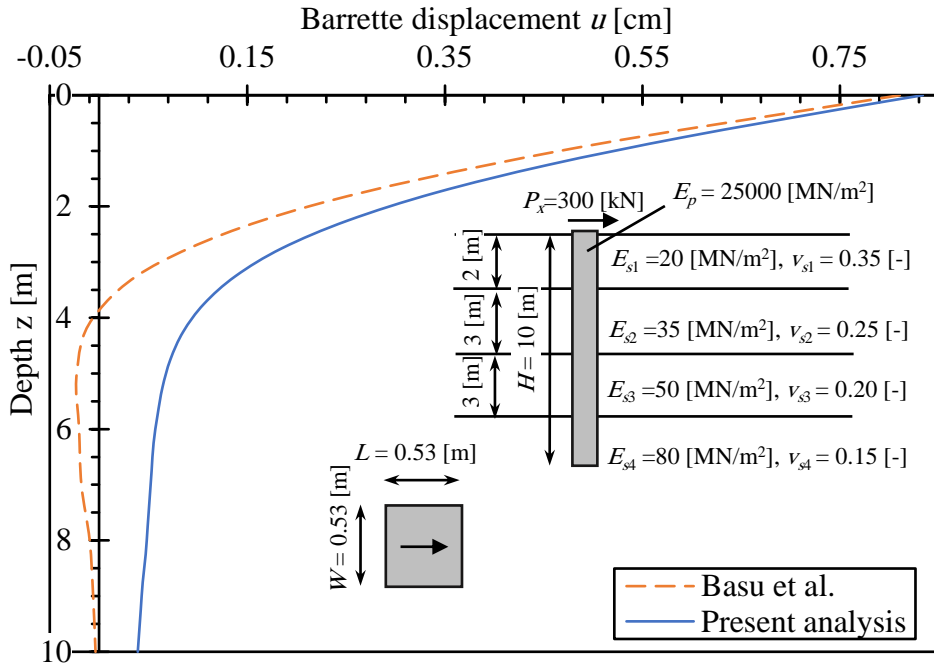


Figure 4.14 Displacement u with the barrette height (case 5).

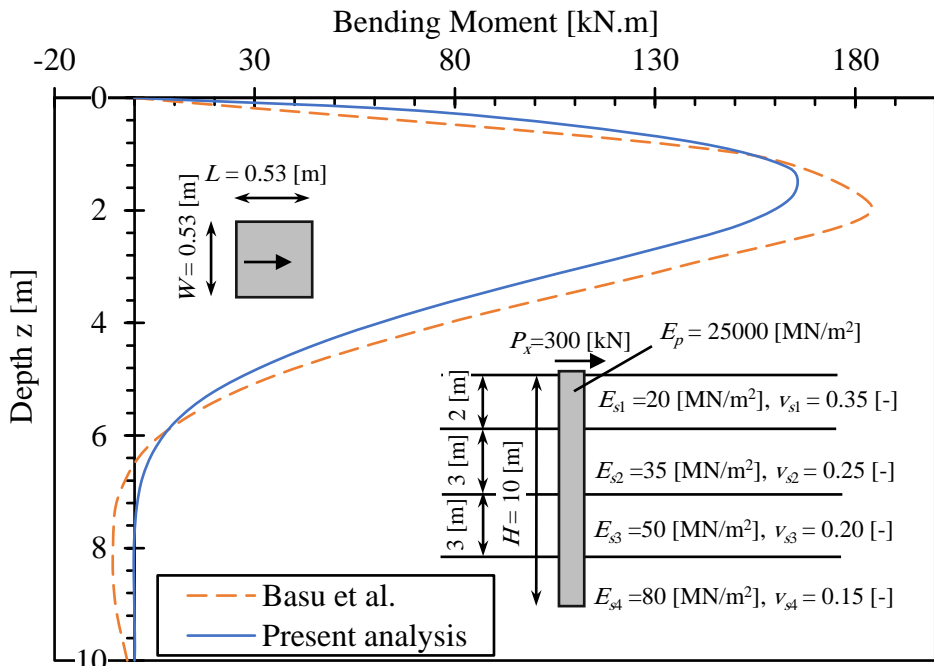


Figure 4.15 Bending moment with the barrette height (case 5).

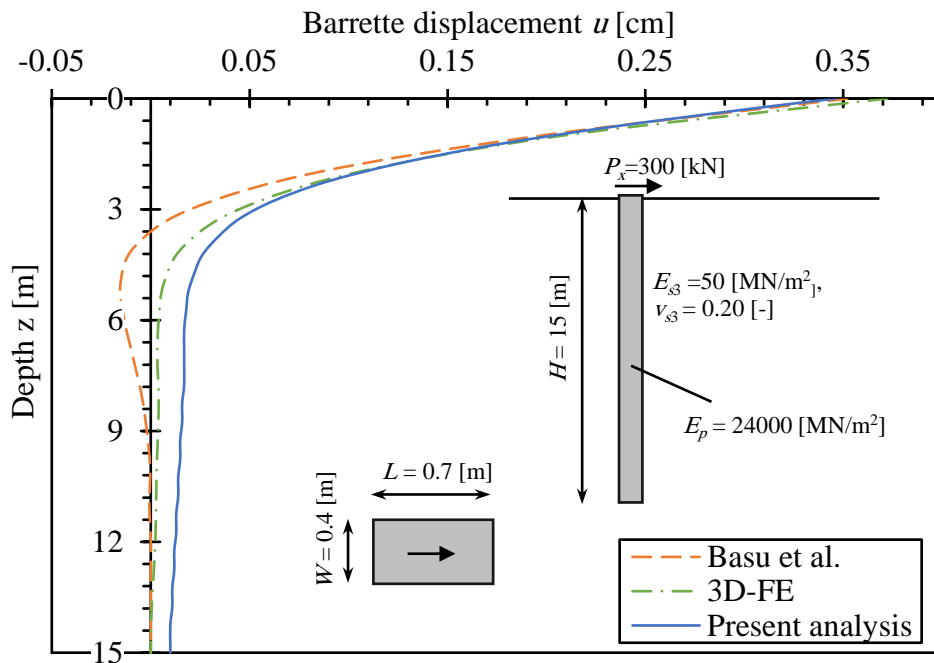


Figure 4.16 Displacement u with the barrette height (case 6).

4.3 The Validity of Dimensionless Barrette Displacements

4.3.1 Description of the test problem

Dimensionless barrette-head displacements obtained by the present analysis are compared with those of *Choi et al. (2014) [14]* to verify the hybrid technique. These dimensionless results are used to investigate the relative stiffness of barrette and soil and the barrette slenderness ratio on square barrettes.

4.3.2 Numerical analysis

Figure 4.17 shows a comparison between results of square barrettes embedded in two-layers soil under lateral force P_x obtained from the present model and *Choi et al. (2014) [14]*. Different values of the modified soil shear modulus ratio $G_{s1}^*/G_{s2}^* = 0.2, 0.5, 2, \text{ and } 5$ with $H/B^* = 50, L/W = 1, \nu_s = 0.3$ and $Ep/G_{s2}^* = 1000$ were considered. Where: B^* is the equivalent pile diameter that produces the same second moment of inertia as that of a circular pile ($B^* = [16WL/3\pi]^{1/4}$), and G^* is the modified shear modulus of the soil ($G_s^* = 0.7G_s(1 + 0.75\nu_s)$) for barrettes, *Choi et al. (2014) [14]*. The thickness h_s of the topsoil layer is varied from zero to H . The ratio $u_{2\text{-layer}}/u_{\text{homog.}}$ of the barrette-head displacement in two-layer and homogenous soil profiles as a function of h_s/H for square barrettes are shown. The barrette-head displacement in homogenous soil $u_{\text{homog.}}$ is computed using G_{s2}^* for the entire soil medium.

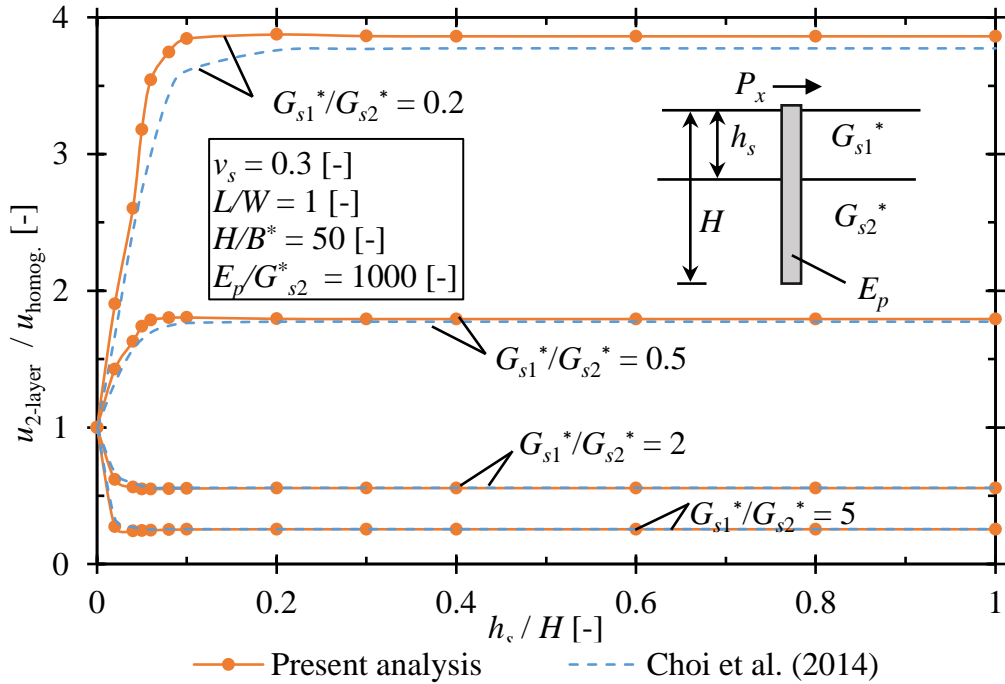


Figure 4.17 The ratio $u_{2\text{-layer}}/u_{\text{homog.}}$ in two-layer soil and versus h_s/H .

A laterally loaded square barrette embedded in a two-layer soil medium was analyzed and compared with *Choi et al. (2014)* [14]. Figure 4.18 shows the relation between the normalized barrette-head displacement u_n and the barrette-soil modulus ratio $E_p/G_s^*_{\text{avg.}}$. The average of the modified soil shear modulus of the soil layers ($G_s^*_{\text{avg.}} = (G_{s1}^* + G_{s2}^*)/2$ or $(G_{s1}^* + G_{s2}^* + G_{s3}^*)/3$) is used to calculate the dimensionless barrette-head displacement u_n . The normalized barrette-head displacement caused by the applied lateral force P_x was defined as $u_n = u|_{z=0} B^* G_s^*_{\text{avg.}} / P_x$, *Choi et al. (2014)* [14], where $u|_{z=0}$ is the barrette-head deflection at the ground surface. Different values of the modified soil shear modulus ratio $G_{s1}^* / G_{s2}^* = 0.2, 0.5, 2, \text{ and } 5$ with $H/B^* = 50$, $L/W = 1$, and $\nu_s = 0.3$ were considered. Also, the topsoil layer thickness h_s is considered to be $h_s = 0.1 H$ (Soil profile (A)) and $0.5 H$ (Soil profile (B)).

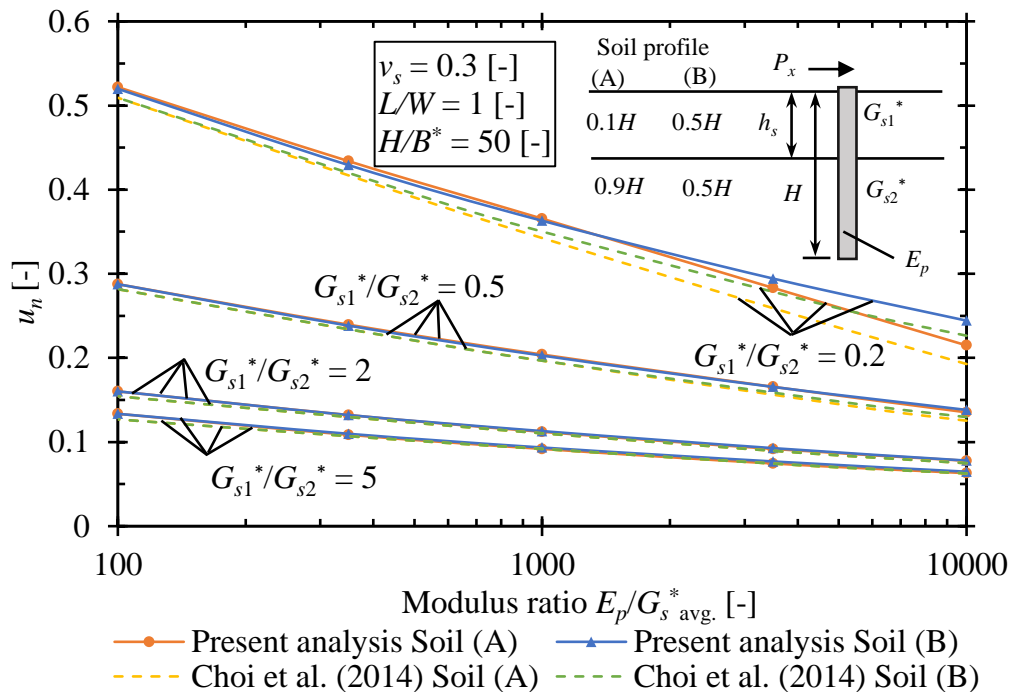


Figure 4.18 The normalized u_n in two-layer soil and versus ratio $E_p/G_s^*_{avg.}$.

Three different cases of three-layer soil medium are considered for analyzing laterally loaded square barrette, as shown in Figure 4.19 and Figure 4.20. For the first case (Case I), the modified soil shear modulus increases with depth, whereas for the third case (Case III), it decreases with depth. For the second case (Case II). The intermediate layer has the smallest modified soil shear modulus. In addition, the top two layers thickness h_s is considered to be $h_{s1} = h_{s2} = 0.1 H$ (Soil profile (A)) and $h_{s1} = h_{s2} = H/3$ (Soil profile (B)). The normalized barrette-head displacement u_n is plotted against the barrette-soil modulus ratio $E_p/G_s^*_{avg.}$ for Cases I-III with $H/B^* = 50$, $L/W = 1$, and $\nu_s = 0.3$, as shown in Figure 4.19. Figure 4.20 shows the normalized barrette-head displacement u_n against the barrette slenderness ratio H/B^* for Cases I-III with $E_p/G_s^*_{avg.} = 1000$, $L/W = 1$, and $\nu_s = 0.3$.

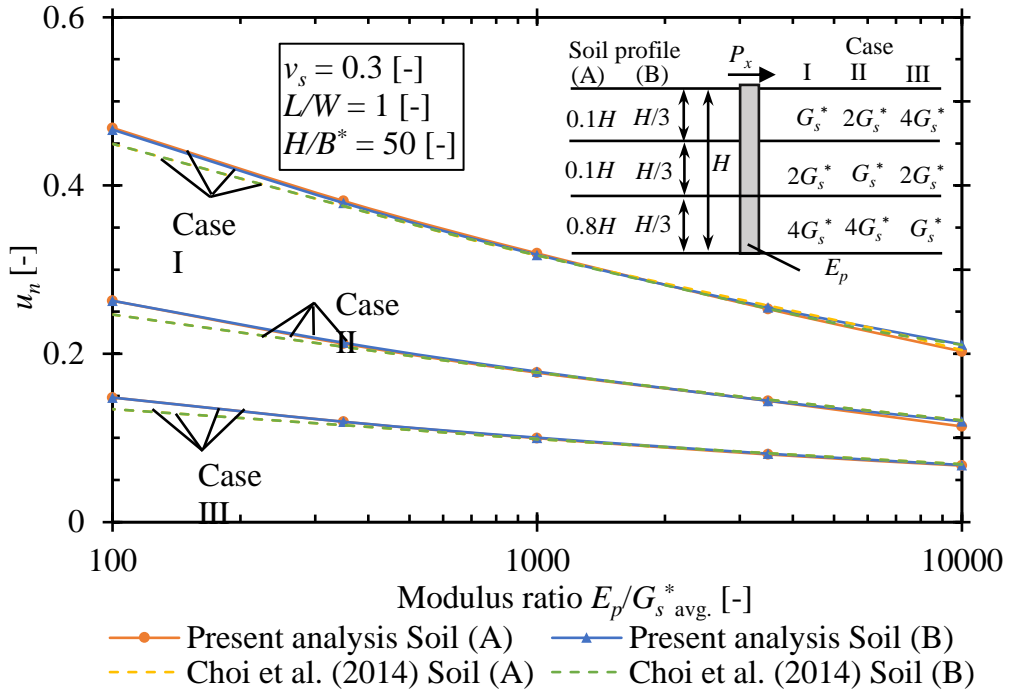


Figure 4.19 The normalized u_n in three-layer soil and versus ratio $E_p/G_s^*_{avg.}$.

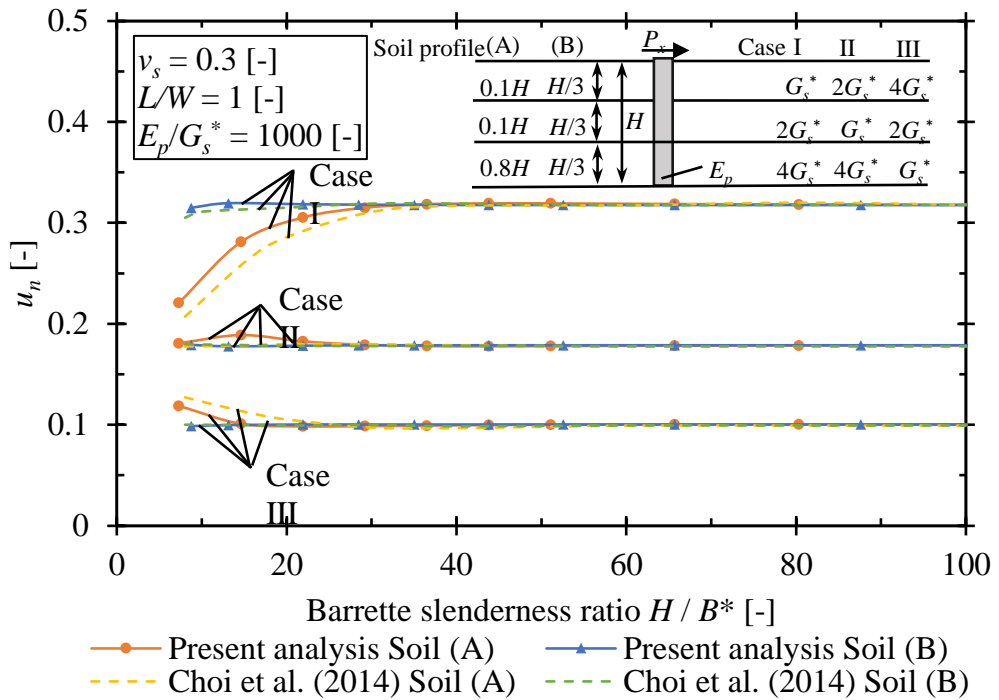


Figure 4.20 The normalized u_n against the ratio H/B^* .

4.3.3 Results and discussion

It can be noticed from [Figure 4.17](#) to [Figure 4.20](#) that a good agreement between the results of the present analysis and those of *Choi et al. (2014)* [14] in all cases.

The thickness of the top layer of the soil is the controlling factor for barrette-head displacement. The horizontal displacement of the barrette is not influenced by the properties of the underlying layers in the case where the topsoil layer thickness exceeds approximately 30% of the barrette height. In the case of a soft layer over a stiff layer (e.g., $G_{s1}^*/G_{s2}^* = 0.2$ or 0.5), $u_{2\text{-layer}}/u_{\text{homog.}}$ increases with an increase in h_s/H . The dimensionless barrette-head displacement decreases as $E_p/G_{s\text{ avg.}}^*$ increases. For long barrettes with barrettes width ratio H/W more than 30 has a very small effect because the barrettes height is reached to the effective-height.

4.4 The Validity of Nonlinear Analysis

4.4.1 Description of the test problem

The barrette results obtained by the present nonlinear-analysis are compared with those obtained by *Poulos et al. (2019)* [48] using 3D FE and using an equivalent circular shafted pile to represent the barrette to verify the present nonlinear analysis of a laterally loaded single barrette.

The single barrette shown in [Figure 4.21](#) is analyzed nonlinearly with different lateral loads values in both the x and the y -directions. Barrette geometry and modulus of elasticity of barrette E_p for the chosen case are listed in [Table 4.4](#). The subsoil of this case consists of two different layers. Each layer has a different modulus of elasticity E_s , and *Poisson's* ratio ν_s are listed in [Table 4.5](#).

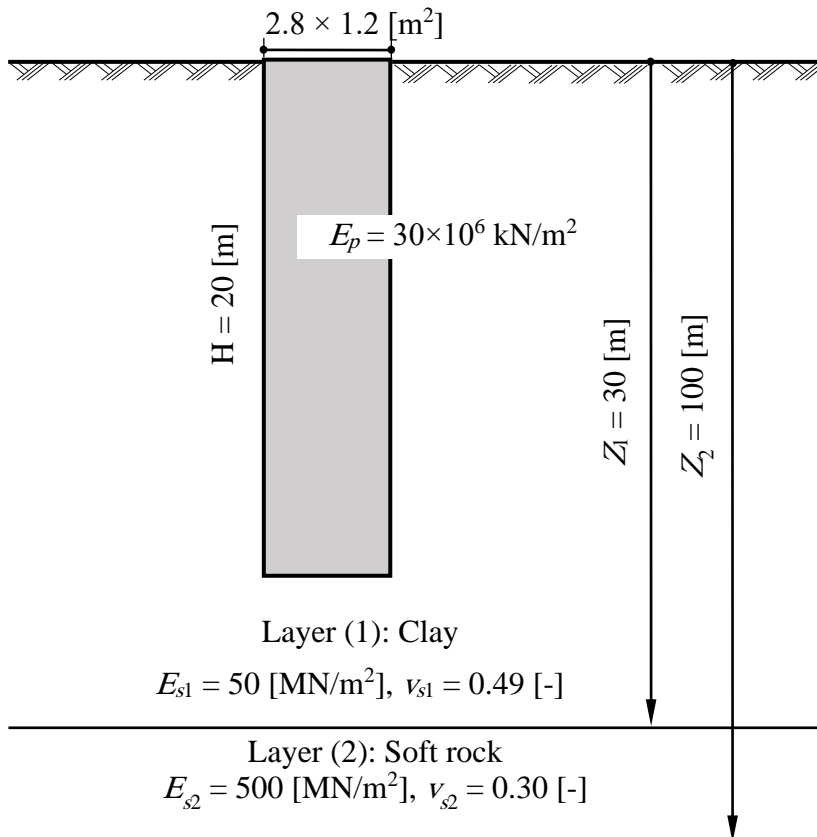


Figure 4.21 Single barrette with subsoil.

Table 4.4 Barrette geometries, *Poulos et al. (2019) [48]*.

Case	Cross-section [m ²]	Height [m]	Modulus of elasticity of the barrette [kN/m ²]
1	1.20 × 2.8	20 m	30 × 10 ⁶

Table 4.5 Subsoil properties, *Poulos et al. (2019) [48]*.

Layer No.	Soil type	Layer depth from the ground surface z [m]	Modulus of elasticity E_s [MN/m ²]	Poisson's ratio v_s [-]
1	Clay	30	50	0.49
2	Soft rock	100	500	0.3

4.4.2 Numerical analysis

A comparison between results obtained from the present analysis and those by *Poulos et al.* (2019) [48] is presented herein. The height of the barrette is divided into equal-elements. Each element has a height of $h = 1.0$ [m]. Both the barrette length and width are taken as two elements, as shown in [Figure 4.22](#). In the analysis, the barrette is analyzed nonlinearly, using a hyperbolic function, to represent the real load-displacement relation. A horizontal limit load H_{lim} [kN] has been used for the nonlinear load-displacement curve. It is usually taken as a ratio of the ultimate load as *Poulos et al.* (2019) [48]. Eq. (36) is used to determine the ultimate lateral load of piles in clay, according to the *ECP 202* [56].

$$H_{ult} = 9 c_u (z - 1.5 D) D \quad (36)$$

Where:

D The diameter of the pile with the same moment of inertia, [m];

z Depth from the ground surface, [m];

c_u Undrained cohesion of clay, [kN/m²]; and

H_{ult} Ultimate lateral load, [kN].

To use this equation D is taken as the diameter of the pile with the same moment of inertia, which will be 2.59 [m] for loads in the x -direction and 1.69 [m] for loads in the y -direction. So, H_{ult} will be 18782 [kN] for loads in the x -direction and 13282 [m] for loads in the y -direction where c_u is 50 [kN/m²]. Limit lateral loads were $H_{lim} = 0.772 H_{ult} = 14.5$ [MN] for loads in the x -direction and $H_{lim} = 0.753 H_{ult} = 10$ [MN] for loads in the y -direction.

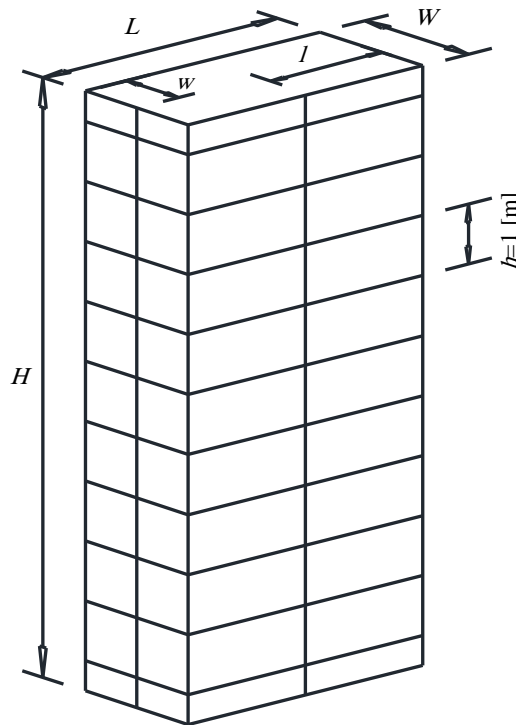


Figure 4.22 The surface element of the barrette.

4.4.3 Results and discussion

The lateral load-displacement curves of the barrette 20 m height in both the x and the y -directions obtained from the present analysis are compared in Figure 4.23 and Figure 4.24 with those obtained by Poulos *et al.* (2019) [48]. The results are in a good agreement.

The load-displacement curve depends on the direction of loading. As reported before by Zhang (2003) [63], El Wakil *et al.* (2013) [23], and Poulos *et al.* (2019) [48], when the loading is toward the largest side of the barrette, it is predicted to carry more load and has a stiffer response than when loaded along the minor axis due to the high resistance of the barrette loaded along the minor axis.

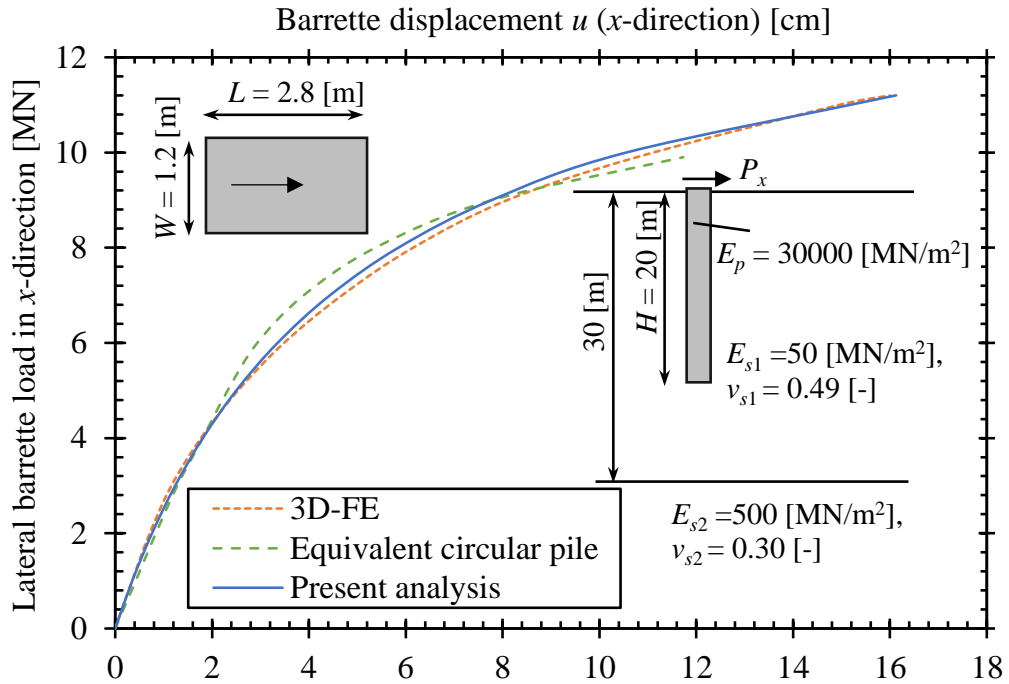


Figure 4.23 Load-displacement curve (x-direction).

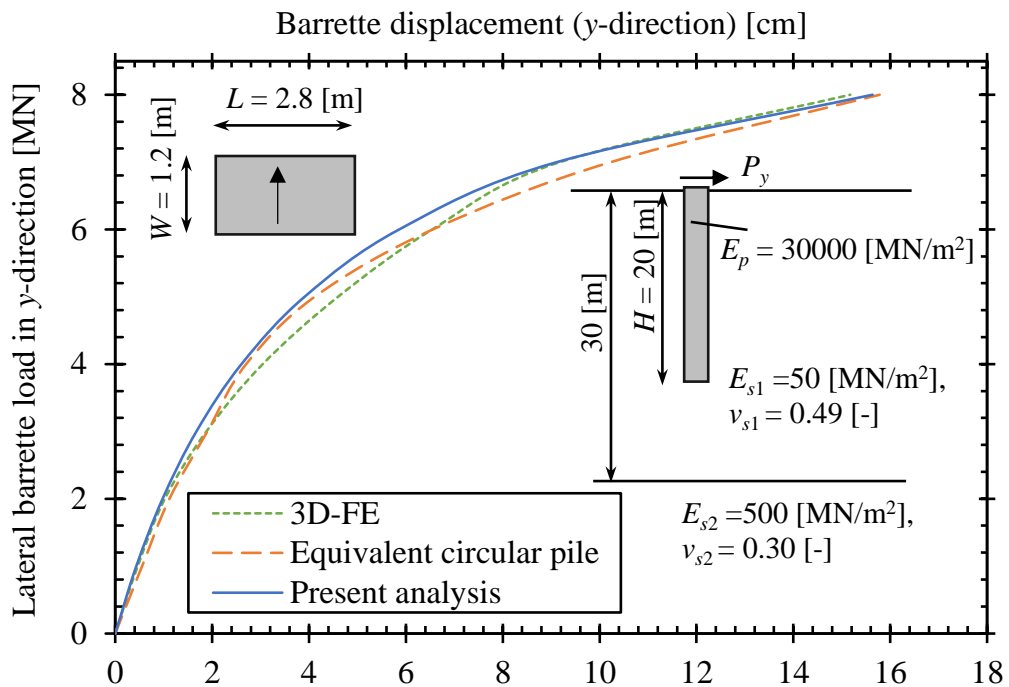


Figure 4.24 Load-displacement curve (y-direction).

4.5 Case Study of Lateral Load Tests

4.5.1 Description of the test problem

Lateral load-displacement relation of the barrette obtained by the present analysis is compared with that presented by *Zhang* (2003) [63], which is obtained from both barrette load test and 3D FE analysis.

Results of load tests of single barrettes having a rectangular cross-section embedded in a multi-layered soil medium are available in the reference *Zhang* (2003) [63]. These tests were performed in Hong Kong.

The barrette in [Figure 4.25](#) is considered and analyzed for different cases. The barrette geometry and modulus of elasticity E_p for these cases are listed in [Table 4.6](#). The soil properties, modulus of elasticity E_s , and *Poisson's* ratio ν_s are listed in [Table 4.7](#) and [Table 4.8](#) and shown in [Figure 4.26](#). E_s was estimated from SPT according to *Bowles* (1996) [9].

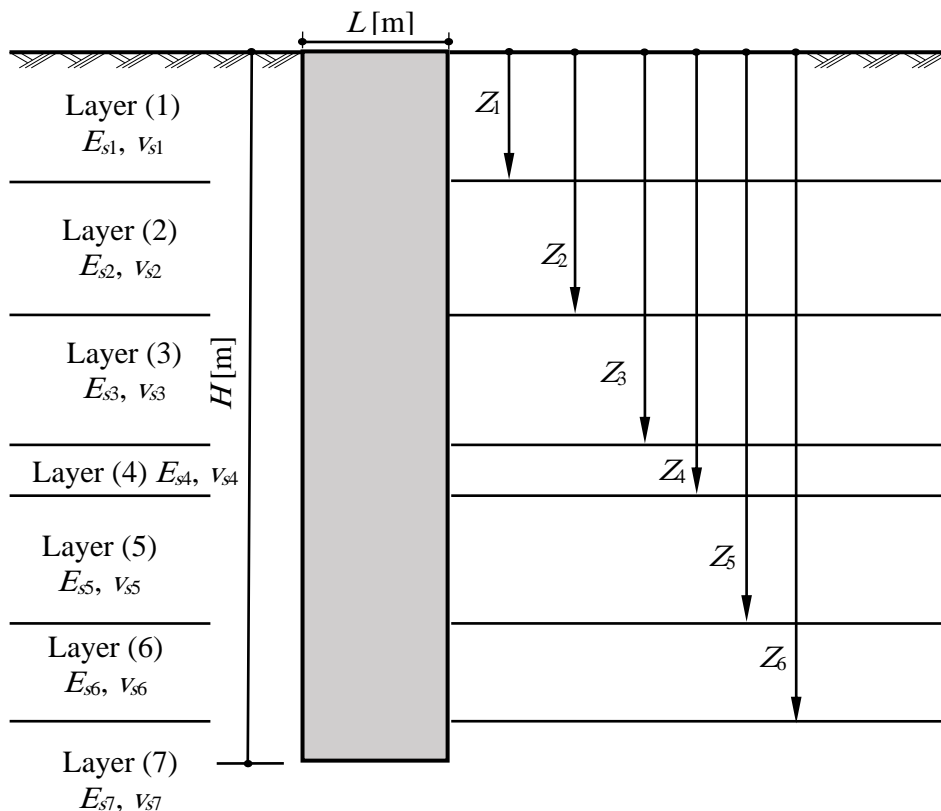
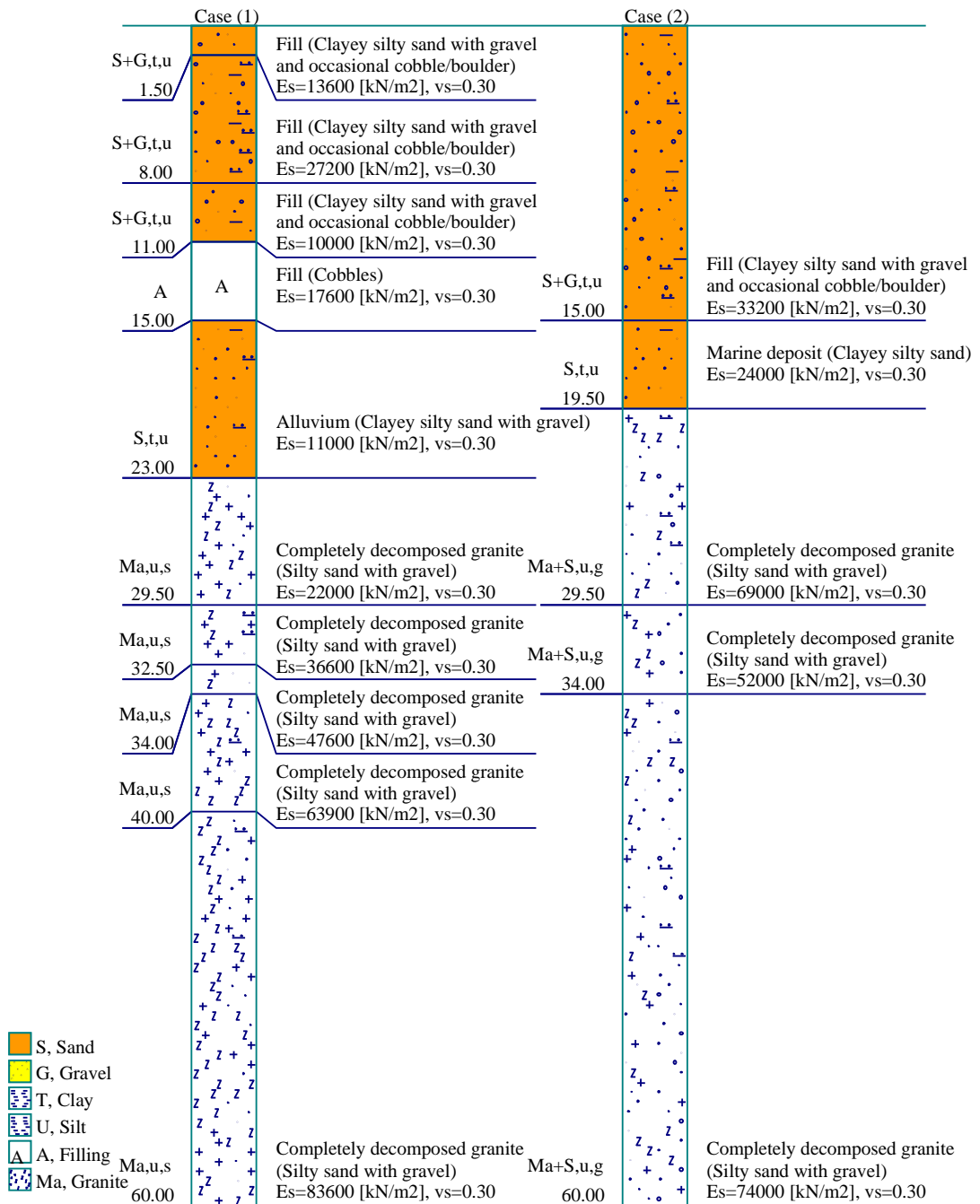


[Figure 4.25](#) Single barrette with subsoil.

Validity of the analysis



Boring Logs

Figure 4.26 Boring logs.

Table 4.6 Barrette geometries, Zhang (2003) [63].

Case	Cross-section [m ²]	Height [m]	Modulus of elasticity of the barrette [kN/m ²]
1	0.86 × 2.8	51	30.3 × 10 ⁶
2	1.20 × 2.7	30	35 × 10 ⁶

Table 4.7 The subsoil properties of case (1), Zhang (2003) [63].

Layer No.	Soil type	Layer depth from the ground surface z [m]	Modulus of elasticity E_s [MN/m ²]	Poisson's ratio ν_s [-]
I				
1	Fill (Clayey silty sand with gravel and occasional cobble/boulder)	1.5	13.6	0.3
2		8	27.2	0.3
3		11	10	0.3
4	Fill (Cobbles)	15	17.6	0.3
5	Alluvium (Clayey silty sand with gravel)	23	11	0.3
6	Completely decomposed granite (Silty sand with gravel)	29.5	22	0.3
7		32.5	36.6	0.3
8		34	47.6	0.3
9		40	63.9	0.3
10		100	83.6	0.3

Table 4.8 Subsoil properties of case (2), *Zhang* (2003) [63].

Layer No. I	Soil type	Layer depth from the ground surface z [m]	Modulus of elasticity E_s [kN/m ²]	<i>Poisson's</i> ratio ν_s [-]
1	Fill (Clayey silty sand with gravel and occasional cobble/boulder)	15	33.2	0.3
2	Marine deposit (Clayey silty sand)	19.5	24	0.3
3	Alluvium (Clayey silty sand with gravel)	28	40.75	0.3
4	Completely decomposed granite (Silty sand with gravel)	29.5	69	0.3
5		34	52	0.3
6		100	74	0.3

4.5.2 Numerical analysis

The height of the barrette is divided into equal-elements. Each element has a height of $h = 2.0$ [m] for case (1) and 1.0 [m] for case (2). Both the barrette length and width are taken as two elements, as shown in [Figure 4.27](#). The barrettes are analyzed nonlinearly using a hyperbolic function. Horizontal limit loads have been assumed from the load-displacement curves of *Zhang* (2003) [63]. These were 6 [MN] and 5.45 [MN] for the first case and 3 [MN] for the second case.

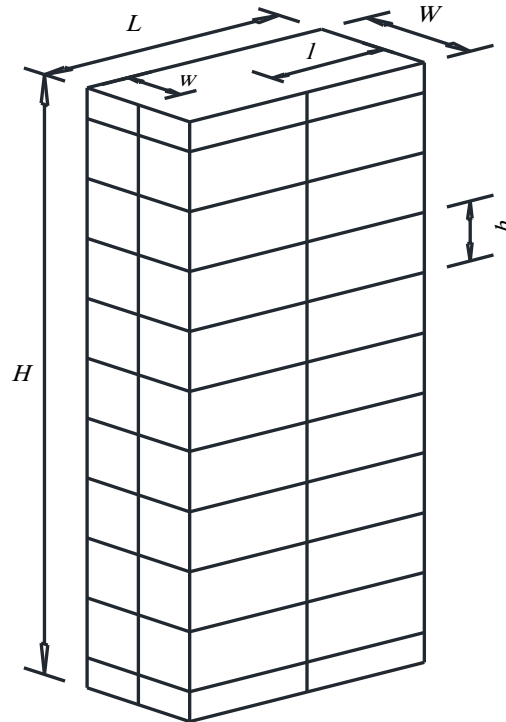


Figure 4.27 The surface element of the barrette.

4.5.3 Results and discussion

The horizontal load-displacement relations of barrettes obtained from the present analysis are compared in Figure 4.28 to Figure 4.30 with that obtained from load tests and from using 3D FE carried out by Zhang (2003) [63].

From the comparison of the linear analysis, it was found that the absolute difference between displacements presented by Zhang (2003) [63] and those of the present technique is less than 0.1 [cm] in case (1) and 0.05 [mm] in the second one.

For nonlinear analysis, the difference between the displacement from the present technique for $H_{lim} = 6$ [MN] and that measured displacement is less than 0.31 [cm] in case (1), except when the load is 4330 [kN], the difference is 3.21 [cm]. But for $H_{lim} = 5.45$ [MN], the absolute difference is increased to 1.90 [cm] in the case of load = 4000 [kN]. The difference decreased to 0.05 [cm] when the load increase to be 4330 [kN]. In case (2), the difference is less than 0.43 [mm]. This difference is too small comparing to the barrette dimensions.

Finally, The verification shows that the lateral load-displacement from the present linear and nonlinear analyses are in good agreement with those of the measured load tests and 3D FE carried out by Zhang (2003) [63].

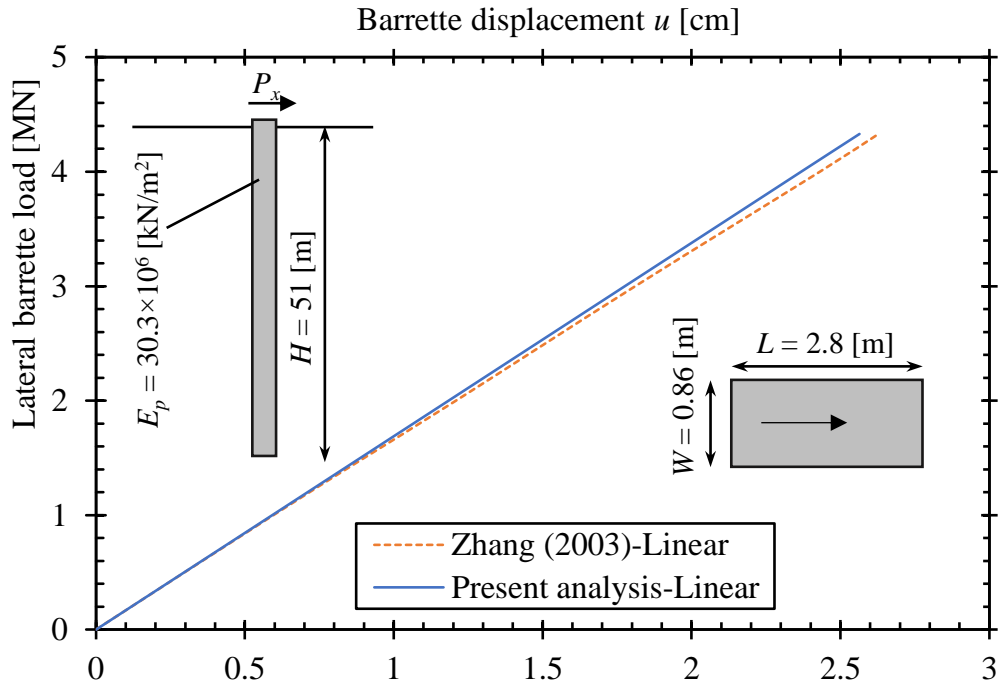


Figure 4.28 Linear load-displacement curve, case (1).

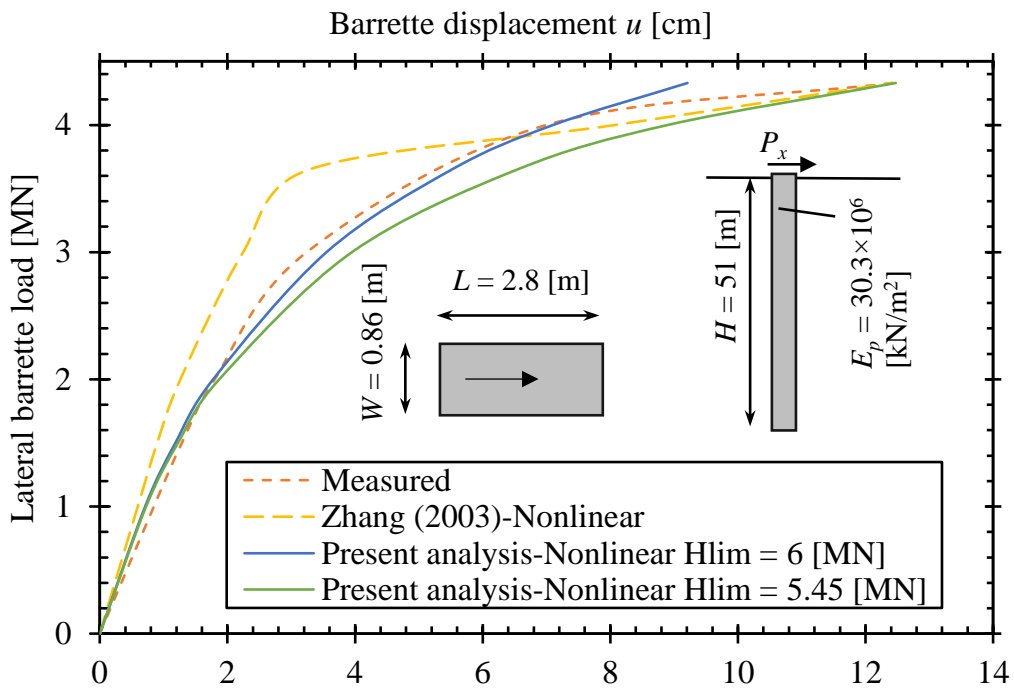


Figure 4.29 Nonlinear load-displacement curve, case (1).

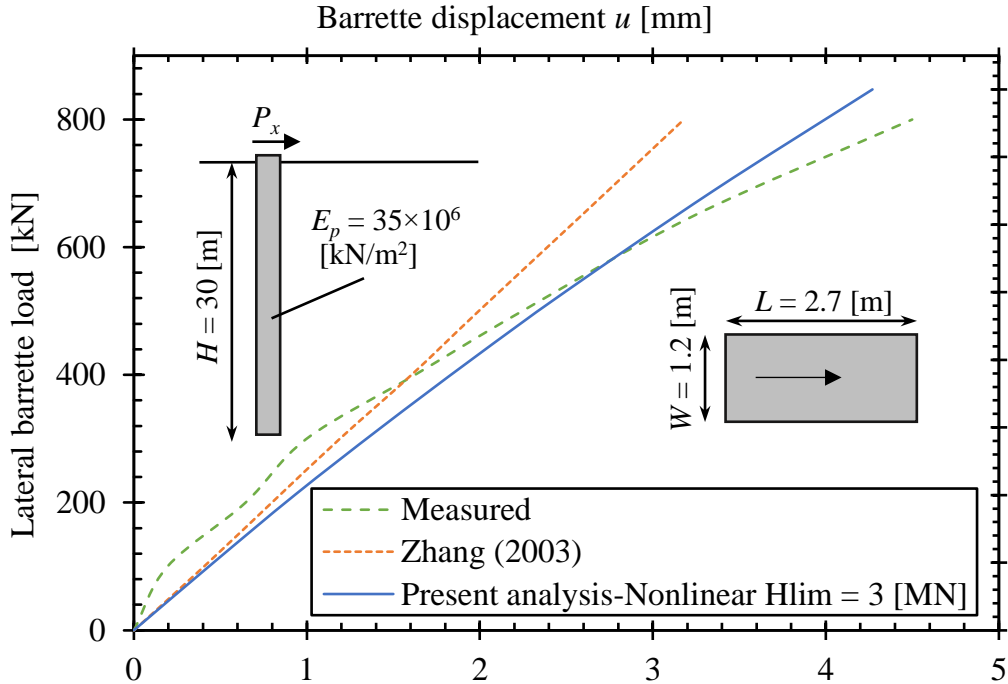


Figure 4.30 Load-displacement curve, case (2).

4.6 Comparative Study of the Present Hybrid Technique

4.6.1 Description of the examination problem

Single barrettes having a rectangular cross-section embedded in subsoil layers is analyzed using different numerical models, as follows:

1. Model (1): Flexibility coefficient model of soil and *CCT* for barrettes.
2. Model (2): Embedded pile in 3D finite element soil.
3. Model (3): Traditional 3D finite element model.

The composed coefficient technique *CCT* is implemented in the flexibility coefficient model presented in this study. In this case, the barrette is treated as one-dimension vertical elements. This technique reduces the time and size of the problem as these two terms considered as main difficulties in three-dimensional problems. In model (2), the barrette is analyzed as an embedded pile. However, treating this pile as one-dimensional beam elements, the soil is treated as block elements. In model (3), the barrette-soil system is treated by block elements. Both models (2) and (3) was analyzed by Plaxis [45].

The results of the three models are compared for verification. Two cases of single barrettes with different dimensions are considered. Each one was analyzed linearly, considering four different types of layered soil. The modulus of elasticity E_s and Poisson's ratio ν_s of these soils are listed in Table 4.9 and shown

in Figure 4.31. Barrette geometry, lateral load on the barrette head, and modulus of elasticity for the chosen cases are listed in Table 4.10.

Table 4.9 Soil properties.

Soil	Layer No.	Soil description	Layer depth from the ground surface z [m]	Modulus of elasticity E_s [MN/m ²]	Poisson's ratio ν_s [-]
(A)	1	Stiff clay	∞	10	0.4
(B)	1	Medium dense sand	∞	25	0.30
(C)	1	Very stiff clay	2	20	0.35
	2	Medium dense sand	5	35	0.25
	3	Dense sand	8	50	0.20
	4	Dense sand	∞	80	0.15
(D)	1	Very stiff clay	1.5	20	0.35
	2	Stiff clay	3.5	10	0.45
	3	Medium dense sand	8.5	40	0.25
	4	Dense sand	∞	80	0.20

Table 4.10 Barrette geometries.

Case	Cross-section [m ²]	Height [m]	Modulus of elasticity of the barrette [kN/m ²]	Load [kN]
1	2.8×0.8	40	30×10^6	3000
2	2.7×1.2	30	30×10^6	3000

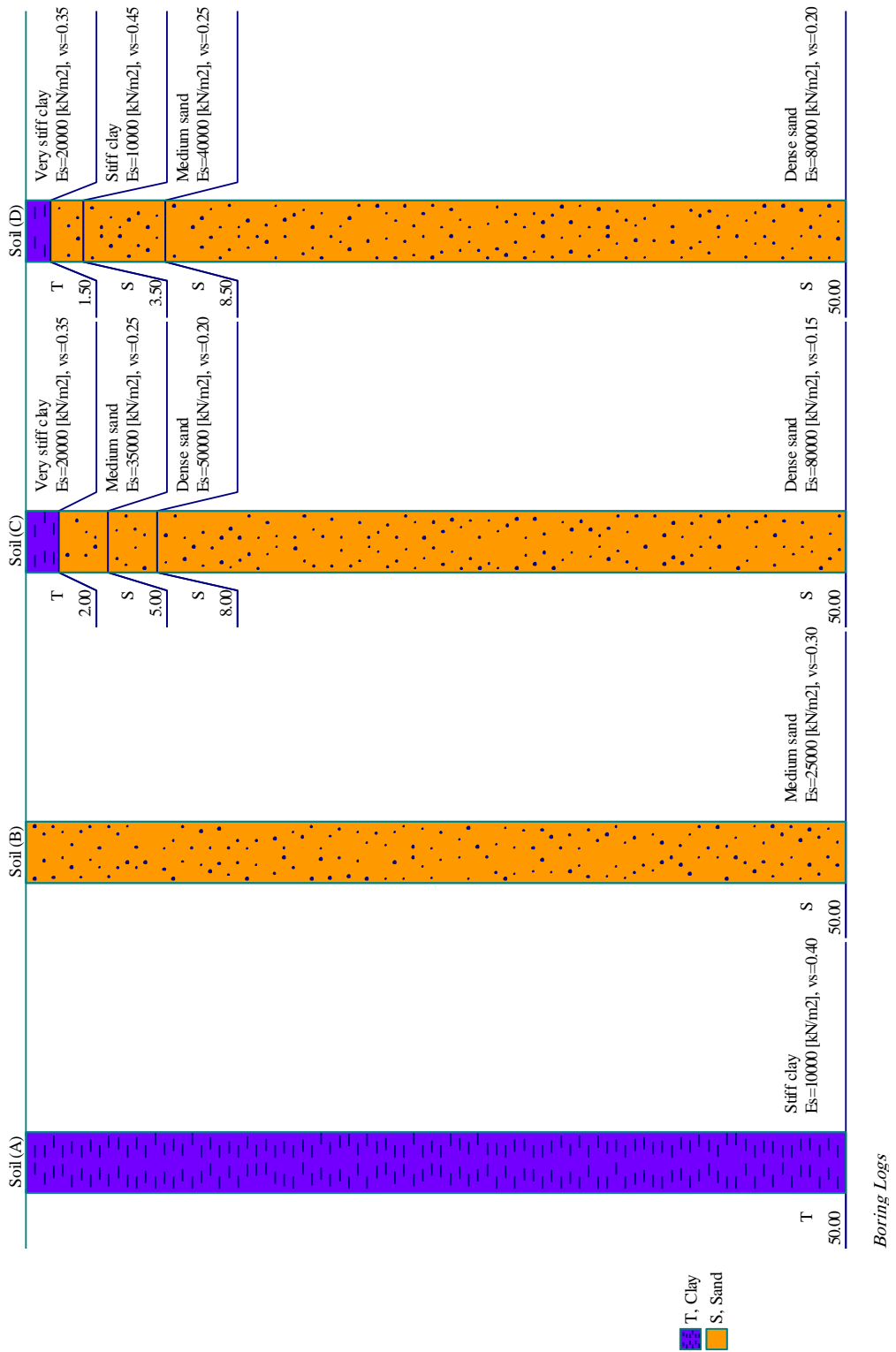


Figure 4.31 Boring logs.

4.6.2 Numerical analysis

For model (1), the barrette height is divided into equal-elements, each of 1.25 [m]. The barrette length and width are divided into four equal-elements. In model (2), the barrette represented as an embedded pile, beam element, and the soil treated as 3D finite elements then analyzed. In model (3), both barrettes and soil are treated as 3D finite elements with interface elements around the barrette then analyzed. In both models (2) and (3), barrettes and soil elements are generated automatically. The soil dimensions around the barrette are extended enough to ensure full interaction between the barrette and soil. It is taken 40 [m] in both the x and the y -directions and twice the barrette height in the z -direction. In this case, the barrette is analyzed linearly. Figure 4.32 to Figure 4.38 shows the element mesh for the single barrettes with different models.

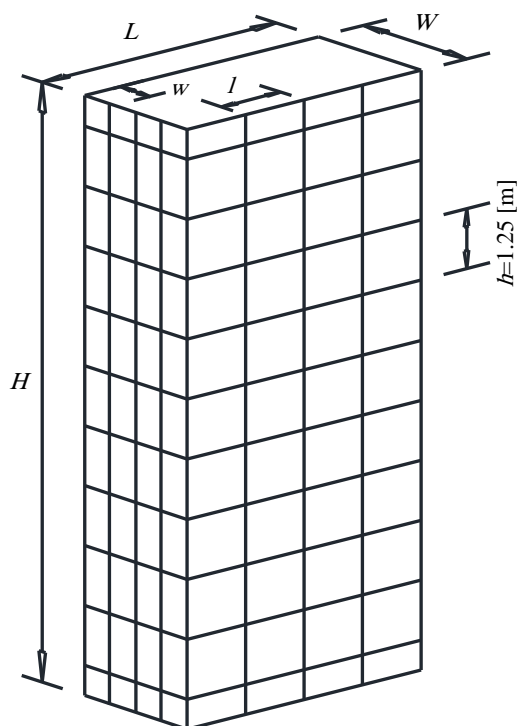


Figure 4.32 The surface element of the barrette for model (1).

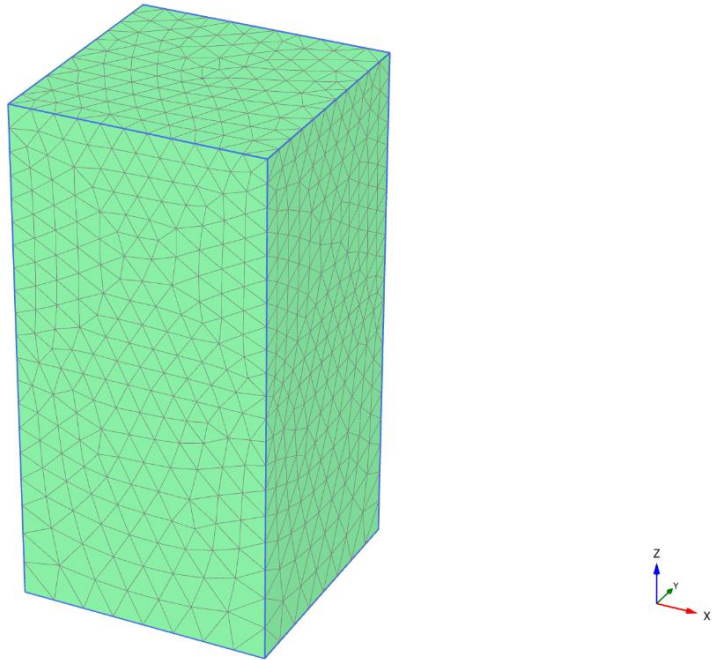


Figure 4.33 Element mesh of the single barrette - model (2) - Soil A&B.

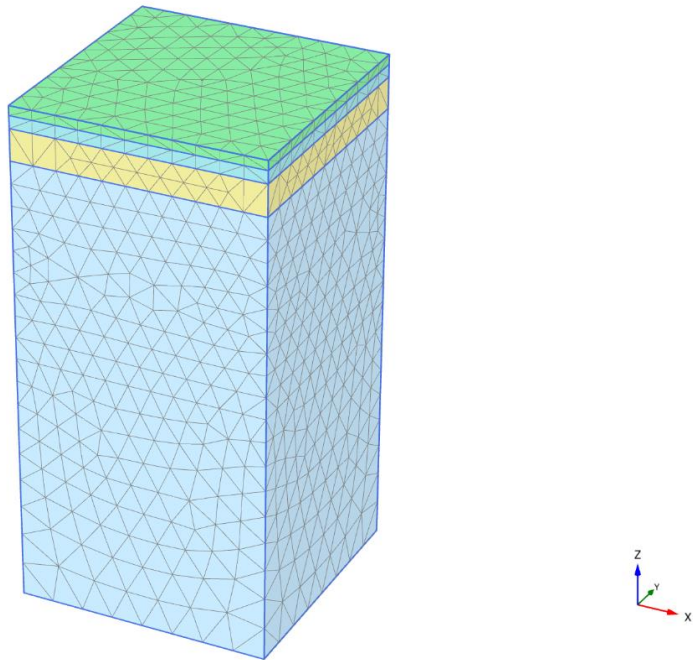


Figure 4.34 Element mesh of the single barrette - model (2) - Soil C&D.

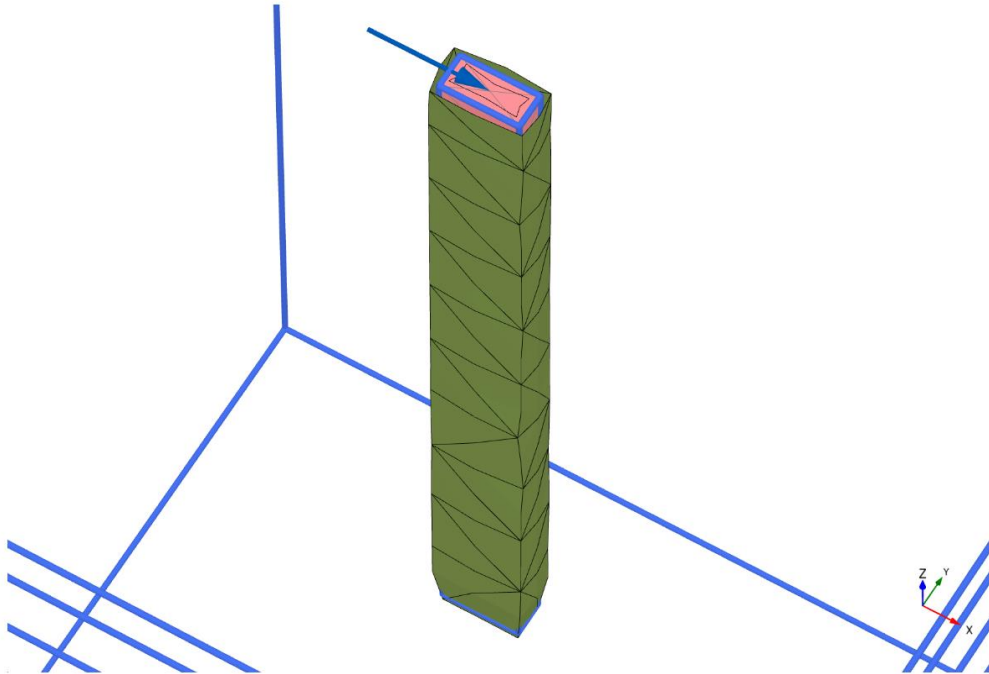


Figure 4.35 Barrette with interface elements - model (3).

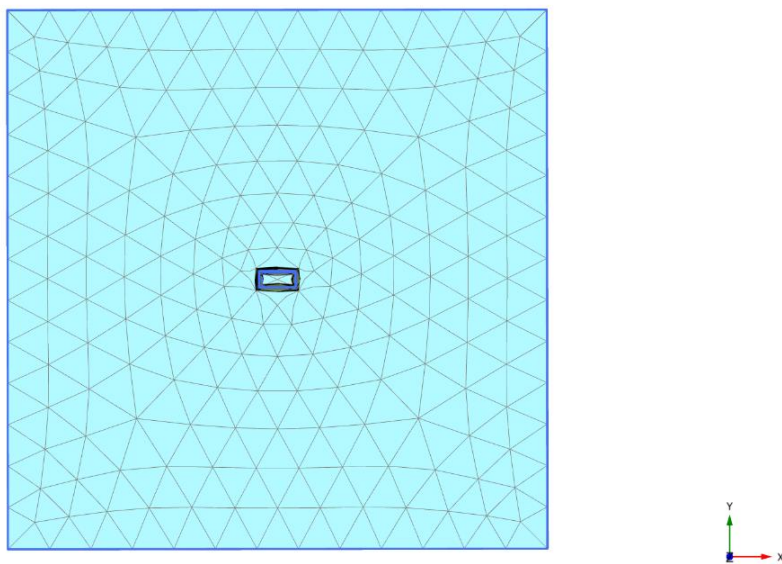


Figure 4.36 Plan of element mesh of the single barrette - model (3).

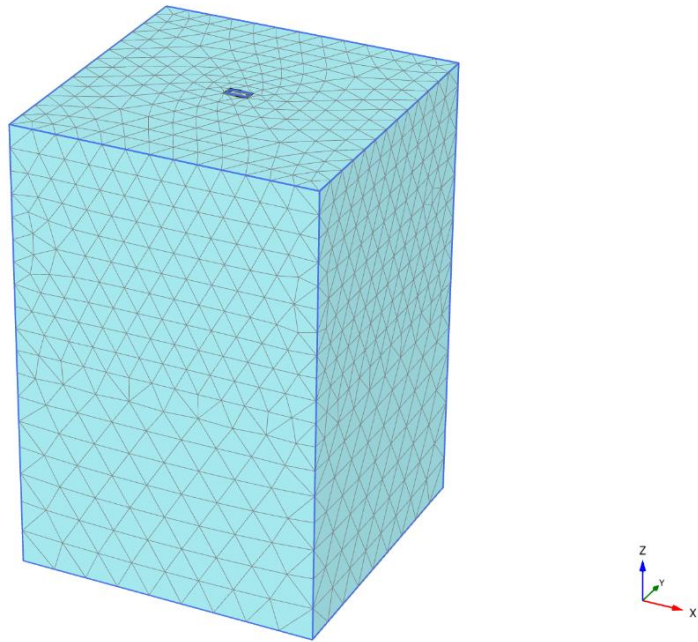


Figure 4.37 Element mesh of the single barrette - model (3) - Soil A&B.

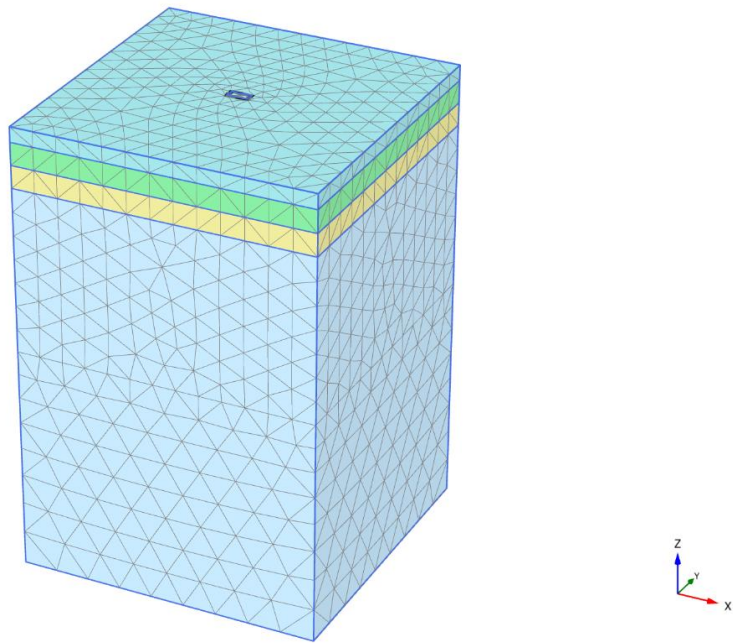


Figure 4.38 Element mesh of the single barrette - model (3) - Soil C&D.

4.6.3 Results and discussion

Barrette deformations and internal forces along the barrette height obtained from the different models are compared. [Figure 4.39](#) to [Figure 4.44](#) show an example. Other comparisons are shown in [APPENDIX \(A\)](#).

Results show that the absolute differences between the barrettes head displacements in the present analysis Models (1) and that by Models (2) and (3), as shown in [Figure 4.39](#), are less than 10.21% compared with Model (2) and 9.22% compared with Model (3), which are 0.22 and 0.13 [cm], respectively.

In addition, the absolute differences between the computed barrettes base displacements in the present analysis Model (1) and those by Models (2) and (3), as shown in [Figure 4.40](#), are less than 0.24 [cm] compared with Model (2) and 0.26 [cm] compared with Model (3). This behavior is noticed for all cases except case (2) with soil type (A), which are 0.55 [cm] and 0.39 [cm], respectively. These differences are too small comparing to the barrette dimensions.

Comparing the maximum bending moments using the present analysis Models (1) and those from Model (2), as shown in [Figure 4.41](#), the differences are less than 16 %. The shear and bending moment results are depending on the element size in the z -direction. In Model (2), the elements are very small so that the shear force isn't smooth curve and the bending moment is greater than the present analysis.

In general, it can be concluded that the results of the present analysis using the flexibility coefficient and CCT are in good agreement with both Models (2) and (3).

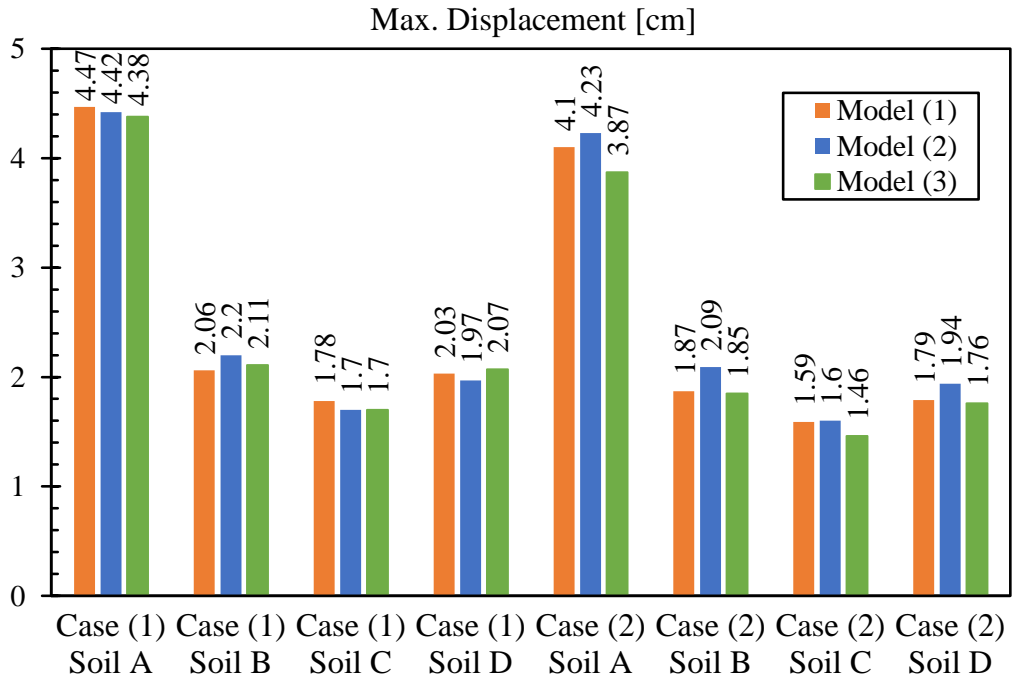


Figure 4.39 Comparison between Max. Displacements.

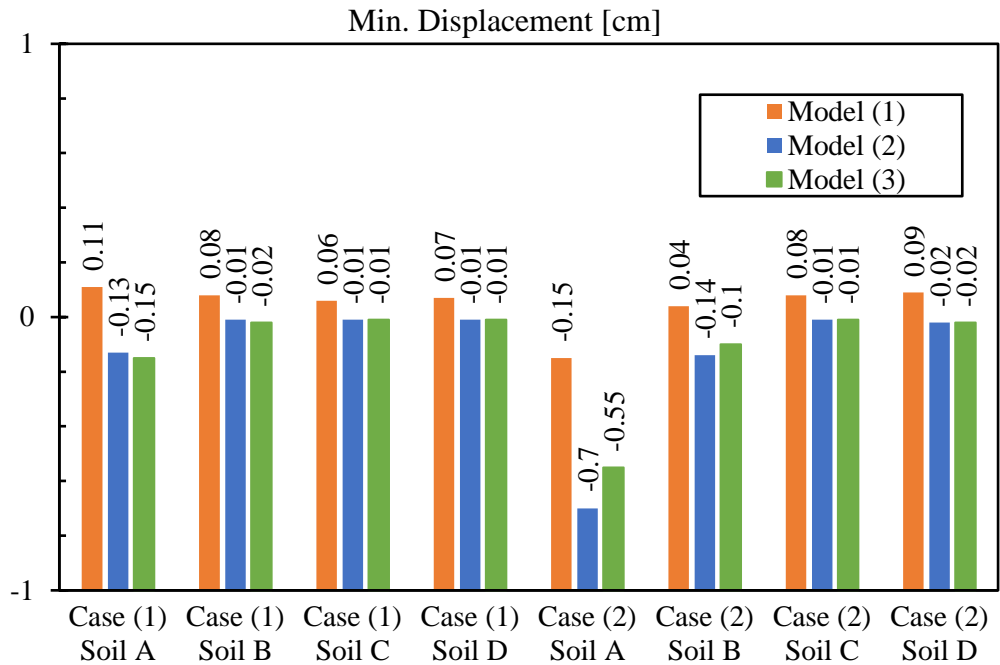


Figure 4.40 Comparison between Min. Displacements.

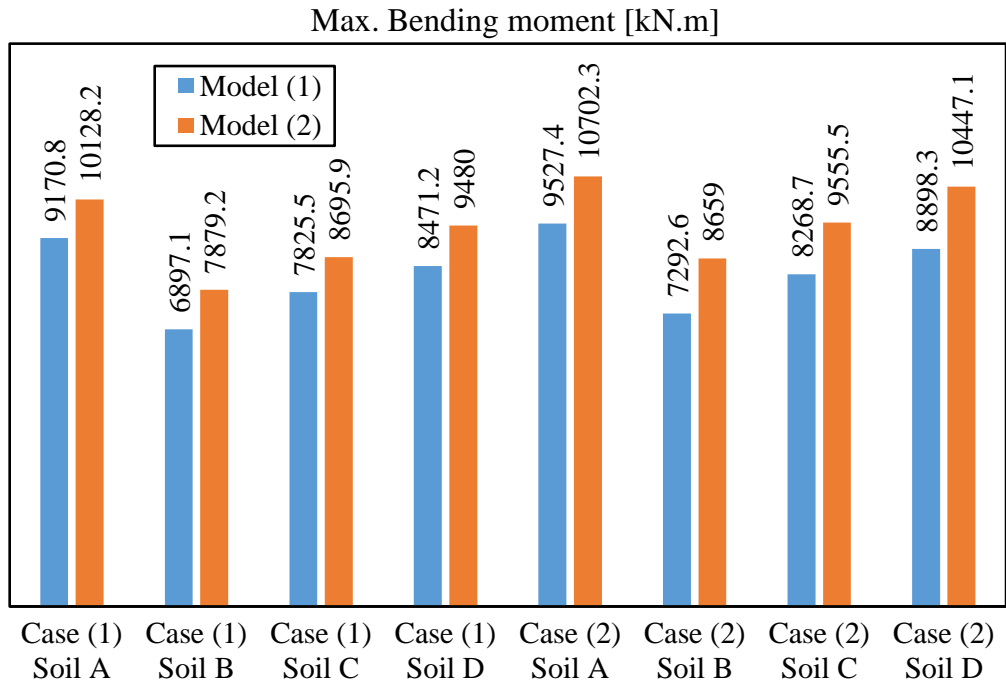


Figure 4.41 Comparison between Max. Bending moments.

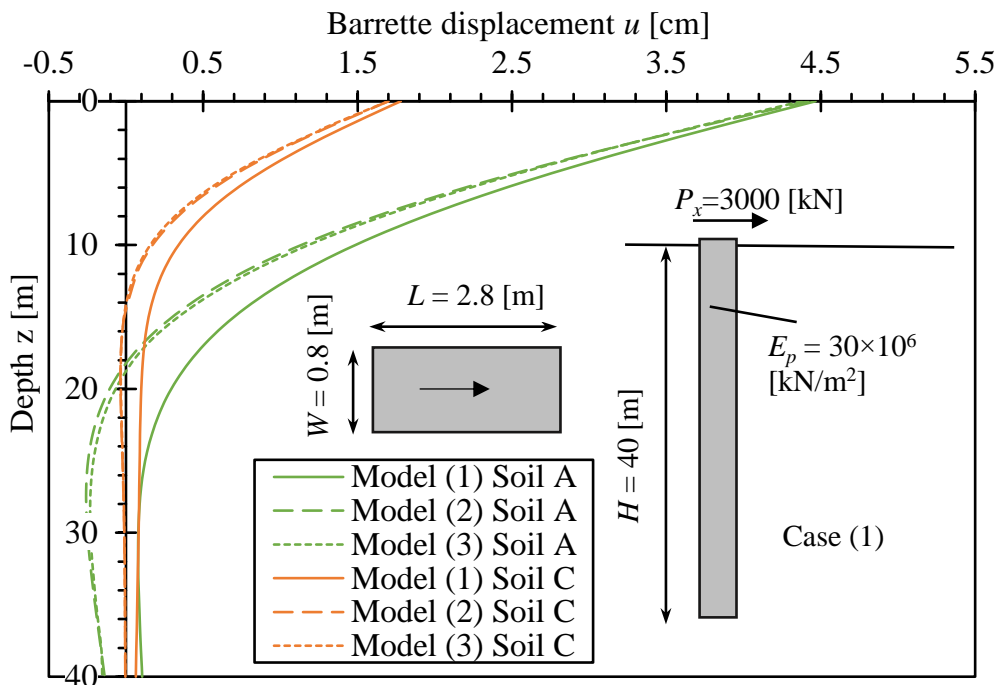


Figure 4.42 Displacement u for case (1) with subsoil (A&C).

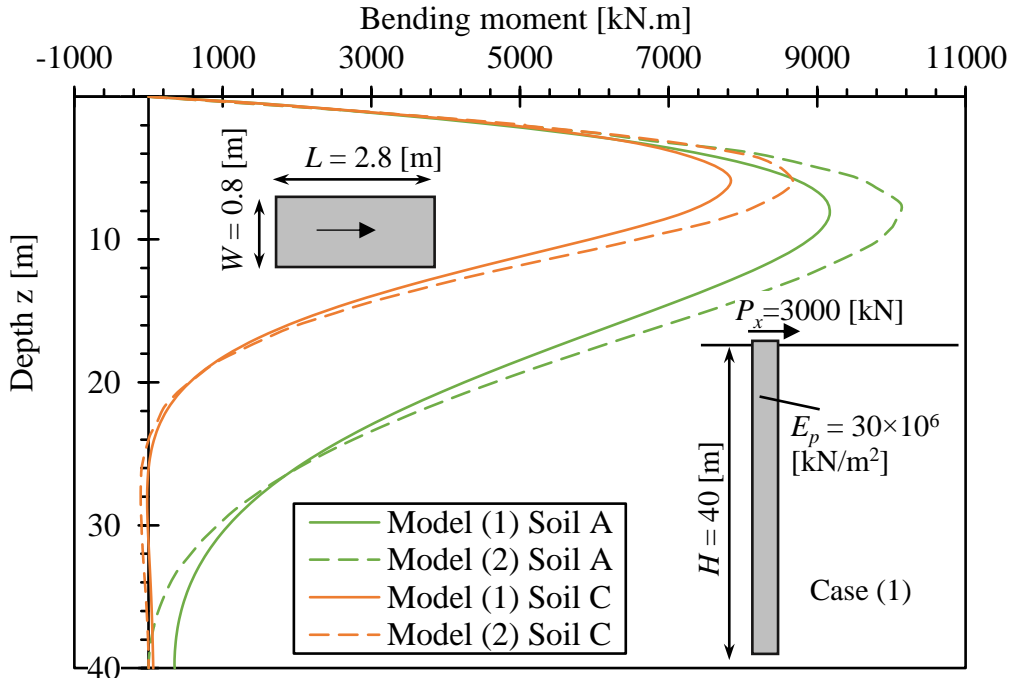


Figure 4.43 Bending moment for case (1) with subsoil (A&C).

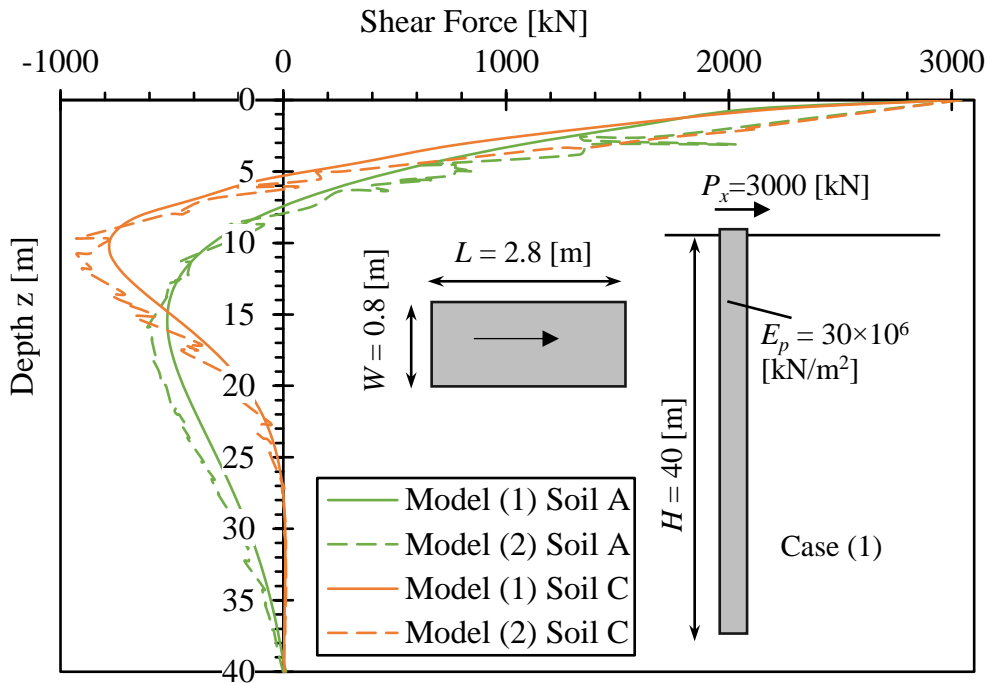


Figure 4.44 Shear force for case (1) with subsoil (A&C).

CHAPTER 5

5 ANALYSIS OF BARRETTES

5.1 Introduction

A comparative study is presented for determining the effective-height of the barrette required for the single barrette subjected to lateral loads in a real-subsoil. The present hybrid analysis is compared with two different methods that are in the *ECP 202* [56]. In addition, soil nonlinearity is studied by comparing results from the linear model with those of nonlinear. Furthermore, a parametric study for analyzing laterally loaded barrettes/barrette groups are presented to investigate the effect of load direction, barrette dimensions, barrettes/soil properties, the spacing between barrettes, and the barrette arrangement.

5.2 Comparative Study of a Single Barrette in a Real Subsoil

5.2.1 Introduction

A comparative study is presented for determining the effective-height of the barrette and provides engineers with guidelines for analyzing laterally loaded single barrettes in east Port-Said, [Figure 5.1](#). In this study, east Port-Said soil properties are considered because this area characterizes by extended soft clay layers. These are similar to the soil formation of London, Frankfurt, Rome, Hong kong, and Dammam.



Figure 5.1 East Port-Said location.

5.2.2 Barrette properties

The barrette material properties are listed in Table 5.1.

Table 5.1 Barrette material properties.

Modulus of elasticity of the barrette material $E_c = 25 \times 10^6$ [kN/m ²]	
Poisson's ratio of the barrette material	$\nu_c = 0.20$ [-]

Studied cases are carried out for a wide range of barrette dimensions, namely barrette lengths L and widths W with different barrette heights H . The effect of these variables on the barrette deformations and internal forces of laterally loaded barrette is investigated. Nine cases of single barrettes are considered, as presented in Table 5.2. Each one is considered and analyzed with various barrette heights H ranging from 20 to 60 [m] to determine the effective-height, in a total of more than 90 cases.

Table 5.2 Studied cases of a single barrette.

Length / Width	$L = 2.5$ [m]	$L = 2.8$ [m]	$L = 3.0$ [m]
$W = 0.8$ [m]	Case 1	Case 2	Case 3
$W = 1.0$ [m]	Case 4	Case 5	Case 6
$W = 1.2$ [m]	Case 7	Case 8	Case 9

5.2.3 Soil properties

The typical subsoil layers of the east Port-Said area presented previously by Hamza *et al.* (2000) [25] are considered in this analysis, as listed in Table 5.3 and shown in Figure 5.2. The subsoil consists of eight layers. Each layer has different unit weight γ_b , effective-shear strength parameters (c' and ϕ'), undrained shear strength c_u , modulus of elasticity E_s , Poisson's ratio ν_s and horizontal modulus of soil reaction n determined according to ECP 202 [56].

Table 5.3 Subsoil properties, Hamza *et al.* (2000) [25].

Layer No.	Soil type	z [m]	γ_b kN/m ³	c' kN/m ²	ϕ' [°]	c_u kN/m ²	E_s MN/m ²	ν_s [-]	n MN/m ³
1	Soft clay	5	17	10	24	20	2.4	0.2	0
2	Medium dense sand	13.5	18.5	0	35	-	30	0.25	6.15
3	Medium stiff clay	28.5	15.5	22	24	46	20.5	0.2	3.7
4	Stiff clay	38.5	15	31	20	61.5	24.7	0.2	3.7
5	Stiff clay	48.5	15	37	20	74	28.1	0.2	3.7
6	Stiff clay	58.5	15	43	20	86	31.4	0.2	3.7
7	Very Stiff clay	92.5	17.5	75	20	150	60	0.2	3.7
8	Dense sand	120	20	0	35	-	144	0.2	11.1

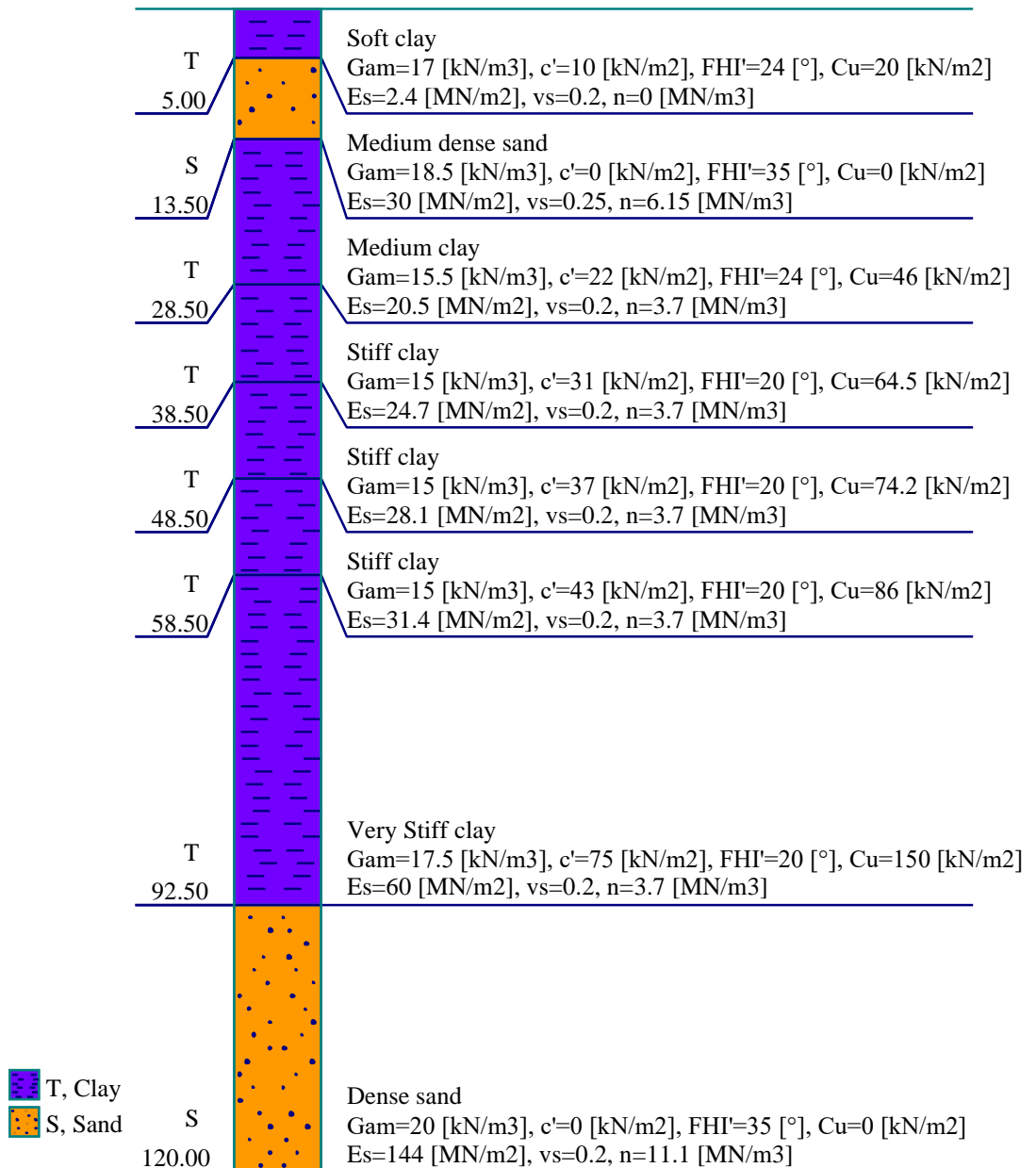


Figure 5.2 East Port-Said boring log.

5.2.4 Effective barrette height

According to the *ECP 202* [56], there are two methods for determining the effective-height. These are approximate methods to assess the effective-height of square or circular piles in homogeneous soil. The first one depends on the horizontal modulus of soil reaction, while the second depends on the soil modulus

of elasticity. The barrette is analyzed many times with different barrette heights ranging from 20 to 60 [m] to investigate the effective-height as follows:

- Method (1): Horizontal modulus of soil reaction.
- Method (2): The soil modulus of elasticity.
- Present analysis.

5.2.4.1 Method (1): Horizontal modulus of soil reaction.

The *ECP 202* [56] equations for determining the effective-height using the horizontal modulus of soil reaction are used in this analysis, equations (37) and (38). In case the barrette crosses layered soil, these moduli are taken as an equivalent horizontal modulus of soil reaction n_{eq} , [kN/m³] according to Eq. (39). This equivalent horizontal modulus is taken as a ratio of the element length that crosses these layers, as shown in Figure 5.3. The effective-barrette height for each case listed in Table 5.2 is determined by substituting this equivalent horizontal modulus into the *ECP 202* [56] equations.

$$t = \sqrt[5]{\frac{E_p I_p}{n}} \quad (37)$$

$$H_e = 4 \times t \quad (38)$$

$$n_{eq} = \frac{\sum n_i H_i}{\sum H_i} \quad (39)$$

Where:

E_p Modulus of elasticity of the barrette material, [kN/m²];

I_p Moment of inertia of the barrette, [m⁴];

t Elastic barrette height, [m];

H_e Effective barrette height, [m];

n_{eq} Equivalent horizontal modulus of soil reaction, [kN/m³];

n_i Horizontal modulus of soil reaction for layer i , [kN/m³]; and

H_i The barrette height that crosses layer i , [m].

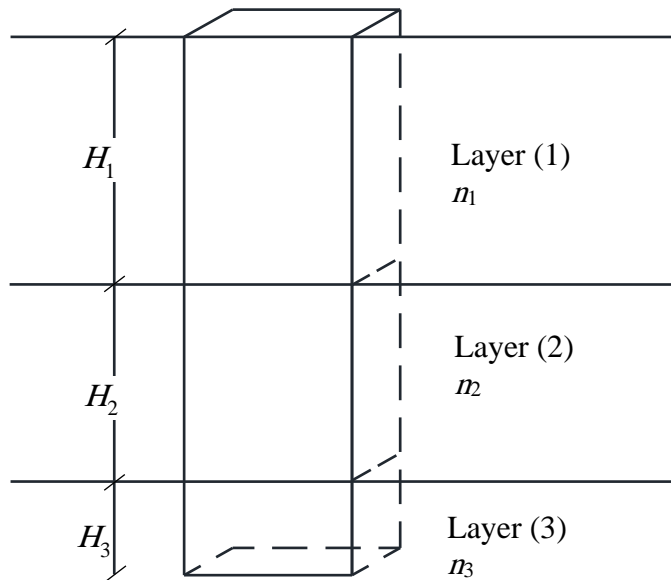


Figure 5.3 The geometry of the barrette lies between different soil layers.

The effective-height is defined as the height in which the analysis results are not influenced by increasing this height. Nine cases are considered to determine that effective-height using the horizontal modulus of soil reaction considering various barrette heights, $H = 20, 30, 40, 50,$ and 60 [m], as listed in Table 5.2. The equivalent horizontal modulus of soil reaction is determined according to Eq. (39), which depends on the barrette height only, as listed in Table 5.4.

Table 5.4 The equivalent horizontal modulus of soil reaction, n_{eq} .

Barrette height H [m]	Layer depth from the ground surface z [m]	Horizontal modulus of soil reaction n [kN/m ³]	Equivalent horizontal modulus of soil reaction n_{eq} [kN/m ³]
20	5	0	3816
	13.5	6150	
	20	3700	
30	5	0	3778
	13.5	6150	
	28.5	3700	
	30	3700	
40	5	0	3758
	13.5	6150	
	28.5	3700	
	38.5	3700	
	40	3700	
50	5	0	3747
	13.5	6150	
	28.5	3700	
	38.5	3700	
	48.5	3700	
	50	3700	
60	5	0	3739
	13.5	6150	
	28.5	3700	
	38.5	3700	
	48.5	3700	
	58.5	3700	
	60	3700	

Substituting the equivalent horizontal modulus of soil reaction n_{eq} listed in [Table 5.4](#) into Eq. (37) leads to:

$$t = \sqrt[5]{\frac{E_p I_p}{n_{eq}}} \quad (40)$$

The effective-height is determined for the nine cases by substituting the elastic-height from Eq. (40) into Eq. (38). Then these are listed in [Table 5.5](#) as the first iteration of determining that effective-height. For case (1) as an example in this

table, it can be concluded that the effective-height is 23.38 [m] while the barrette height is 20 [m]. In this condition, the equivalent horizontal modulus of soil reaction n_{eq} doesn't represent the soil surrounding the barrette, which needs to be recalculated according to a barrette height equal to this effective-height. Otherwise, the effective-height seems to be approximately constant when increasing the barrette height to 30 [m] or more for this case. So, the effective-height for this case is between 20 and 30 [m]. Accordingly, the next iteration considered the barrette height to be the effective-height of the first iteration 23.43 [m]. Applying this methodology for determining the effective-height of the nine cases listed in Table 5.2 leads to Table 5.6.

Table 5.5 Effective barrette height using method (1), first iteration.

Barrette Width W , [m]	Barrette Height H , [m]	Barrette Length L , [m]		
		2.5	2.8	3.0
0.8	20	23.38	25.03	26.08
	30	23.43	25.08	26.14
	40	23.45	25.10	26.16
	50	23.47	25.12	26.18
	60	23.48	25.13	26.19
1.0	20	24.45	26.17	27.27
	30	24.50	26.22	27.33
	40	24.52	26.25	27.36
	50	24.54	26.26	27.37
	60	24.55	26.28	27.39
1.2	20	25.36	27.14	28.29
	30	25.41	27.20	28.34
	40	25.43	27.22	28.37
	50	25.45	27.24	28.39
	60	25.46	27.25	28.40

Table 5.6 Effective barrette height, Method (1).

Length / Width	$L = 2.5$ [m]	$L = 2.8$ [m]	$L = 3.0$ [m]
$W = 0.8$ [m]	23.40	25.06	26.12
$W = 1.0$ [m]	24.48	26.21	27.32
$W = 1.2$ [m]	25.39	27.18	28.34

5.2.4.2 Method (2): The soil modulus of elasticity.

The *ECP 202* [56] equation for determining the effective-height using the soil modulus of elasticity is used in this analysis, Eq. (41). In case the barrette crosses layered soil, these moduli are taken as an equivalent soil modulus of elasticity E_{seq} , [kN/m²] according to Eq. (42). This equivalent modulus is taken as a ratio of the element length that crosses these layers, as shown in Figure 5.4. The effective-height for each case listed in Table 5.2 is determined by substituting this equivalent modulus into the *ECP 202* [56] equations.

$$H_e = 4.44 \times \sqrt[4]{\frac{E_p I_p}{E_s}} \quad (41)$$

$$E_{seq} = \frac{\sum E_{si} H_i}{\sum H_i} \quad (42)$$

Where:

- H_e Effective barrette height, [m];
- E_p Modulus of elasticity of the barrette material, [kN/m²];
- I_p Moment of inertia of the barrette, [m⁴];
- E_s Modulus of elasticity of the soil, [kN/m²];
- E_{seq} Equivalent soil modulus of elasticity, [kN/m²];
- E_{si} Soil modulus of elasticity for layer i , [kN/m²]; and
- H_i The barrette height that crosses layer i , [m].

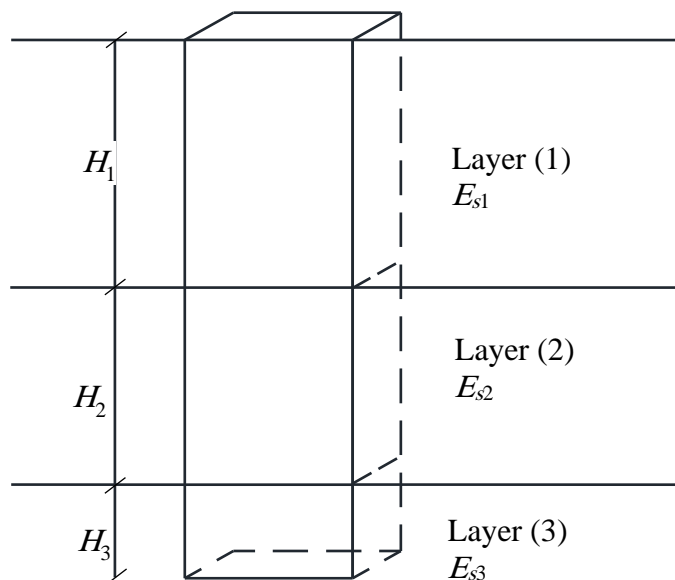


Figure 5.4 The geometry of the barrette lies between different soil layers.

Nine cases are considered to determine that effective-height using the modulus of elasticity considering various barrette heights, $H = 20, 30, 40, 50,$ and 60 [m], as listed in Table 5.2. The equivalent modulus of elasticity is determined according to Eq. (42), which depends on the barrette height only, as listed in Table 5.7.

Table 5.7 The equivalent modulus of elasticity, E_{seq} kN/m².

Barrette height H [m]	Layer depth from the ground surface z [m]	Modulus of elasticity E_s [kN/m ²]	Equivalent modulus of elasticity E_{seq} [kN/m ²]
20	5	2400	20013
	13.5	30000	
	20	20500	
30	5	2400	20385
	13.5	30000	
	28.5	20500	
	30	24700	
40	5	2400	21591
	13.5	30000	
	28.5	20500	
	38.5	24700	
	40	28100	
50	5	2400	22992
	13.5	30000	
	28.5	20500	
	38.5	24700	
	48.5	28100	
	50	31400	
60	5	2400	25108
	13.5	30000	
	28.5	20500	
	38.5	24700	
	48.5	28100	
	58.5	31400	
	60	60000	

Substituting the equivalent modulus of elasticity E_{seq} listed in Table 5.7 into Eq. (41) leads to:

$$H_e = 4.44 \times \sqrt[4]{\frac{E_p I_p}{E_{seq}}} \quad (43)$$

The effective-height for the nine cases is determined according to Eq. (43). Then these are listed in Table 5.5 as the first iteration of determining that effective-height. For case (9) as an example in this table, it can be concluded that the effective-height is 33.84 [m] while the barrette height is 20 [m]. In this condition, the equivalent modulus of elasticity E_{seq} doesn't represent the soil surrounding the barrette, which needs to be recalculated according to a barrette height equal to this effective-height. Otherwise, the effective-height seems to be approximately constant when increasing the barrette height to 30 [m] or more for this case. So, the effective-height for this case is between 30 and 40 [m]. Accordingly, the next iteration considered the barrette height to be the effective-height of the first iteration 33.68 [m]. Applying this methodology for determining the effective-height of the nine cases listed in Table 5.2 leads to Table 5.9.

Table 5.8 Effective barrette height using method (2), first iteration.

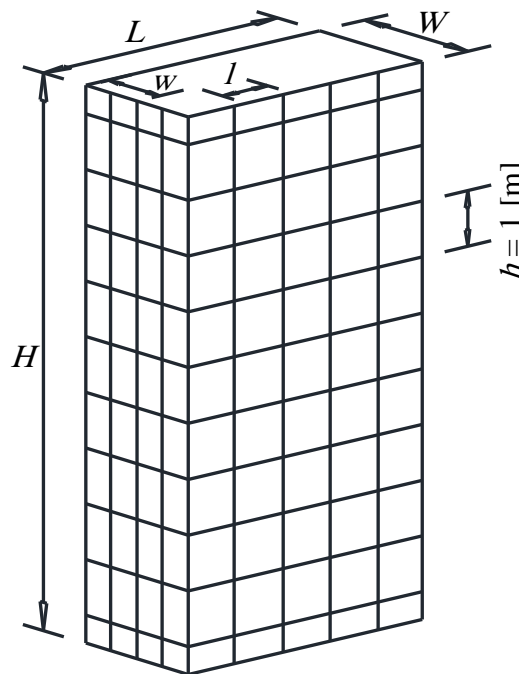
Barrette Width W , [m]	Barrette Height H , [m]	Barrette Length L , [m]		
		2.5	2.8 m	3 m
0.8	20	26.67	29.03	30.57
	30	26.54	28.90	30.43
	40	26.17	28.49	30.00
	50	25.76	28.04	29.53
	60	25.20	27.43	28.89
1.0	20	28.20	30.70	32.33
	30	28.07	30.56	32.18
	40	27.67	30.12	31.72
	50	27.24	29.65	31.23
	60	26.64	29.01	30.55
1.2	20	29.51	32.13	33.84
	30	29.38	31.98	33.68
	40	28.96	31.53	33.20
	50	28.51	31.03	32.68
	60	27.88	30.36	31.97

Table 5.9 Effective barrette height, Method (2).

Length / Width	$L = 2.5$ [m]	$L = 2.8$ [m]	$L = 3.0$ [m]
$W = 0.8$ [m]	26.63	28.96	30.41
$W = 1.0$ [m]	28.15	30.55	32.09
$W = 1.2$ [m]	29.41	31.90	33.51

5.2.4.3 Using the present analysis

A comparative test of the numerical model for analyzing laterally loaded single barrette in east Port-Said is performed to determine the effective-height using the present analysis. Nine cases are considered in this analysis, as listed in [Table 5.2](#). Each one is considered and analyzed with various barrette heights H ranging from 20 to 60 [m] to determine the effective-height. The barrette-soil interface is divided into elements with a height of $h = 1.0$ [m]. The barrette length and width are divided into equal five- and four-elements, respectively, as shown in [Figure 5.5](#). The barrette is considered to be an elastic body in a continuum soil medium. And the load-displacement relation is determined according to the linear analysis of single barrettes. The lateral load on the barrette head is taken constant for all cases and equal to 1000 [kN].



[Figure 5.5](#) The surface element of the single barrette.

[Figure 5.6](#) to [Figure 5.10](#) shows displacements u , reaction forces R_x , shear forces Q_x , bending moments M_y and barrette rotations Θ_{y-y} with different barrette heights obtained by the present analysis, for case (1) as an example. From these figures, it can be concluded that the analysis results are not influenced by increasing the barrette height to more than 30 [m] for this case. So, the effective-height for this case is between 20 and 30 [m]. Accordingly, this case is considered and analyzed with various barrette heights H ranging from 20 to 30 [m]. Applying this methodology for determining the effective-height of the nine cases listed in [Table 5.2](#) leads to [Table 5.10](#).

Table 5.10 Effective barrette height, the present analysis.

Length / Width	$L = 2.5$ [m]	$L = 2.8$ [m]	$L = 3.0$ [m]
$W = 0.8$ [m]	29	31	33
$W = 1.0$ [m]	31	33	34
$W = 1.2$ [m]	32	34	36

Other comparisons of displacements u , reaction forces R_x , shear forces Q_x , bending moments M_y and barrette rotations Θ_y for different cases with different barrette heights are shown in **APPENDIX (B)**.

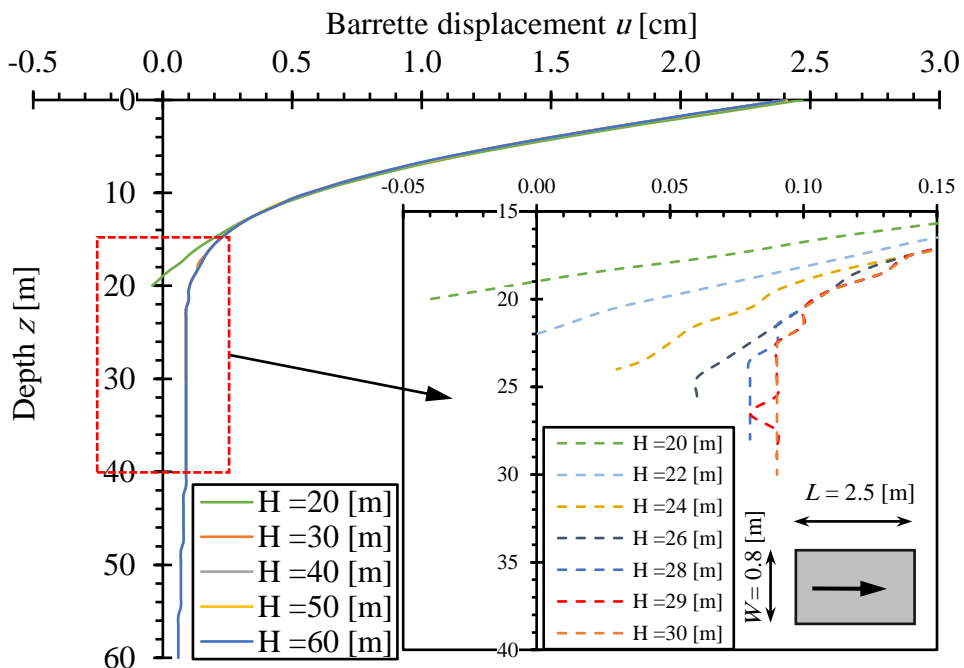


Figure 5.6 Displacement u with the barrette height (case 1).

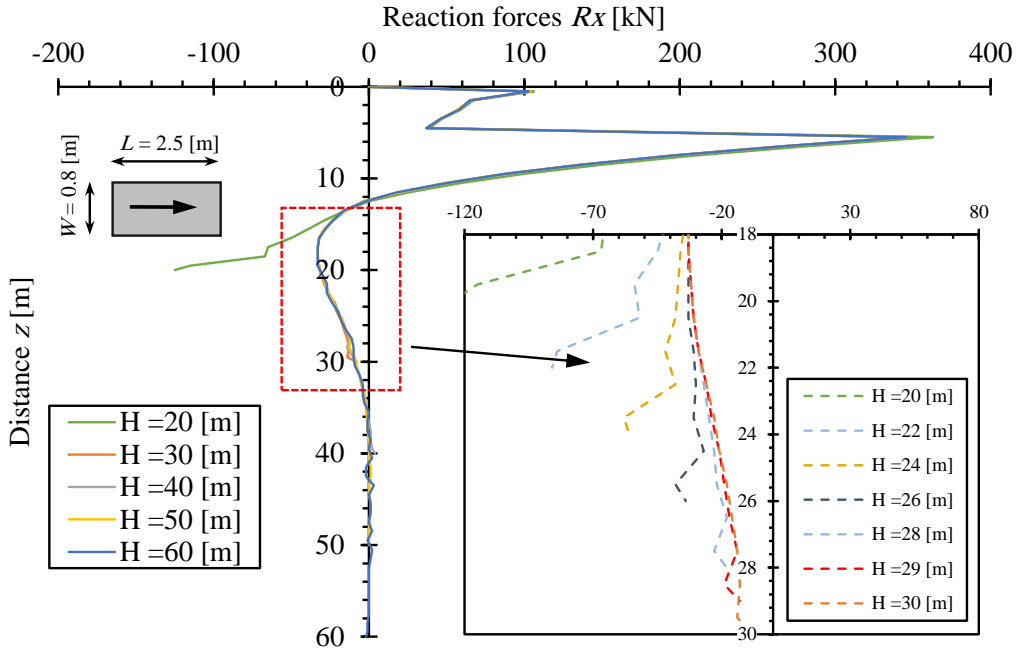


Figure 5.7 Reaction forces R_x with the barrette height (case 1).

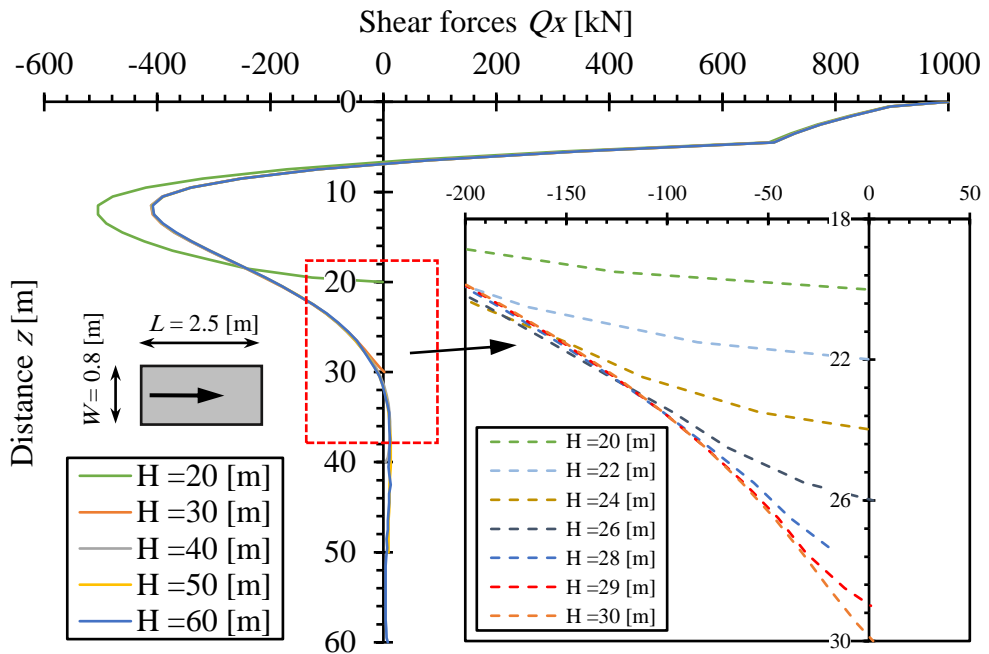


Figure 5.8 Shear forces Q_x with the barrette height (case 1).

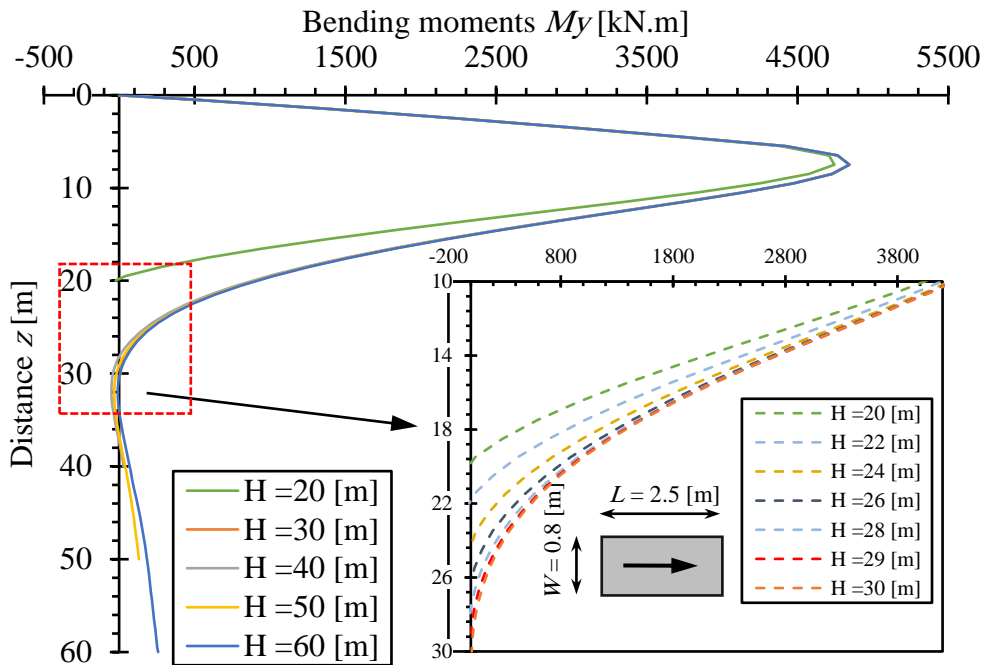


Figure 5.9 Bending moments M_y with the barrette height (case 1).

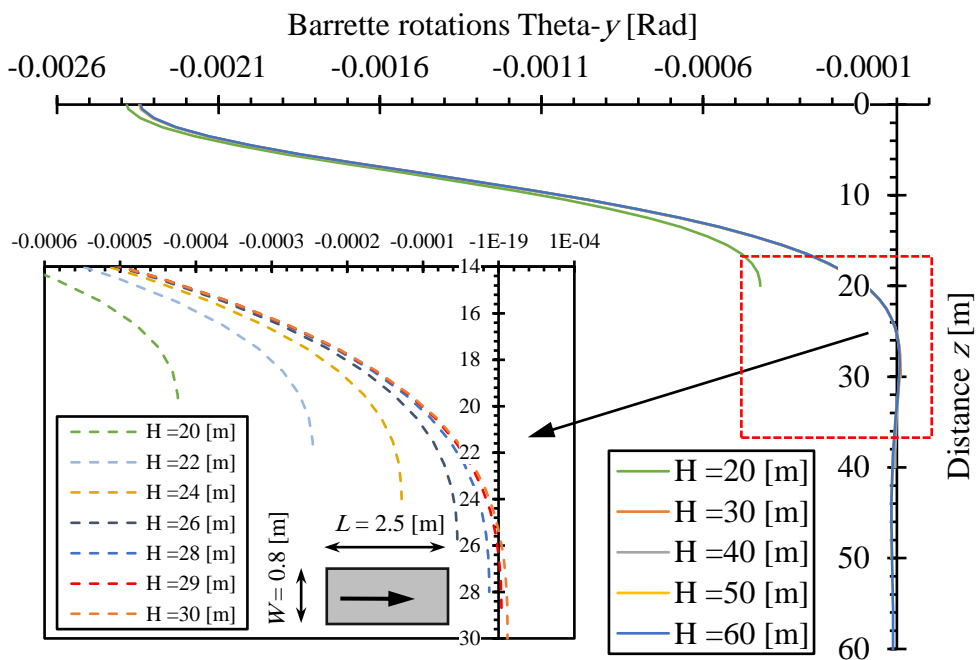


Figure 5.10 Barrette rotations Θ_{-y} with the barrette height (case 1).

5.2.4.4 Results and discussion

Figure 5.11 presents a comparison of effective-height L_e using different methods with that of the present analysis for the nine cases listed in Table 5.2, which shows that the absolute differences in results between the present hybrid-technique and both the first and second methods (1) and (2) are 23.70% to 26.63%, and 5.95% to 10.12%, respectively.

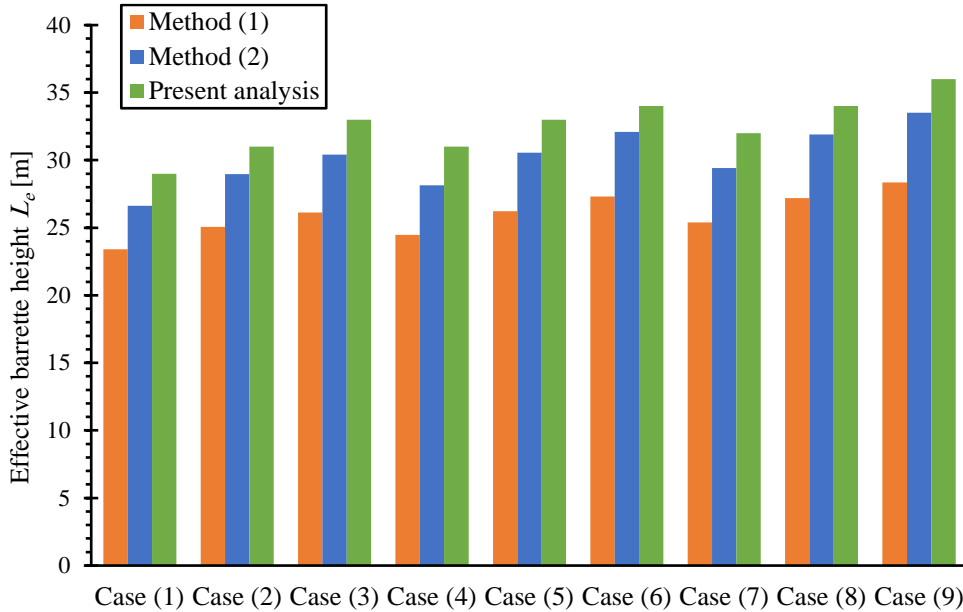


Figure 5.11 Comparison of effective barrettes height L_e .

Equations (38) and (43) for determining the effective-height of a square or a circular pile in a homogeneous soil can be modified to be used for determining the effective-height in multi-layered soil to be equations (44) and (45) for both the first and second methods.

$$H_e = 5 \times t \quad (44)$$

$$H_e = 4.8 \times \sqrt[4]{\frac{E_p I_p}{E_{seq}}} \quad (45)$$

Figure 5.12 presents a comparison of effective barrettes heights L_e using different modified methods with that of the present analysis for the nine cases listed in Table 5.2, which shows that the absolute difference between the present hybrid-technique and modified methods (1) and (2) is 0.07% to 1.62% and 0.08% to 1.99%, respectively.

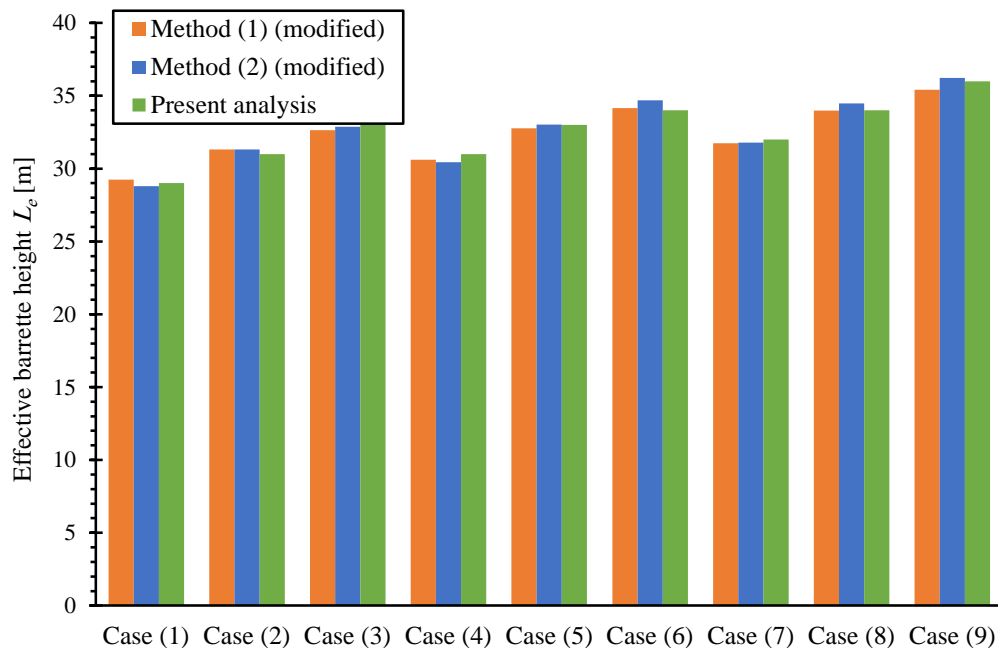


Figure 5.12 Comparison of modified effective barrettes height L_e .

From this study, it can be concluded that the behavior of laterally loaded single barrette with a height less than 20 [m] is relatively rigid. The analysis results are not influenced by increasing the barrette height to more than 40 [m]. The maximum bending moment happens at 22% to 26% of the effective barrette height.

5.2.5 The maximum bending moment and barrette head displacement

The *ECP 202* [56] equations for determining the maximum bending moment and the pile head displacement of the laterally loaded pile with free head support are used in this analysis, equations (46) and (47).

$$u_o = 2.4 \frac{P_{xo} t^3}{E_p I_p} + \frac{1.55 M_{yo} t^3}{E_p I_p} \quad (46)$$

$$M_{max} = 0.77 (P_{xo} t + M_{yo}) \quad (47)$$

Where:

E_p Modulus of elasticity of the barrette material, [kN/m²];

I_p Moment of inertia of the barrette, [m⁴];

t Elastic barrette height, [m];

P_{xo} The lateral load at the barrette head, [kN];

M_{yo} The bending moment at the barrette head, [kN.m];

u_o The barrette head displacement, [cm]; and

M_{max} The maximum bending moment along the barrette height , [kN.m].

5.2.5.1 Barrette subjected to lateral load only ($M_{y_0} = \text{Zero}$).

The maximum bending moment and barrette head displacement for each case listed in Table 5.2 is determined with M_{y_0} equal to Zero and then compared with the present analysis results and shown in Figure 5.13 and Figure 5.14.

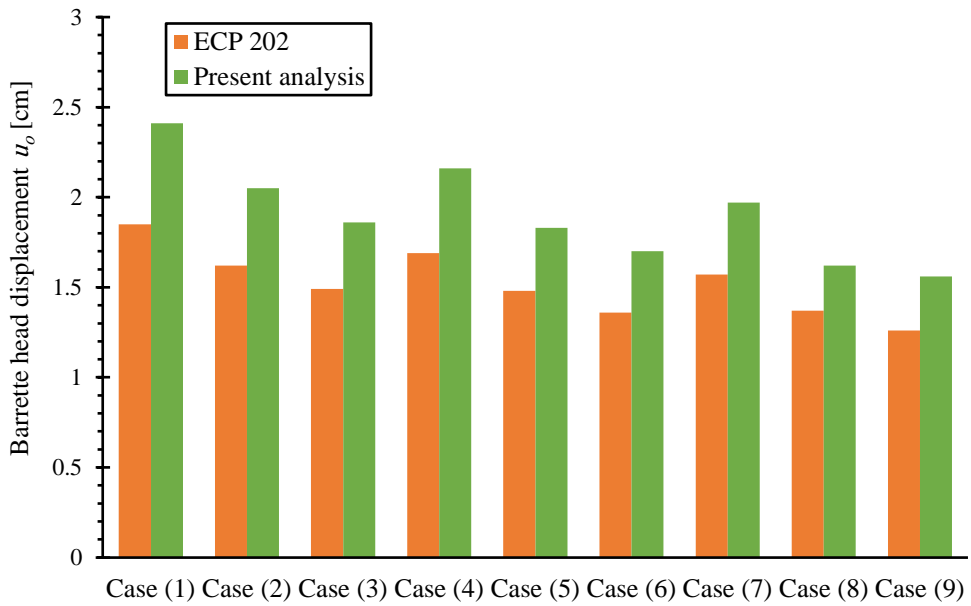


Figure 5.13 Comparison of barrette head displacement u_o ($M_{y_0} = 0$).

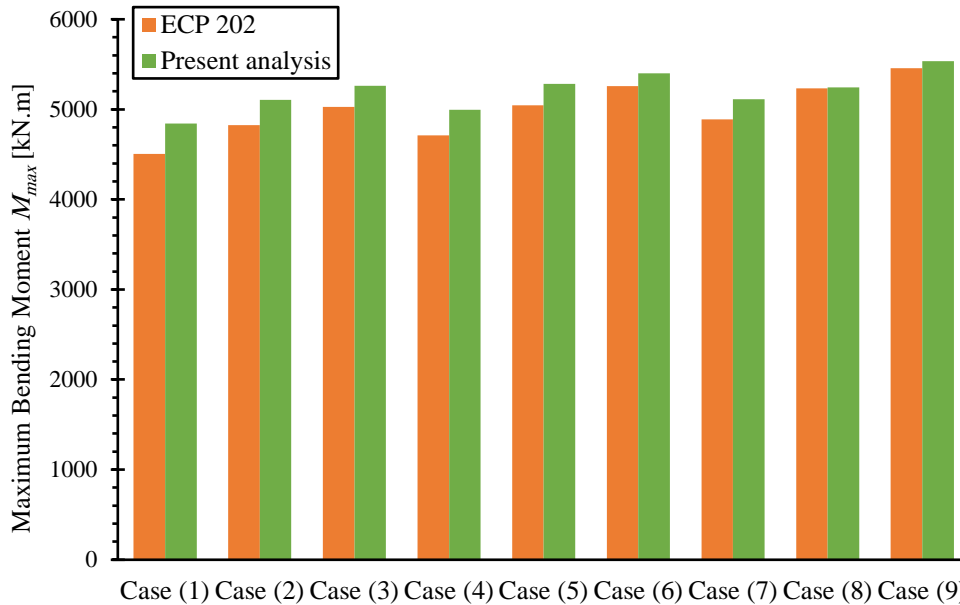


Figure 5.14 Comparison of maximum bending moment of the barrette M_{max} ($M_{yo}=0$).

Figure 5.13 and Figure 5.14 show that the absolute differences in results between the present hybrid-technique and the *ECP 202* [56] equations for determining the maximum bending moment and the pile head displacement are 0.20% to 7.48%, and 18.25% to 30.27%, respectively.

Equations (46) and (47) can be modified to be used for determining the maximum bending moment and barrette head displacement to be equations (48) and (49) when M_{yo} equal to Zero.

$$u_o = 3 \frac{P_{xo} t^3}{E_p I_p} \quad (48)$$

$$M_{max} = 0.8 (P_{xo} t) \quad (49)$$

Figure 5.15 and Figure 5.16 presents a comparison of the maximum bending moment and barrette head displacement using modified equations (48) and (49) with that of the present analysis, which shows that the absolute difference between the present hybrid-technique and modified equations is 0.64% to 3.55% for the maximum bending moment and 0.41% to 3.77% for and the barrette head displacement.

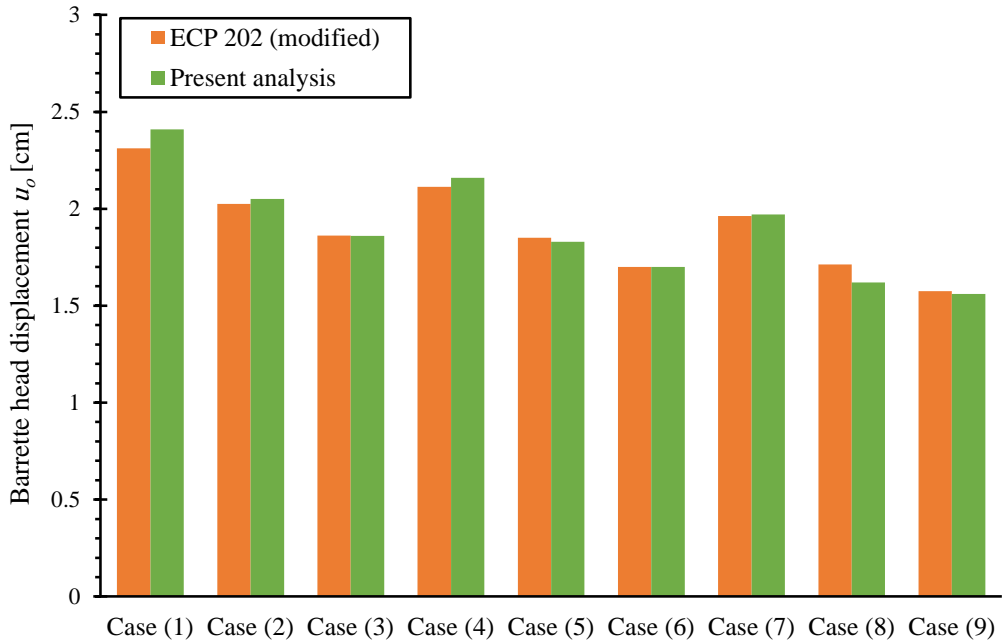


Figure 5.15 Comparison of modified barrette head displacement u_o ($M_{yo} = 0$).

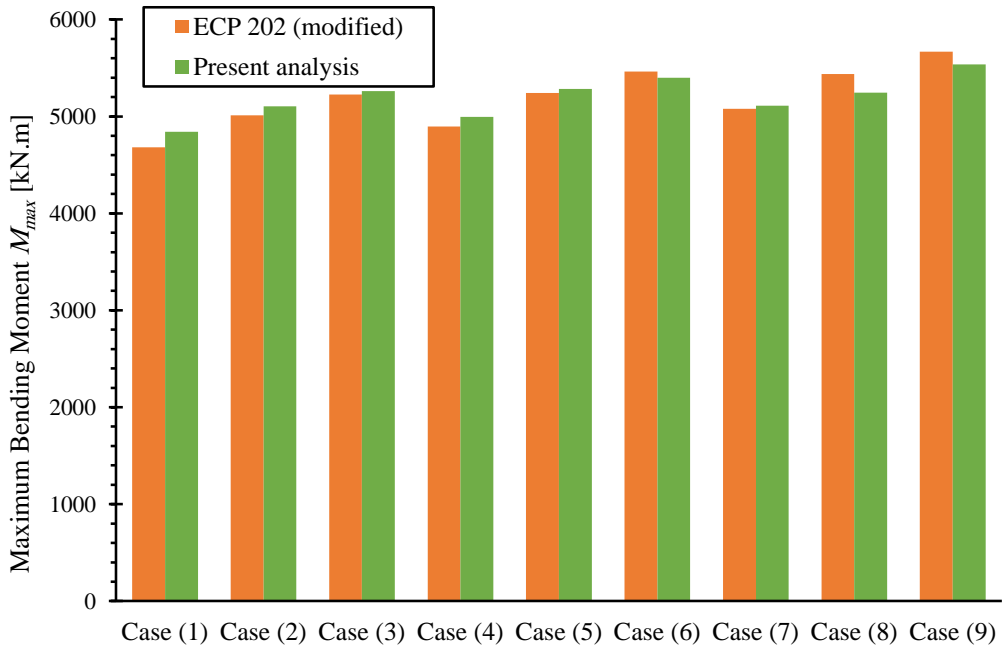


Figure 5.16 Comparison of modified maximum bending moment of the barrette M_{max} ($M_{yo} = 0$).

5.2.5.2 Barrette subjected to bending moment only ($P_{xo} = \text{Zero}$).

The barrette head displacement for each case listed in Table 5.2 is determined with P_{xo} equal to Zero and then compared with the present analysis results and shown in Figure 5.17. In this case, The maximum bending moment = M_{yo} , which is taken to be 2000 [kN.m]. It was found that the absolute difference is ranging from 18.25% to 30.27%.

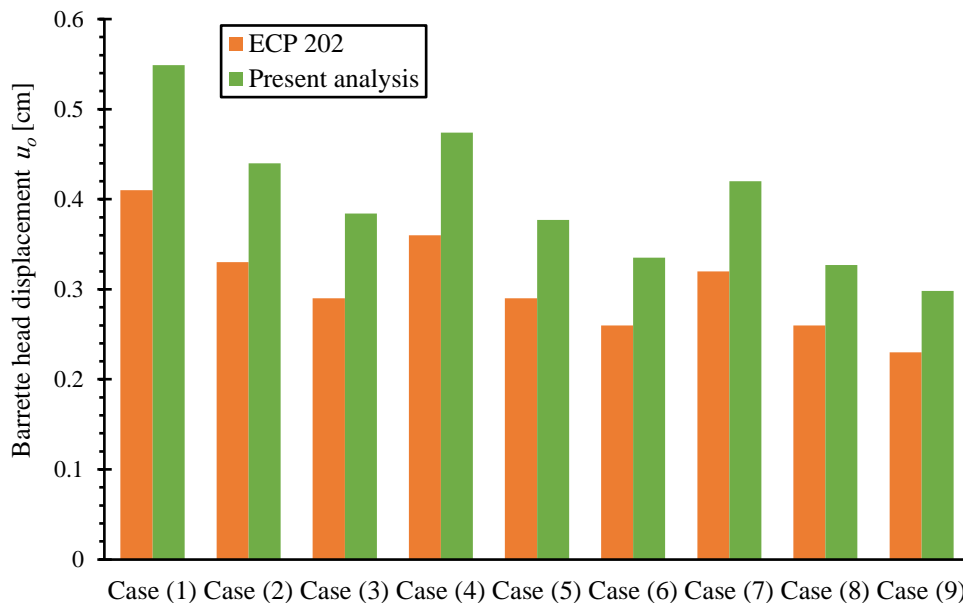


Figure 5.17 Comparison of barrette head displacement u_o ($P_{xo} = 0$).

Eq. (46) for determining the pile head displacement of a square or a circular pile with free head support can be modified to be used for determining the barrette head displacement to be eq. (56) when $P_{xo} = 0$.

$$u_o = \frac{2M_{yo}t^3}{E_p I_p} \tag{50}$$

Figure 5.18 presents a comparison of the barrette head displacement using eq. (56) with that of the present analysis for the nine cases listed in Table 5.2, which shows that the absolute difference between the present hybrid-technique and modified equation is 0.14% to 3.77% for the barrette head displacement.

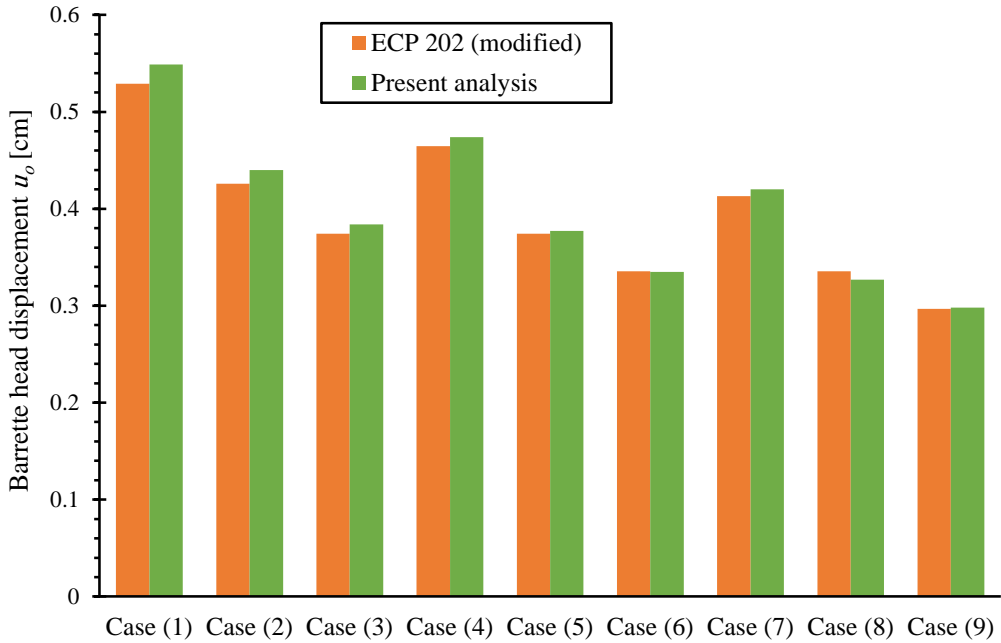


Figure 5.18 Comparison of modified barrette head displacement u_o ($P_{x0}=0$).

5.2.5.3 Barrette subjected to lateral load and bending moment.

The *ECP 202* [56] equations for determining the maximum bending moment and the pile head displacement of the laterally loaded pile with free head support equations (46) and (47) can be written as equations (51) and (52) to be used for the laterally loaded single barrette. The results using these equations are compared with those from the present analysis for the nine cases listed in Table 5.2, as shown in Figure 5.19 and Figure 5.20 where $M_{y0} = 2000$ [kN.m] and $P_{x0} = 1000$ [kN].

$$u_o = 3 \frac{P_{x0} t^3}{E_p I_p} + \frac{2M_{y0} t^3}{E_p I_p} \quad (51)$$

$$M_{max} = (0.8 P_{x0} t + M_{y0}) \quad (52)$$

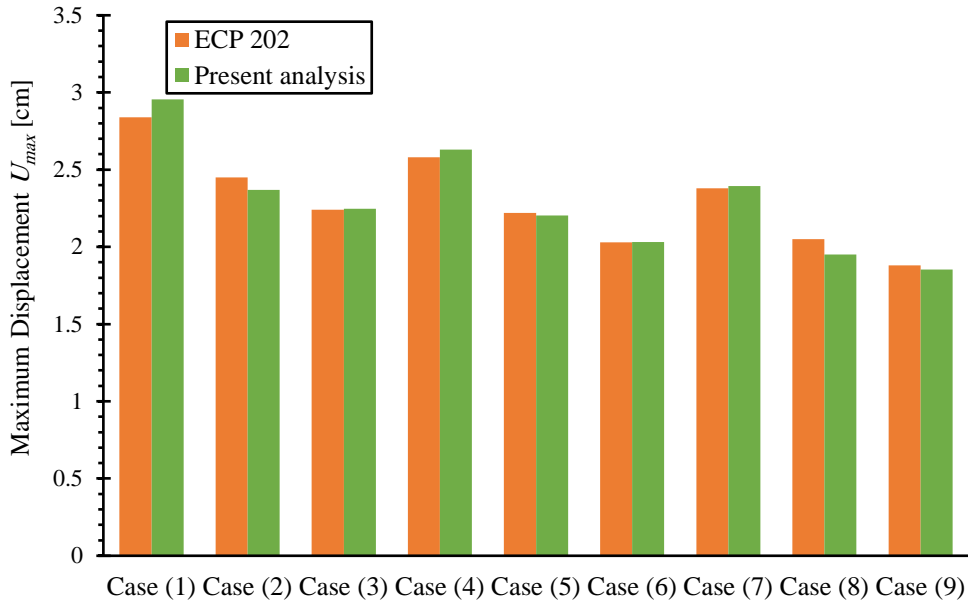


Figure 5.19 Comparison of barrette head displacement u_o .

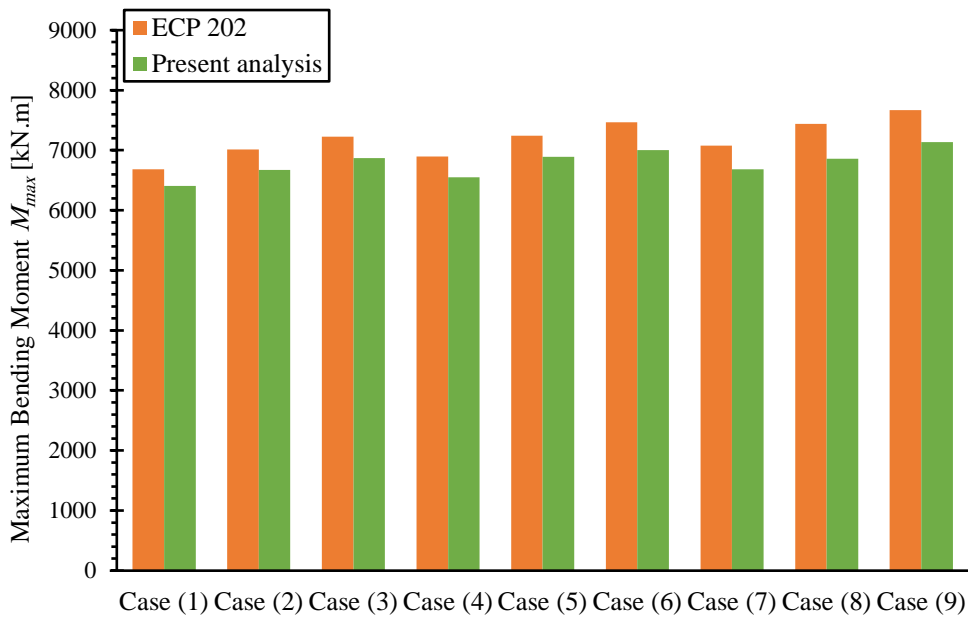


Figure 5.20 Comparison of maximum bending moment of the barrette M_{max} .

Figure 5.19 and Figure 5.20 show that absolute differences in results between the present hybrid-technique and the modified equations (51) and (52) for determining the maximum bending moment and the barrette head displacement are ranging from 0.4.13% to 7.75%, and 0.06% to 2.51%, respectively.

Eq. (52) for determining the maximum bending moment can be modified to be Eq. (53). The results using this equation are compared with those from the present analysis for the nine cases listed in Table 5.2, as shown in Figure 5.21. The absolute differences in results are decreased to be 0.06% to 2.51%.

$$M_{max} = 0.8 (P_{xo}t + M_{yo}) \quad (53)$$

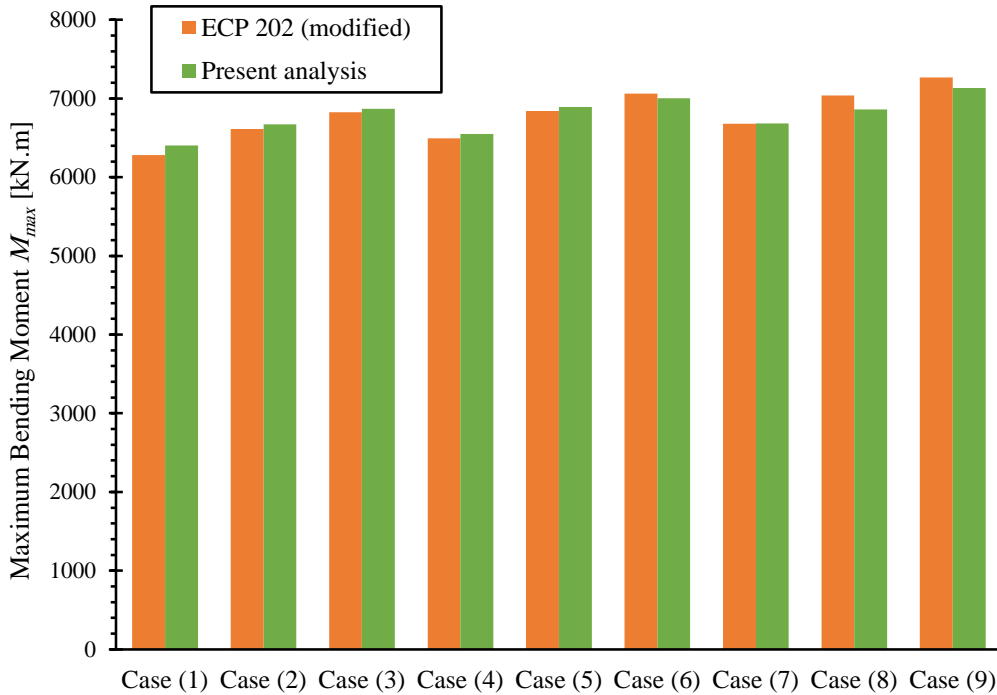


Figure 5.21 Comparison of modified maximum bending moment of the barrette M_{max} .

5.2.6 Limit barrette load

A horizontal limit load H_{lim} [kN] has been used for the nonlinear load-displacement curve. It is usually taken as a ratio of the ultimate load as *Poulos et al.* (2019) [48], it has been considered to be 0.772 as verified before in Section 4.4.

Broms equations (1964a, 1964b) [10], [11] for determining the ultimate lateral load of piles in both sand and clay are used by the *ECP 202* [56]. These equations have been checked by many researchers *Kulhawy et al.* (1995) [31], *Zhang et al.* (2005) [62], *Fleming et al.* (2008) [24], and *Russo* (2016) [52] by considering horizontal loading tests on piles, which are well documented to allow a back analysis of the results. They suggested a slightly different case of the *Broms'* method. The improvement consists simply of the adoption of the ultimate lateral load for sand presented by *Barton* (1984) [3] Eq. (54). That by

replacing *Broms* equations [10]. Equations (54) and (55) are used to determine the ultimate lateral load of piles in sand and clay, respectively.

$$H_{ult} = 0.5 K_p^2 \gamma' z^2 D \tag{54}$$

$$H_{ult} = 9 c_u z D \tag{55}$$

Where:

K_p Passive earth pressure coefficient, [-];

γ' Submerged unit weight of soil, [kN/m³];

D The diameter of the pile with the same moment of inertia, [m];

z Depth from the ground surface, [m];

c_u Undrained cohesion of clay, [kN/m²]; and

H_{ult} Ultimate lateral load, [kN].

To use these equations to determine the ultimate lateral load of single barrettes, D is taken as the diameter of the pile with the same moment of inertia. The ultimate lateral load of single barrettes H_{ult} and the horizontal limit load of single barrettes H_{lim} are calculated and listed in Table 5.11 and Table 5.12.

Table 5.11 The ultimate lateral load of the barrettes H_{ult} , [kN].

Length / Width	$L = 2.5$ [m]	$L = 2.8$ [m]	$L = 3.0$ [m]
$W = 0.8$ [m]	67130	75798	82680
$W = 1.0$ [m]	73616	83015	88934
$W = 1.2$ [m]	78428	88388	96244

Table 5.12 The horizontal limit load of the barrettes H_{lim} , [kN].

Length / Width	$L = 2.5$ [m]	$L = 2.8$ [m]	$L = 3.0$ [m]
$W = 0.8$ [m]	51824	58516	63829
$W = 1.0$ [m]	56832	64088	68657
$W = 1.2$ [m]	60546	68235	74300

5.2.7 Guideline for analyzing single barrettes

Guidelines for engineers when analyzing laterally loaded barrettes in east Port-Said or similar formations are presented. Single barrettes of different lateral loads and geometries are analyzed linearly and nonlinearly using the hyperbolic function. The limit lateral displacements for single barrettes in this analysis is taken as 5% of the barrette width B . This value is considered as an acceptable practical value for analyzing barrettes. Table 5.13 lists a summary of the analysis results. In this table, barrette loads for each case study are listed, in addition to the maximum bending moments when applying these loads. Figure 5.22 shows

the load-displacement curve according to the hyperbolic function for case 1 as an example. Other comparisons are shown in **APPENDIX (C)**.

Table 5.13 Summary results of analyzing single barrettes using nonlinear analysis.

Case	Cross-section [m ²]	Height [m]	Limit displacement [cm]	Load P_x [kN]	Max. Bending moment M_{max} [kN.m]
1	2.5 × 0.8	29	4	1610	7795
2	2.8 × 0.8	31	4	1885	9622
3	3.0 × 0.8	33	4	2078	10934
4	2.5 × 1.0	31	5	2228	11131
5	2.8 × 1.0	33	5	2627	13880
6	3.0 × 1.0	34	5	2827	15265
7	2.5 × 1.2	32	6	2896	14801
8	2.8 × 1.2	34	6	3506	18387
9	3.0 × 1.2	36	6	3665	20292

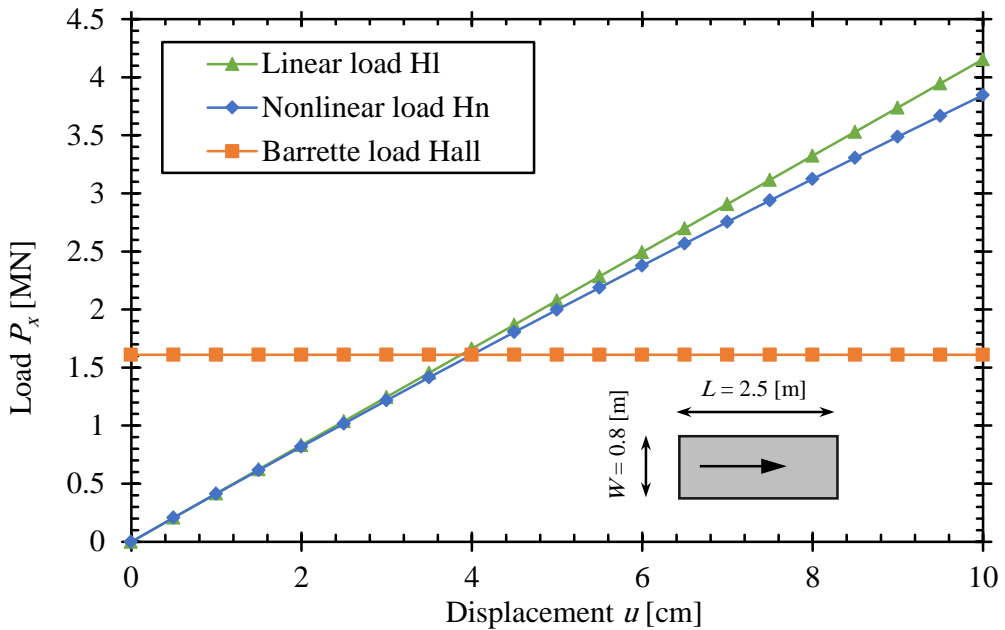


Figure 5.22 The load-displacement curve for Case (1).

5.3 Parametric Study of Single Barrettes

5.3.1 Introduction

An application of the proposed hybrid technique is used to investigate the effect of barrette width W , barrette length L , barrette height H , modulus of elasticity of the barrette material E_p , modulus of elasticity of the soil E_s , *Poisson's* ratio of the soil ν_s , and load direction α on the barrette displacement.

The effect of load direction on the displacement of a single barrette is studied. Displacements with different load directions α are compared to those of the same single barrette with load direction $\alpha = 0^\circ$. The change of displacement is expressed by displacement ratio R_s [-], which is given by Eq. (56):

$$R_s = u_s / u_0 \quad (56)$$

Where:

R_s Single barrette displacement ratio R_s , [-];

u_s Studied single barrette displacement with different load directions α , [m];
and

u_0 Single barrette displacement with load direction $\alpha = 0^\circ$, [m].

5.3.2 Material properties and parameters of interest

Table 5.14 lists groups of dimensionless parameters that are considered. A barrette width of $W = 1$ m and lateral load is taken to be that causes a barrette-head displacement equal to 5% of the barrette width W . This displacement could be an acceptable value of an allowable lateral displacement of the single barrette.

Table 5.14 Dimensionless groups of parameters used in the analysis.

Dimensionless group	Notation	Considered values
Barrette height to width ratio	H / W	10, 25, 50
Barrette length to width ratio	L / W	1.0, 1.5, 2.0, 2.5, 3.0
Barrette-soil elasticity ratio	E_p / E_s	1000, 2000, 3000, 4000, 5000
<i>Poisson's</i> ratio of the soil	ν_s	0.1, 0.2, 0.3, 0.4, 0.5
Load direction	α	$0^\circ, 22.5^\circ, 45^\circ, 67.5^\circ, 90^\circ$

5.3.3 Results and discussion

5.3.3.1 Effect of load direction, Barrette length to width ratio, and Barrette - soil elasticity ratio

Figure 5.23 to Figure 5.27 presents the evolution of the displacement ratio R_s as a function of the load direction α for various barrette length to width ratios L/W , load direction α , and barrette-soil elasticity ratios E_p/E_s , as listed in Table 5.14.

The barrette height to width ratio $H/W = 25$ [-] and *Poisson's* ratio of the soil $\nu_s = 0.3$ [-]. The increasing displacement ratio R_s with increasing load direction α are shown according to the previously mentioned comments. The displacement ratio increases as L/W increases, load direction increases, and E_p/E_s decreases, where barrettes become stiffer. Except for the square barrette (pile), the displacement ratio will be constant while increasing the load direction.

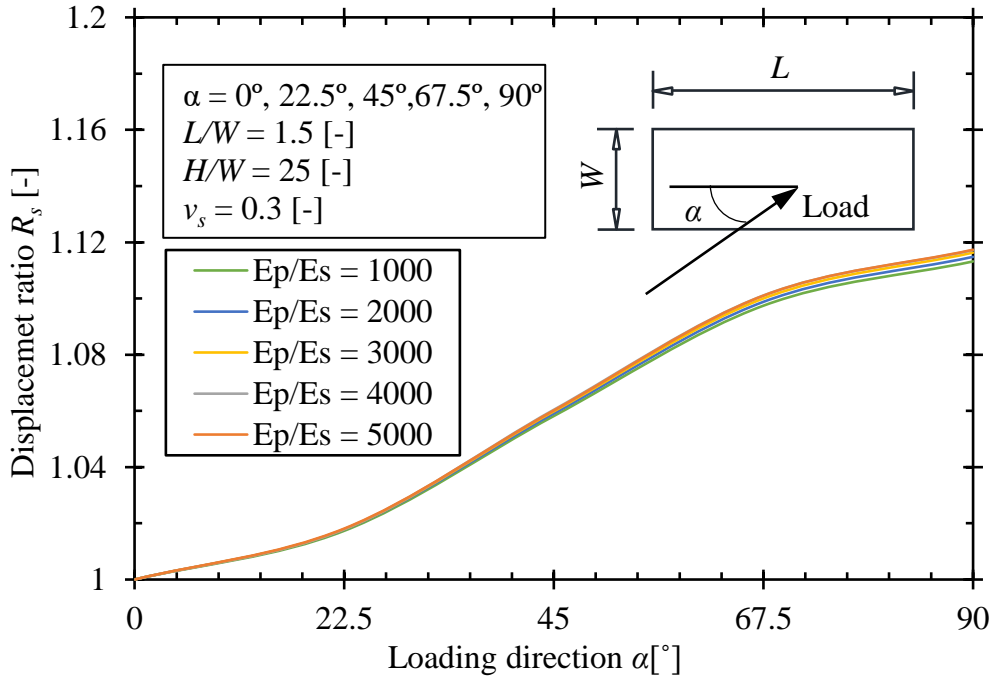


Figure 5.23 The displacement ratio R_s for $L/W = 1.5$ [-].

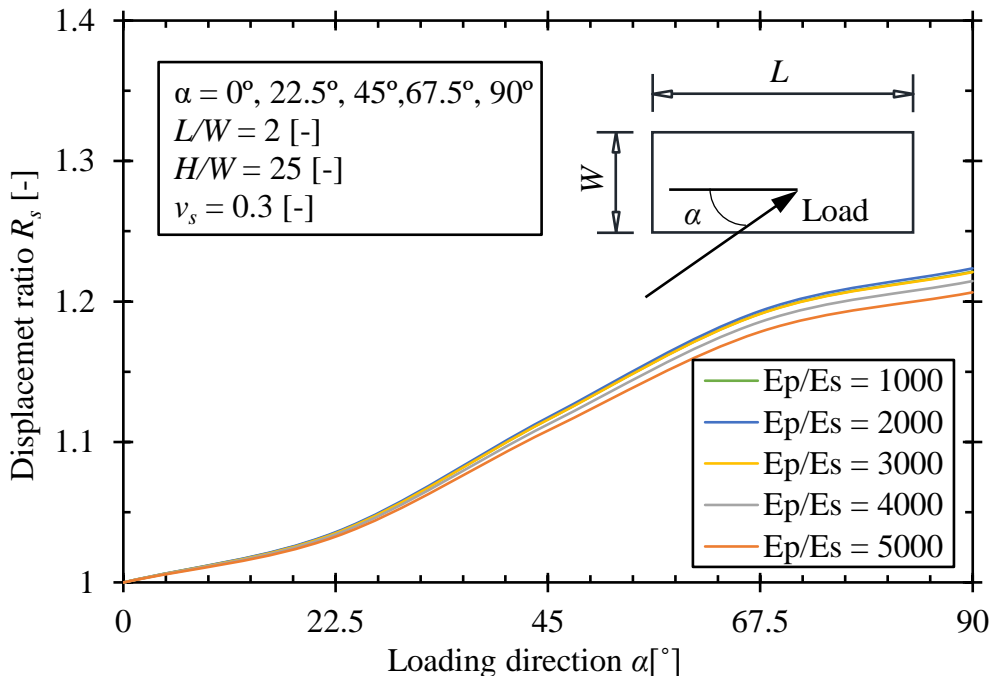


Figure 5.24 The displacement ratio R_s for $L/W = 2.0$ [-].

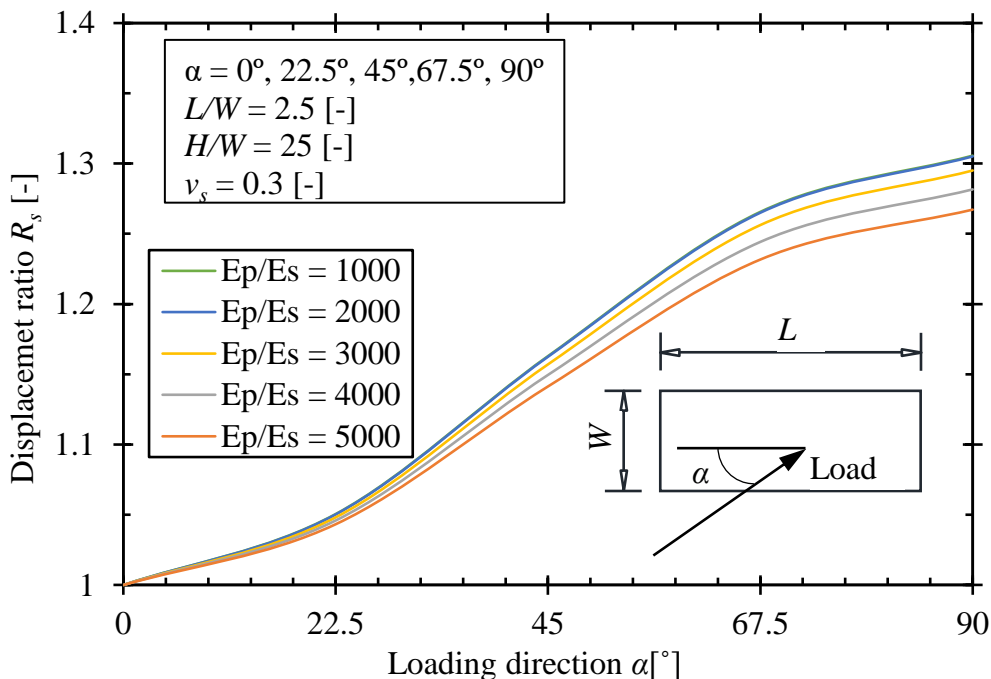


Figure 5.25 The displacement ratio R_s for $L/W = 2.5$ [-].

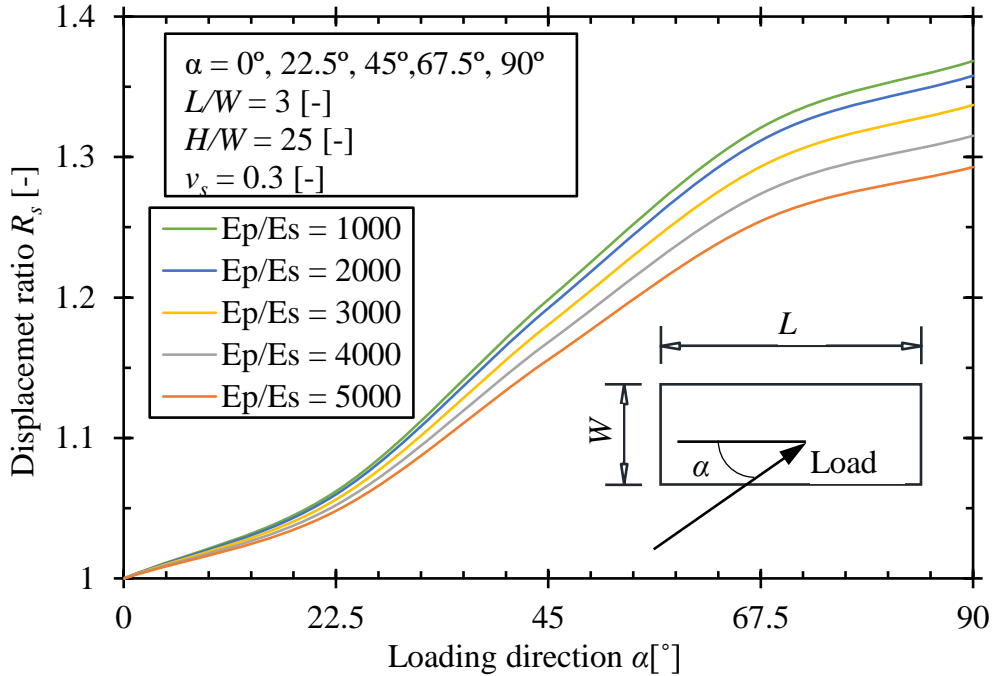


Figure 5.26 The displacement ratio R_s for $L/W = 3.0$ [-].

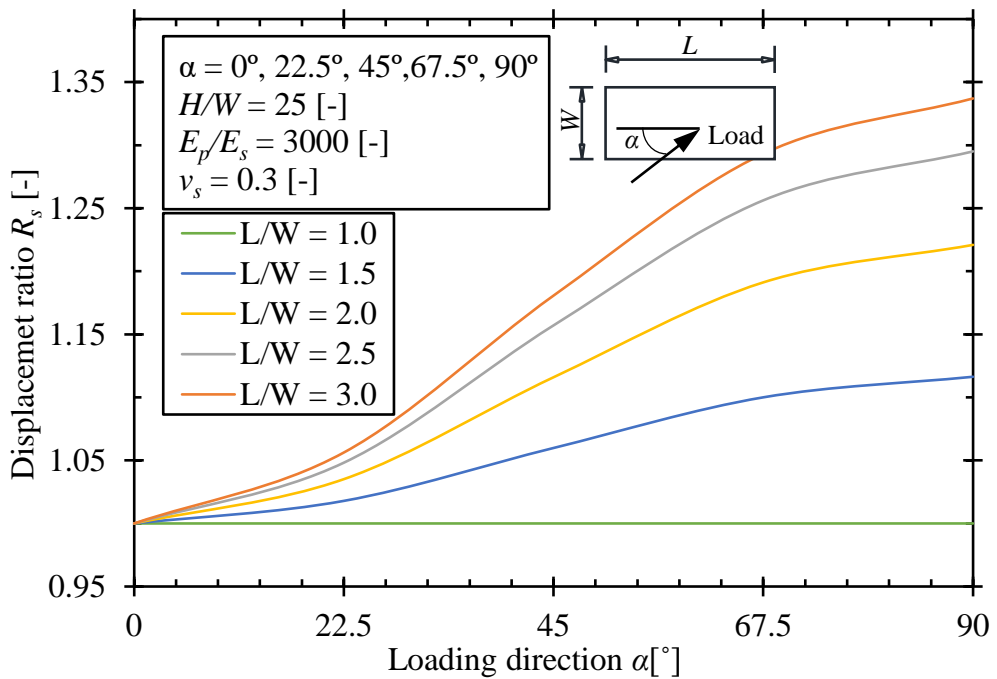


Figure 5.27 The displacement ratio R_s for various barrette L/W .

5.3.3.2 Effect of Poisson's ratio of the soil

Figure 5.28 presents the evolution of the displacement ratio R_s as a function of the load direction α for various Poisson's ratio of the soil and load direction α , as listed in Table 5.14. The barrette length to width ratios $L/W = 2.0$ [-], barrette height to width ratio $H/W = 25$ [-] and barrette-soil elasticity ratios $E_p/E_s = 3000$ [-]. The increasing displacement ratio R_s with increasing load direction α are shown according to the previously mentioned comments. The displacement ratio decreases with increasing Poisson's ratio of the soil ν_s .

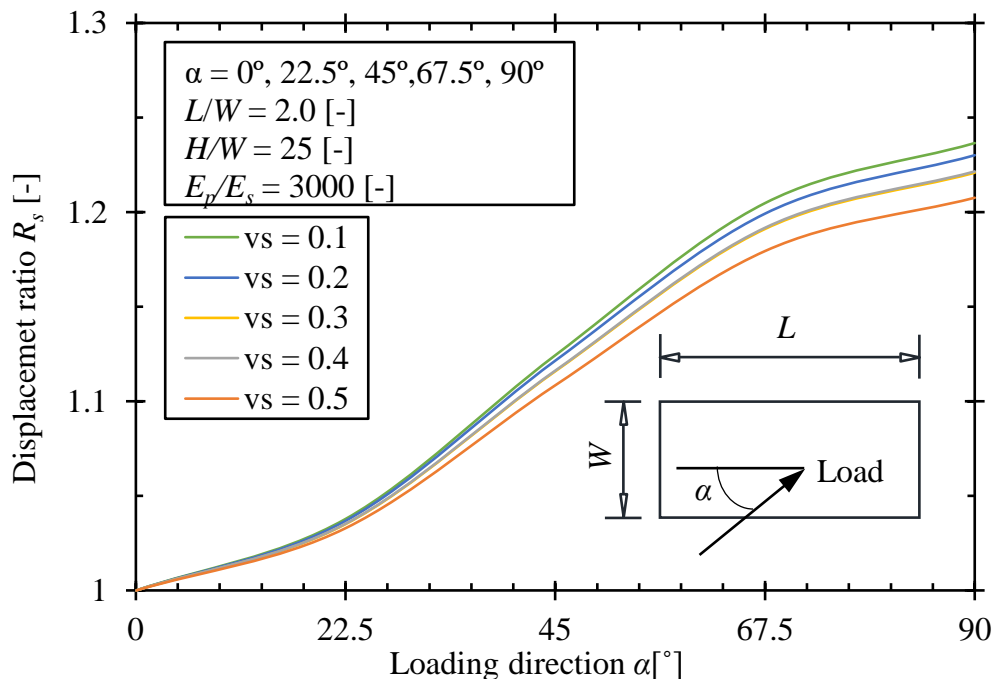


Figure 5.28 The displacement ratio R_s for the effect of ν_s .

5.3.3.3 Effect of barrette height to width ratio

Figure 5.29 presents the evolution of the displacement ratio R_s as a function of the load direction α for various barrette height to width ratio H/W and load directions α , as listed in Table 5.14. The barrette length to width ratios $L/W = 2.0$ [-], barrette-soil elasticity ratios $E_p/E_s = 3000$ [-] and Poisson's ratio of the soil $\nu_s = 0.3$ [-]. The increasing displacement ratio with increasing load direction α is shown according to the previously mentioned comments. Although the displacement ratio R_s decreases with decreasing the barrette height to width ratio H/W , where the barrette becomes more rigid, increasing the barrette height to width ratio H/W more than 30 has a very small effect, where the barrette height is reached to the effective-height of the barrette.

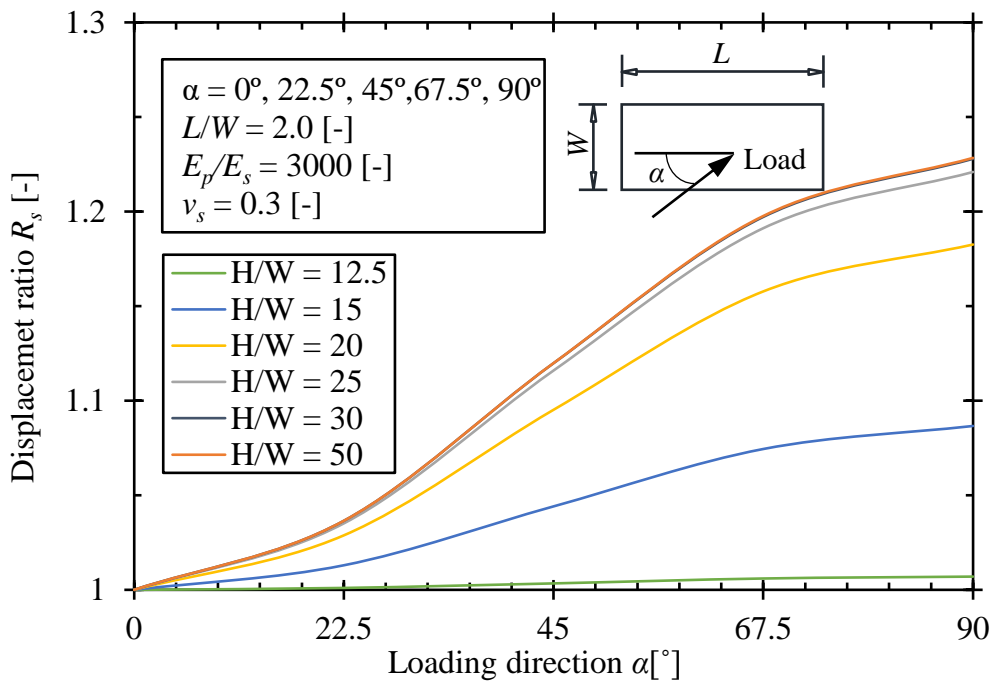


Figure 5.29 The displacement ratio R_s for the effect of H/W .

5.4 Parametric Study of Barrette Groups

5.4.1 Introduction

An application of the proposed hybrid technique is used to investigate the effect of barrette width W , barrette length L , barrette height H , barrette spacing S , number of barrettes, modulus of elasticity of the barrette material E_p , Modulus of elasticity of the soil E_s , *Poisson's* ratio of the soil ν_s , and load direction α on the barrette group displacement.

Two barrettes are considered in this study to investigate the lateral load effect on the barrette group displacement, as shown in [Figure 5.30](#).

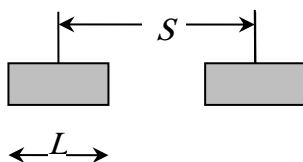


[Figure 5.30](#) The geometry of two barrettes as a barrette group.

The group effect is illustrated by studying the ratio between the barrette group displacements to that of a single barrette. The group effect is expressed by displacement ratio R_g [-], which is given by [Eq. \(57\)](#):

$$R_g = u_g / u_s \quad (57)$$

Where:

R_g Barrette group displacement ratio R_g , [-];

u_g Studied barrette group displacement, [m]; and

u_s Single barrette displacement, [m].

5.4.2 Material properties and parameters of interest

[Table 5.15](#) lists groups of dimensionless parameters that are considered. A barrette width of $W = 1$ m and lateral load is taken to be that causes a barrette-head displacement equal to 5% of the barrette width W . This displacement could be an acceptable value of an allowable lateral displacement of the single barrette.

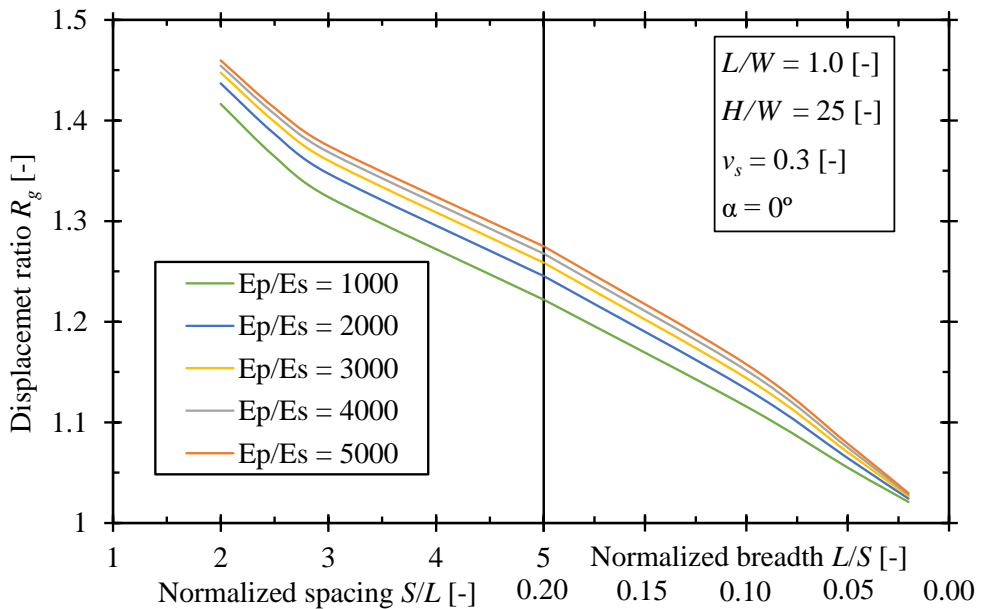
Table 5.15 Dimensionless groups of parameters used in the analysis.

Dimensionless group	Notation	Considered values
Barrette spacing ratio	S / L	2, 2.5, 3, 5, 10, 20, 50
Barrette breadth ratio	L / S	0.5, 0.4, 0.33, 0.2, 0.1, 0.05, 0.02
Barrette height to width ratio	H / W	10, 25, 50
Barrette length to width ratio	L / W	1.0, 1.5, 2.0, 2.5, 3.0
Barrette-soil elasticity ratio	E_p / E_s	1000, 2000, 3000, 4000, 5000
<i>Poisson's</i> ratio of the soil	ν_s	0.1, 0.2, 0.3, 0.4, 0.5
Load direction	α	0° , 22.5° , 45° , 67.5° , 90°
Number of barrettes	-	2, 3, 4

5.4.3 Results and discussion

5.4.3.1 Effect of Barrette spacing, Barrette length to width ratio, and Barrette - soil elasticity ratio

Figure 5.31 to Figure 5.36 presents the evolution of the displacement ratio R_g as a function of the spacing between barrettes for various barrette length to width ratios L/W and barrette-soil elasticity ratios E_p/E_s , as listed in Table 5.15. The barrette height to width ratio $H/W = 25$ [-], load direction $\alpha = 0^\circ$, and *Poisson's* ratio of the soil $\nu_s = 0.3$ [-]. The displacement ratio R_g decrease with increasing the normalized center to center distance between barrettes S/L , as shown according to the previously mentioned comments. The displacement ratio R_g decreases as L/W increases and E_p/E_s decreases, where barrettes become stiffer.

**Figure 5.31** The displacement ratio R_g for $L/W = 1.0$ [-].

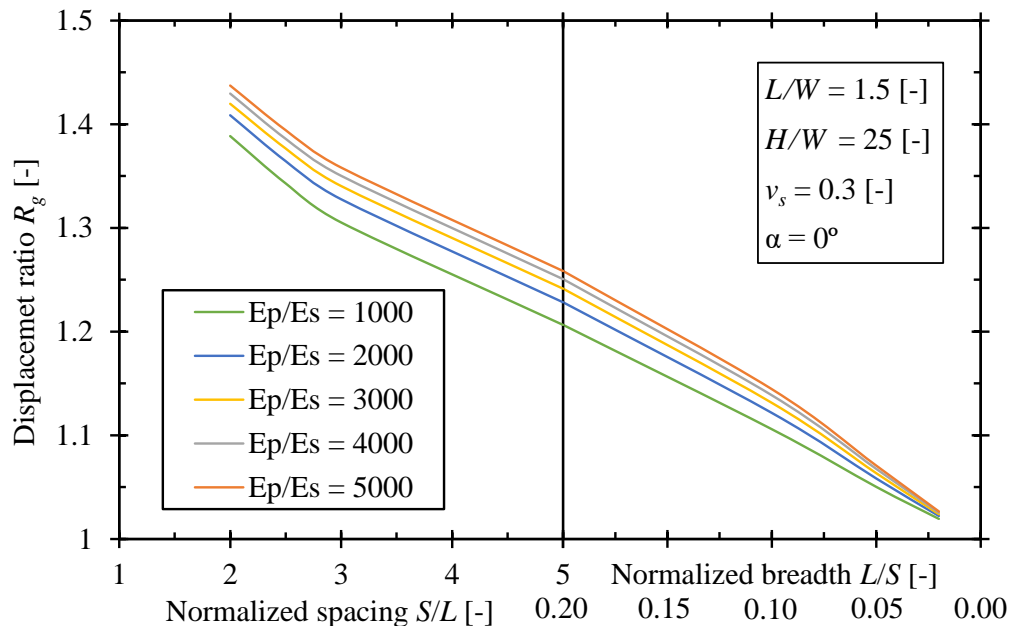


Figure 5.32 The displacement ratio R_g for $L/W = 1.5$ [-].

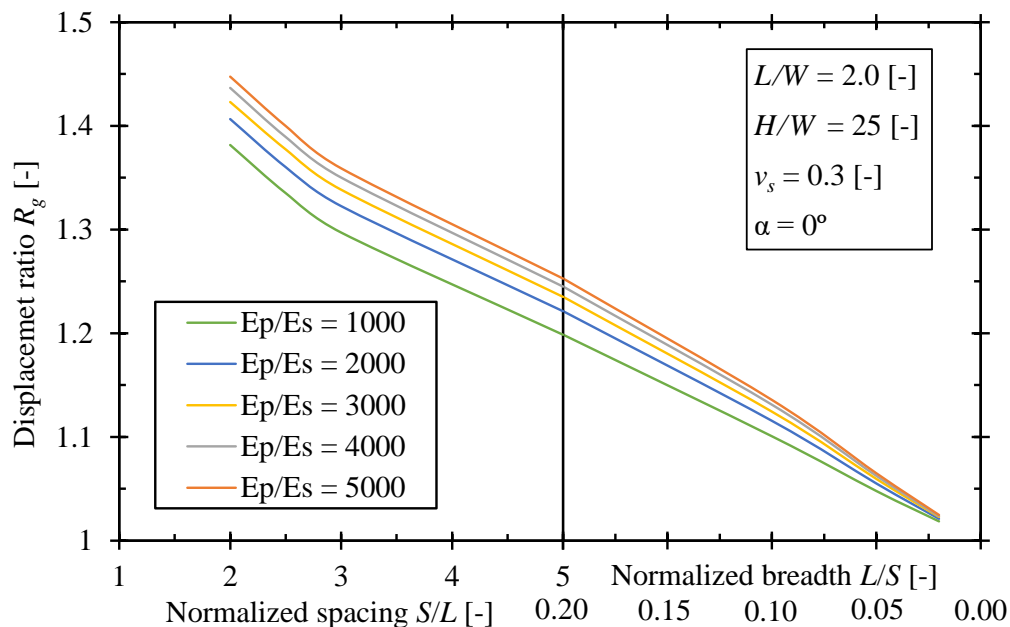


Figure 5.33 The displacement ratio R_g for $L/W = 2.0$ [-].

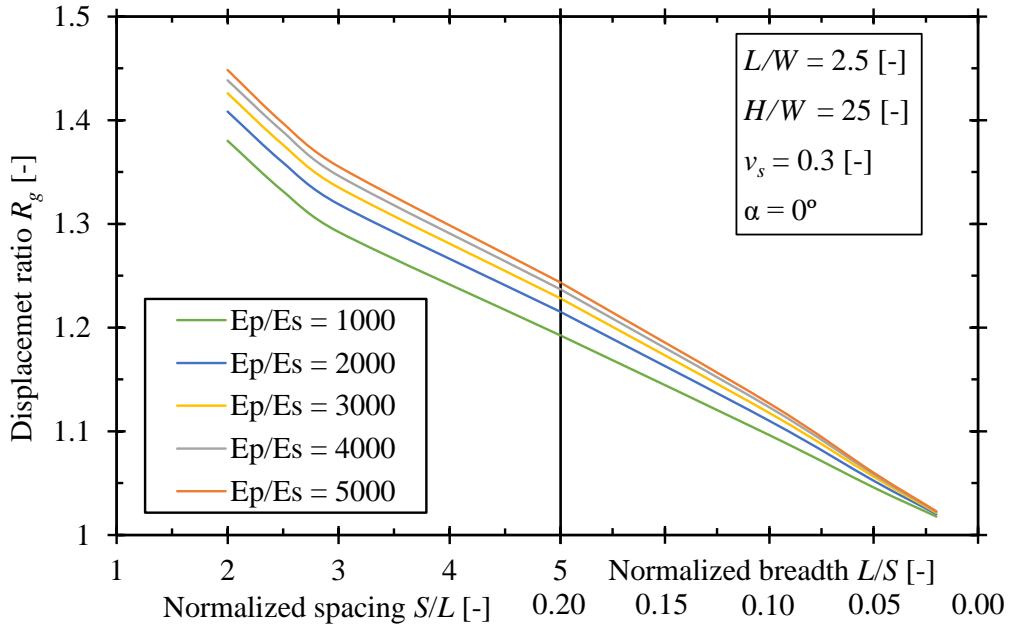


Figure 5.34 The displacement ratio R_g for $L/W = 2.5$ [-].

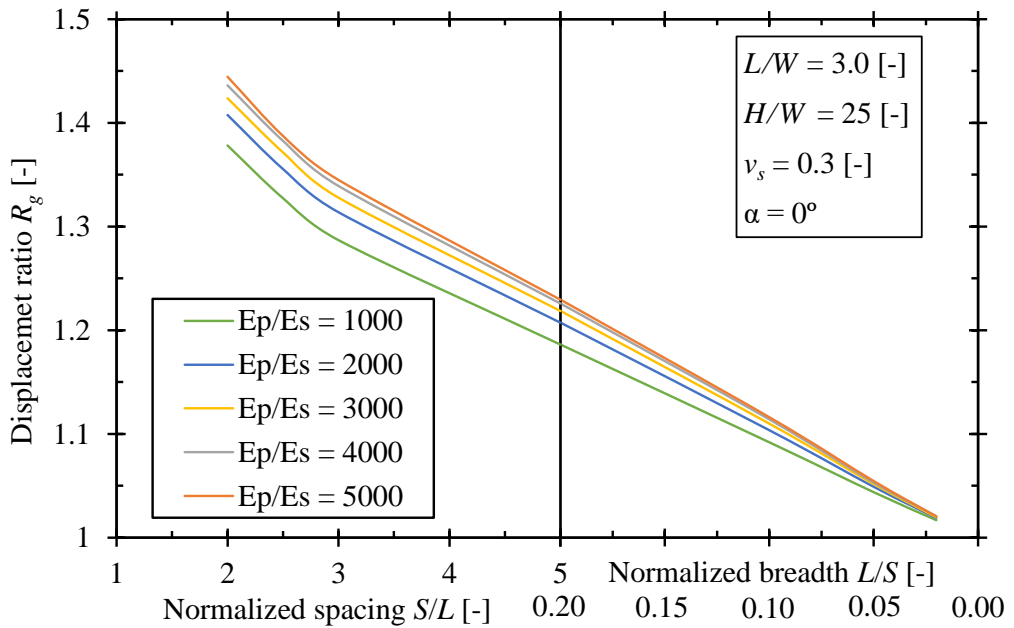


Figure 5.35 The displacement ratio R_g for $L/W = 3.0$ [-].

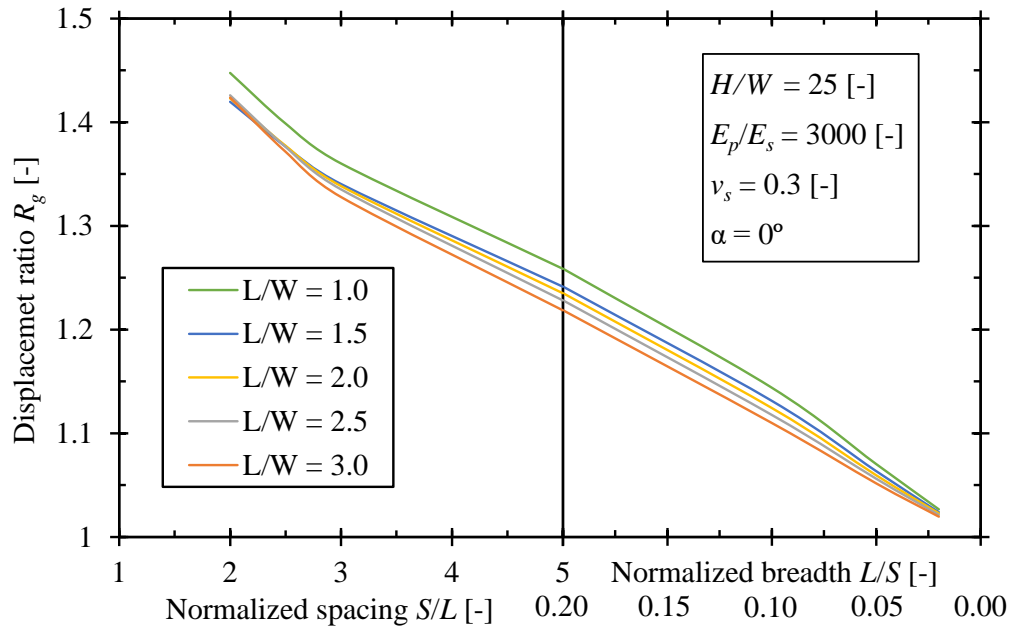


Figure 5.36 The displacement ratio R_g with various L/W .

5.4.3.2 Effect of Poisson's ratio of the soil

Figure 5.37 presents the evolution of the displacement ratio R_g as a function of the normalized center to center distance between barrettes S/L for various Poisson's ratio of the soil, as listed in Table 5.15. The barrette length to width ratios $L/W = 2.0$ [-], barrette height to width ratio $H/W = 25$ [-], barrette-soil elasticity ratios $E_p/E_s = 3000$ [-], and load direction $\alpha = 0^\circ$. The displacement ratio R_g decrease with increasing the normalized center to center distance between barrettes S/L , as shown according to the previously mentioned comments. The displacement ratio R_g decreases as Poisson's ratio of the soil ν_s decreases.

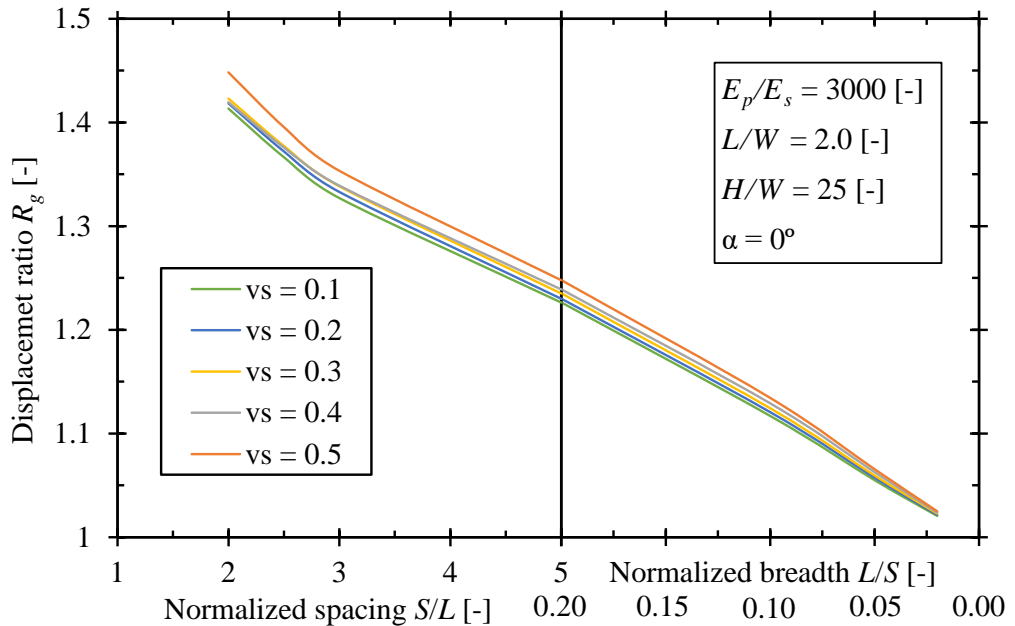


Figure 5.37 The displacement ratio R_g for the effect of ν_s .

5.4.3.3 Effect of barrette height to width ratio

Figure 5.38 presents the evolution of the displacement ratio R_g as a function of the normalized center to center distance between barrettes S/L for various barrette height to width ratio H/W , as listed in Table 5.15. The barrette length to width ratios $L/W = 2.0$ [-], load direction $\alpha = 0^\circ$, barrette-soil elasticity ratios $E_p/E_s = 3000$ [-], and Poisson's ratio of the soil $\nu_s = 0.3$ [-]. The displacement ratio R_g decrease with increasing the normalized center to center distance between barrettes S/L , as shown according to the previously mentioned comments. Although the displacement ratio R_g decreases with decreasing the barrette height to width ratio H/W , where the barrettes become more rigid, increasing the barrette height to width ratio H/W more than 30 has a very small effect, where barrettes height are reached to the effective-height of the barrette.

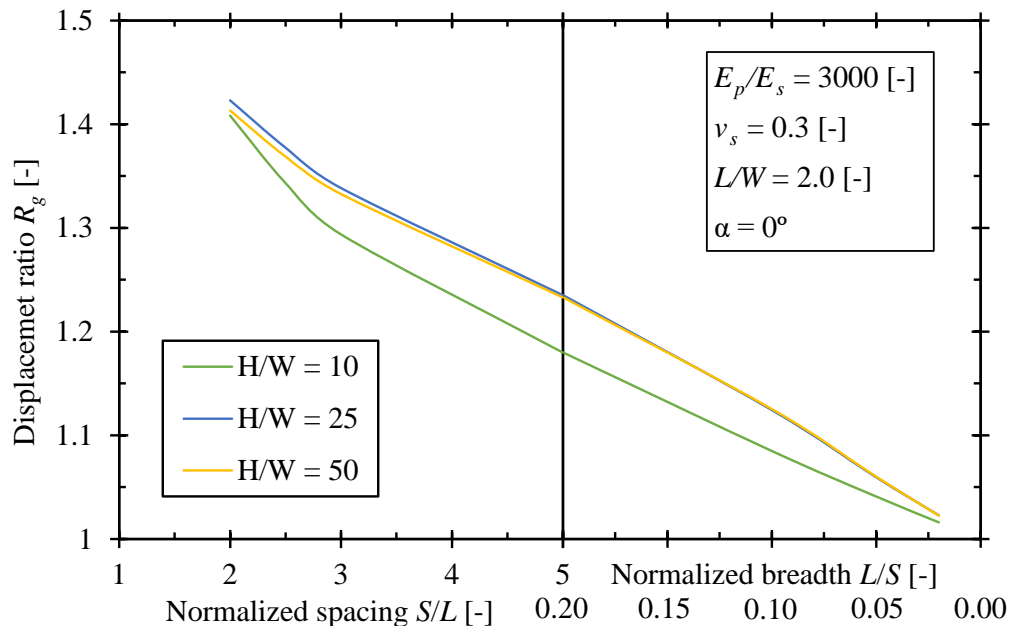


Figure 5.38 The displacement ratio R_g for the effect of H/W .

5.4.3.4 Effect of numbers of barrettes

The groups of three and four barrettes are considered to study the effect of the number of barrettes, as shown in Figure 5.39 and Figure 5.40.

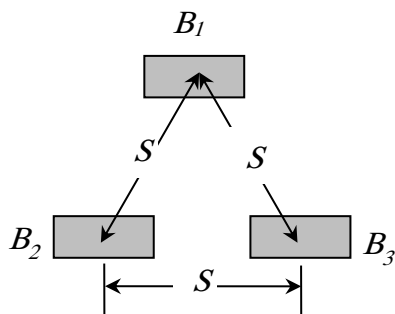


Figure 5.39 The groups of three barrettes.

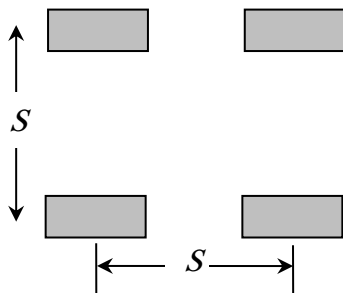


Figure 5.40 The groups of four barrettes.

Figure 5.41 presents the evolution of the displacement ratio R_g as a function of the normalized center to center distance between barrettes S/L for a various number of barrettes, as shown in Figure 5.39 and Figure 5.40, and listed in Table 5.15. The barrette length to width ratios $L/W = 2.0$ [-], barrette height to width ratio $H/W = 25$ [-], load direction $\alpha = 0^\circ$, barrette-soil elasticity ratios $E_p/E_s = 3000$ [-], and *Poisson's* ratio of the soil $\nu_s = 0.3$ [-]. The displacement ratio R_g decrease with increasing the normalized center to center distance between barrettes S/L , as shown according to the previously mentioned comments. The displacement ratio R_g decreases with decreasing the number of barrettes in the barrette group.

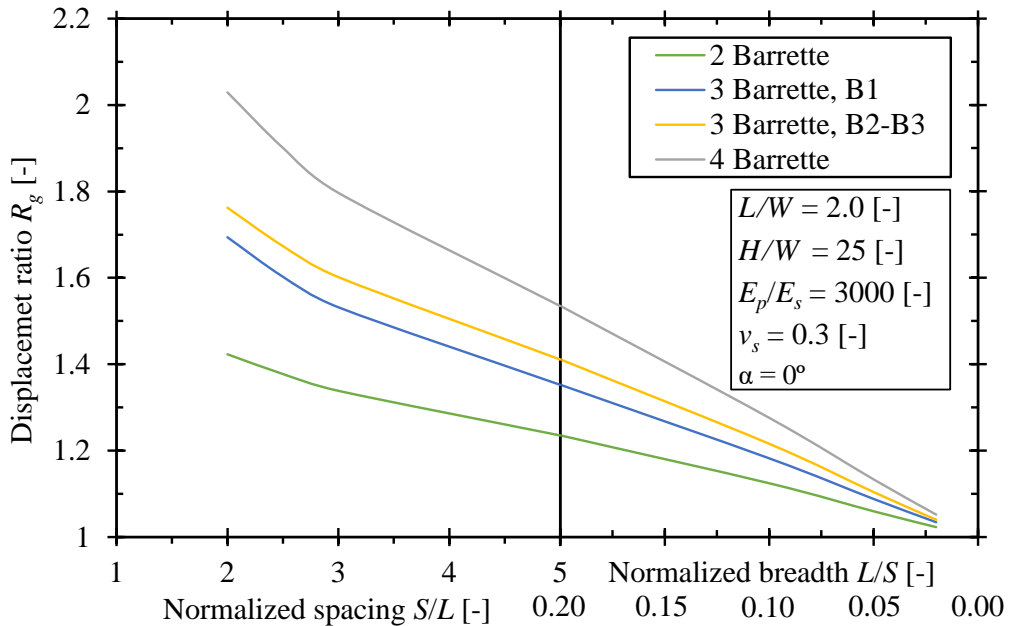


Figure 5.41 The displacement ratio R_g for the effect of barrettes number.

5.4.3.5 Effect of load direction

Finally, Figure 5.42 to Figure 5.45 present the evolution of the displacement ratio R_g as a function of the normalized center to center distance between barrettes S/L for various load direction α and a various number of barrettes, as listed in Table 5.15. The barrette height to width ratio $H/W = 25$ [-], the barrette length to width ratios $L/W = 2.0$ [-], the barrette - soil elasticity ratios $E_p/E_s = 3000$ [-] and *Poisson's* ratio of the soil $\nu_s = 0.3$ [-]. The displacement ratio R_g decreases with increasing center to center of barrettes distance, as shown according to the previously mentioned comments. The displacement ratio R_g decreases as load direction increases.

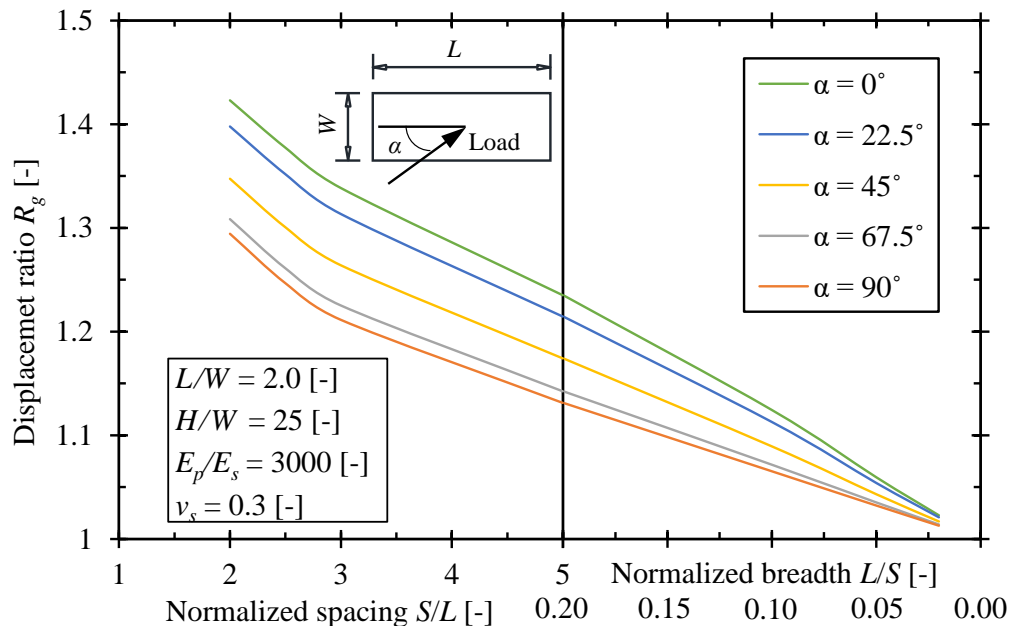


Figure 5.42 The displacement ratio R_g for the effect of α , Group of 2 barrettes.

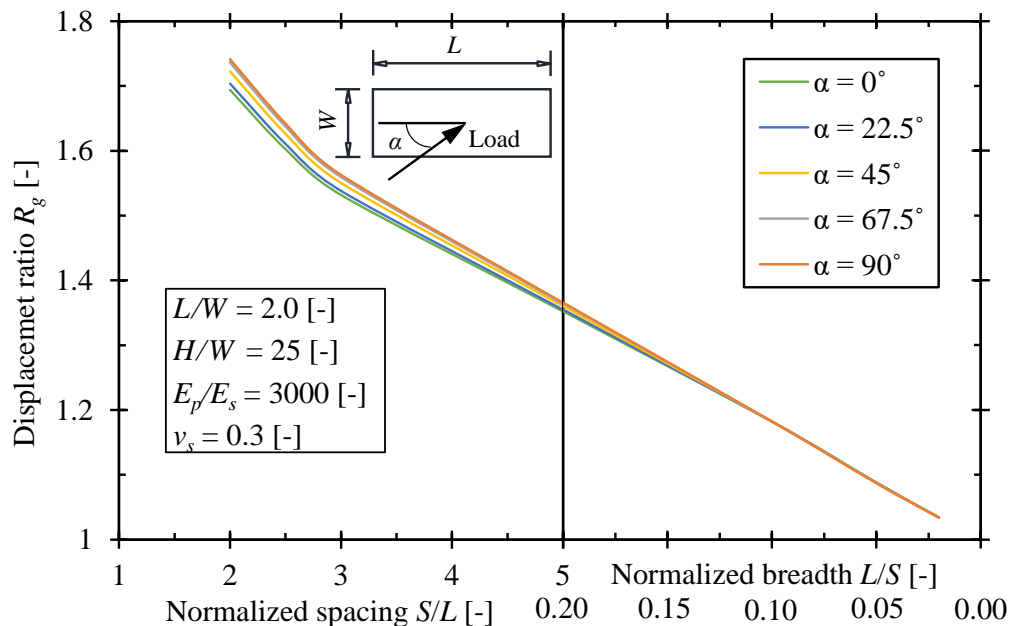


Figure 5.43 The displacement ratio R_g for the effect of α , Group of 3 barrettes, B1.

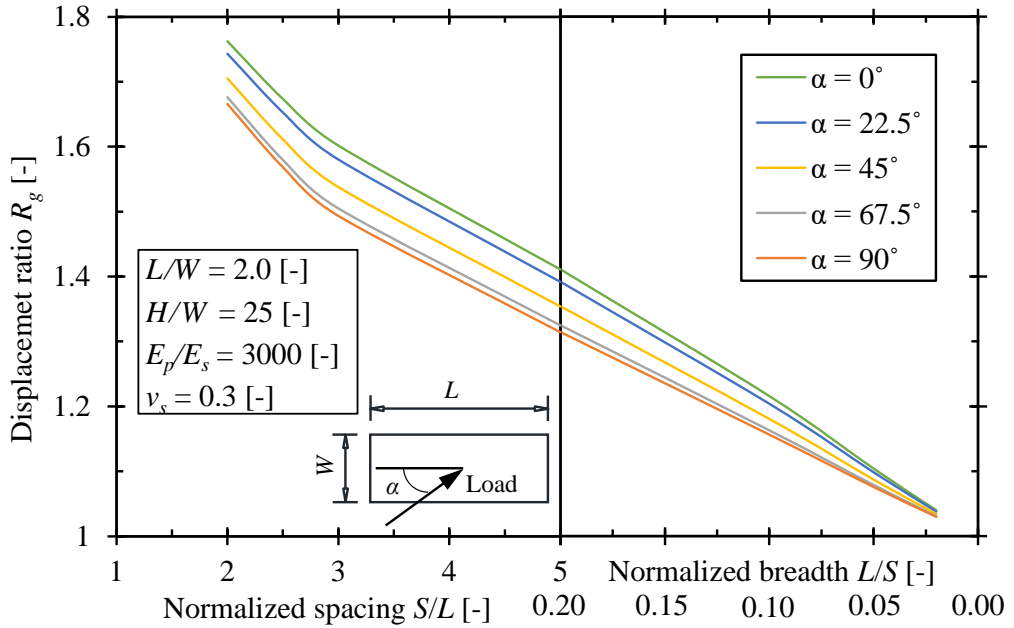


Figure 5.44 The displacement ratio R_g for the effect of α , Group of 3 barrettes, B2&B3.

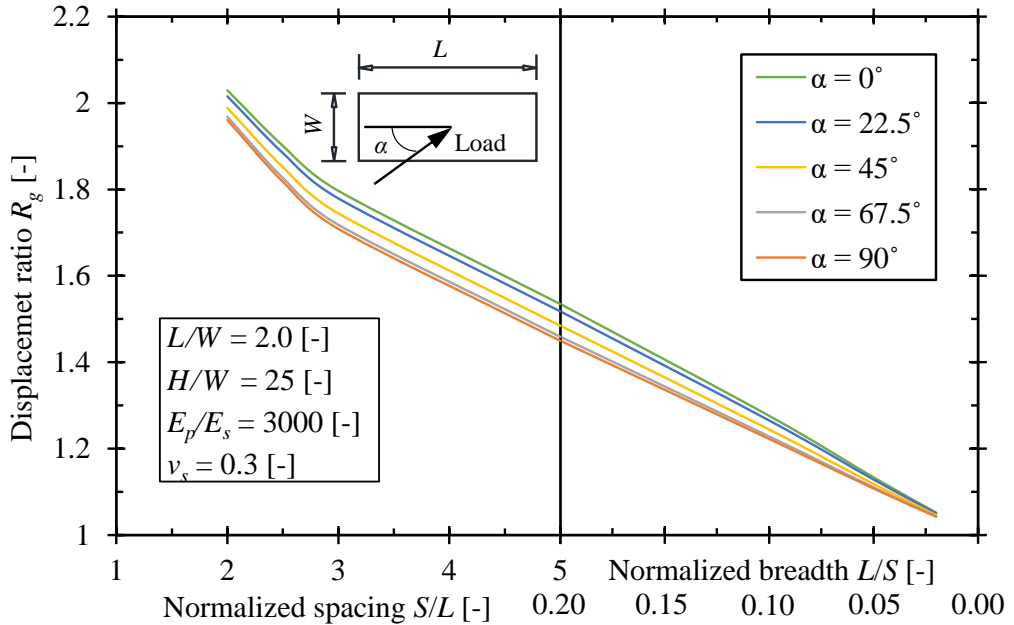


Figure 5.45 The displacement ratio R_g for the effect of α , Group of 4 barrettes.

CHAPTER 6

6 CONCLUSIONS AND RECOMMENDATIONS

6.1 Summary

Most researches on barrettes were performed using three-dimensional finite element methods. While this technique considered the full interactions between barrettes and the surrounding soil, it leads to a huge-stiffness matrix. Therefore, large-systems of equations have to be solved. Consequently, this analysis is time consuming even for the fast computers of today. Methods for analyzing piles are used to simplify this problem. In those methods, barrettes are treated as piles with an equivalent cross-sectional area. The disadvantage of using these methods in barrettes analyses is that the three-dimensional natural geometry of barrettes and soil was neglected.

In this thesis, a numerical technique for analyzing vertically loaded barrettes previously presented by the author (2016) [18] is extended to analyze laterally loaded single barrettes and barrette groups. The full three-dimensional interactions between barrettes, surrounding soil, and the group interaction of every single barrette on the barrette group is considered by generating the full soil-stiffness matrix. The presented technique is based on the flexibility coefficients of *Mindlin's* solution and one-dimensional finite elements. The *CCT* is used to compose the full soil-stiffness matrix. The resulting matrix is added to the barrette stiffness generating the full stiffness matrix of barrette groups to be solved. The developed technique considerably reduces the problem size and the computing time. This hybrid technique is coded in a user-friendly computer program.

The presented hybrid technique is used for linear and nonlinear analysis of laterally loaded barrettes/barrette groups embedded in multi-layered soil models. It has been verified by comparing linear and nonlinear results from analyzing single barrettes embedded in multi-layered soil with those obtained analytically in the available literature. Furthermore, a case study is carried out to compare the present technique results with those from load tests and 3D-FE models. In addition, two different 3D-FE models are used to compare the results from these models with those obtained by the hybrid technique.

A comparative study of laterally loaded single barrettes in a real-subsoil is carried out, in which east Port-Said soil properties are considered. These are similar to the soil formation of London, Frankfurt, Rome, Hong kong, and Dammam. In this study, different methods available in the *ECP 202* [56] for determining the effective-height of the barrette are used. Also, the linear and nonlinear soil models are compared to study soil nonlinearity. Finally, a parametric study is

carried out to investigate the behavior of laterally loaded single barrettes and barrette groups with different barrette dimensions, spacing, numbers, arrangement, material, and soil properties.

6.2 Conclusions

From studies carried out in this thesis, it could be concluded that:

- The technique can be effectively used in linear and nonlinear analyses of laterally loaded single barrettes and barrette groups in layered soil medium.
- Due to the lower number of nodes in the converted one-dimensional model rather than the three-dimensional finite element model, the first model consumes less computation time in the analysis. That enables analysis of large barrette foundations such as barrette group and barrette raft.
- Verification examination of the present analysis for analyzing laterally loaded barrettes shows that results are in good agreement with those obtained numerically by 3D FE.
- Good agreement is noticed while comparing the nonlinear analysis of laterally loaded barrette and measured values obtained from load tests.
- Although the barrette head displacements of the present linear analysis of laterally loaded barrettes are very close comparing to those obtained numerically by 3D FE, the distribution of barrette lateral displacements along the barrette length is relatively softer (giving higher displacements) in the present analysis. The absolute difference in results of the base displacements is very small. It is less than 0.1 cm comparing to the barrette dimensions. In which the barrette head displacement is the effective displacement in this case of analysis.
- In general, it can be concluded that the results of the present hybrid technique are in good agreement with those of 3D-FE models.
- The comparative study presents guidelines when analyzing laterally loaded single barrettes in the east Port-Said area and similar soil formations around the world, such as London, Frankfurt, Rome, Hong kong, and Dammam.
- The *ECP 202* [56] equations for determining effective heights of square or circular piles in homogeneous soil is modified to determine effective barrette heights in multi-layered soil.
- The *ECP 202* [56] equations for determining the maximum bending moment and maximum displacement of square or circular piles with free head support is modified to determine these of single barrettes.

- The *ECP 202* [56] equations for determining the ultimate lateral load of square or circular piles in sand using *Broms* (1964a) [10] method need to be updated with the one suggested by *Barton* (1984) [3], which is the more accurate one for piles in sand.
- The maximum bending moment happens at 22% to 26% of the effective barrette height.
- Determining the ultimate load capacity of laterally loaded single barrette needs more comparisons with field load tests.
- The behavior of laterally loaded single barrettes analyzed in soil formations like that existing in east Port-Said is close to being linear when considering displacement criteria for every single barrette to be is taken as 5% of the barrette width. This value is considered as an acceptable practical value for analyzing barrettes.
- The thickness of the topsoil layer is a controlling factor for the barrette-head displacement.
- The horizontal displacement of the barrette/barrette group is not influenced by the properties of the underlying layers in the case where the topsoil layer thickness exceeds approximately 30% of the barrette height.
- The lateral barrette/barrette group load capacity is affected by loading direction due to the dependence of the flexural stiffness of barrettes on barrette inertia.
- Increasing the barrette/barrette group height to width ratio H/W more than 30 has a very small effect because the barrette/barrette group height is reached to the effective-height of the barrette.
- From the parametric study, the normalized spacing S/L is suggested to be equal or greater than three since the displacement ratio R_g decreases linearly.

6.3 Recommendations for Future Works

The scope for future studies based on the presented hybrid technique may also include:

- Analyzing of nonrectangular cross-sections barrettes.
- Analyzing Mono-piles.
- Analyzing barrettes subjected to torsion load.
- Analyzing barrettes under dynamic loads.

It should be emphasized here that the above mentioned concluding remarks are specially related to the studied cases. Further future studies are strongly

recommended, including site measurements and back analysis. That to assess the validity and accuracy of the barrettes and barrette raft calculations in east Port-Said.

6.4 Research extracted from this thesis

- [1] *El Gendy, M., Ibrahim, H., and El Arabi, I.* (2020) "Analysing Rectangular Pile Using One Dimensional Finite Element" *Geotechnical and Geological Engineering*, vol. 38 (5): 4617–4635.
Doi: <https://doi.org/10.1007/s10706-020-01314-5>
- [2] *El Gendy, M., Ibrahim, H., and El Arabi, I.* (2020) "Developing the composed coefficient technique for analyzing laterally loaded barrettes" *Innovative Infrastructure Solutions*, vol. 5 (2): no. 43:1-14.
Doi: <https://doi.org/10.1007/s41062-020-00294-y>
- [3] *El Gendy, M., Ibrahim, H., and El Arabi, I.* (2021) " The behavior of laterally loaded barrette groups using hybrid flexibility coefficient and finite element technique" *Innovative Infrastructure Solutions*.
Doi: <https://doi.org/10.1007/s41062-021-00535-8>

7 REFERENCES

- [1] ABAQUS, Dassault Systèmes, Vélizy-Villacoublay, France.
- [2] Abbas, J., Chik, Z., and Taha, M. (2008) "Single pile simulation and analysis subjected to lateral load" *Electronic Journal of Geotechnical Engineering*, vol. 13: 1-15.
- [3] Barton, O. (1984) "Response of pile groups to lateral loading in the centrifuge" presented at the Proceedings of Symposium on Appl. of Centrifuge Modelling to Geotech. In Design, Balkema, Rotterdam, The Netherlands.
- [4] Basu, D. (2006) "Analysis of laterally loaded piles in layered soil" PHD Thesis, Purdue University, West Lafayette, Indiana, U.S.A.
- [5] Basu, D., Prezzi, M., Salgado, R., and Chakraborty, T. (2008) "Settlement analysis of piles with rectangular cross sections in multi-layered soils" *Computers and Geotechnics*, vol. 35 (4): 563-575.
Doi: <https://doi.org/10.1016/j.compgeo.2007.09.001>
- [6] Basu, D., and Salgado, R. (2007) "Elastic analysis of laterally loaded pile in multi-layered soil" *Geomechanics and Geoengineering*, vol. 2 (3): 183-196.
Doi: <https://doi.org/10.1080/17486020701401007>
- [7] Basu, D. and Salgado, R. (2008) "Analysis of laterally loaded piles with rectangular cross sections embedded in layered soil" *International Journal for Numerical and Analytical Methods in Geomechanics*, vol. 32 (7): 721-744.
Doi: <https://doi.org/10.1002/nag.639>
- [8] Behloul, D. and Moussai, B. (2016) "Three-dimensional analysis of laterally loaded barrette foundation using Plaxis 3D" in *7th Civil Engineering Conference in the Asian Region*, Waikiki, Hawaii, USA.
- [9] Bowles, J. "Foundation Analysis and Design" 5 Ed. New York: McGraw-Hill, (1996).
- [10] Broms, B. B. (1964) "Lateral resistance of piles in cohesionless soils" *Journal of the Soil Mechanics and Foundations Division*, vol. 90 (2): 123-156.
- [11] Broms, B. B. (1964) "Lateral resistance of piles in cohesive soils" *Journal of the Soil Mechanics and Foundations Division*, vol. 90 (2): 27-63.
- [12] Cao G., Zhu M., Gong W., Wang X., Dai G. (2020) "Dynamic response of vertically loaded rectangular barrettes in multilayered viscoelastic soil" *Geomechanics and Engineering*, vol. 23 (3): 275-287.
Doi: <https://doi.org/10.12989/gae.2020.23.3.275>

- [13] Charles, N. and Lei, G. (2003) "Performance of Long Rectangular Barrettes in Granitic Saprolites" *Journal of Geotechnical and Geoenvironmental Engineering*, vol. 129 (8).
Doi: [https://doi.org/10.1061/\(ASCE\)1090-0241\(2003\)129:8\(685\)](https://doi.org/10.1061/(ASCE)1090-0241(2003)129:8(685))
- [14] Choi, Y. S., Basu, D., Salgado, R., and Prezzi, M. (2014) "Response of Laterally Loaded Rectangular and Circular Piles in Soils with Properties Varying with Depth" *Journal of Geotechnical and Geoenvironmental Engineering*, vol. 140 (4). Doi: [https://doi.org/10.1061/\(ASCE\)GT.1943-5606.0001067](https://doi.org/10.1061/(ASCE)GT.1943-5606.0001067)
- [15] Choi, Y. S., Basu, D., Prezzi, M., and Salgado, R. (2015) "Study on laterally loaded piles with rectangular and circular cross sections" *Geomechanics and Geoengineering*, vol. 10 (2): 139-152.
Doi: <https://doi.org/10.1080/17486025.2014.902119>
- [16] Conte, E., Troncone, A., and Vena, M. (2013) "Nonlinear three-dimensional analysis of reinforced concrete piles subjected to horizontal loading" *Computers and Geotechnics*, vol. 49 123-133.
Doi: <https://doi.org/10.1016/j.compgeo.2012.10.013>
- [17] El Gendy, M. (2007) "Formulation of a composed coefficient technique for analyzing large piled raft" *Ain Shams Engineering Journal*, vol. 42 29-56.
- [18] El Gendy, M. (2016) "Behavior of Large-Section Supports under Heavy Loaded Structures" MSc Thesis, Port Said University, Port Said, Egypt.
- [19] El Gendy, M., El Gendy, A., El Gendy, O. (2018) "Analysis of Piled raft of Burj Khalifa in Dubai by the program ELPLA" GEOTEC Software Inc., Canada.
- [20] El Gendy, M., Ibrahim, H., and El Arabi, I. (2017) "Analyzing Single Barrette as Rigid Support by Composed Coefficient Technique" *Malaysian Journal of Civil Engineering*, vol. 29 (3): 273-288.
Doi: <https://doi.org/10.11113/mjce.v29.53>
- [21] El Gendy, M., Ibrahim, H., and El Arabi, I. (2018) "Modeling Single Barrettes as Elastic Support by CCT" *Malaysian Journal of Civil Engineering*, vol. 30 (2): 296-312.
Doi: <https://doi.org/10.11113/mjce.v30n2.481>
- [22] El Gendy, M., Ibrahim, H., and El Arabi, I. (2019) "Composed Coefficient Technique for Modelling Barrette Groups" *Malaysian Journal of Civil Engineering*, vol. 31 (1): 23-33.
Doi: <https://doi.org/10.11113/mjce.v31n1.510>

- [23] *El Wakil, A. Z. and Nazir, A. K.* (2013) "Behavior of laterally loaded small scale barrettes in sand" *Ain Shams Engineering Journal*, vol. 4 (3): 343-350.
Doi: <https://doi.org/10.1016/j.asej.2012.10.011>
- [24] *Fleming, K., Weltman, J., Randolph, F., and Elson, K.* "Piling Engineering" (Surrey University Press). New York: Halsted Press, (1985).
- [25] *Hamza, M. and Hamed, H.* (2000) "Three Dimensional Soil-Structure Analysis of Port-Said East Quay Wall" *WIT Transactions on The Built Environment*, to be published vol. 51: 371-380.
- [26] *Hsu, M., YU, C., and Chen, C.* (2017) "Case studies for side resistance of barrette piles using results of ultimate load tests" *Journal of GeoEngineering*, vol. 12 (2): 65-79.
Doi: [http://dx.doi.org/10.6310/jog.2017.12\(2\).3](http://dx.doi.org/10.6310/jog.2017.12(2).3)
- [27] *Ibranim, H., El Arabi, I., and El Gendy, M.* (2016) "Analyzing Barrettes as Large-Section Supports by CCT" *Port-Said Engineering Research Journal*, vol. 20 (2): 27-39.
Doi: <https://dx.doi.org/10.21608/pserj.2016.33578>
- [28] *Nasser, A.* (2020) "Lateral Behavior of Single Pile in Cohesionless Soil Subjected to Both Vertical and Horizontal Loads" MSc Thesis, Cairo University, Egypt.
- [29] *Kacprzak, G.* (2015) "Proposition of designing method for barrettes as a non-direct foundation of engineering construction" *Technical Transactions*, vol. 24: 71-77.
Doi: <https://doi.org/10.4467/2353737XCT.15.228.4614>
- [30] *Keawsawasvong, S. and Ukritchon, B.* (2016) "Ultimate lateral capacity of two dimensional plane strain rectangular pile in clay" *Geomechanics and Engineering*, vol. 11 (2): 235-252.
Doi: <http://dx.doi.org/10.12989/gae.2016.11.2.235>
- [31] *Kulhawy, H., and Chen, J.* (1995) "A thirty year perspective of Broms' lateral loading models, as applied to drilled shafts" presented at the Bengt B. Broms Symposium on Geotechnical Engineering, Geotechnical Research Centre, Singapore.
- [32] *Kumari A., Thakare S.W., and Dhatrak A.I.* (2020) Lateral and Uplift Capacities of Barrette Pile in Sandy Soil. In: Latha Gali M., Raghuvver Rao P. (eds) *Construction in Geotechnical Engineering. Lecture Notes in Civil Engineering*, vol 84. Springer, Singapore.
Doi: https://doi.org/10.1007/978-981-15-6090-3_15

- [33] *Lei, G.* (2001) "Behavior of Excavated rectangular piles (Barrettes) in granitic saprolites" PHD Thesis, Hong Kong University of science and technology, Clear Water Bay, Kowloon, Hong Kong.
- [34] *Lei, G. H., Hong, X., and Shi, J. Y.* (2007) "Approximate three-dimensional analysis of rectangular barrette-soil-cap interaction" *Canadian Geotechnical Journal*, vol. 44 (7): 781-796.
Doi: <https://doi.org/10.1139/t07-017>
- [35] *Leszczynski, M.* (2009) "Barretted raft design for high-rise building applying 3D numerical tool" in *The 17th International Conference on Soil Mechanics and Geotechnical Engineering*, Bibliotheca Alexandrina, Alexandria, Egypt.
Doi: <https://doi.org/10.3233/978-1-60750-031-5-1263>
- [36] *Lin, S., Lu, F., Kuo, C., Su, T., and Mulowayi, E.* (2014) "Axial capacity of barrette piles embedded in gravel layer" *Journal of GeoEngineering*, vol. 9 103-107. Doi: [http://dx.doi.org/10.6310/jog.2014.9\(3\).3](http://dx.doi.org/10.6310/jog.2014.9(3).3)
- [37] *Manoj S., Choudhury D., and Alzaylaie M.* (2020) "Value engineering using load-cell test data of barrette foundations – La Maison, Dubai" *Geotechnical Engineering*. Doi: <https://doi.org/10.1680/jgeen.19.00246>
- [38] *Mansour M.M., Fayed A.L., Morsi M.M.* (2021). "Numerical simulation for the nonlinear behavior of laterally loaded barrettes" *Innovative Infrastructure Solutions*, vol. 6:26. Doi: <https://doi.org/10.1007/s41062-020-00392-x>
- [39] *Mert, M., Ozkan, and M.T.* (2020) "A new hyperbolic variation method for settlement analysis of axially loaded single friction piles" *Arab J Geosci*, vol. 13, 794. Doi: <https://doi.org/10.1007/s12517-020-05791-z>
- [40] *Mindlin, R. D.* (1936) "Force at a Point in the Interior of a Semi-Infinite Solid" *Physics*, vol. 7 (5): 195-202.
Doi: <https://doi.org/10.1063/1.1745385>
- [41] *Musarra, M. and Massad, F.* (2015) "Static Load Tests in an Instrumented Rock Socket Barrette Pile" *Soils and Rocks*, vol. 38 (2): 163-177.
- [42] *Nguyen, H., Fellenius, B., Puppala, A., Aravind, P., and Tran, Q.* (2016) "Bidirectional Tests on Two Shaft-Grouted Barrette Piles in Mekong Delta, Vietnam" *Geotechnical Engineering Journal of the SEAGS & AGSSEA*, vol. 74 (1): 15-25.
- [43] *Nossan, A., Nossan, V., Stanić, B., and Mihaljević, I.* (2009) "A bridge foundation resisting sliding soil mass" presented at The 17th International Conference on Soil Mechanics and Geotechnical Engineering, Bibliotheca Alexandrina, Alexandria, Egypt, 5-9 October 2009.
Doi: <https://doi.org/10.3233/978-1-60750-031-5-1495>

- [44] Pereira, G., Rodriguez Quet, F., Voster, T. E. B., and Wojtowicz, G. (2019) "Overview of the dual foundation system of the Dubai Creek Tower" in *ECSMGE 2019 – XVII European Conference on Soil Mechanics and Geotechnical Engineering*, Harpa Conference Centre, Iceland.
Doi: <https://doi.org/10.32075/17ECSMGE-2019-0703>
- [45] PLAXIS 3D, Bentley Systems, Delft, Netherlands.
- [46] Poulos, H. G., and Bergère, A. (2017) "Deep foundation systems of ultra high-rise buildings: the Entisar tower in Dubai" in *The 19th International Conference on Soil Mechanics and Geotechnical Engineering*, Seoul.
- [47] Poulos, H. G., and Davis, E. H. (1968) "The Settlement Behavior of Single Axially Loaded Incompressible Piles and Piers" *Géotechnique*, vol. 18 (3): 351-371. Doi: <https://doi.org/10.1680/geot.1968.18.3.351>
- [48] Poulos, H. G., Chow, H.S.W., and Small, J. C. (2019) "The Use of Equivalent Circular Piles to Model the Behavior of Rectangular Barrette Foundations" *Geotechnical Engineering Journal of the SEAGS & AGSSEA*, vol. 50 (3): 106-109.
- [49] Rabaiotti, C. and Malecki, C. (2018) "In situ testing of barrette foundations for a high retaining wall in molasse rock" *Géotechnique*, vol. 68 (12): 1056-1070. Doi: <https://doi.org/10.1680/jgeot.17.P.144>
- [50] Rafa, S. A., and Moussai, B. (2018) "Three-Dimensional Analyses of Bored Pile and Barrette Load Tests Subjected to Vertical Loadings" *Soil Mechanics and Foundation Engineering*, vol. 55 (3): 146-152.
Doi: <https://doi.org/10.1007/s11204-018-9518-0>
- [51] Russo, G. (1998) "Numerical analysis of piled rafts" *International Journal for Numerical and Analytical Methods in Geomechanics*, vol. 22 (6): 477-493.
Doi: [https://doi.org/10.1002/\(SICI\)1096-9853\(199806\)22:6%3C477::AID-NAG931%3E3.0.CO;2-H](https://doi.org/10.1002/(SICI)1096-9853(199806)22:6%3C477::AID-NAG931%3E3.0.CO;2-H)
- [52] Russo, G. (2016) "A method to compute the non-linear behavior of piles under horizontal loading" *Soils and Foundations*, vol. 56 (1): 33-43.
Doi: <https://doi.org/10.1016/j.sandf.2016.01.003>
- [53] Russo, G., Abagnara, V., Poulos, H. G., and Small, J. C. (2012) "Re-assessment of foundation settlements for the Burj Khalifa, Dubai" *Acta Geotechnica*, vol. 8 (1): 3-15.
Doi: <https://doi.org/10.1007/s11440-012-0193-4>
- [54] Seo, H., Basu, D., Prezzi, M., and Salgado, R. (2009) "Load-Settlement Response of Rectangular and Circular Piles in Multilayered Soil" *Journal of Geotechnical and Geoenvironmental Engineering*, vol. 135 (3): 420-430.
Doi: [https://doi.org/10.1061/\(ASCE\)1090-0241\(2009\)135:3\(420\)](https://doi.org/10.1061/(ASCE)1090-0241(2009)135:3(420))

- [55] Shulyatiev, O., Dzagov, A., Bokov, I., and Shuliatev, S. (2013) "Correction of soil design parameters for the calculation of the foundation based on the results of barrettes static load test" in *The 18th International Conference on Soil Mechanics and Geotechnical Engineering*, Paris.
- [56] Standing Committee to prepare Egyptian Code for Soil mechanics, d. a. i. o. f.-P. f. D. f. "Egyptian Code for Soil mechanics, design and implementation of foundations" Part four: Deep foundations, The National Center for Housing and Building Research, Egypt, (2007).
- [57] Teparaksa W., Sinkinson M., and Teparaksa J. (2018) "Vertical Capacity of Large and Deep Barrette Pile for Bangkok Subsoils" presented at the Proceedings of China-Europe Conference on Geotechnical Engineering. Springer Series in Geomechanics and Geoengineering. Springer, Cham. Doi: https://doi.org/10.1007/978-3-319-97115-5_31
- [58] Thasnanipan, N., Anwar, M., Maung, A. W., and Tanseng, P. (1999) "Performance comparison of bored and excavated piles in the layered soils of Bangkok" in *Innovative Solutions in Structural and Geotechnical Engineering*, Pathumthani, Thailand.
- [59] Thasnanipan, N., Maung, A., and Aye, A. (2001) "Record load test on a large barrette and its performance in the layered soils of Bangkok" in *5th International Conference on Deep Foundation Practice incorporating Piletalk*, Singapore.
- [60] Thasnanipan, N., Maung, A. W., and Tanseng, P. (1998) "Barrettes Founded in Bangkok Subsoils, Construction and Performance" in *the Thirteenth Southeast Asian Geotechnical*, Taipei, Taiwan.
- [61] Ukritchon, B. and Keawsawasvong, S. (2017) "Undrained Lateral Capacity of Rectangular Piles under a General Loading Direction and Full Flow Mechanism" *KSCE Journal of Civil Engineering*, vol. 22 (7): 2256-2265. Doi: <https://doi.org/10.1007/s12205-017-0062-7>
- [62] Zhang, L., Silva, F., Grismala, R. (2005) "Ultimate Lateral Resistance to Piles in Cohesionless Soils" *journal of geotechnical and geoenvironmental engineering*, vol. 131 (1): 78-83. Doi: [https://doi.org/10.1061/\(ASCE\)1090-0241\(2005\)131:1\(78\)](https://doi.org/10.1061/(ASCE)1090-0241(2005)131:1(78))
- [63] Zhang, L. M. (2003) "Behavior of Laterally Loaded Large-Section Barrettes" *Journal of Geotechnical and Geoenvironmental Engineering*, vol. 129 (7): 639-648. Doi: [https://doi.org/10.1061/\(ASCE\)1090-0241\(2003\)129:7\(639\)](https://doi.org/10.1061/(ASCE)1090-0241(2003)129:7(639))
- [64] Znamenskii, V. V., Bakhoidin, B. V., Parfenov, E. A., and Musatova, M. V. (2019) "Investigation of the Load-Carrying Capacity of Barrettes for a 56-

References

- Storey Residential Building" *Soil Mechanics and Foundation Engineering*, vol. 56 (1): 1-6. Doi: <https://doi.org/10.1007/s11204-019-09561-2>
- [65] <http://www.soletanchefreyssinet.com/projet/projet-test-2/dubai-creek-tower-2-2>
- [66] <https://calatrava.com/news/reader/dubai-creek-tower-sets-new-milestone-with-completion-of-pile-cap.html>
- [67] <https://www.ffgb.be/en/techniques/piles/large-diameter-bored-piles/barrette>

8 APPENDIX

8.1 APPENDIX (A)

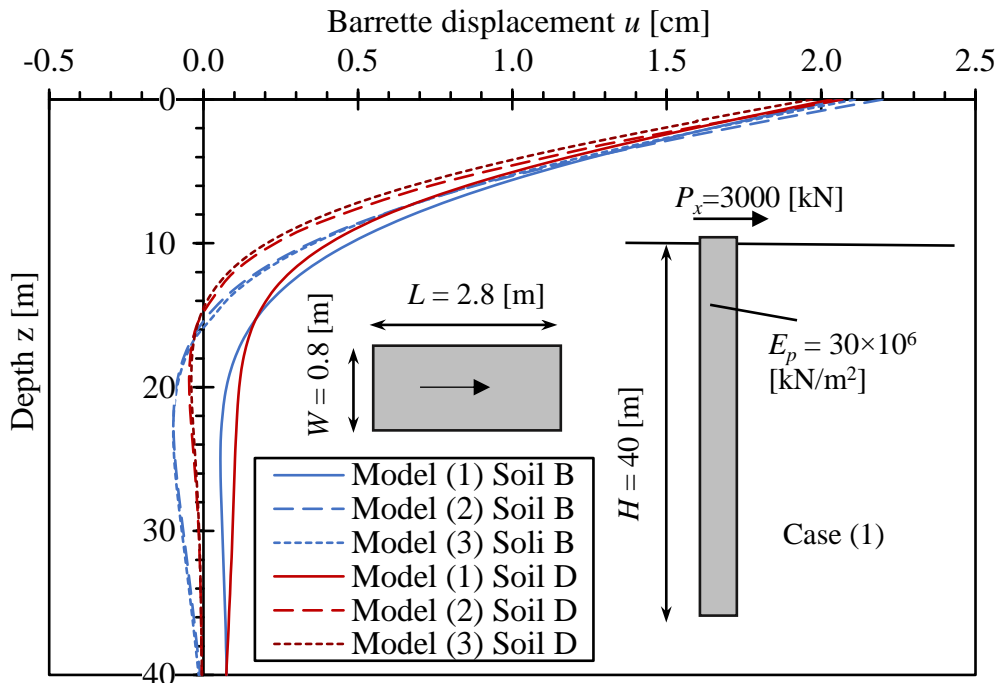


Figure A.1 Displacement for case (1) with subsoil (B&D).

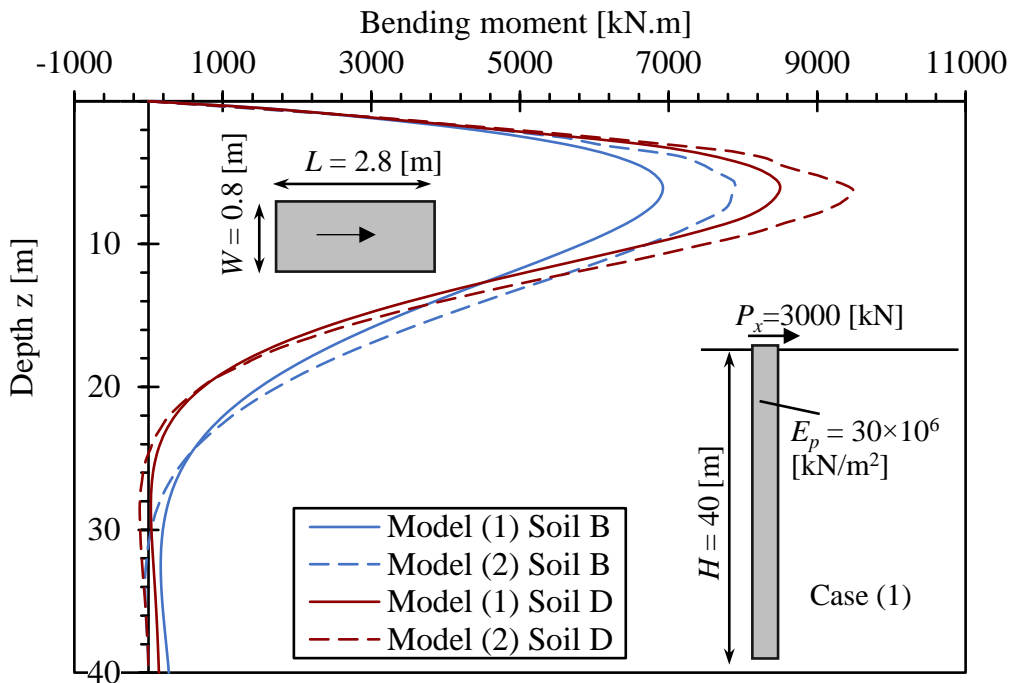


Figure A.2 Bending moment for case (1) with subsoil (B&D).

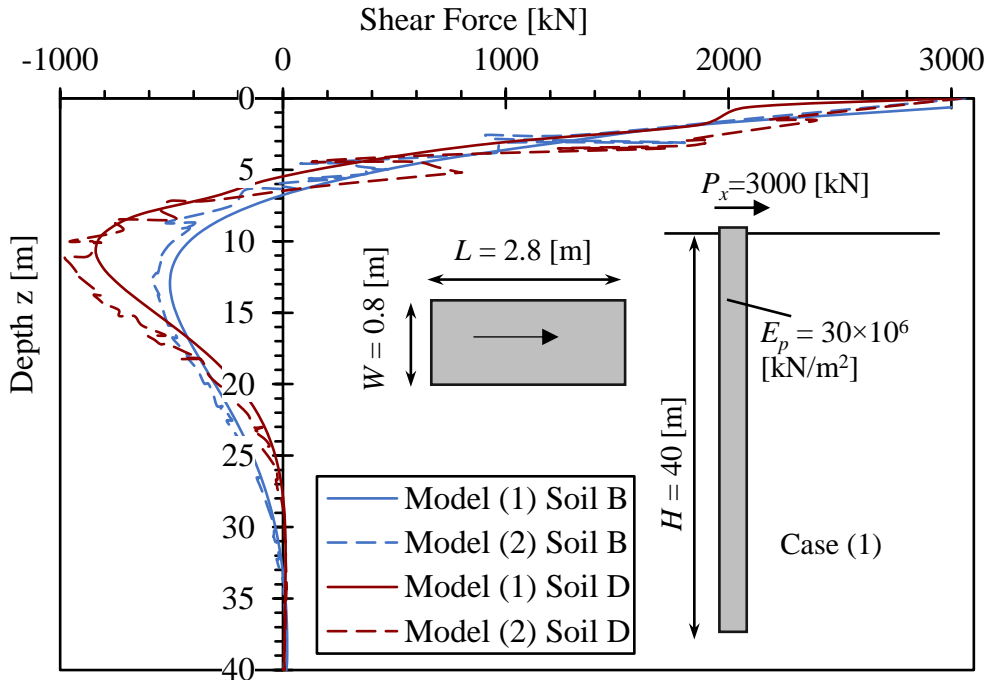


Figure A.3 Shear force for case (1) with subsoil (B&D).

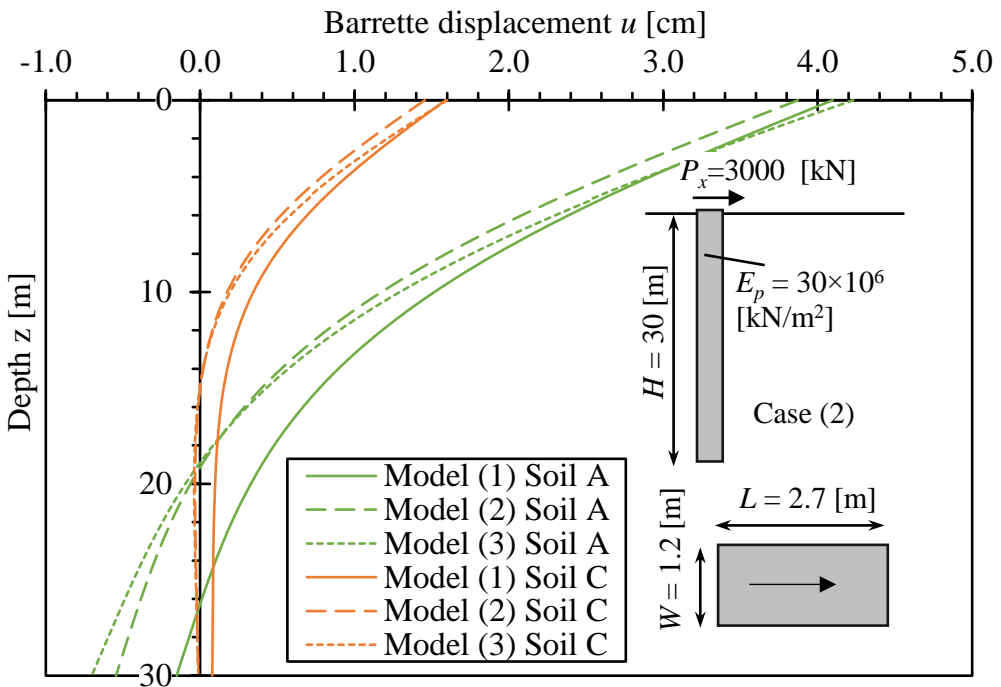


Figure A.4 Displacement u for case (2) with subsoil (A&C).

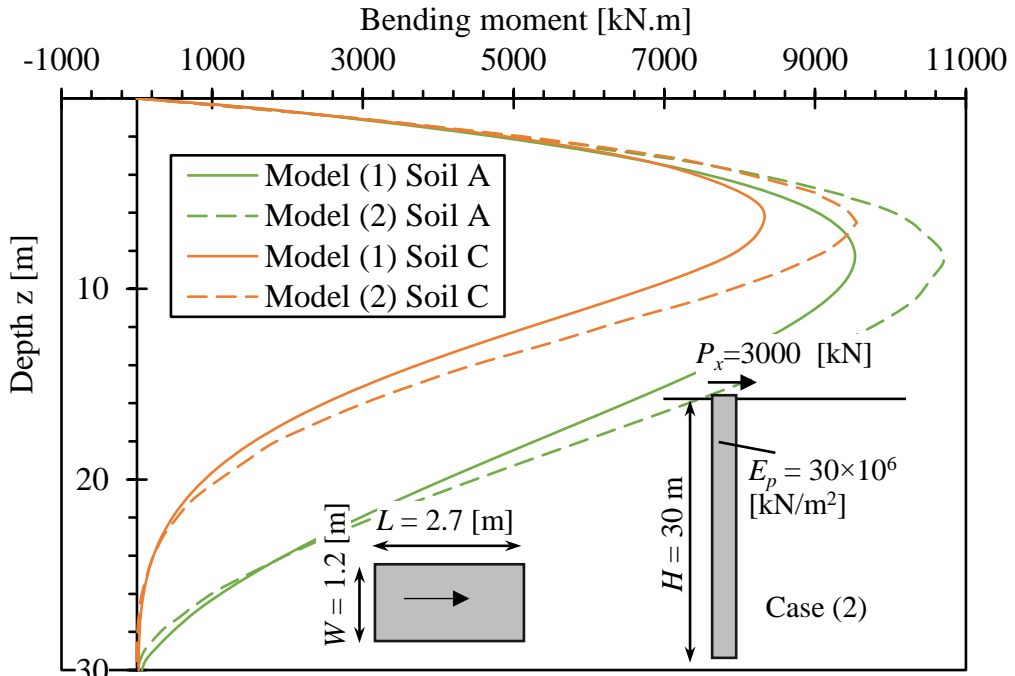


Figure A.5 Bending moment for case (2) with subsoil (A&C).

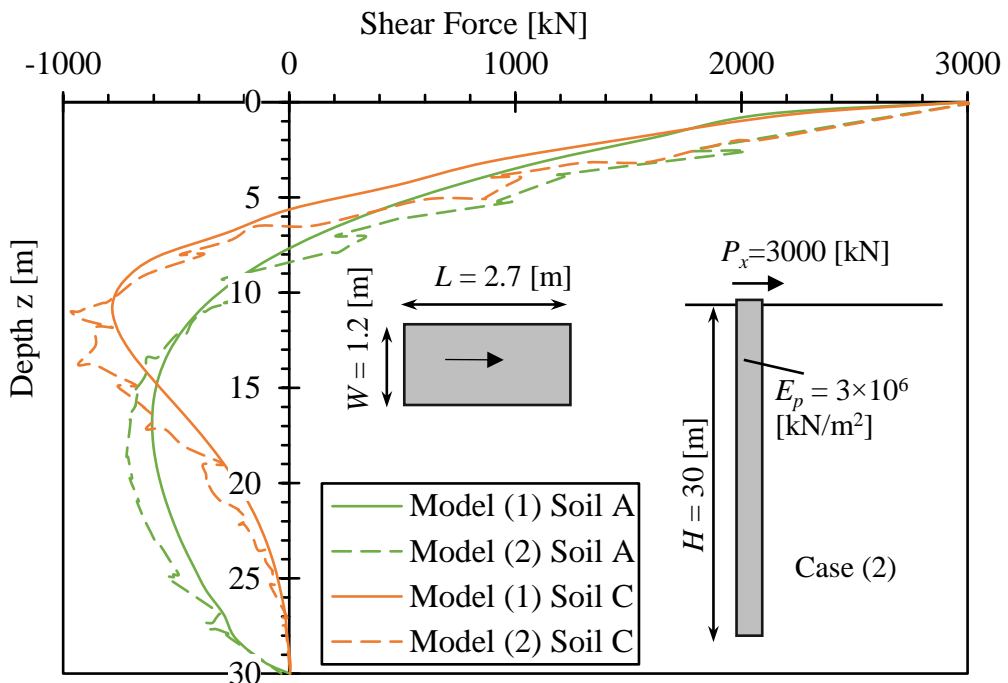


Figure A.6 Shear force for case (2) with subsoil (A&C).

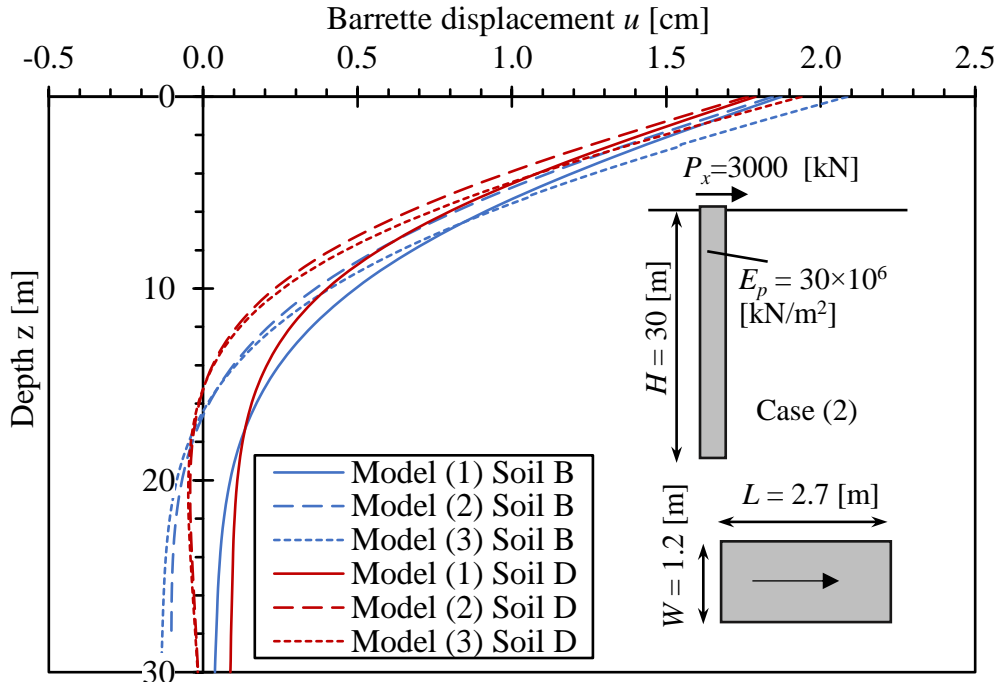


Figure A.7 Displacement u for case (2) with subsoil (B&D).

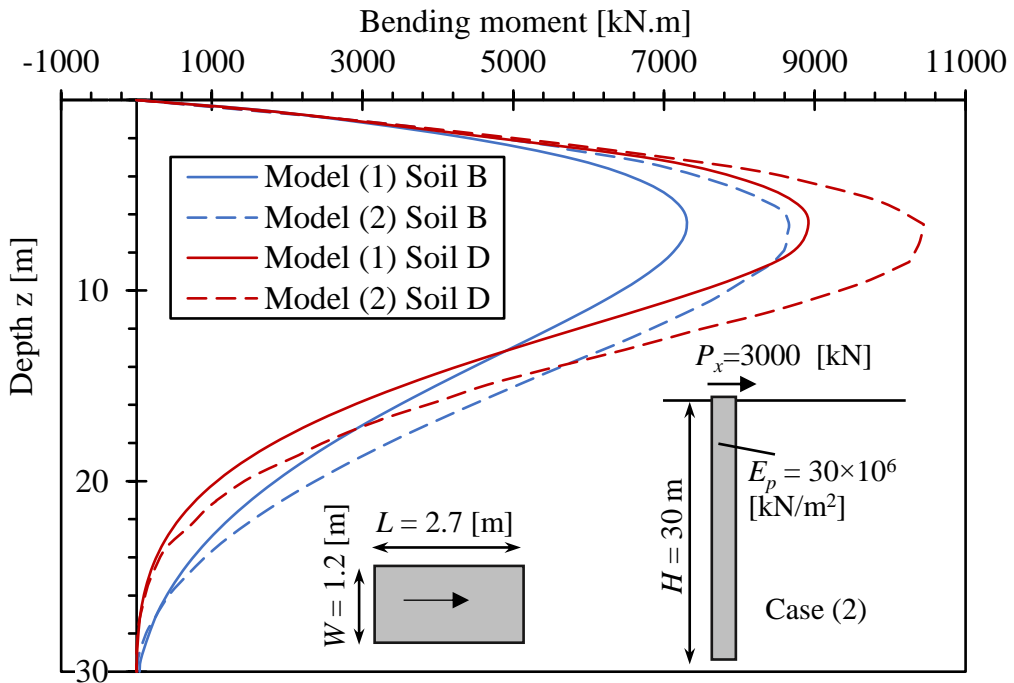


Figure A.8 Bending moment for case (2) with subsoil (B&D).

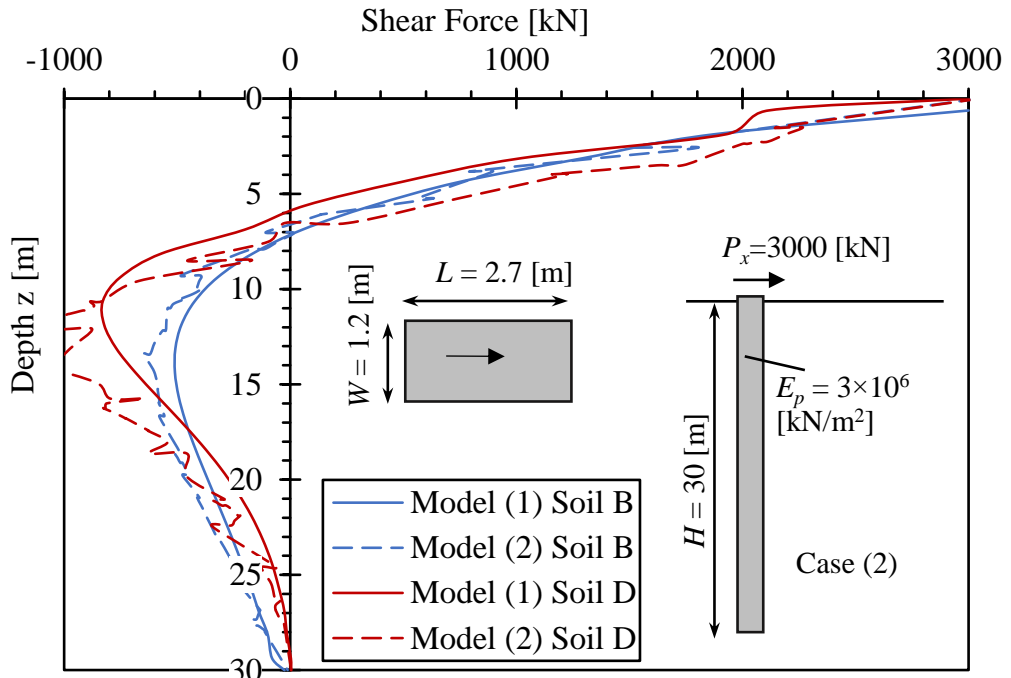


Figure A.9 Shear force for case (2) with subsoil (B&D).

8.2 APPENDIX (B)

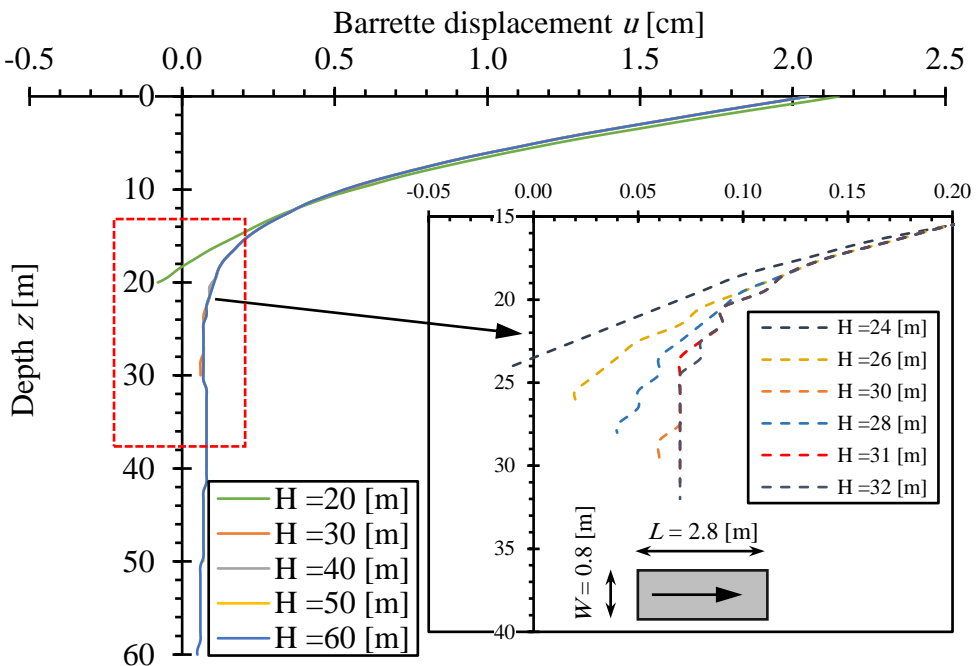


Figure A.10 Displacement u with the barrette height (case 2).

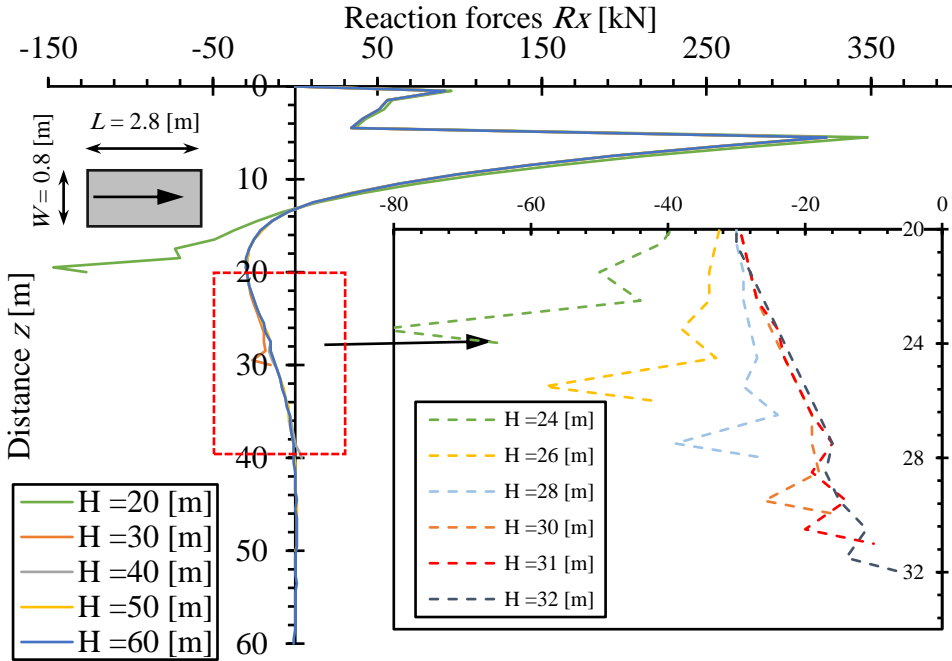


Figure A.11 Reaction forces R_x with the barrette height (case 2).

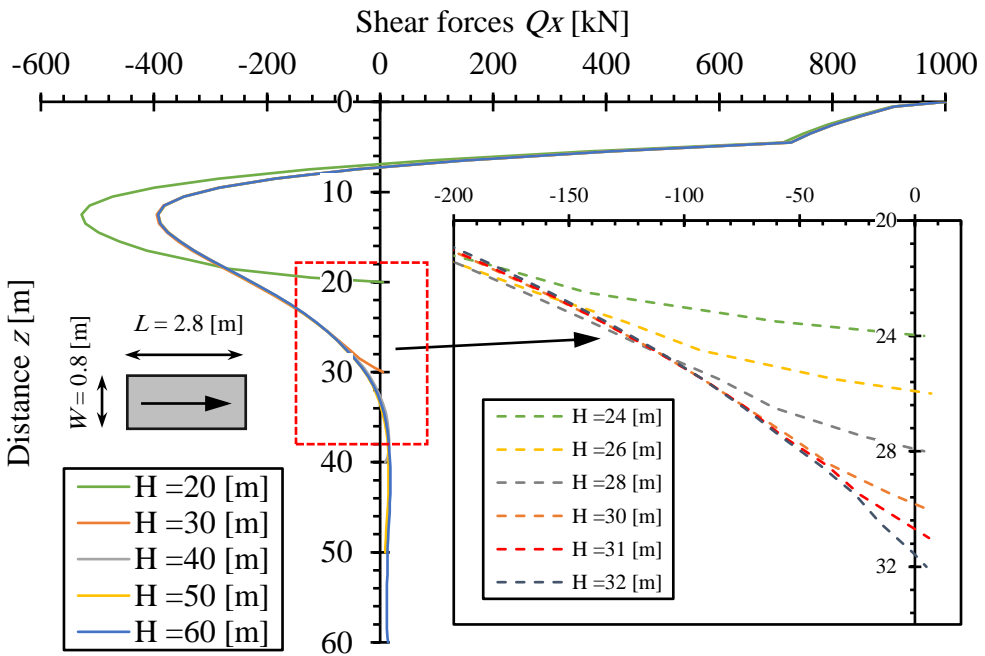


Figure A.12 Shear forces Q_x with the barrette height (case 2).

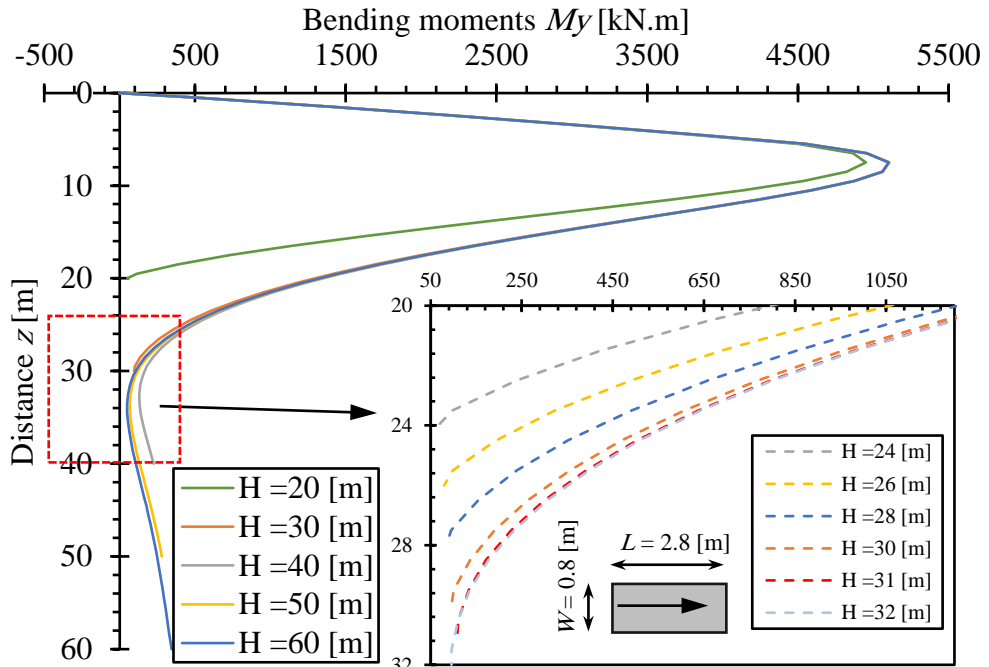


Figure A.13 Bending moments M_y with the barrette height (case 2).

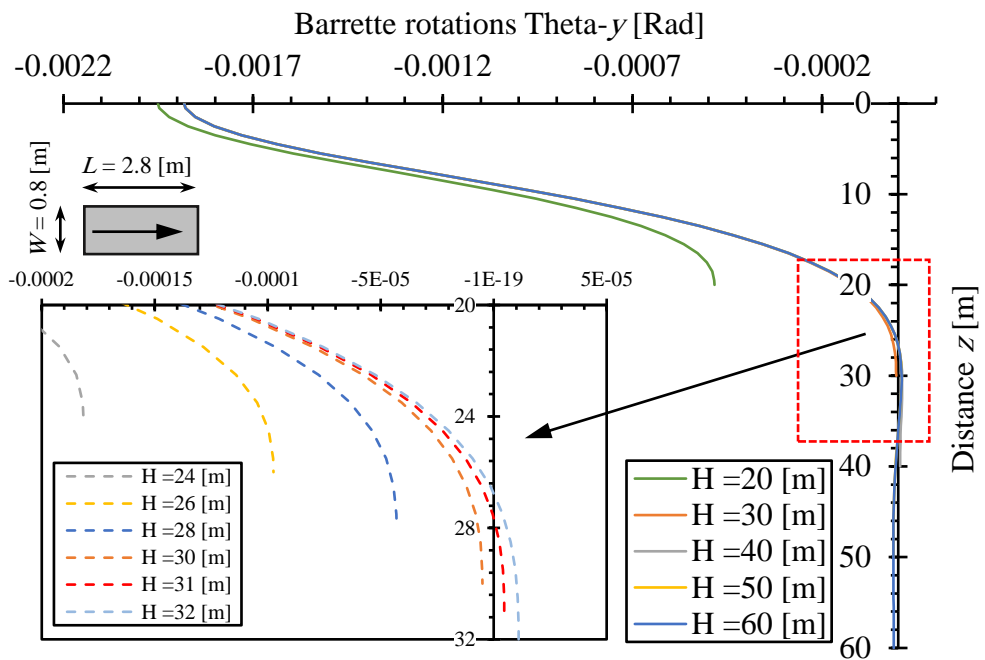


Figure A.14 Barrette rotations Θ_{-y} with the barrette height (case 2).

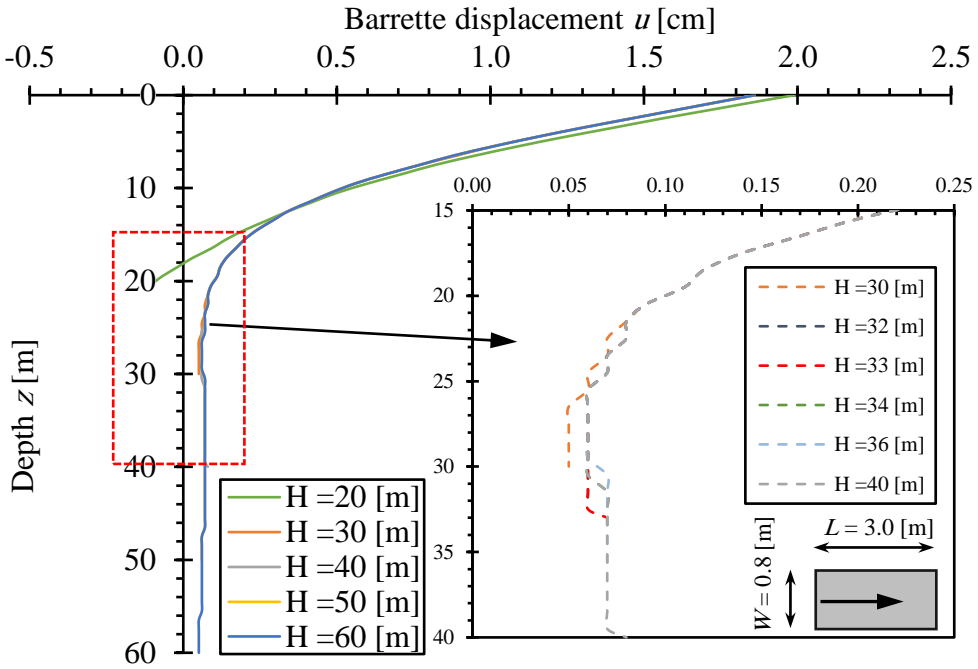


Figure A.15 Displacement u with the barrette height (case 3).

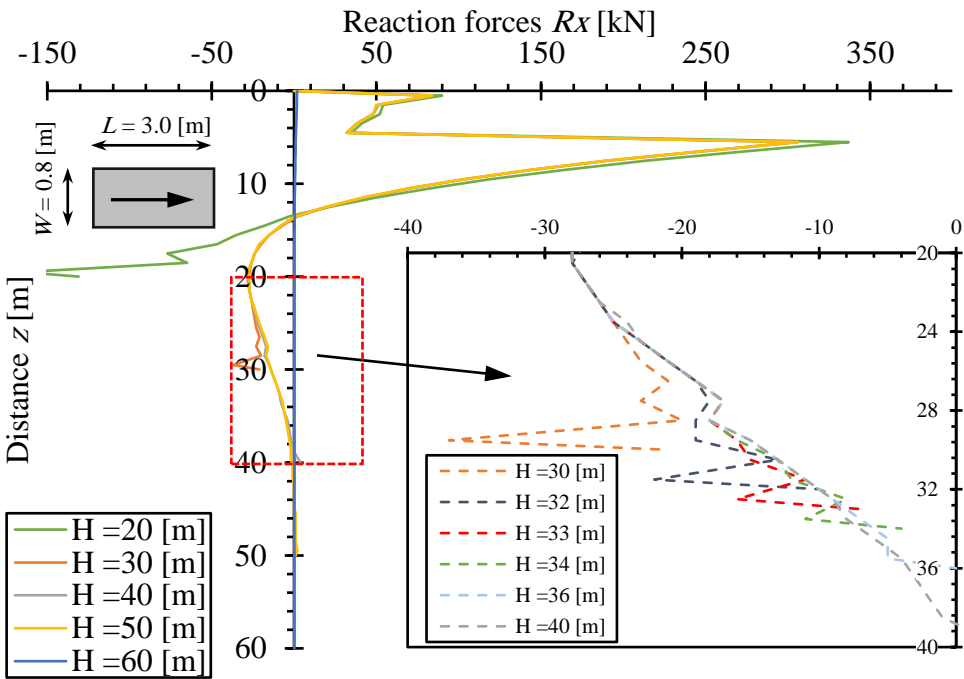


Figure A.16 Reaction forces R_x with the barrette height (case 3).

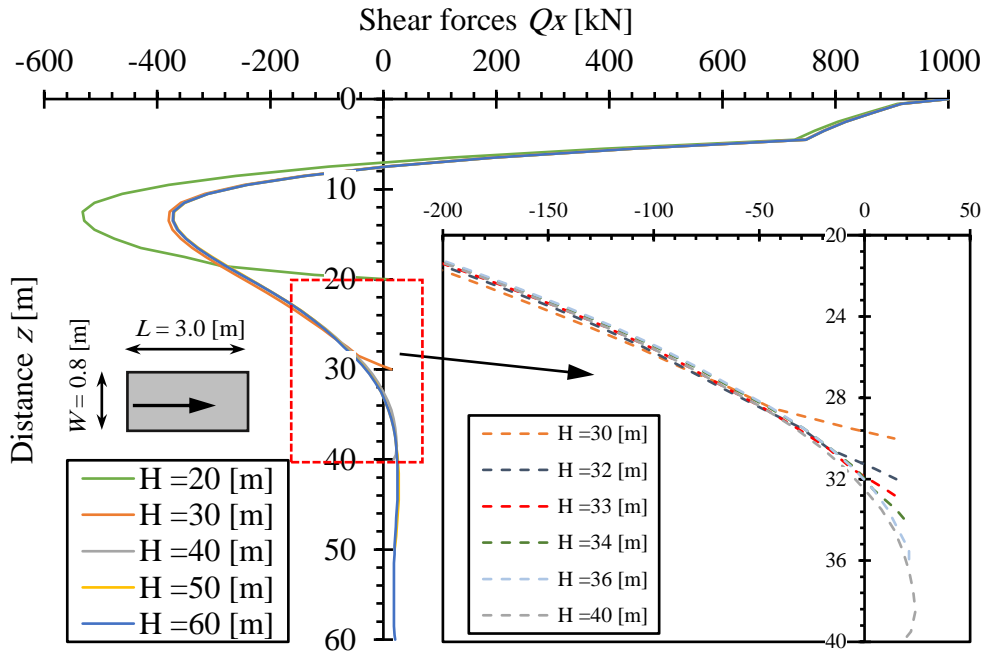


Figure A.17 Shear forces Q_x with the barrette height (case 3).

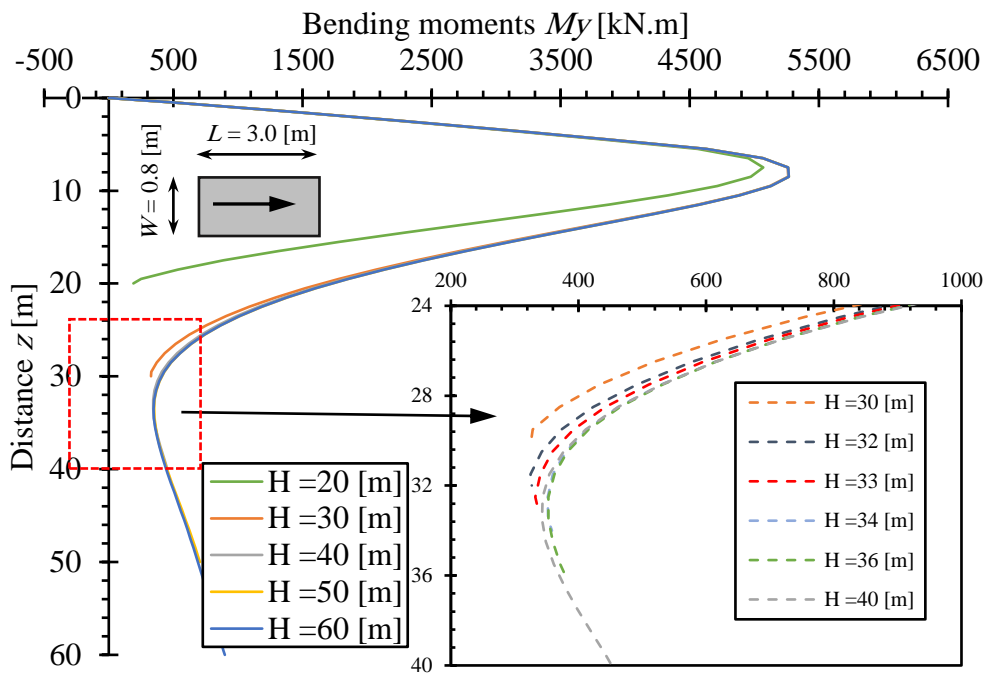


Figure A.18 Bending moments M_y with the barrette height (case 3).

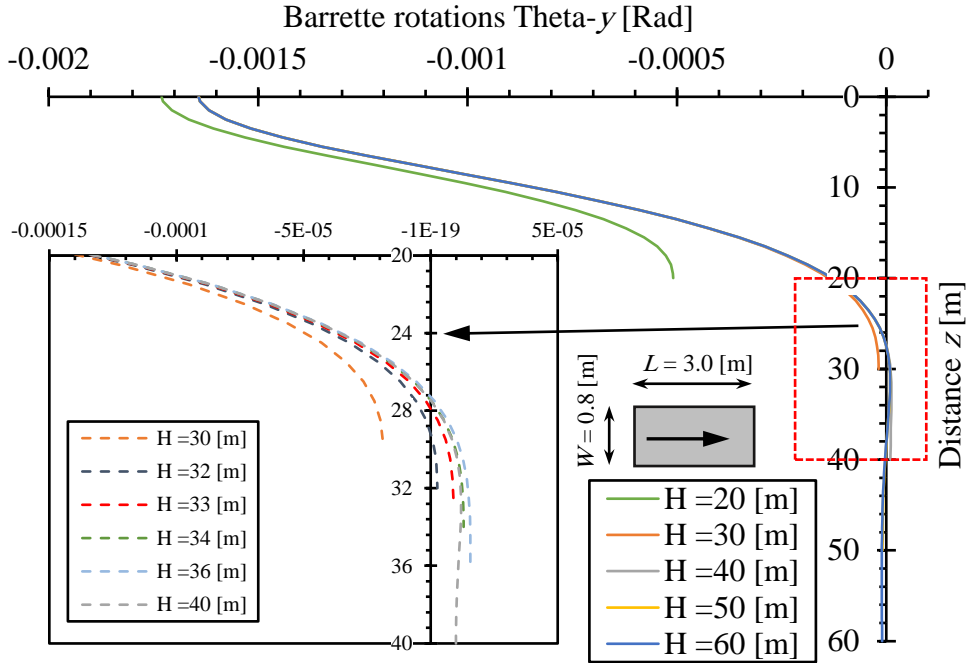


Figure A.19 Barrette rotations Θ_{-y} with the barrette height (case 3).

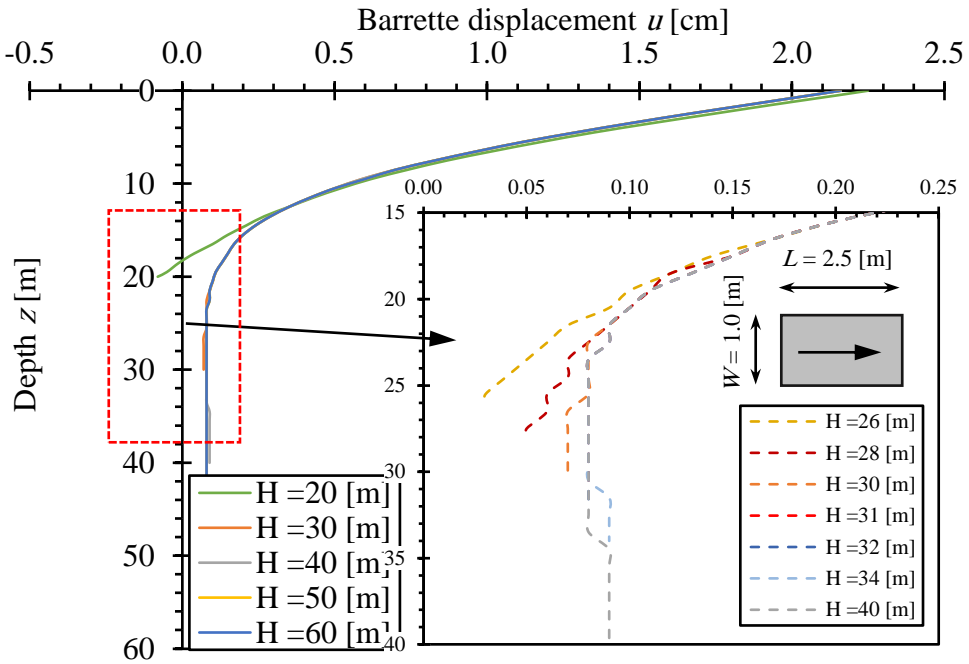


Figure A.20 Displacement u with the barrette height (case 4).

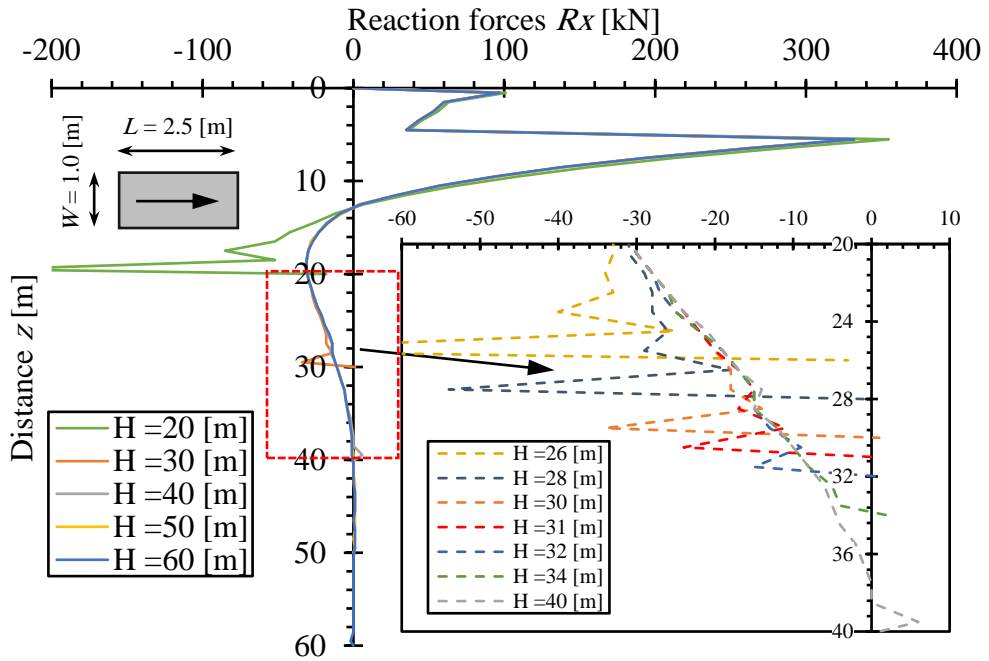


Figure A.21 Reaction forces R_x with the barrette height (case 4).

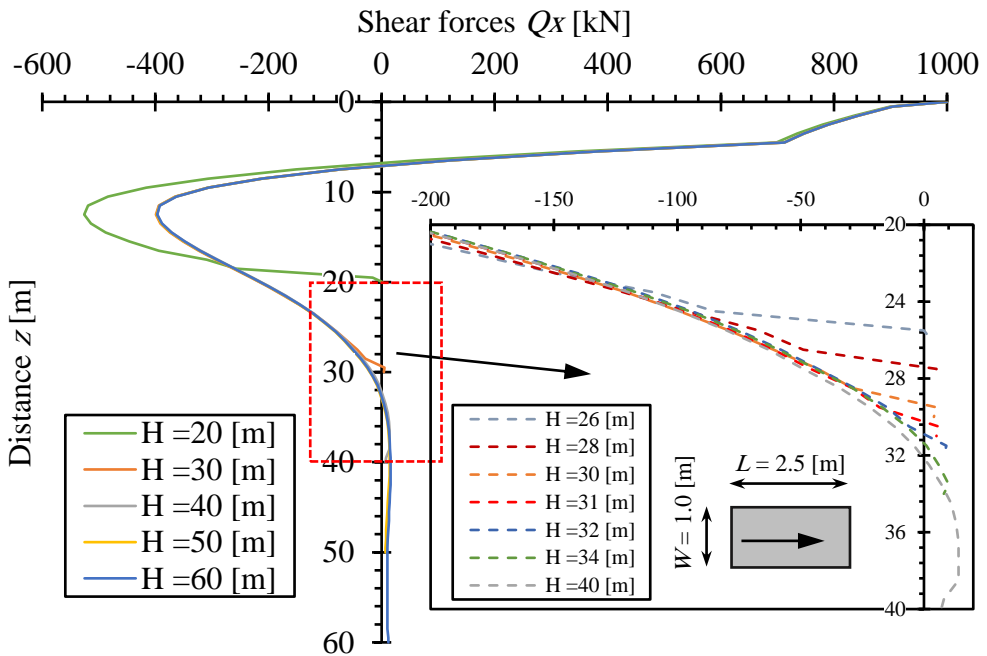


Figure A.22 Shear forces Q_x with the barrette height (case 4).

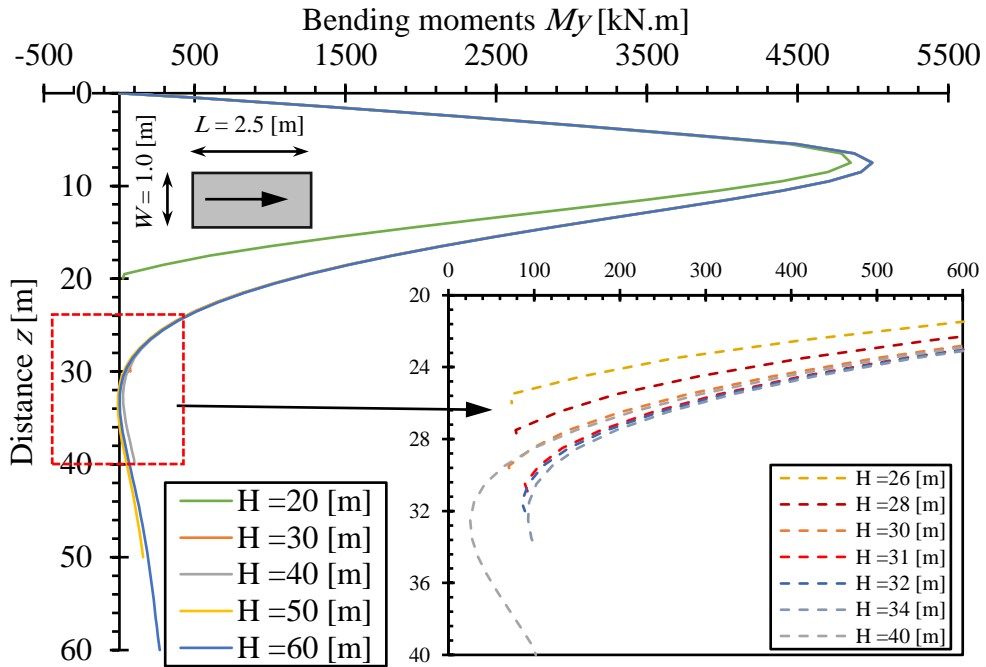


Figure A.23 Bending moments M_y with the barrette height (case 4).

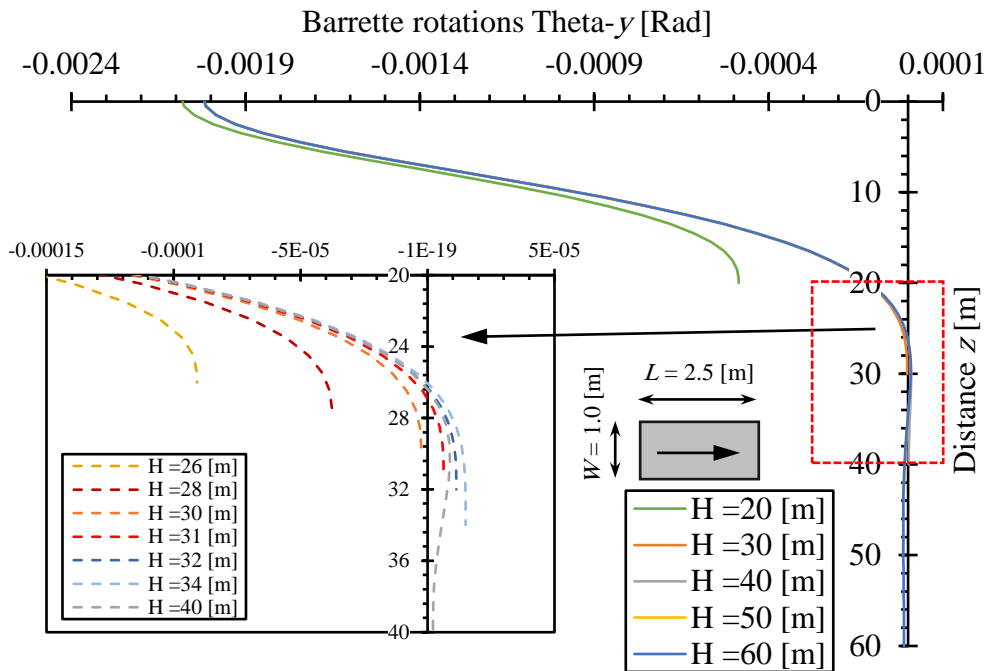


Figure A.24 Barrette rotations Θ_{y} with the barrette height (case 4).

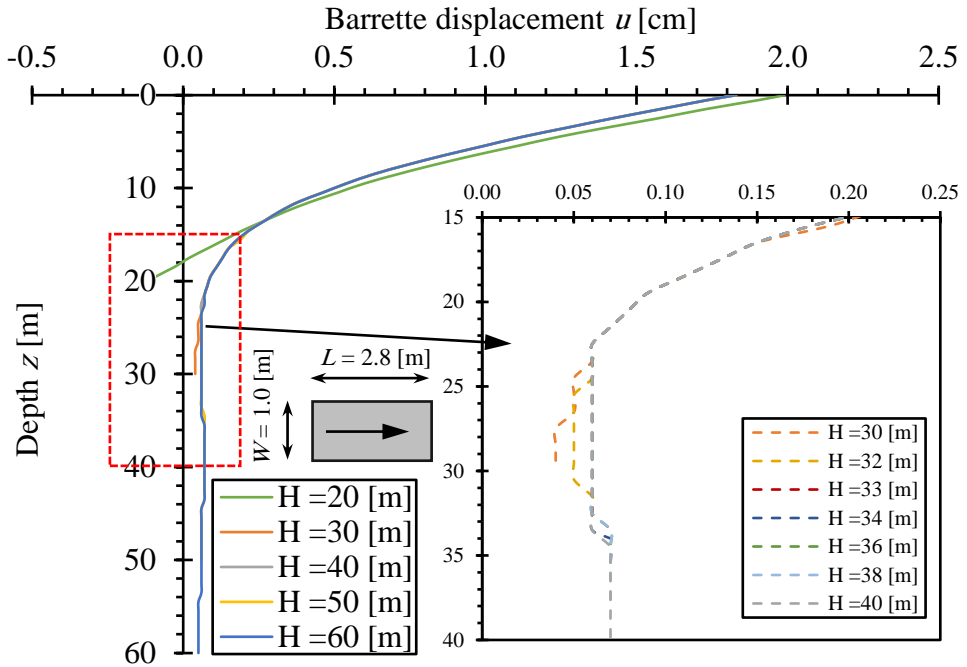


Figure A.25 Displacement u with the barrette height (case 5).

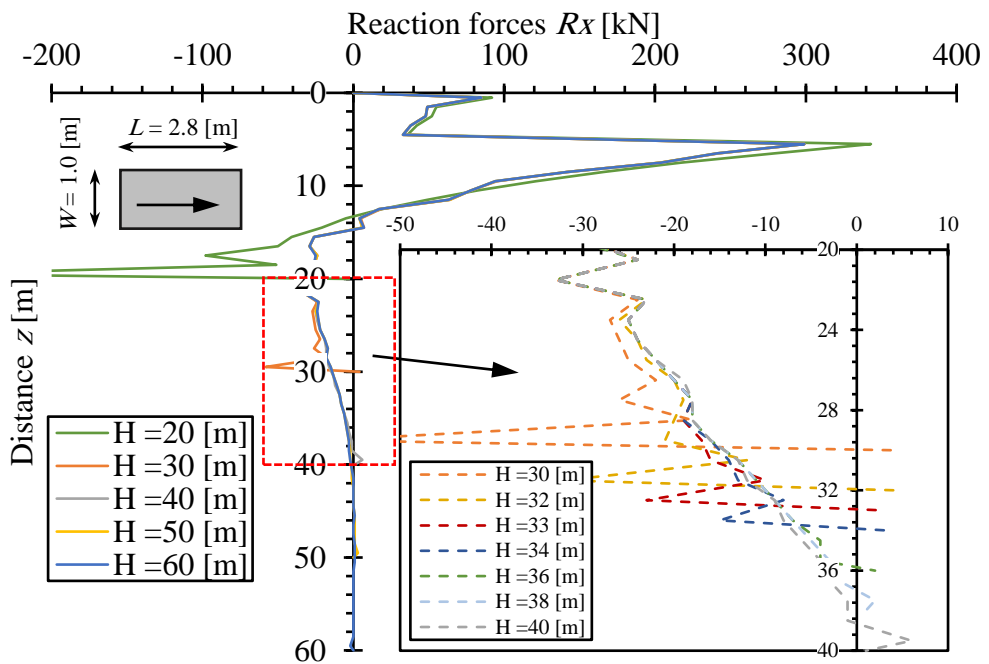


Figure A.26 Reaction forces R_x with the barrette height (case 5).

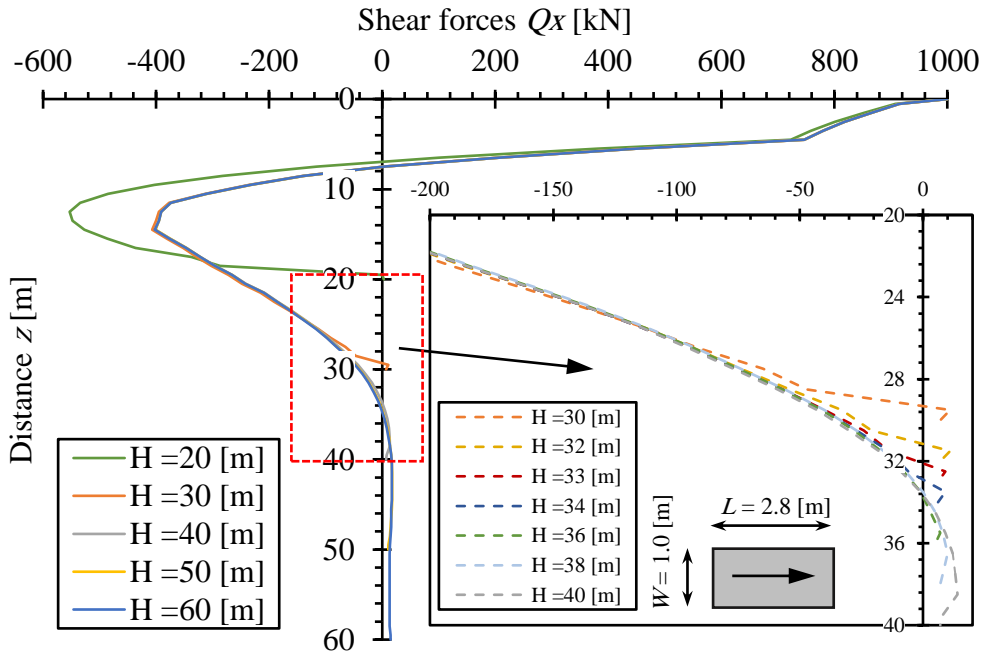


Figure A.27 Shear forces Q_x with the barrette height (case 5).

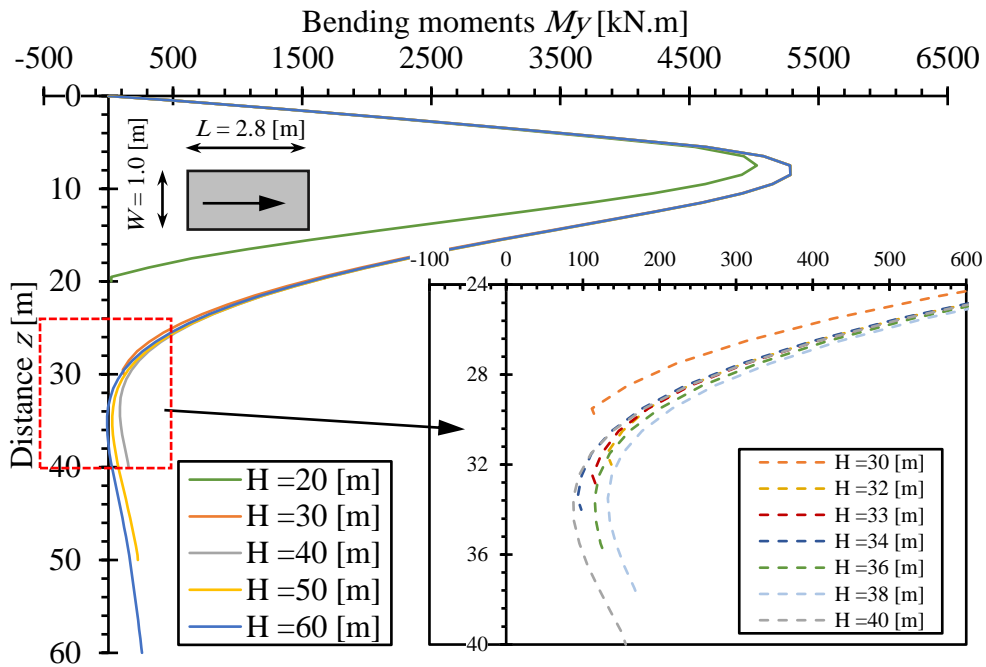


Figure A.28 Bending moments M_y with the barrette height (case 5).

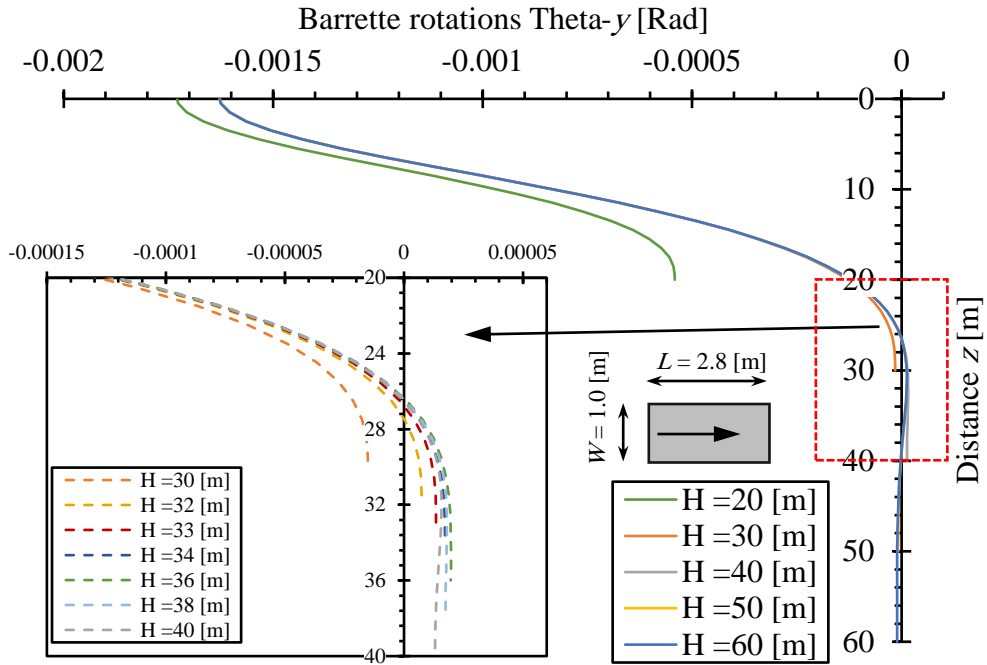


Figure A.29 Barrette rotations Θ_{-y} with the barrette height (case 5).

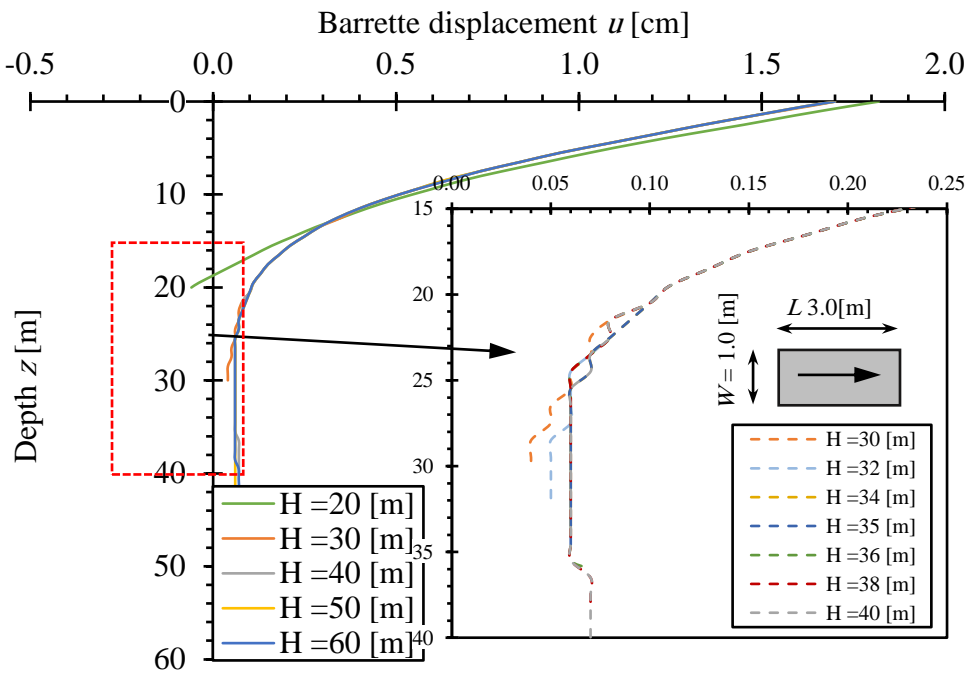


Figure A.30 Displacement u with the barrette height (case 6).

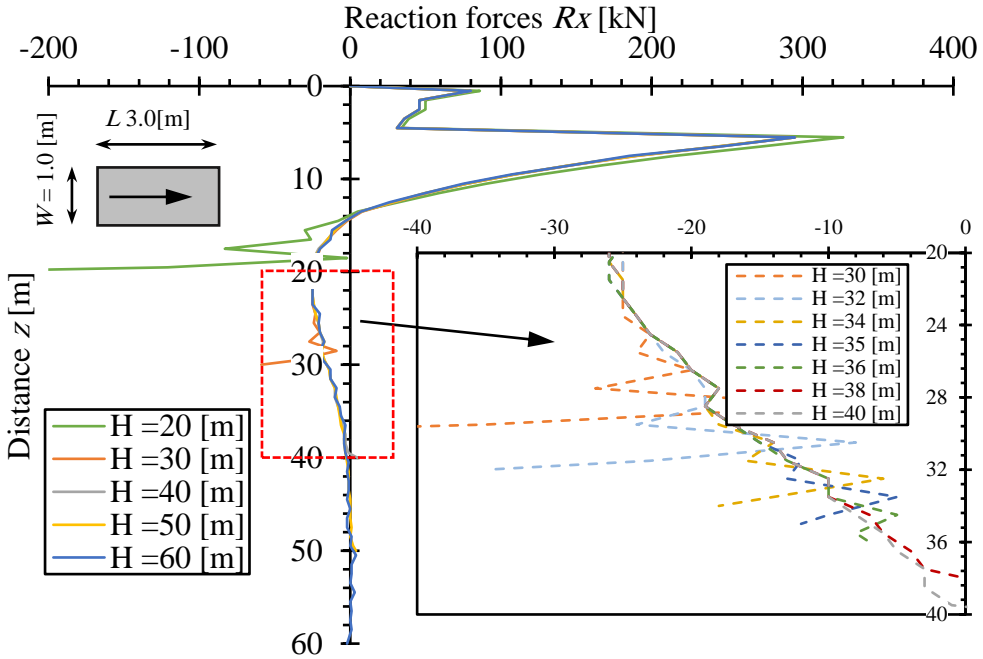


Figure A.31 Reaction forces R_x with the barrette height (case 6).

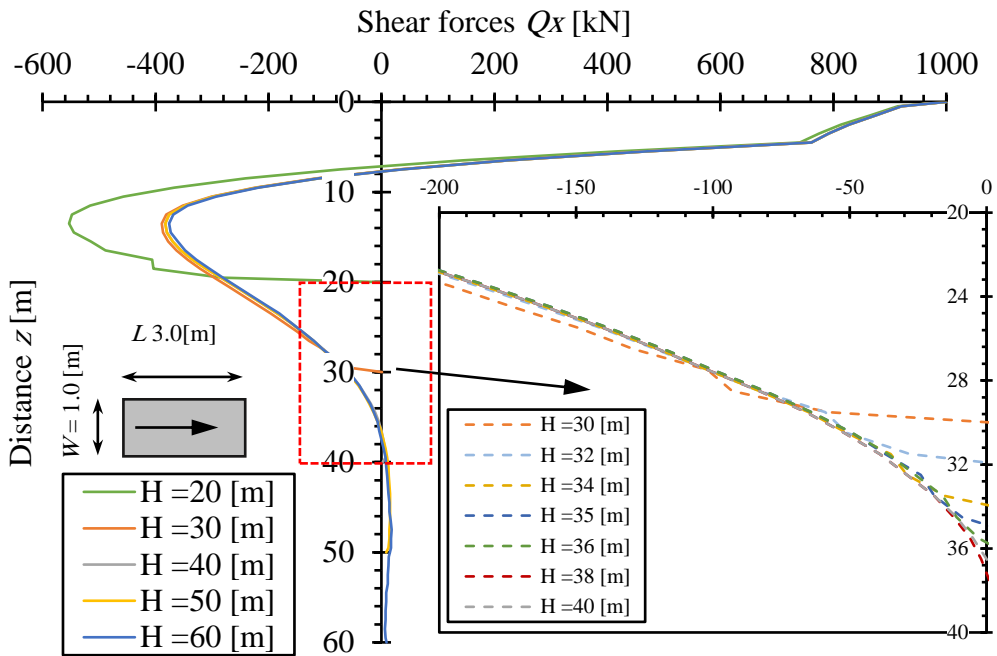


Figure A.32 Shear forces Q_x with the barrette height (case 6).

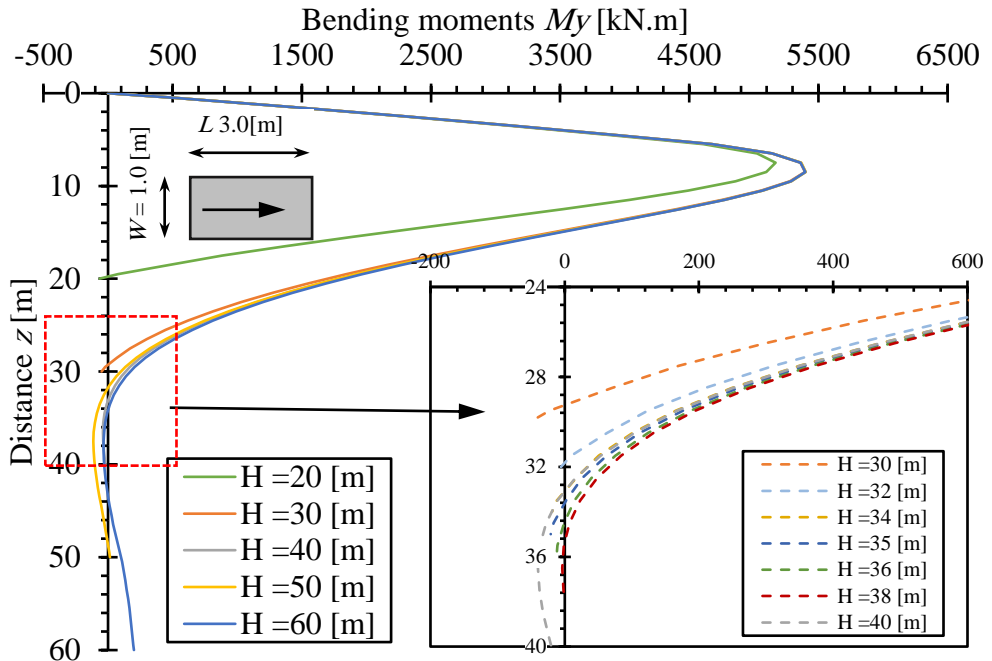


Figure A.33 Bending moments M_y with the barrette height (case 6).

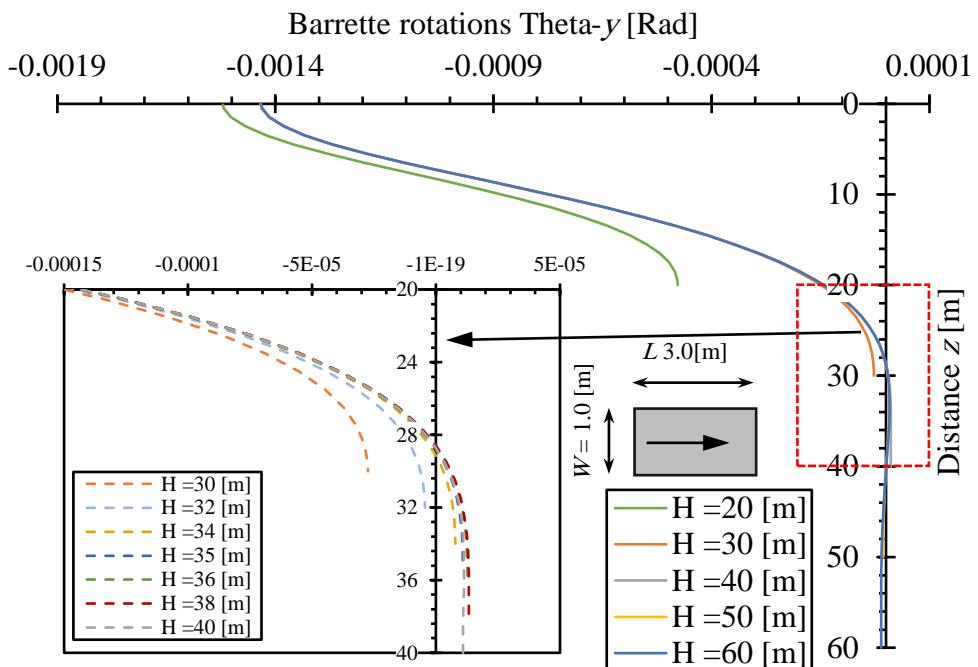


Figure A.34 Barrette rotations $\Theta_{theta-y}$ with the barrette height (case 6).

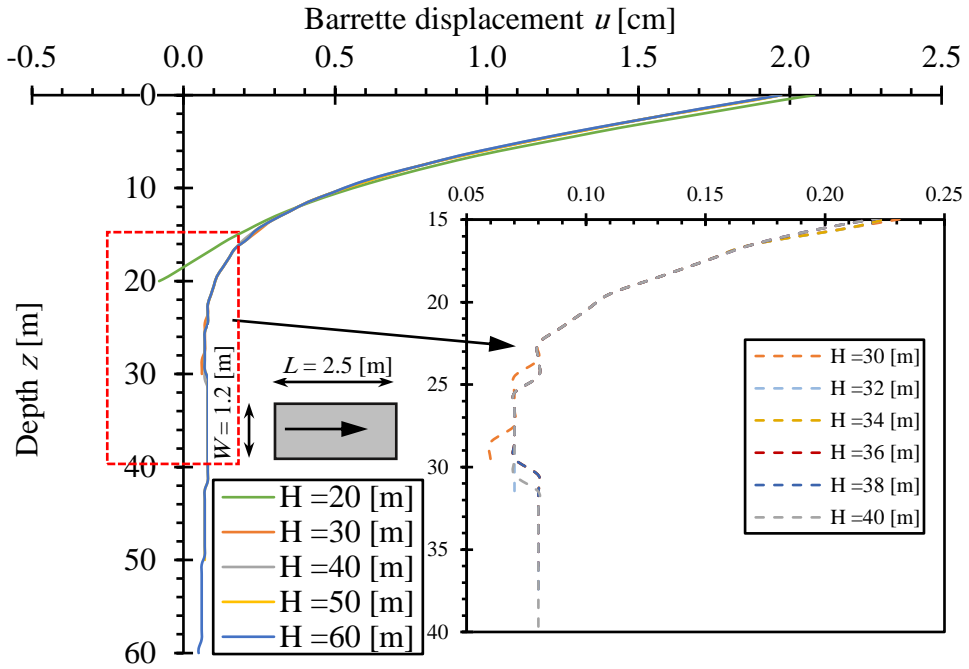


Figure A.35 Displacement u with the barrette height (case 7).

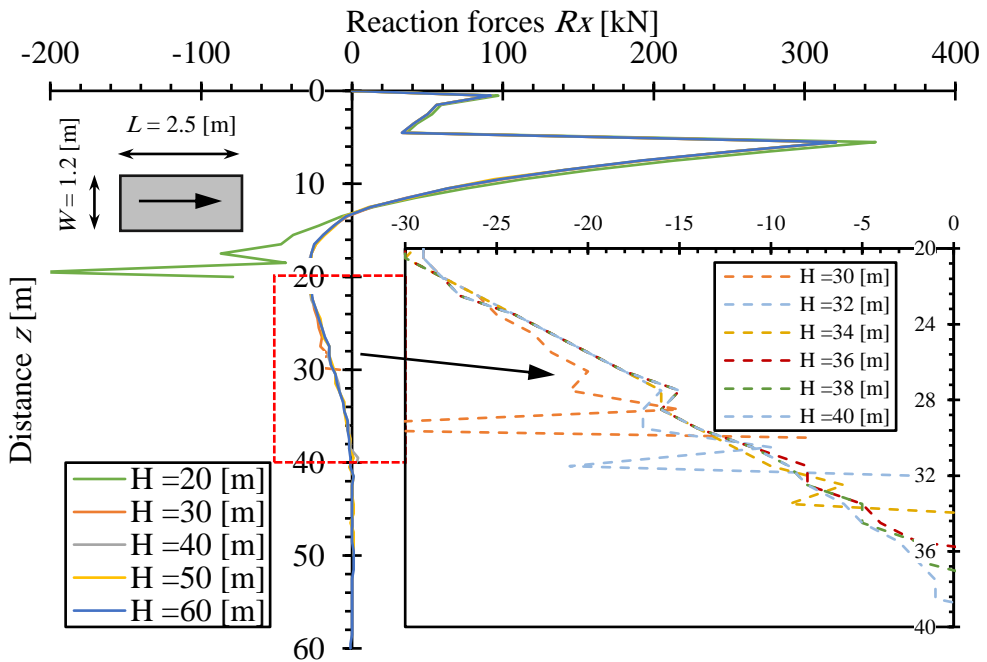


Figure A.36 Reaction forces R_x with the barrette height (case 7).

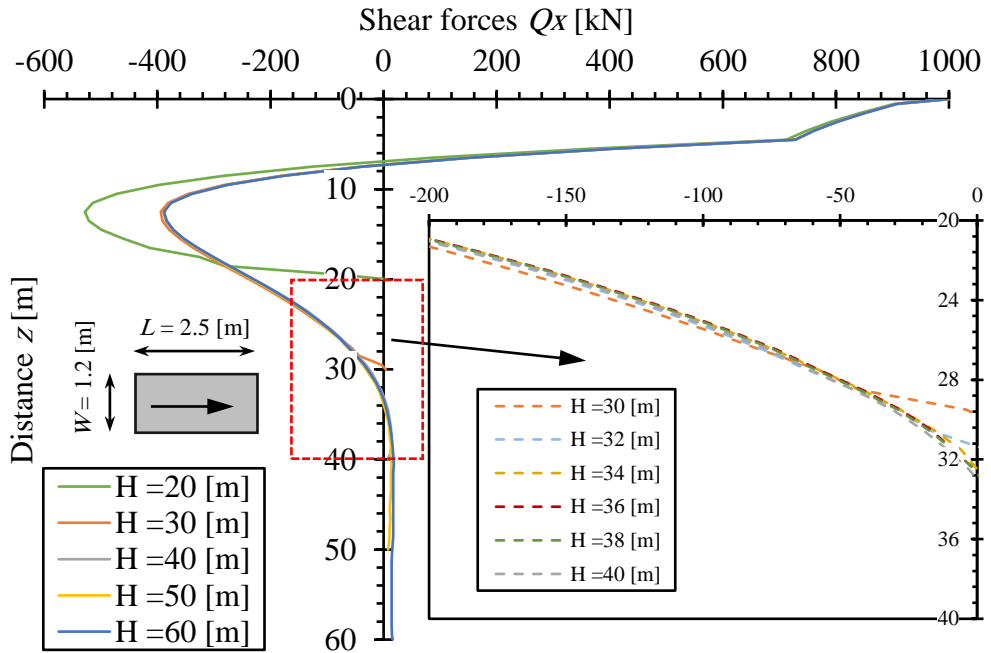


Figure A.37 Shear forces Q_x with the barrette height (case 7).

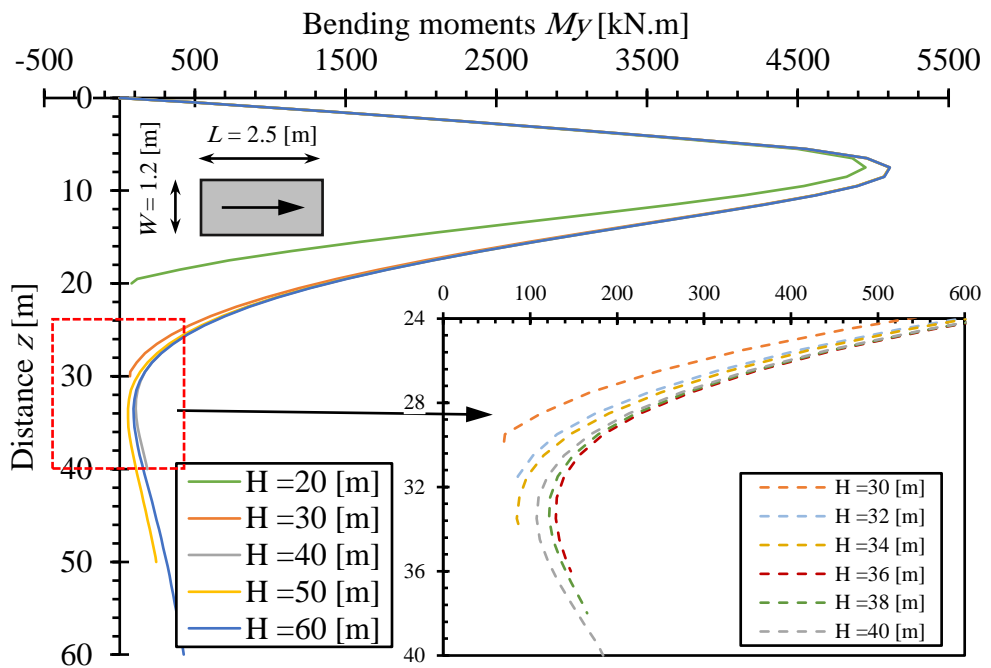


Figure A.38 Bending moments M_y with the barrette height (case 7).

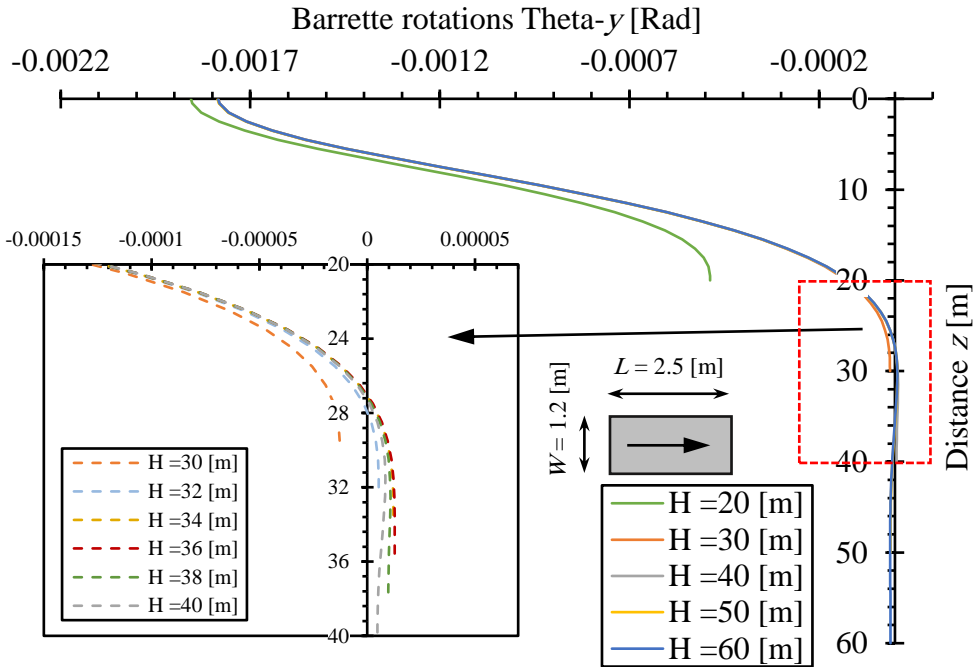


Figure A.39 Barrette rotations $\Theta\text{-}y$ with the barrette height (case 7).

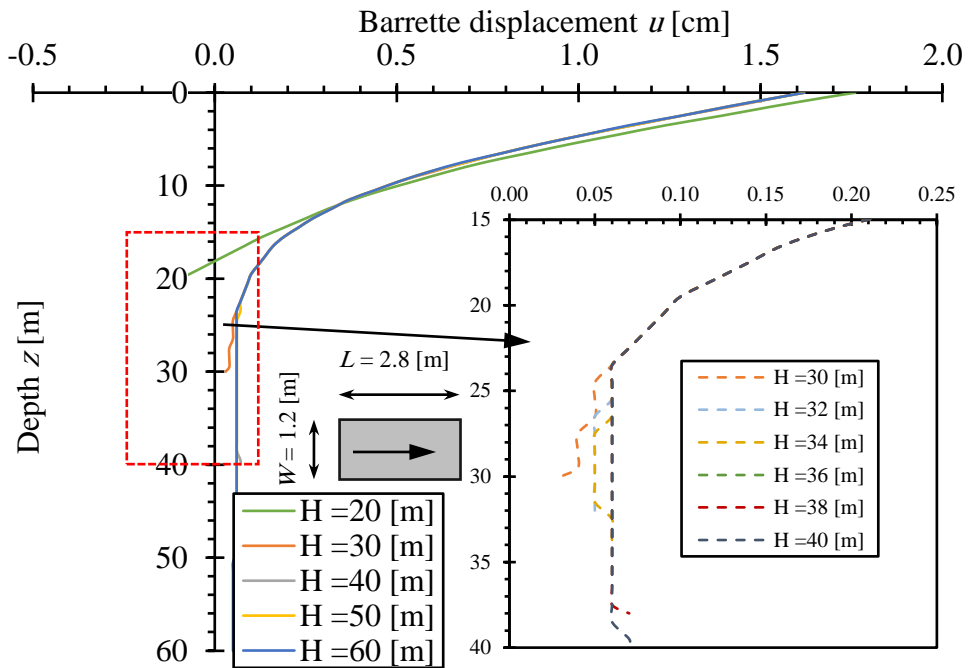


Figure A.40 Displacement u with the barrette height (case 8).

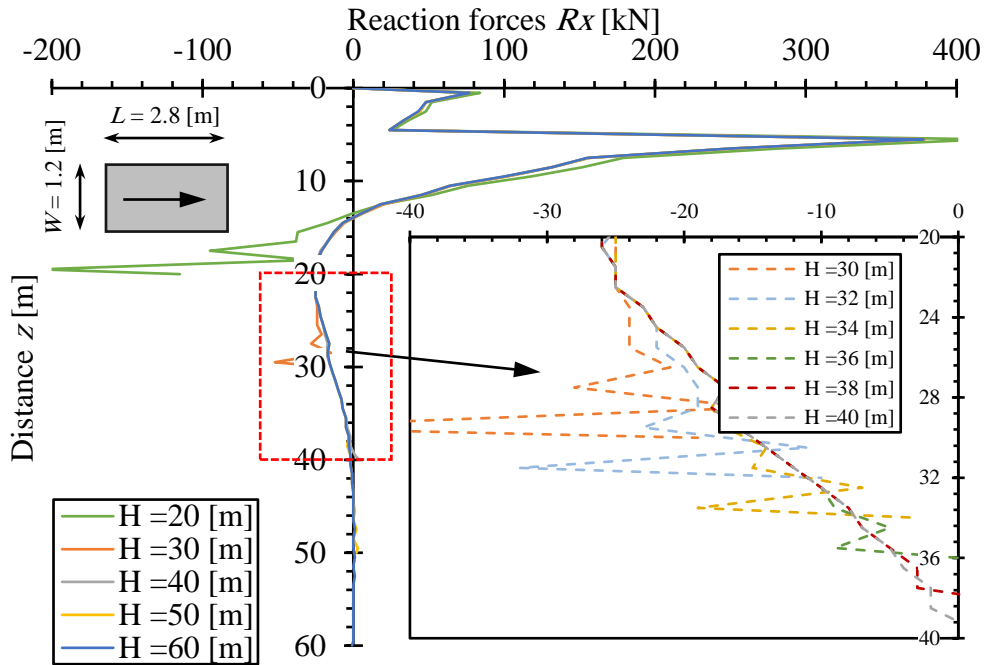


Figure A.41 Reaction forces R_x with the barrette height (case 8).

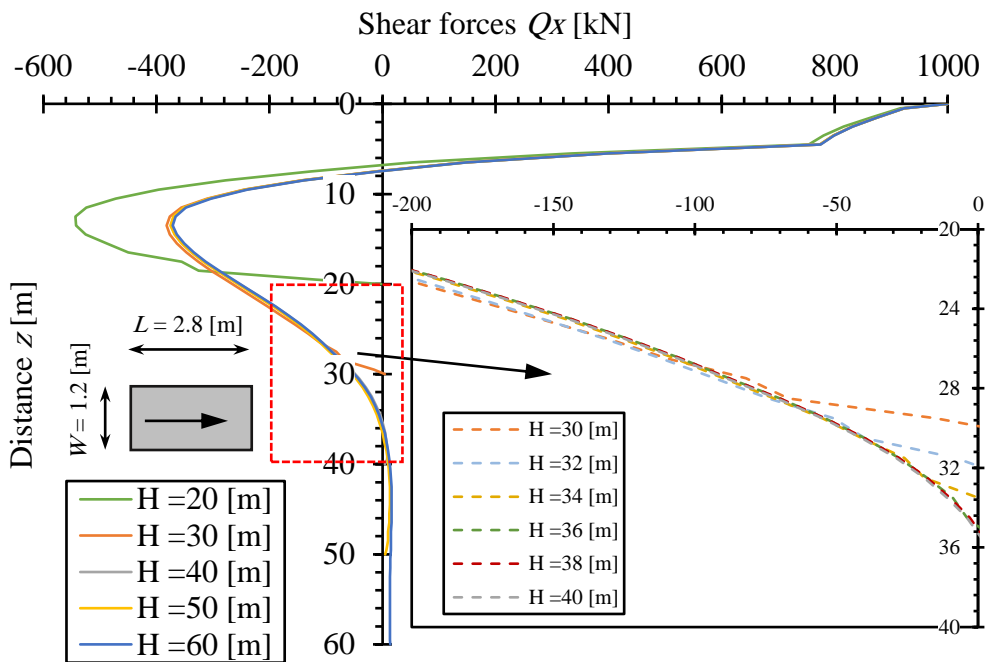


Figure A.42 Shear forces Q_x with the barrette height (case 8).

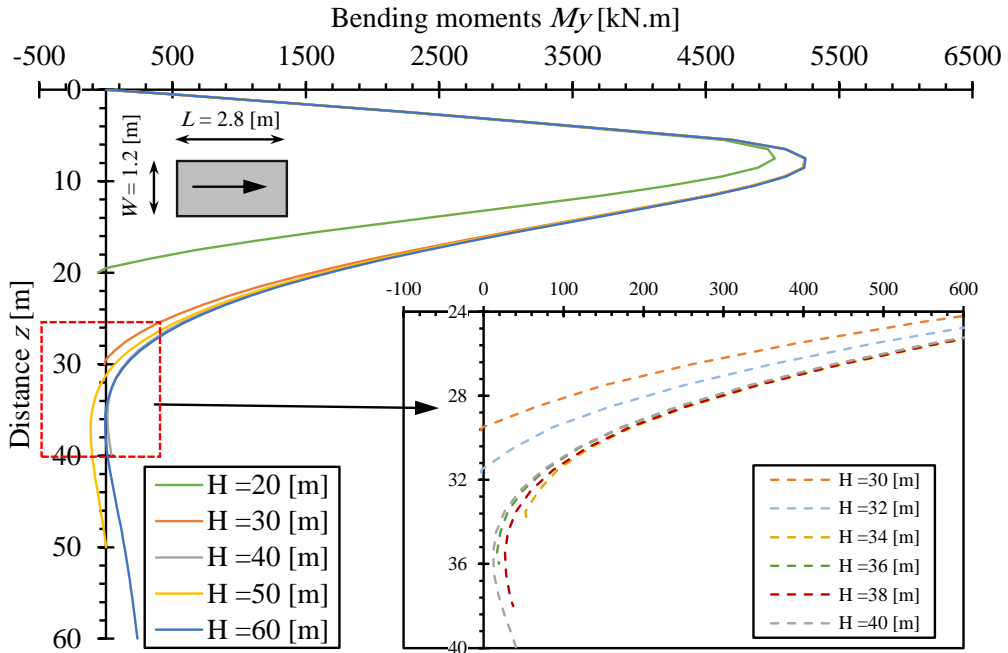


Figure A.43 Bending moments M_y with the barrette height (case 8).

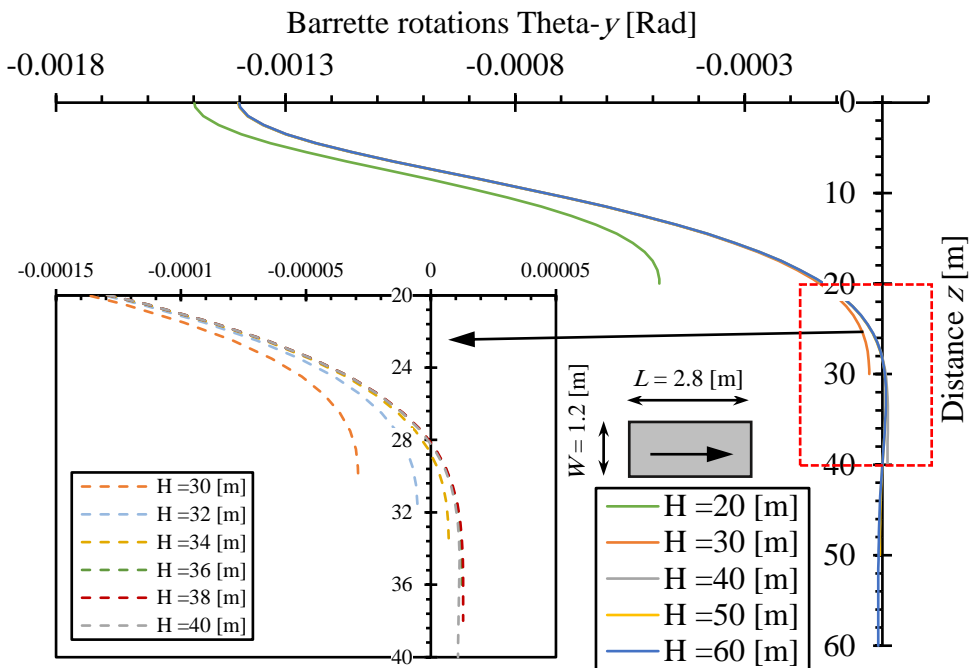


Figure A.44 Barrette rotations Θ_{-y} with the barrette height (case 8).

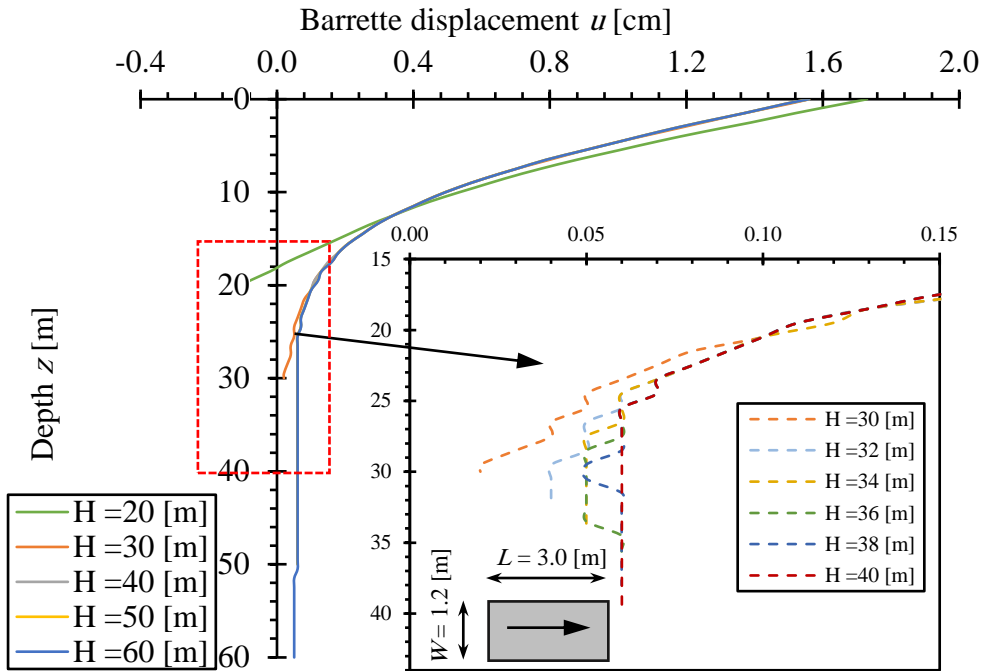


Figure A.45 Displacement u with the barrette height (case 9).

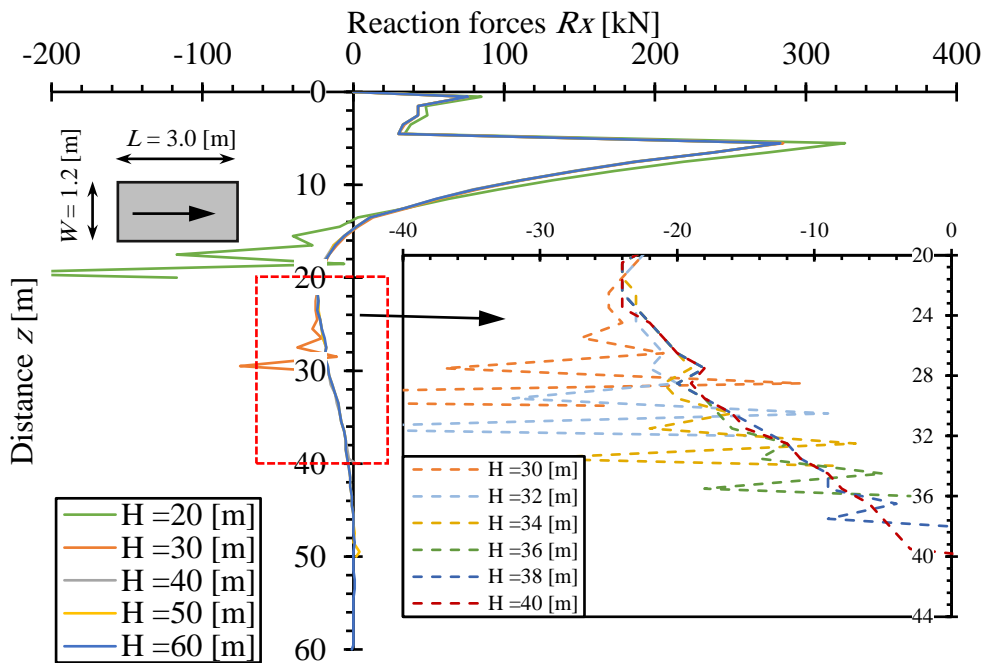


Figure A.46 Reaction forces R_x with the barrette height (case 9).

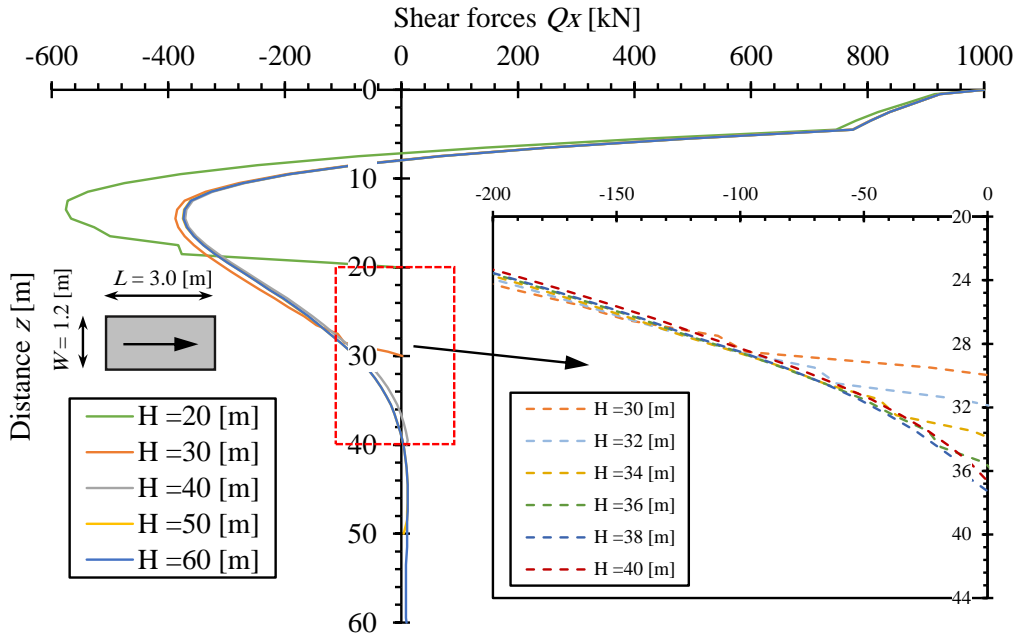


Figure A.47 Shear forces Q_x with the barrette height (case 9).

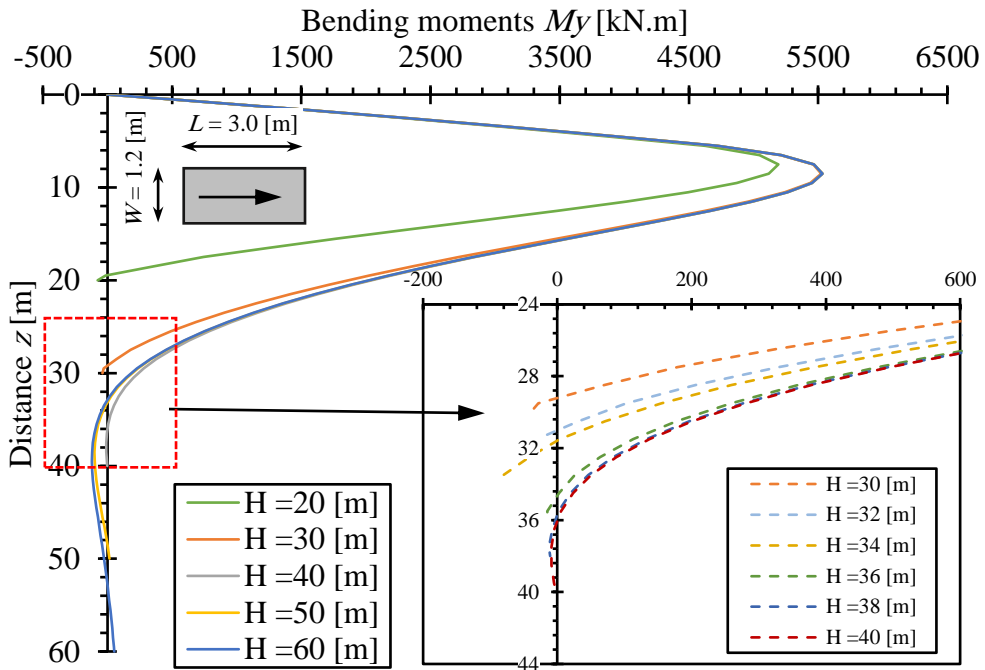


Figure A.48 Bending moments M_y with the barrette height (case 9).

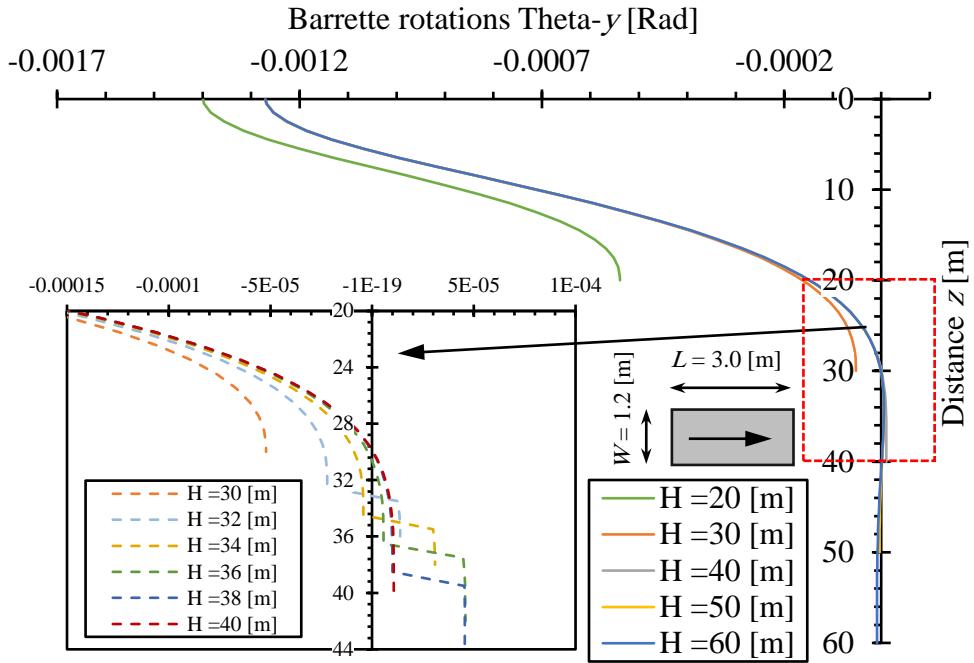


Figure A.49 Barrette rotations Θ_{-y} with the barrette height (case 9).

8.3 APPENDIX (C)

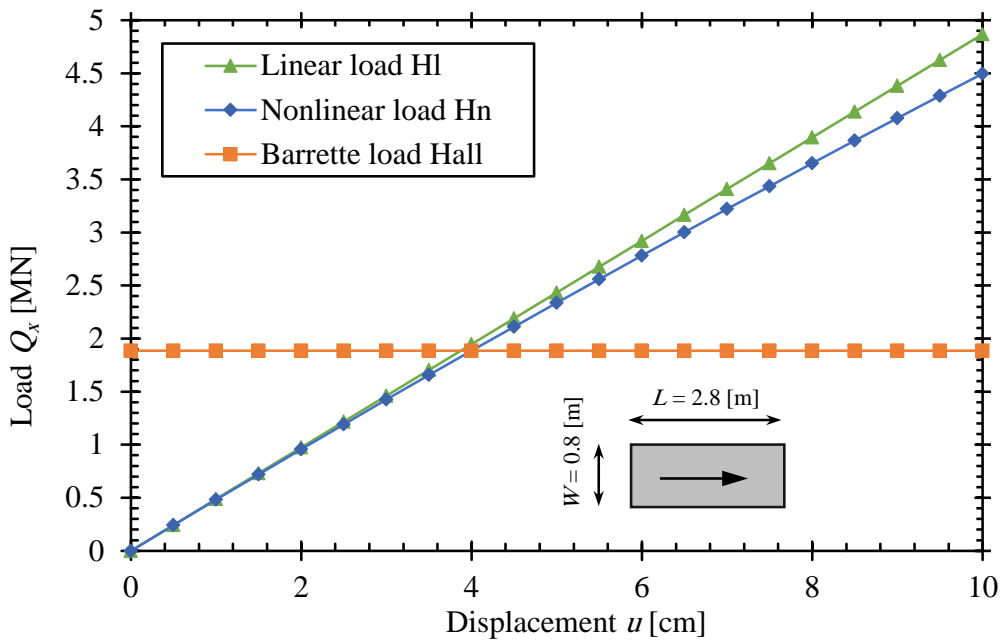


Figure A.50 The load-displacement curve for Case (2).

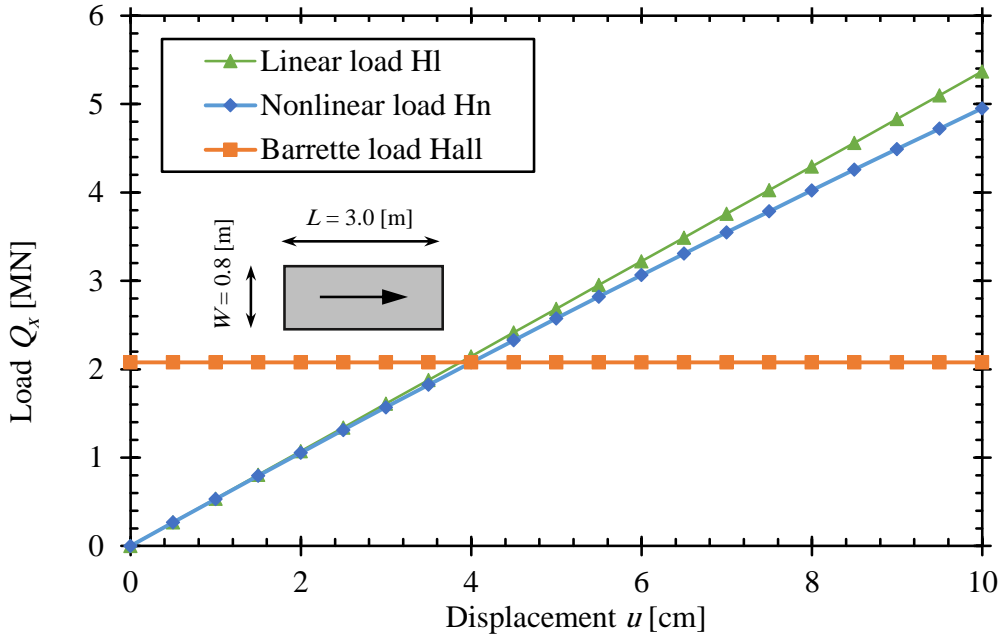


Figure A.51 The load-displacement curve for Case (3).

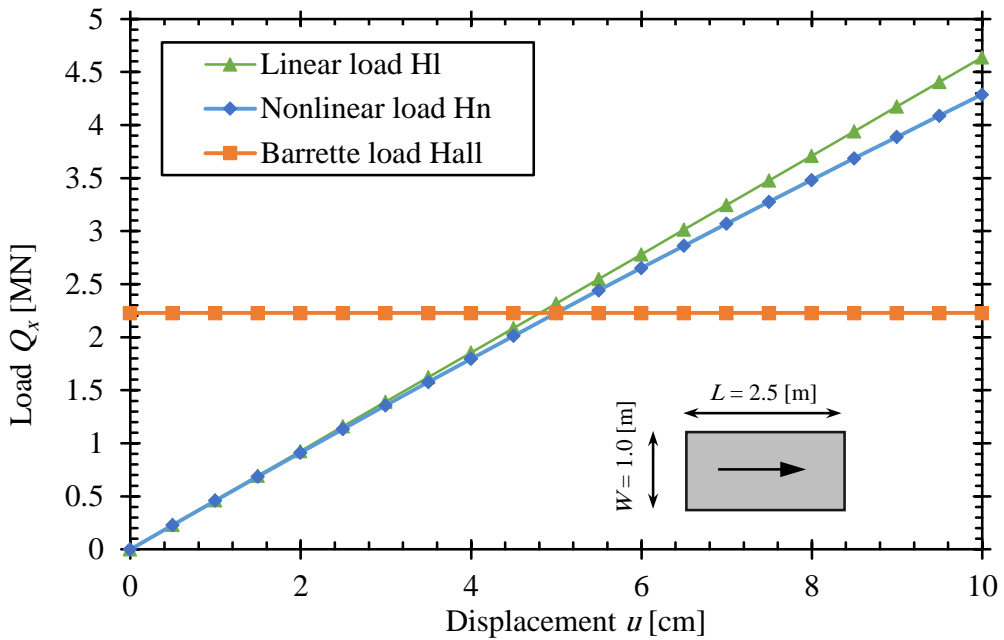


Figure A.52 The load-displacement curve for Case (4).

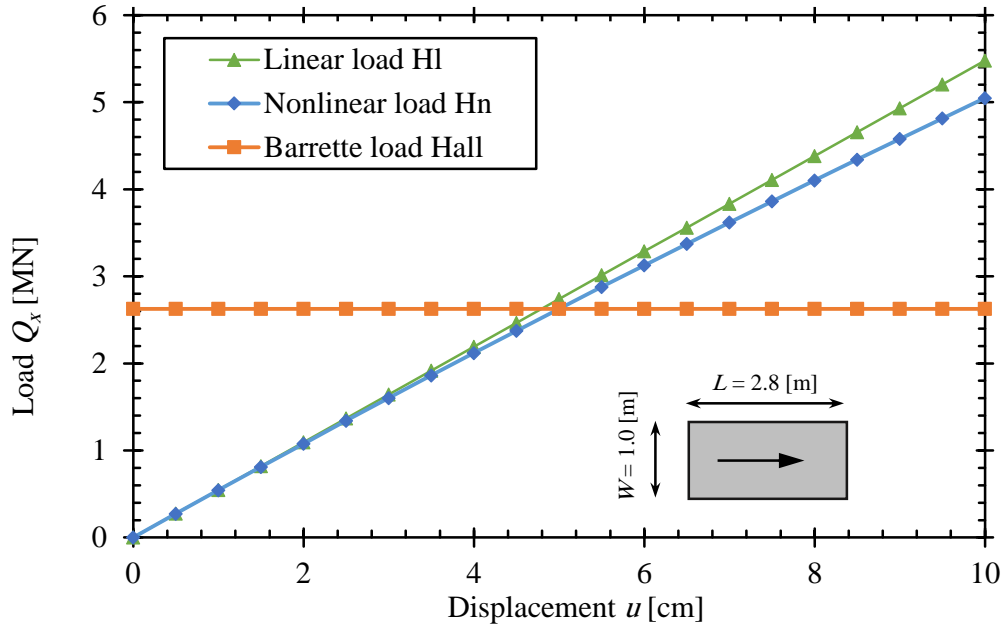


Figure A.53 The load-displacement curve for Case (5).

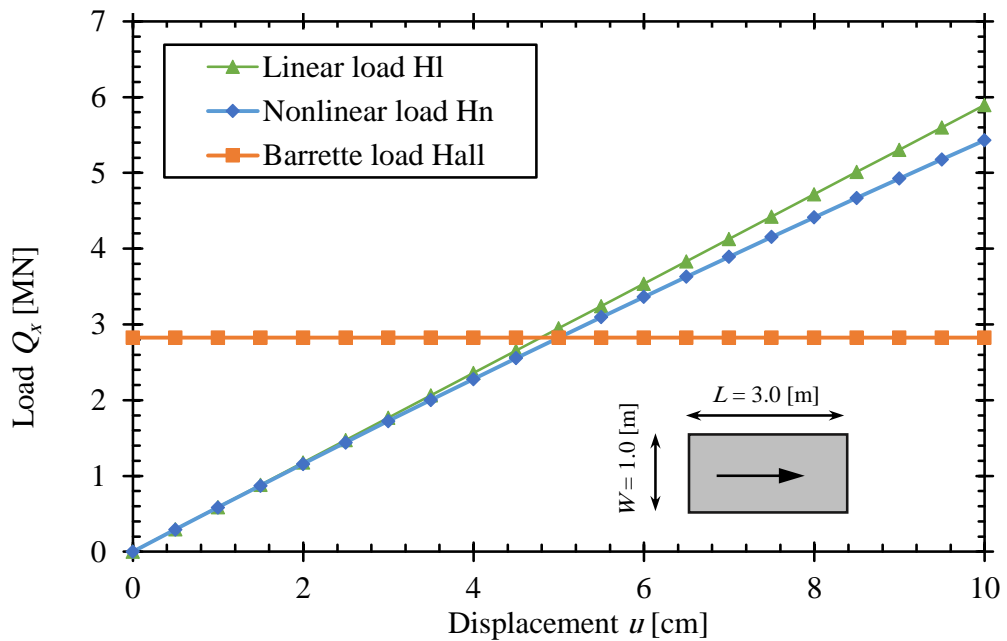


Figure A.54 The load-displacement curve for Case (6).

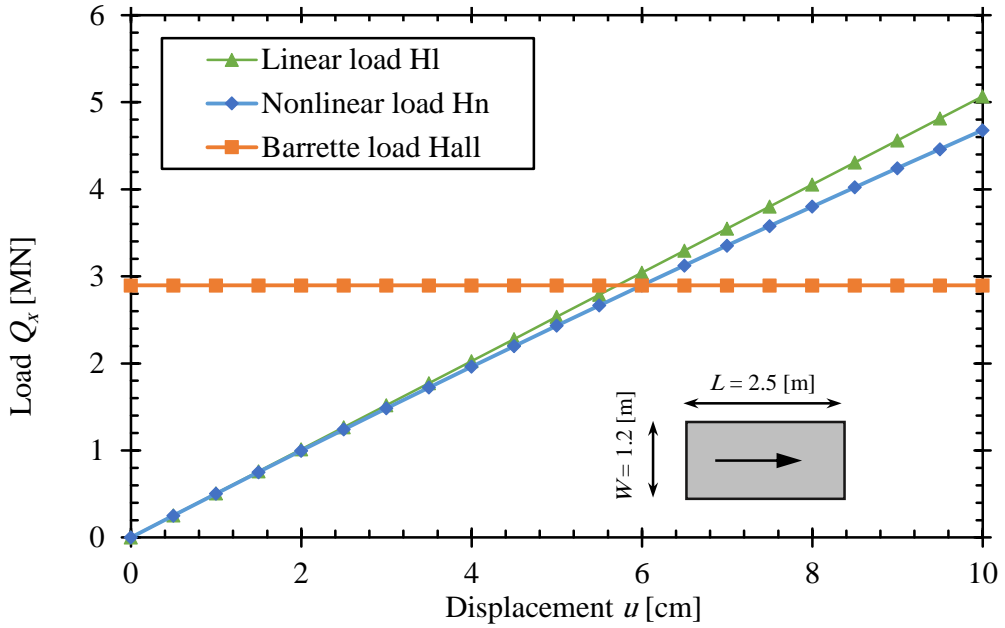


Figure A.55 The load-displacement curve for Case (7).

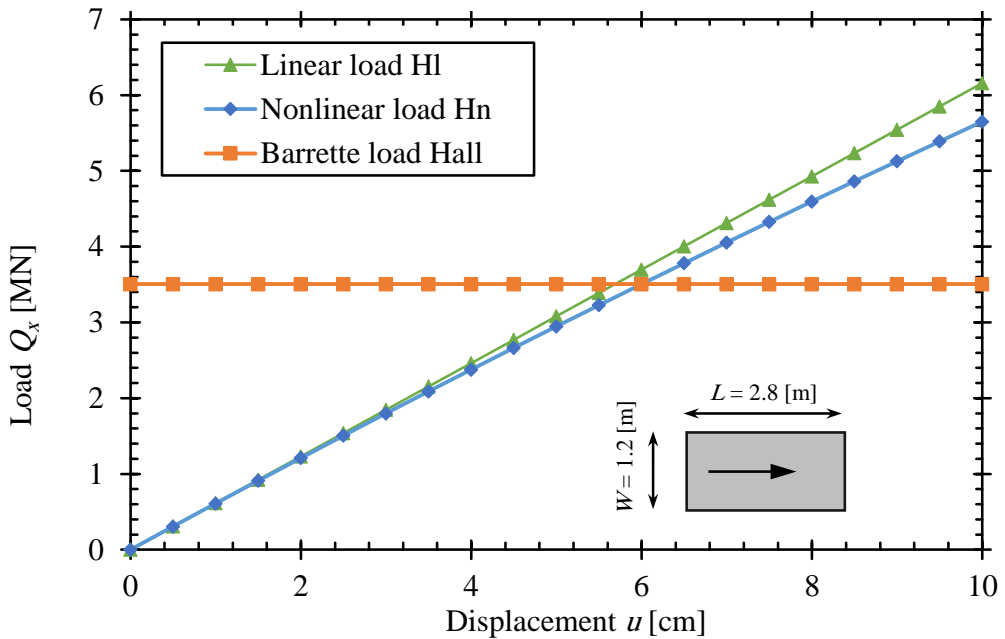


Figure A.56 The load-displacement curve for Case (8).

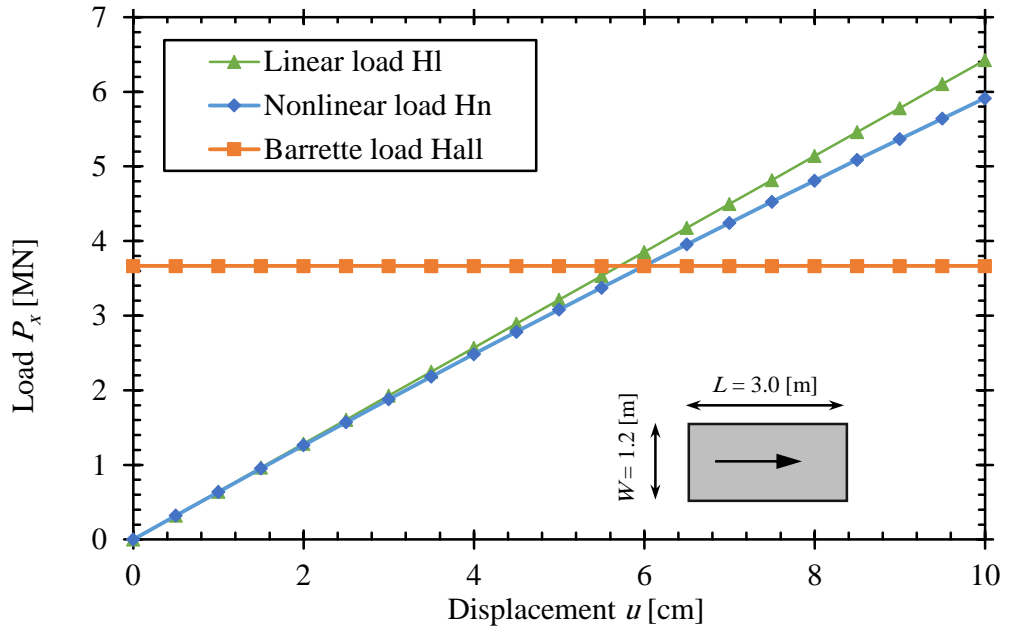


Figure A.57 The load-displacement curve for Case (9).

”نمذجة الأساسات الباريتية تحت تأثير الأحمال الجانبية“

ملخص الرسالة

التطور الحضاري الذي تشهده مصر في الآونة الأخيرة، مثل بناء العديد من المدن الجديدة، بناء أعلى برج في إفريقيا بارتفاع ٣٤٥ م، مسجد الفتح العليم، كاتدرائية المهدي، أبراج العلمين الجديدة، تطوير البنية التحتية والموانئ وغيرها. كل هذه المنشآت الضخمة تحتاج إلى تأسيس جيد لتجنب مشاكل التربة. قد يكون التأسيس على الباريت حلاً رئيسياً لتجنب مشاكل التربة. معظم الدراسات السابقة التي تمت لتحليل التفاعل التبادلي بين الباريت والتربة استخدم فيها طريقة العناصر المحددة ثلاثية الأبعاد. ويحتاج هذا التمثيل إلى شبكة كبيرة من العناصر المحددة مما يؤدي إلى وجود نظام كبير من المعادلات التي تحتاج إلى حل. وبالتالي، فإن هذا التحليل يستغرق وقتاً طويلاً حتى بالنسبة لأجهزة الكمبيوتر السريعة اليوم. في هذه الرسالة، تم تعديل تقنية تكوين المعامل لتحليل الباريت المفرد ومجموعة من الباريت المحمل جانبياً. وتأخذ هذه التقنية في الاعتبار التفاعل التبادلي ثلاثي الأبعاد بين الباريت المحملة جانبياً والتربة المحيطة بعين الاعتبار. إلى جانب ذلك، تقلل هذه التقنية بشكل كبير من عدد المعادلات التي يجب حلها، ويمكن استخدام تلك التقنية في كلا من التحليل الخطي وغير الخطي مع اختلاف تكوين التربة. تم دراسة مجموعة من الأمثلة والتطبيقات ومقارنة نتائج التحليل للنموذج المقترح في هذا البحث مع النتائج المنشورة بالأبحاث السابقة، وذلك للتحقق من دقة طرق التحليل المقترحة. بالإضافة إلى ذلك، تم إجراء دراسة باستخدام التحليل الحالي لمقارنة النتائج مع نتائج اختبارات التحميل الجانبي للباريت. ثم تمت مقارنة النتائج التي تم الحصول عليها بواسطة العناصر ثلاثية الأبعاد باستخدام نموذجين مختلفين مع النتائج التي تم الحصول عليها بواسطة التحليل الحالي. كما تم إجراء دراسات مقارنة للباريت المفردة المحملة جانبياً باستخدام بيانات التربة لجسه حقلية لموقع حقيقي بمنطقة شرق بورسعيد. تقدم دراسات الحالة إرشادات للمهندسين عند تحليل الباريت المحمل جانبياً في منطقة شرق بورسعيد أو المناطق ذات خصائص التربة المماثلة حول العالم. وأخيراً بحثت الدراسات المقارنة سلوك الباريت المفرد ومجموعات الباريت المحملة جانبياً ذات أبعاد، تباعد، عدد، ترتيب، خصائص مواد، وخصائص التربة مختلفة.

الرسالة هي دراسة علمية في موضوع التفاعل التبادلي بين الباريت المحمل جانبياً والتربة وتحتوي على خمسة أبواب على النحو التالي:

الباب الأول:

يحتوي على مقدمة عن البحث، والغرض منه، ومكوناته، مع عرض مشكلة تحليل الباريت الحمل جانبياً.

الباب الثاني:

يعرض هذا الباب ملخص للأبحاث السابقة المتاحة عن هذا الموضوع.

الباب الثالث:

يحتوي هذا الباب على النماذج الرياضية المستخدمة والتي تم تطويرها وتطبيقها في هذا البحث. وذلك باستخدام طريقة معامل المرونة وطريقة العناصر المحددة المعتمدين على تقنية تكوين المعامل. كما يشمل أيضاً أساسيات تحليل الباريت المفرد ومجموعة من الباريت.

الباب الرابع:

ويتم فيه دراسة مجموعة من الأمثلة والتطبيقات ومقارنة نتائج التحليل للنموذج المقترح في هذا البحث مع النتائج المنشورة بالأبحاث السابقة، وذلك للتحقق من دقة طرق التحليل المقترحة. بالإضافة إلى ذلك، تم إجراء دراسة باستخدام التحليل الحالي لمقارنة النتائج مع نتائج اختبارات التحميل الجانبي للباريت. ثم، تمت مقارنة النتائج التي تم الحصول عليها بواسطة العناصر ثلاثية الأبعاد باستخدام نموذجين مختلفين مع النتائج التي تم الحصول عليها بواسطة التحليل الحالي.

الباب الخامس:

ويتم فيه إجراء دراسات مقارنة للباريت المفردة المحملة جانبياً باستخدام بيانات التربة لجلسه حقلية لموقع حقيقي بمنطقة شرق بورسعيد. تقدم دراسات الحالة إرشادات للمهندسين عند تحليل الباريت الحمل جانبياً في منطقة شرق بورسعيد أو المناطق ذات خصائص التربة المماثلة حول العالم. وأخيراً بحثت الدراسات المقارنة سلوك الباريت المفرد ومجموعات الباريت المحملة جانبياً ذات أبعاد، تباعد، عدد، ترتيب، خصائص مواد، وخصائص التربة مختلفة.

الباب السادس:

يشتمل على ملخص البحث وخلاصة ما تم التوصل إليه من نتائج والتوصيات للبحوث المستقبلية والأبحاث المستخلصة من الرسالة.

بسم الله الرحمن الرحيم

هذه الكلمات شكر و عرفان لمن ساهموا في خروج هذا العمل.

أولا أتقدم بخالص الشكر والامتنان لوالدي أ.د./ محمد مسعد الجندي وعمي د./ أمين مسعد الجندي مؤلفي برنامج **ELPLA**، فلولا مساعداتهم ما خرج هذا العمل إلي النور.

ثانيا أتوجه لأمي وزوجتي بالشكر والعرفان على تشجيعهما لي، وصبرهما معي.

ثالثا أتوجه بالشكر والتقدير إلى المشرفين أ.د./ حسن محمد حسن و د./ إبراهيم أحمد العربي على مساعدتهم والمراجعة والتدقيق لإخراج هذا العمل.

رابعا أتوجه بالشكر والتقدير إلى أ.د./ طارق نجيب سالم , أ.د./ عادل هاشم همام و د./ داروين فوكس علي مجهوده الكبير في المراجعة والتدقيق.

محمود الجندي

اسم صاحب الرسالة	محمود محمد مسعد الجندي
عنوان الرسالة	نمذجة الأساسات الباريتية تحت تأثير الأحمال الجانبية
الكلية	كلية الهندسة
القسم العلمي المانح للرسالة	الهندسة المدنية
موقع الكلية	بورسعيد
الدرجة العلمية	الدكتوراه
تاريخ المنح	٢٠٢١/٧/٧
لغة الرسالة	الإنجليزية
هيئة الإشراف	أ.د/ حسن محمد حسن إبراهيم أ.م.د/ إبراهيم أحمد أحمد العربي
هيئة التحكيم	أ.د/ طارق نجيب عبد الله سالم أ.د/ حسن محمد حسن إبراهيم أ.د./ عادل هاشم همام محمد

الموجز العربي	
<p>الباريت هو حل حيوي لتقليل المشاكل الناتجة عن إزاحة التربة أسفل الهياكل الضخمة نظراً لقدرات التحميل المحورية والجانبية العالية. الطرق التقليدية لتحليل الباريت تعتمد بشكل أساسي على نمذجة الباريت والتربة المحيطة باستخدام العناصر المحددة ثلاثية الأبعاد. تتطلب هذه النماذج جهداً حسابياً ضخماً. في هذه الرسالة، تم تطوير تقنية هجينة لتحليل الباريت المحملة جانبياً سواء كان مفرداً أو في مجموعة. في هذه التقنية، يتم استخدام معامل المرونة لتحديد تشوه التربة بناءً على حلول مندلين مع مراعاة التفاعل الكامل بين الباريت والتربة المحيطة. أيضاً، يأخذ في الاعتبار التفاعل الجماعي لكل باريت على مجموعة الباريت. من ناحية أخرى، يتم تقسيم الباريت في الاتجاه الرأسي إلى عناصر محدودة أحادية البعد. يتم تجميع مصفوفة صلابة التربة على طول سطح المشبك بواسطة تقنية المعامل المركب لتكون أحادية البعد على طول المحور الرأسي للباريت ذو الإزاحة المتغيرة على طول ارتفاعه. تتيح هذه التقنية إضافة مصفوفة صلابة التربة إلى مصفوفة صلابة الباريت، مما يؤدي إلى إنشاء مصفوفة الصلابة الكاملة للباريت المفرد أو في مجموعة. نتيجة لذلك، يتم تقليل عدد المعادلات. تم إجراء عدد كبير من عمليات التحقق للتأكد من دقة التقنية الهجينة المقدمة. بالإضافة إلى ذلك، تم إجراء دراسة مقارنة للباريت المفردة المحملة جانبياً في باطن الأرض الحقيقي، حيث تم النظر في خصائص تربة شرق بورسعيد. أيضاً، تم إجراء دراسات بارامترية للتحقيق في سلوك الباريت المفرد أو في مجموعة والمحملة جانبياً. تقدم الدراسة إرشادات لتحليل الباريت المفرد أو في مجموعة المحملة جانبياً.</p>	
الكلمات الدالة	التفاعل التبادلي بين التربة والمنشأ، الأساسات العميقة، الخوازيق المستطيلة، الباريت المفرد، مجموعات الباريت، الأحمال الجانبية، تقنية تكوين المعامل.

نمذجة الأساسات الباريتية تحت تأثير الأحمال الجانبية

رسالة مقدمة

للحصول على درجة الدكتوراه في الهندسة المدنية

إعداد

م / محمود محمد مسعد الجندي

أجيزت بواسطة

أ.د/ طارق نجيب عبد الله سالم

.....
أستاذ ميكانيكا التربة والأساسات بكلية الهندسة، جامعة
الزقازيق.

أ.د/ حسن محمد حسن إبراهيم

.....
أستاذ المنشآت الخرسانية بكلية الهندسة، جامعة بورسعيد.

أ.د. / عادل هاشم همام محمد

.....
أستاذ ميكانيكا التربة والهندسة الجيوتقنية، المركز القومي
لبحوث الإسكان والبناء.

أ.د/ هبة الكيلاني

وكيل كلية الهندسة لشؤون الدراسات العليا

أ.د/ حسن محمد حسن

عميد كلية الهندسة



جامعة بورسعيد



كلية الهندسة

نمذجة الأساسات الباريتية تحت تأثير الأحمال الجانبية

إعداد

محمود محمد مسعد الجندي

ماجستير الهندسة المدنية

كلية الهندسة، جامعة بورسعيد، ٢٠١٦

رسالة مقدمة

للحصول على درجة الدكتوراه في الهندسة المدنية

تحت إشراف

د/ إبراهيم أحمد أحمد العربي

أستاذ مساعد الهندسة الإنشائية بقسم الهندسة

المدنية، كلية الهندسة بجامعة بورسعيد

أ.د/ حسن محمد حسن إبراهيم

أستاذ المنشآت الخرسانية بقسم الهندسة

المدنية، كلية الهندسة بجامعة بورسعيد

٢٠٢١